UNIVERSIDAD COMPLUTENSE DE MADRID
FACULTAD DE FARMACIA

TESIS DOCTORAL

Sistemas de liberación controlada multicargados para crear modelos animales y plataformas neuroprotectoras

Multi-loaded drug delivery systems to create animal models and neuroprotective platforms

MEMORIA PARA OPTAR AL GRADO DE DOCTOR

PRESENTADA POR

Alba Aragón Navas

Directoras

Rocío Herrero Vanrell
Irene Bravo Osuna
Vanessa Andrés Guerrero

Madrid

UNIVERSIDAD COMPLUTENSE DE MADRID

FACULTAD DE FARMACIA

TESIS DOCTORAL

Sistemas de liberación controlada multicargados para crear modelos animales y plataformas neuroprotectoras / Multi-loaded drug delivery systems to create animal models and neuroprotective platforms.

MEMORIA PARA OPTAR AL GRADO DE DOCTOR

PRESENTADA POR

Alba Aragón Navas

DIRECTORAS

Dra. Rocío Herrero Vanrell

Dra. Irene Bravo Osuna

Dra. Vanessa Andrés Guerrero

UNIVERSIDAD COMPLUTENSE DE MADRID

FACULTAD DE FARMACIA

PROGRAMA DE DOCTORADO EN FARMACIA

TESIS DOCTORAL

Sistemas de liberación controlada multicargados para crear modelos animales y plataformas neuroprotectoras / Multi-loaded drug delivery systems to create animal models and neuroprotective platforms.

MEMORIA PARA OPTAR AL GRADO DE DOCTOR

PRESENTADA POR

Alba Aragón Navas

DIRECTORAS

Dra. Rocío Herrero Vanrell

Dra. Irene Bravo Osuna

Dra. Vanessa Andrés Guerrero

AGRADECIMIENTOS

No te das cuenta de toda la gente que se cruza en tu camino durante estos años hasta que tienes que escribir los agradecimientos. Quiero aprovechar este espacio para darles gracias.

En primer lugar, me gustaría agradecer a mis directoras de tesis. A la doctora Rocío Herrero Vanrell por haberme dirigido y haberme dado la oportunidad de trabajar en su grupo de investigación, por haberme enseñado a "dormir" las cosas y por todo el esfuerzo que ha realizado, especialmente durante los últimos meses. A la doctora Irene Bravo Osuna por sus consejos y sus ánimos sobre todo en la parte final de la tesis. Y a la doctora Vanessa Andrés Guerrero por su ayuda y consejos durante estos años. Gracias a las tres por compartir vuestros conocimientos, consejos, ánimos, paciencia y dedicación durante estos 5 años de tesis doctoral.

También me gustaría agradecer al resto de supervisoras del grupo de investigación, las doctoras Irene Molina Martínez y Marta Vicario de la Torre por su disponibilidad siempre que he necesitado su ayuda y sus consejos durante estos años.

A los directores del departamento de Farmacia Galénica y Tecnología Alimentaria, la doctora Emilia Barcia Hernández y el doctor Damián Córdoba Díaz por haberme permitido realizar la tesis en el departamento.

Al Ministerio de Ciencia, Innovación y Universidades (actualmente Ciencia e Innovación) por la concesión del contrato de Formación del Personal Investigador, con el cual he podido realizar esta tesis y una de las estancias.

A la doctora Esther Gil Alegre, profesora del departamento de Farmacia Galénica y Tecnología Alimentaria, por haberme enseñado qué es la Tecnología Farmacéutica en tercero de carrera y que, gracias a ella, conociera el departamento durante los años de estudiante.

I would also like to thank doctor Wenxin Wang's group and Blafar Ltd for letting me to perform my secondment in their laboratories. Part of the results of these experiments are gathered in chapter III. Thank you, Melissa Johnson, for your help with the hyaluronic acid hydrogels. Muchas gracias también a los doctores Irene Lara Sáez y Darío

Manzanares Sandoval por dedicar vuestro tiempo y paciencia en enseñarme cultivos celulares, además de vuestra ayuda.

Moreover, I would like to thank doctor Michael Young, from the Department of Ophthalmology, Schepens Eye Research Institute, Harvard Medical School, for giving me the opportunity of performing my second secondment in his laboratory. It is undeniable that this experience has enriched both my research and life experiences.

También me gustaría expresar mi agradecimiento a los doctores Luis Pablo Júlvez, Elena García Martín y María Jesús Rodrigo Sanjuán, del Grupo de Investigación e Innovación Miguel Servet Oftalmología (GIMSO), en Zaragoza, por habernos permitido desarrollar los trabajos en colaboración con ellos, aportando el punto de vista clínico a estos y dando un valor añadido a nuestra investigación.

Me gustaría agradecer al doctor Manuel Guzmán Navarro por su disponibilidad y ayuda con los experimentos del GPC que se nos quedaron pendientes cuando nuestro equipo dejó de funcionar. Gracias a la Unidad de Bioanálisis y Control de Calidad del Centro de Química Aplicada y Biotecnología por permitirnos realizar estos análisis en sus instalaciones.

Gracias también a todas las personas que han pasado por nuestro laboratorio, ya fueran estudiantes o compañeros que ya terminaron. Gracias a la doctora Alicia Arranz Romera por enseñarme las técnicas más básicas en el laboratorio. Gracias al doctor Sergio Esteban Pérez, quien me enseñó a mantener los equipos, nos sacaba de "excursión" por Madrid y que, junto con Javier, me descubrió el mundo de las cervezas. Gracias también al doctor David García Herranz por haberme enseñado gran parte de lo que sé en el laboratorio, por mostrar siempre su punto de vista y por haber trabajado codo con codo conmigo durante estos años. Gracias a Miriam Ana González-Cela Casamayor, que empezamos juntas, y la casualidad (y la pandemia) ha hecho que nuestras estancias hayan sido prácticamente a la vez, siendo un apoyo la una de la otra cuando estábamos fuera de España. Gracias a Marco Brugnera, por tu paciencia, tranquilidad, por tus consejos y tu ayuda siempre que la he necesitado. Por asegurarte de que todas las botellas del laboratorio quedaran cerradas herméticamente. Gracias también a Elena Moreno López y Cristina Morilla Lomeña que, aunque no haya trabajado tanto con vosotras, sé que estabais ahí para lo que necesitara. Gracias también a los

compañeros del laboratorio de al lado, Mónica Villa Hermosilla y el doctor Mario Alonso González, por alegrarnos los días.

Y gracias a ti, por supuesto, a mi compañero, amigo y pareja, el doctor José Javier López Cano, por estar a mi lado desde un poquito antes de que esta aventura empezara. Gracias por tu apoyo incondicional, por todos los consejos, por desarrollar y enseñarme a sintetizar el polímero de los capítulos finales de esta tesis, por intentar ayudarme siempre que has podido, por aguantar mis ausencias durante las estancias… casi podría escribir otra tesis enumerando motivos por los que agradecerte. Gracias también por aguantarme y comprenderme. A veces no ha sido fácil pues tras salir del laboratorio nos llevábamos nuestras preocupaciones a casa. Pero, sobre todo, gracias por transmitir tu pasión por la ciencia, por estar siempre dispuesto a ayudar independientemente de si conocías el experimento o no y por ser un ejemplo para mí. Espero seguir a tu lado el camino que recorramos y compartir nuestros éxitos juntos.

También quiero agradecer a mi amiga Sara Abalo Cano, a quien conozco desde la infancia, y que, aunque no nos veamos mucho espero que sigamos manteniendo esta amistad. A mi amiga Lara Masó Álvarez por hacerme salir de la burbuja de la tesis para vernos y cenar juntas y compartirme su experiencia en la industria. Gracias también a Blanca Ojosnegros Gozalo por apoyarme y estar pendiente de cómo iba la tesis.

También me gustaría agradecer a Vicente López Coronado y Sacramento Cano Romero, los padres de Javier, por su disponibilidad y su hospitalidad cada vez que tenía experimentos en Zaragoza. Por hacerme sentir parte de la familia y aconsejarme siempre. Y, por supuesto, gracias por ayudarme con el diseño de la portada de esta tesis.

Por último, y no menos importante, quiero agradecer a mi familia (tíos, tías, primo, primas…) por su apoyo durante esta etapa. Especialmente, gracias a mis abuelos y aitites quienes no terminan de comprender lo que hago y han tenido que aguantar largas temporadas sin que fuera a visitarles. Gracias a mi hermana Rocío, por haberme enseñado que a veces hay que desviarse del camino para llegar a la meta. Gracias también por tus consejos. Gracias a mi padre por enseñarme que hay que trabajar duro y gracias también por tus consejos técnicos sobre compresores (porque sí, la tesis es un ámbito multidisciplinar). Gracias a mi madre por apoyarme, escuchar todos mis problemas y preocupaciones e intentar aconsejarme en la medida de lo posible. Gracias

a los dos por vuestro sacrificio para ofrecerme las mejores oportunidades posibles y por advertirme desde pequeña de los sacrificios que conlleva la investigación.

"No es la más fuerte de las especies la que sobrevive, ni la más inteligente, sino la que mejor se adapta a los cambios"

Charles Darwin

A mis padres y a mi hermana

ÍNDICE

ÍNDICE

ÍNDICE

ABREVIATURAS

σ-1-r: Receptores sigma-1

A_1/O/A_2: Acuo-óleo-acuosa

Ad5: Adenovirus 5

ADN: Ácido desoxirribonucleico

AINE: Antiinflamatorio no esteroideo

AMPA: Ácido α-amino-3-hidroxi-5-metil-4-isoxazolapropiónico

AMPc: Adenosín monofosfato cíclico

ATP: Adenosín trifosfato

BDNF: Factor neurotrófico derivado del cerebro (del inglés "Brain Derived Neurotrophic Factor")

BSA: Albúmina sérica bovina (del inglés "Bovine serum albumin")

CNTF: Factor neurotrófico ciliar (del inglés "Ciliary Neurotrophic Factor")

DHA: Ácido docohexanoico

DMAE: Degeneración macular asociada a la edad

DX: Dexametasona

DXP: Dexametasona fosfato

ELISA: Ensayo por inmunoabsorción ligado a enzimas (del inglés "Enzyme-linked inmunosorbent assay")

EMA: Agencia europea del medicamento (del inglés "European Medicines Agency")

EMD: Edema macular diabético

ERG: Electrorretinografía (en inglés: Electroretinography)

ET-1: Endotelina-1

EtOH: Etanol

FDA: Agencia americana de alimentos y fármacos (del inglés "Food and Drug Administration")

GCL: Capa de células ganglionares (del inglés "Ganglion cells layer")

GDNF: Factor neurotrófico derivado de la glía (del inglés "Glial cell line-derived neurotrophic factor")

GPC: Cromatografía de permeación en gel (del inglés "Gel permeation chromatography")

HA: Ácido hialurónico

HPLC: Cromatografía líquida de alta eficacia (del inglés "High-performance liquid chromatography)

HPLC/MS: Cromatografía líquida de alta eficacia acoplada a espectrometría de masas (del inglés "High-performance liquid chromatography-mass spectrometry)

ICAM-1: Molécula de adhesión intercelular (del inglés "Intercellular Adhesion Molecule 1")

IL: Interleucina

IODDS: Sistemas intraoculares de liberación controlada (del inglés "Intraocular drug delivery systems")

IOP: Intraocular pressure

MC: Diclorometano (del inglés "Methylene chloride")

MCP-1: Proteína quimioatrayente de monocitos 1 (del inglés "Monocyte chemoattractant protein-1")

MeOH: metanol

MSs: Microesferas

MSsDexafibro: Microesferas co-cargadas con dexametasona y fibronectina

NMDA: N-metil-D-aspartato

NOHL: Neuropatía óptica hereditaria de Leber

NTG: Glaucoma normotensivo (del inglés "Normal tensión glaucoma")

O/A: Óleo-acuosa

OHT: Hipertensión ocular (del inglés "ocular hipertensión")

OCT: Tomografía de coherencia óptica (del inglés "optical coherence tomography")

PBS: Tampón fostato salino (Phosphate buffered saline)

PCL: Policaprolactona (en inglés "poly(caprolactone")

PEDF: Factor derivado del epitelio pigmentario (del inglés "Pigment epithelium-derived factor")

PEG: Polietilenglicol

PhNR: Respuesta fotópica negativa (del inglés "Photopic Negative Response")

PIO: Presión intraocular

PLGA: Ácido poli(láctico-co-glicólico) (del inglés "Poly(lactic-co-glycolic) acid")

PVA: Alcohol polivinílico (del inglés "Poly(vinyl) alcohol")

R: Retina polo posterior (del inglés "Retina posterior pole")

RD: Retinopatía diabética

RNFL: Capa de fibras nerviosas de la retina (del inglés "Retina nerve fiber layer")

ROP: Método de la apertura del anillo (del inglés "Ring opening method")

ROS: Especies de oxígeno reactivas (de sus siglas en inglés "Reactive oxygen species")

RP: Retinitis pigmentaria

RPE: Epitelio pigmentario de retina (del inglés "Retinal pigmented epithelium")

RGCs: Células ganglionares de la retina (del inglés "Retinal ganglion cells")

S/O/A: Sólido-óleo-acuoso

S/O/O: sólido-óleo-oleoso

SEM: Microscopía electrónica de barrido (del inglés "Scanning electron microscopy")

SOD: Superóxido dismutasa

TEM: Microscopía electrónica de transmisión (del inglés "Transmission electron microscopy")

TNF-α: Factor de necrosis tumoral alfa (del inglés ""Tumoral Necrosis Factor α")

TrkB: Receptor de tropomiosina relacionado a la quinasa B (del inglés "Tropomyosin receptor kinase B")

TUDCA: Ácido tauroursodeoxicólico (del inglés "Tauroursodeoxycholic Acid")

UDCA: Ácido ursodesoxicólico (del inglés "Ursodeoxycholic acid")

VCAM-1: Proteína de adhesión celular vascular 1 (del inglés "Vascular cell adhesion protein 1")

VEGF: Factor de crecimiento endotelial vascular (del inglés "Vascular endothelial growth factor")

Vit E: Vitamina E

W/O/W: Water-in-oil-in-water

RESUMEN – SUMMARY

RESUMEN

SISTEMAS DE LIBERACIÓN CONTROLADA MULTICARGADOS PARA CREAR MODELOS ANIMALES Y PLATAFORMAS NEUROPROTECTORAS.

El glaucoma es una enfermedad crónica neurodegenerativa que afecta al segmento posterior del ojo y que cursa con la pérdida paulatina de la visión, principalmente con pérdida progresiva de las células ganglionares de la retina (RGCs) y daño en el nervio óptico. El proceso de neurodegeneración que aparece en la enfermedad es multifactorial, estando implicados distintos mecanismos dentro de los que destacan el estrés oxidativo, la disfunción mitocondrial, la inflamación, la excitotoxicidad o la deprivación de factores neurotróficos. El único factor de riesgo conocido modificable es la elevación de la presión intraocular (PIO). Sin embargo, no todos los pacientes que padecen glaucoma cursan con una elevación de la PIO, y en muchos otros casos la restauración de valores normales de la PIO no impide que se siga produciendo degeneración de la retina.

Muchos de los mecanismos fisiopatológicos que provocan esta enfermedad son también desconocidos. Su conocimiento es esencial a la hora de desarrollar nuevas terapias que sean efectivas y puedan prevenir o detener su progresión. Por ello, el desarrollo de modelos animales que simulen las condiciones fisiopatológicas en humanos es de gran interés. Actualmente, existen una gran variedad de modelos animales inducidos por distintos mecanismos, ya sean dependientes o independientes de la PIO. Sin embargo, todavía ninguno de los modelos desarrollados ha conseguido imitar la elevación gradual y sostenida de la PIO que ocurre en el glaucoma humano.

Los principales tratamientos actuales de la enfermedad están destinados a reducir la PIO, pero, no son siempre suficientes y en ocasiones, no resultarían necesarios. Por ello, la neuroprotección es un enfoque que tiene cada vez más relevancia en el tratamiento de esta enfermedad. Además, debido a su carácter multifactorial, la combinación de varios principios activos con actividades neuroprotectoras y cuyas dianas farmacológicas sean distintas es una estrategia prometedora.

Al tratarse, el glaucoma, de una patología crónica, los sistemas de liberación controlada capaces de mantener las concentraciones efectivas de los principios activos durante largos periodos de tiempo resultan de gran interés.

Por todo ello, en esta tesis doctoral se han desarrollado sistemas de liberación controlada para dar solución a dos problemas diferentes, aunque relacionados. Por un lado, se ha elaborado un sistema microparticular biodegradable de co-administración de sustancias capaces de generar hipertensión ocular, que ha permitido la creación de un modelo murino de glaucoma crónico mediante su inyección en cámara anterior. Por otro lado, se ha procedido al diseño y desarrollo de distintos sistemas de liberación modificada basados en microsistemas y en hidrogeles capaces de co-liberar varias sustancias neuroprotectoras simultáneamente para el tratamiento neuroprotector del glaucoma y que podrían ser también de utilidad en el tratamiento de otras enfermedades neurodegenerativas del segmento posterior del ojo. Esto demuestra la doble utilidad de la tecnología farmacéutica, no sólo para el tratamiento de las patologías, como se hace tradicionalmente, sino también como herramienta útil capaz de crear modelos animales de enfermedad.

En el **capítulo I** de esta tesis doctoral se procedió a la elaboración de microesferas biodegradables del ácido poli(láctico-co-glicólico) (PLGA), co-cargadas con dos agentes activos capaces de actuar sobre la malla trabecular e inducir un aumento de la presión intraocular (dexametasona y fibronectina) con el objetivo de inyectarlas en cámara anterior para crear un modelo de glaucoma crónico en ratas. La liberación *in vitro* de ambos compuestos mostró un perfil multifásico característico de las microesferas de PLGA con una liberación inicial rápida, seguida de la alternancia de fases con liberaciones más lentas y rápidas.

La inyección intracameral de las microesferas en ratas Long-Evans de una suspensión al 10% (p/v) produjo un aumento gradual de la PIO durante 24 semanas debido, por un lado, a un daño físico producido por el bloqueo de la salida del humor acuoso ocasionado por la propia presencia de las microesferas en la malla trabecular y, además, un daño farmacológico producido por la dexametasona y por la fibronectina. Solo se necesitó una inyección de las microesferas para elevar la presión durante 24 semanas y

se obtuvieron valores considerados como hipertensión ocular a la semana 11. Así mismo, se observó una degeneración progresiva de la retina mediante electrorretinogramas y OCT.

En paralelo a la creación del modelo de glaucoma crónico en ratas, se estableció como siguiente objetivo principal el desarrollo de varias plataformas neuroprotectoras de liberación sostenida. Para ello, cada uno de los siguientes capítulos se dedicó al desarrollo de cada uno de estos sistemas. Así, el **capítulo II** se enfocó en el desarrollo y optimización de microesferas cargadas con tres principios activos de distinta naturaleza con actividades neuroprotectoras. Como primer objetivo de este capítulo se estableció la optimización de las microesferas cargadas con un antiinflamatorio (dexametasona) y un agente antiapoptótico (ácido ursodesoxicólico; UDCA) para posteriormente incluir el agente neurotrófico GDNF (glial cell-line derived neurotrophic factor). Las microesferas fueron elaboradas a partir de una emulsión sólido/óleo/acuosa en la que el compuesto proteico fue incorporado en estado sólido.

La optimización de estas microesferas se realizó incorporando un co-solvente más soluble en agua en la fase interna de la emulsión, además de la inclusión de distintas cantidades de dexametasona seleccionando para la inclusión de la proteína en estado sólido las elaboradas con una mezcla 80:20 de diclorometano:etanol en la fase orgánica y 60 mg de dexametasona.

Tras la inclusión de GDNF al estado sólido en la fase interna de la emulsión, se determinó la eficacia encapsulación de los tres principios activos, la dispersión de la proteína dentro de la matriz polimérica, así como la liberación *in vitro*. Esta fue ajustada a diferentes modelos cinéticos, mostrando que el modelo de Gallagher-Corrigan, con la corrección propuesta por Gorrasi, podía describir perfectamente los perfiles de liberación *in vitro* de los tres compuestos en su totalidad. Mediante este modelo matemático se pudo hipotetizar, además, que la encapsulación de un segundo compuesto dentro de las microesferas modifica principalmente el primer estadio de la liberación, que es el producido por la disolución de los principios activos.

En el **capítulo III** se desarrollaron dos tipos diferentes de hidrogeles inteligentes basados en ácido hialurónico (HA) funcionalizado, y en el polímero tribloque PLGA-PEG-PLGA, como plataformas para la liberación controlada de sustancias activas para el tratamiento de patologías crónicas oculares.

Los hidrogeles de ácido hialurónico fueron formados mediante la reticulación de HA funcionalizado con grupos tiol (HA-SH) y aldehído (HA-CHO). Se evaluaron sus propiedades reológicas mostrando una gelificación rápida cuyo módulo de almacenamiento aumentaba con el tiempo. También mostró propiedades de autocuración, una característica interesante para su aplicación como inyectable.

En el caso de los hidrogeles de PLGA-PEG-PLGA, se recurrió a la optimización del tiempo necesario para disolver el tribloque, ya que su disolución en medio acuoso tenía inicialmente una duración de 3 días. Para ello, se recurrió al cambio del polímero PEG utilizado en su síntesis por uno de un mayor peso molecular y la inclusión de distintas sustancias crioprotectoras en el tampón acuoso para su posterior liofilización.

El hidrogel de HA mostró una degradación más rápida (7 días) en comparación con las formulaciones finales de hidrogeles de PLGA-PEG-PLGA (14 días). En cuanto a la liberación *in vitro* de la sustancia modelo empleada (dexametasona fosfato), los hidrogeles de HA también mostraron una liberación del compuesto superior a las 24 horas.

De acuerdo con los resultados obtenidos, se seleccionaron los hidrogeles de PLGA-PEG-PLGA como candidatos finales para el posible tratamiento de patologías crónicas y se procedió a realizar los correspondientes estudios de tolerancia, proliferación y migración *in vitro* en células epiteliales de retina (RPE-1).

Finalmente, en el **capítulo IV**, se procedió a la combinación de los distintos sistemas desarrollados con anterioridad (microesferas tri-cargadas e hidrogeles termosensibles) para formar un sistema híbrido. Aunque, en esta tesis doctoral se han utilizado estrategias tecnológicas durante el proceso de co-microencapsulación con éxito, se observó una liberación inicial rápida de parte de su contenido que durante el proceso de microencapsulación queda retenido cerca de la superficie de las microesferas o

incluidas en poros de fácil acceso. Por esta razón, en el capítulo IV se ha procedido a evaluar otra estrategia interesante, como es la formación de un sistema híbrido mediante la dispersión de las microesferas en los hidrogeles termosensibles derivados del PLGA-PEG-PLGA. La combinación de microesferas dentro de los hidrogeles, además de producir una disminución de la liberación inicial también favorece la agregación inicial de las microesferas en la zona de administración cuando son inyectadas y puede tener un potencial papel de protección frente a la degradación *in vivo*. Como beneficio adicional, la suspensión de las microesferas en el hidrogel podría evitar la pérdida de estas por adhesión a la jeringa en el momento de la inyección.

La caracterización fisicoquímica del sistema híbrido demostró que la inclusión de las microesferas no produjo modificaciones relevantes en las características del hidrogel con la incoporación de sustancias crioprotectoras. El hidrogel cuyo tampón contenía manitol mostró una degradación en peso más rápida que el elaborado con trehalosa. Sin embargo, eso no afectó a la liberación de los principios activos.

Además, la liberación de los tres compuestos fue ajustada al modelo cinético de Gallagher-Corrigan con la corrección de Gorrasi confirmando también los hallazgos de la disminución en la liberación inicial.

Finalmente, los estudios de tolerancia celular mostraron una viabilidad óptima de las formulaciones finales de hidrogeles en RPE-1. Además, las formulaciones híbridas también presentaron buenas propiedades de inyectabilidad.

SUMMARY.

MULTI-LOADED DRUG DELIVERY SYSTEMS TO CREATE ANIMAL MODELS AND NEUROPROTECTIVE PLATFORMS.

Glaucoma is a chronic neurodegenerative disease that affects the posterior segment of the eye and causes gradual vision loss, mainly with progressive loss of retinal ganglion cells (RGCs) and optic nerve damage. The process of neurodegeneration that appears in the disease is multifactorial, with different mechanisms being involved, including oxidative stress, mitochondrial dysfunction, inflammation, excitotoxicity and neurotrophic factor deprivation. The only known modifiable risk factor is elevated intraocular pressure (IOP). However, not all patients with glaucoma have elevated IOP, and in many cases restoration of normal IOP does not prevent further retinal degeneration.

Many of the pathophysiological mechanisms that cause this disease are also unknown. Knowledge of these mechanisms is essential to develop new therapies that are effective and can prevent or halt the progression of the disease. Therefore, the development of animal models that simulate the pathophysiological conditions in humans is of great interest. Currently, there are a wide variety of animal models induced by different mechanisms, either IOP-dependent or IOP-independent. However, none of the models developed have yet succeeded in mimicking the gradual and sustained IOP elevation that occurs in human glaucoma.

The current main treatments for the disease are aimed at lowering IOP, but they are not always sufficient and may not always be necessary. Neuroprotection is therefore an increasingly important approach in the treatment of this disease. Moreover, due to its multifactorial nature, the combination of several active ingredients with neuroprotective activities and different drug targets is a promising strategy.

As glaucoma is a chronic pathology, controlled release systems capable of maintaining effective concentrations of active ingredients over long periods of time are of great interest.

Therefore, in this doctoral thesis, controlled release systems have been developed to solve two different, although related, problems. On the one hand, a biodegradable microparticular system for co-administration of substances capable of generating ocular hypertension has been developed, which has allowed the creation of a murine model of chronic glaucoma by injection into the anterior chamber. On the other hand, we have designed and developed different modified release systems based on microsystems and hydrogels capable of co-releasing several neuroprotective substances simultaneously for the neuroprotective treatment of glaucoma and which could also be useful in the treatment of other neurodegenerative diseases of the posterior segment of the eye. This demonstrates the dual utility of pharmaceutical technology, not only for the treatment of pathologies, as is traditionally done, but also as a useful tool capable of creating animal models of disease.

In **chapter I** of this doctoral thesis, biodegradable microspheres of poly(lactic-co-glycolic acid) (PLGA), co-loaded with two active agents capable of acting on the trabecular meshwork and inducing an increase in intraocular pressure (dexamethasone and fibronectin) were developed for injection into the anterior chamber to create a model of chronic glaucoma in rats. *In vitro* release of both compounds showed a multiphase profile characteristic of PLGA microspheres with an initial rapid release, followed by alternating phases with slower and faster releases.

Intracameral injection of the microspheres into Long-Evans rats of a 10% (w/v) suspension resulted in a gradual increase in IOP over 24 weeks due, on the one hand, to physical damage caused by blocking the outflow of aqueous humour caused by the presence of the microspheres in the trabecular meshwork and, on the other hand, to pharmacological damage caused by dexamethasone and fibronectin. Only one injection of the microspheres was needed to raise the pressure for 24 weeks and values considered as ocular hypertension were obtained at week 11. Progressive retinal degeneration was also observed by electroretinograms and OCT.

In parallel to the creation of the model of chronic glaucoma in rats, the development of several sustained-release neuroprotective platforms was established as the next main objective. To this end, each of the following chapters was devoted to the development of each of these systems. Thus, **chapter II** focused on the development and optimisation

of microspheres loaded with three different types of active substances with neuroprotective activities. The first objective of this chapter was the optimisation of microspheres loaded with an anti-inflammatory (dexamethasone) and an anti-apoptotic agent (ursodeoxycholic acid; UDCA) to subsequently include the neurotrophic agent GDNF (glial cell-line derived neurotrophic factor). The microspheres were prepared from a solid-in-oil-in-water emulsion in which the protein compound was incorporated in a solid state.

These microspheres were optimised by incorporating a more water-soluble co-solvent in the internal phase of the emulsion, in addition to the inclusion of different amounts of dexamethasone, selecting those made with an 80:20 mixture of dichloromethane:ethanol in the organic phase and 60 mg of dexamethasone for the inclusion of the protein in the solid state.

After inclusion of GDNF in the solid state in the internal phase of the emulsion, the encapsulation efficiency of the three active ingredients, the dispersion of the protein within the polymeric matrix, as well as the *in vitro* release were determined. This was fitted to different kinetic models, showing that the Gallagher-Corrigan model, with the correction proposed by Gorrasi, could perfectly describe the *in vitro* release profiles of the three compounds in their entirety. Using this mathematical model, it was also hypothesised that the encapsulation of a second compound inside the microspheres mainly modifies the first stage of the release, which is the one produced by the dissolution of the active ingredients.

In **chapter III**, two different types of smart hydrogels based on functionalised hyaluronic acid (HA) and the triblock polymer PLGA-PEG-PLGA were developed as platforms for the controlled release of active substances for the treatment of chronic ocular pathologies.

Hyaluronic acid hydrogels were formed by cross-linking functionalised HA with thiol (HA-SH) and aldehyde (HA-CHO) groups. Their rheological properties were evaluated showing rapid gelation whose storage modulus increased with time. It also showed self-healing properties, an interesting feature for its application as an injectable.

In the case of PLGA-PEG-PLGA hydrogels, the time needed to dissolve the triblock was optimised, as its dissolution in aqueous media initially lasted 3 days. For this purpose, the PEG polymer used in its synthesis was changed to one of a higher molecular weight and the inclusion of different cryoprotective substances in the aqueous buffer for its subsequent freeze-drying.

The HA hydrogel showed a faster degradation (7 days) compared to the final PLGA-PEG-PLGA hydrogel formulations (14 days). Regarding the *in vitro* release of the model substance used (dexamethasone phosphate), the HA hydrogels also showed a higher release of the compound after 24 hours.

Based on the results obtained, PLGA-PEG-PLGA hydrogels were selected as final candidates for the possible treatment of chronic pathologies and the corresponding *in vitro* tolerance, proliferation and migration studies were carried out on retinal epithelial cells (RPE-1).

Finally, in **chapter IV**, the different systems previously developed (tri-loaded microspheres and thermosensitive hydrogels) were combined to form a hybrid system. Although, in this doctoral thesis, technological strategies have been used during the co-microencapsulation process with success, an initial rapid release of part of its content was observed, which during the microencapsulation process is retained near the surface of the microspheres or included in easily accessible pores. For this reason, another interesting strategy, the formation of a hybrid system by dispersing the microspheres in the PLGA-PEG-PLGA-derived thermosensitive hydrogels, has been evaluated in chapter IV. The combination of microspheres within the hydrogels, besides producing a decrease in initial release, also favours the initial aggregation of the microspheres at the site of administration when injected and may have a potential protective role against degradation *in vivo*. As an additional benefit, suspension of the microspheres in the hydrogel could prevent loss of the microspheres by adhesion to the syringe at the time of injection.

The physicochemical characterisation of the hybrid system showed that the inclusion of the microspheres did not produce relevant modifications in the characteristics of the hydrogel with the incorporation of cryoprotective substances. The hydrogel containing

mannitol in the buffer showed a faster degradation by weight than the one made with trehalose. However, this did not affect the release of the active ingredients.

Furthermore, the release of the three compounds was fitted to the Gallagher-Corrigan kinetic model with Gorrasi correction also confirming the findings of decreased initial release.

Finally, cell tolerance studies showed optimal viability of the final hydrogel formulations on RPE-1. In addition, the hybrid formulations also showed good injectability properties.

INTRODUCCIÓN

1. Anatomofisiología ocular

El ojo o globo ocular es un órgano par con forma esferoidal achatada, con un volumen de 6,5 mL y un peso de 7 gramos. Tiene un diámetro aproximado de 24 mm y ocupa el 25% de la órbita. El espacio restante es ocupado por los músculos extraoculares, nervios, vasos sanguíneos, tejido adiposo orbital y tejido conectivo. La órbita es una estructura ósea piramidal con una inclinación de 23° hacia el exterior con respecto a la línea media del cráneo. Ésta rodea la mayor parte del globo ocular, siendo únicamente la córnea y la parte anterior del globo, los que exceden sus límites (Figura 1) (1,2).

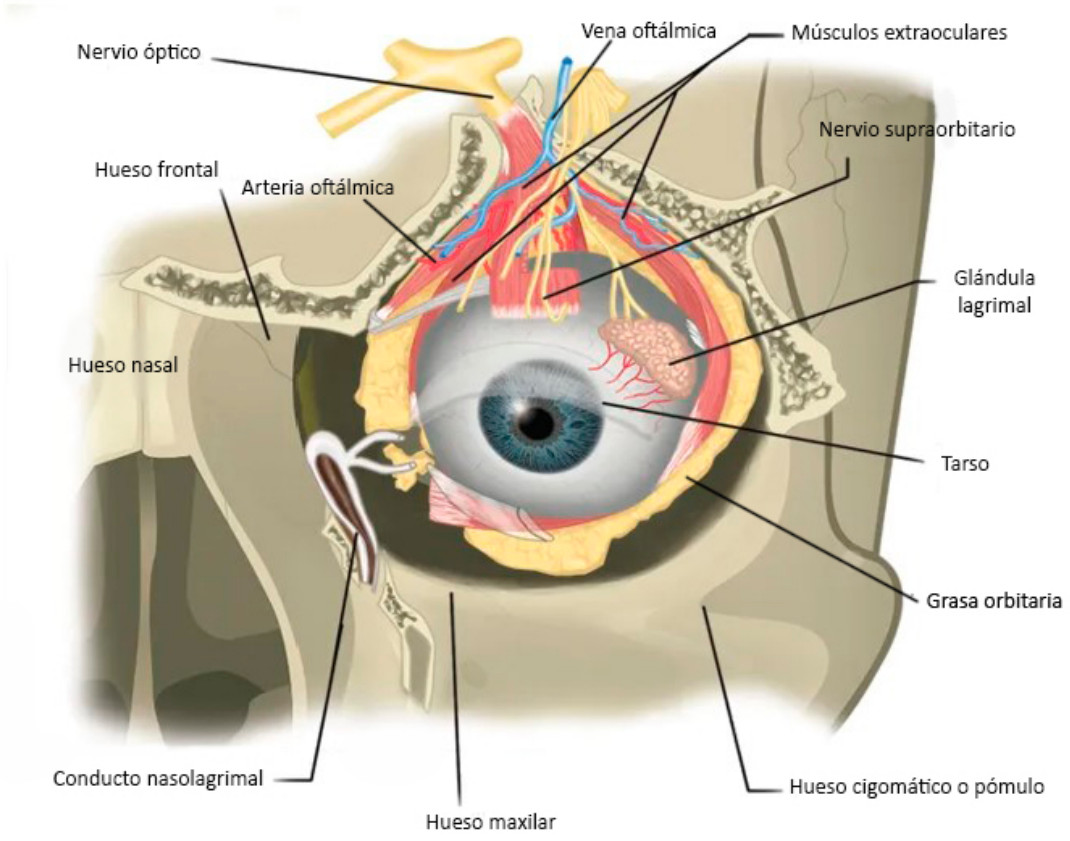

Figura 1. Vista anterior de la cavidad orbital. Imagen extraída y adaptada de https://neupsykey.com/.

Anatómicamente, el globo ocular se puede dividir en 3 capas distintas o túnicas (Figura 3), que se disponen desde el exterior hacia el interior de la siguiente manera:

- Túnica fibrosa. Está formada por la córnea (en la zona anterior) y la esclera (en la zona posterior).

- La córnea es una capa transparente avascular que cubre el iris. Está formada por 6 capas: epitelio corneal, membrana de Bowman, estroma, capa de Dúa, membrana de Descemet y endotelio corneal (3).
- La esclera es una capa blanca, densa, de tejido conectivo, formada principalmente por fibras de colágeno y fibroblastos. Cubre la mayor parte del globo ocular exceptuando la córnea, y se encarga de dar forma al mismo, ser sitio de anclaje de los músculos extraoculares además de tener funciones de protección. En la unión de la esclera con la córnea se encuentra el canal de Schlemm, donde el humor acuoso es drenado desde la malla trabecular (4).

- Túnica vascular o úvea. Se encuentra formada por la coroides, los cuerpos ciliares y el iris.
  - La coroides es un tejido pigmentado y altamente vascularizado que se encuentra entre la esclerótica y la retina. Debido a su gran número de vasos sanguíneos, suministra nutrientes a la parte posterior de la retina. La coroides produce el pigmento melanina que hace que esta capa tenga un color marrón oscuro característico lo que permite que pueda absorber los rayos de luz directos, previniendo, de esta manera, su reflejo y dispersión dentro del globo ocular.
  - El iris es la parte coloreada del ojo que se encuentra suspendido entre la córnea y el cristalino, anclado en su margen exterior a los procesos ciliares. La cantidad de melanina es la que determina el color de los ojos, siendo más oscuros los que más cantidad contienen y más claros los que tienen menos concentración. El iris posee fibras musculares lisas que son las encargadas de contraerlo o dilatarlo, regulando así el tamaño de la pupila y, por tanto, la cantidad de luz que entra al globo ocular, siendo esta última, la principal función del iris.
  - El cuerpo ciliar es la continuación de la coroides en la parte anterior de la túnica vascular. Posee también un color marrón oscuro debido a la presencia de melanocitos productores de melanina. El cuerpo ciliar está compuesto por los procesos ciliares y el músculo ciliar (Figura 2). Los procesos ciliares son protuberancias o pliegues de la superficie interna

de los cuerpos ciliares y contienen capilares sanguíneos que participan en la producción del humor acuoso. A continuación de los procesos ciliares, se encuentran las fibras zonulares, zónula o ligamento suspensorio del cristalino, entre otros nombres, que se encargan de mantener en su posición al cristalino y permiten que el músculo ciliar actúe sobre él. El músculo ciliar consiste en una banda circular de músculo liso que se puede contraer o relajar y esto altera la tensión de las fibras zonulares y, por tanto, la forma del cristalino, adaptándolo a la visión cercana o lejana (1,4).

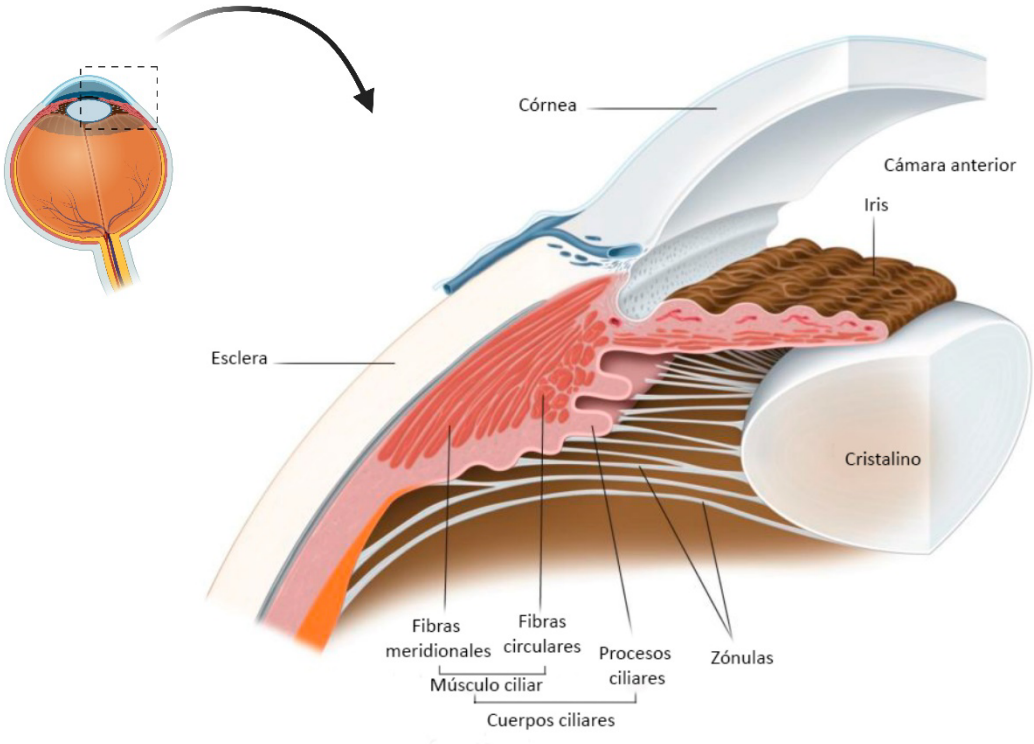

Figura 2. Anatomía del segmento anterior con mayor detalle de los cuerpos ciliares y zónulas. Imagen extraída y adaptada de © 2022 American Academy of Ophthalmology (http://www.aao.org). Imagen creada con Biorender.com.

- Túnica nerviosa o retina. Es la capa más interna del globo ocular. Se trata de una capa transparente, delgada y delicada que cubre tres cuartas partes del globo ocular y el primer paso en la ruta de la visión. Está formada por 10 capas diferentes que desde el punto de vista funcional se dividen en dos: una capa pigmentada y otra neural.

- La capa pigmentada también se llama epitelio pigmentario de la retina, ya que está formada por células epiteliales que contienen melanina. Se localiza entre la coroides y la capa neural y como en la coroides, la melanina ayuda a absorber los rayos de luz directos, teniendo un papel de protección frente a ellos. Además, también sirve de soporte metabólico a la retina neural o sensorial.
- La capa neural o capa sensorial se puede considerar una extensión del cerebro que procesa los datos visuales antes de enviar los impulsos nerviosos al nervio óptico. Se encuentra formada por 3 capas de neuronas de la retina (capa de fotorreceptores -conos y bastones-, capa de células bipolares y la capa de las células ganglionares) que se encuentran separadas entre sí por dos zonas (capa sináptica interna y externa) donde tienen lugar las sinapsis. Además, en la capa de células bipolares existen otros dos tipos de células llamadas células horizontales y amacrinas que poseen funciones de nutrición y soporte.

  La capa de fotorreceptores se compone de dos tipos de células especializadas: conos y bastones. Los conos son los encargados de la visión a color y hay tres tipos, los sensibles a la luz azul, verde y a la luz roja; los bastones son sensibles a la luminosidad y al contraste.

  Las señales visuales pueden formar parte de un circuito de vías con sentido tanto horizontal como vertical. Primero la información visual es procesada por los fotorreceptores. Estos establecen sinapsis con las células bipolares ya sea de forma directa o indirecta a través de las células horizontales. A su vez, las células bipolares establecen sinapsis con las células ganglionares y amacrinas. Finalmente, los axones de las células ganglionares se extienden al disco óptico, saliendo del globo ocular a través nervio óptico. El disco óptico, es también conocido como papila óptica o punto ciego, ya que no contiene fotorreceptores.

  La mácula lútea que se localiza en el centro exacto de la retina dispone de una zona central en la que se encuentra la fóvea, que consiste en una pequeña depresión que solamente contiene conos. Como resultado, la fóvea es la zona con mayor agudeza visual o resolución (1,4).

Además, la retina posee células gliales que juegan un papel importante en la homeostasia neuronal. Están compuestas por tres tipos celulares: las células gliales de Müller y los astrocitos, ambos conforman la macroglia, y las células microgliales. En la retina de los vertebrados, las células gliales de Müller son las principales y, en concreto, la retina humana posee entre 4 y 5 millones. Tienen funciones de soporte homeostático, metabólico y funcional neuronal. Constituyen un enlace anatómico y funcional entre las neuronas retinianas y aquellos compartimentos donde se produce intercambio de moléculas (como pueden ser la cámara vítrea, los vasos sanguíneos retinianos o el espacio subretiniano). Las células de Müller eliminan, además, los productos de desecho y modulan de forma directa o indirecta la excitabilidad y transmisión neuronal (5,6).

Con respecto a los astrocitos, diversos estudios han demostrado que están implicados en la vascularización retiniana y en el mantenimiento de la barrera hemato-retiniana y que son los principales productores de VEGF (factor de crecimiento endotelial vascular). Asimismo, contribuyen a varias funciones homeostáticas gliales en las que de igual forma están involucradas las células de Müller, como son la eliminación de dióxido de carbono, la regulación del pH extracelular y la retirada del potasio sobrante del líquido extracelular, procedente de la actividad neuronal, que es transferido a zonas con baja concentración de potasio (6,7).

La microglía tiene funciones de protección de las neuronas de la muerte celular y media la regeneración de tejidos. También elimina productos tóxicos, patógenos, restos celulares y produce factores neurotróficos y citoquinas pro y antiinflamatorias, siendo, por tanto, una mediadora crucial en la neuroinflamación. De hecho, alteraciones en su funcionalidad están implicadas en la neurodegeneración (6,8).

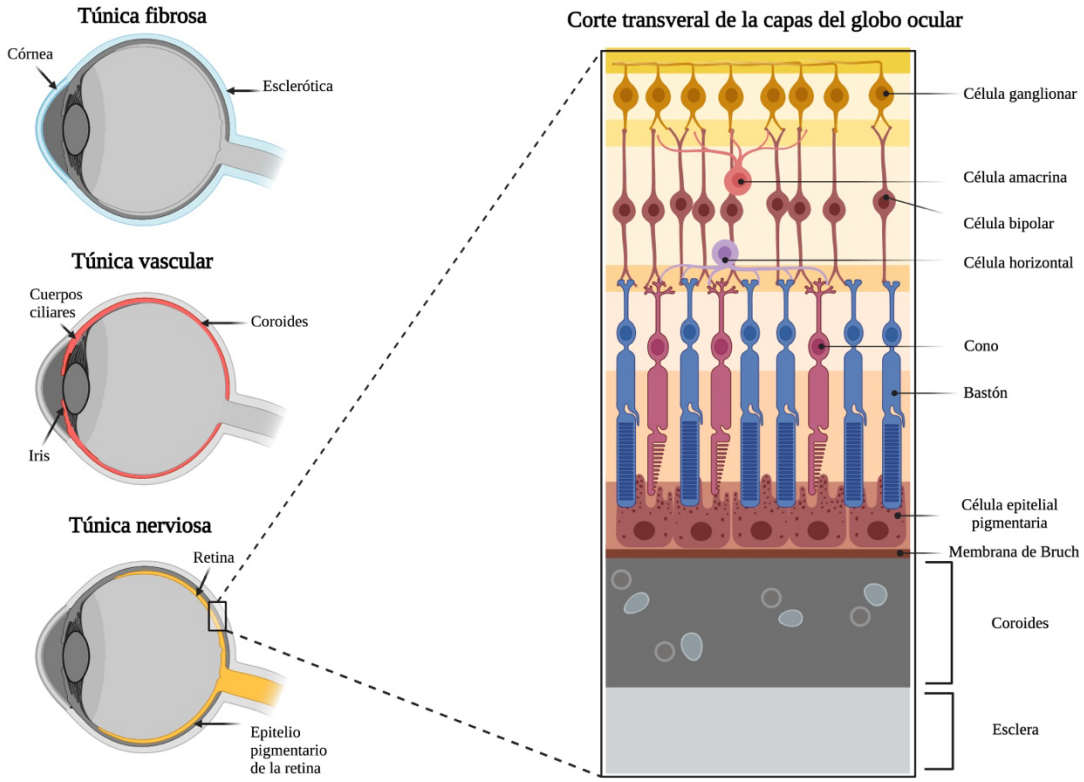

Figura 3. Clasificación y corte transversal de las distintas capas de conforman el globo ocular. Descripción breve de las células que forman la capa neural de la retina. Imagen basada en López-Cano, JJ (2022). Nanosistemas de administración oftálmica para el tratamiento de patologías crónicas e inflamatorias. [Tesis doctoral] Universidad Complutense de Madrid. Imagen creada con Biorender.com.

El globo ocular se encuentra dividido por el cristalino en dos segmentos: anterior y posterior.

- El segmento anterior ocupa 1/3 del ojo y se sitúa en la parte más externa del mismo. Está formado por el cristalino (suspendido de los cuerpos ciliares por las zónulas), el iris y la córnea. Se encuentra delimitado a su vez en dos cámaras: anterior y posterior, y ambas contienen el humor acuoso (Figura 4).
    - *La cámara anterior* se encuentra delimitada en la parte anterior por la córnea y en la posterior por el iris y parte de los cuerpos ciliares. Contiene el humor acuoso que se comunica con la cámara posterior por la pupila.
    - *La cámara posterior* es un espacio triangular que contiene humor acuoso. Se encuentra delimitada por el iris y parte de los cuerpos ciliares, en la parte posterior está delimitada por el cristalino y las zónulas y finalmente en la parte lateral por los cuerpos ciliares.

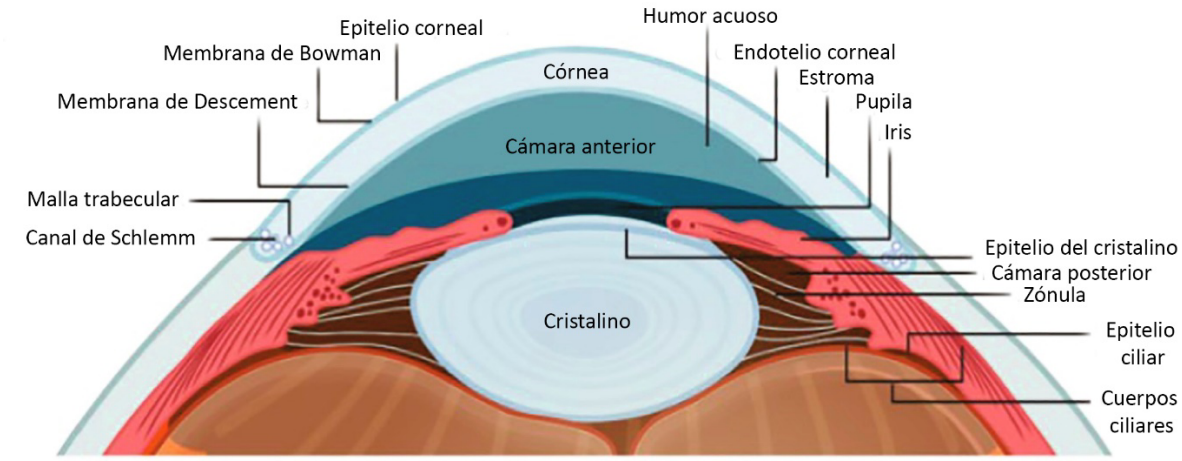

Figura 4. Estructura del segmento anterior del ojo. Imagen extraída y adaptada de "Morris J, Myer C, Cornet T, Junk AK, Lee RK, Bhattacharya SK. Proteomics of pseudoexfoliation materials in the anterior eye segment. Adv Protein Chem Struct Biol. 2021; 127:271-290."

El **humor acuoso** es un líquido claro que baña ambas cámaras del segmento anterior en diferente volumen, siendo este de 0,25 mL en la cámara anterior y de 0,06 mL en la posterior. Está formado en un 99,9% de agua y el 0,1% restante de sólidos entre los cuales destacan proteínas, aminoácidos y otras sustancias no coloides como son glucosa, urea, ácido ascórbico, ácido láctico, inositol, oxígeno en forma disuelta e iones (Na^+, K^+, Cl^-, HCO_3^-). Se produce en los cuerpos ciliares y fluye desde la cámara anterior de forma mayoritaria hacia la malla trabecular y el canal de Schlemm. Desde aquí, el humor acuoso entra en los canales colectores que drenan hacia las venas epiesclerales. A nivel metabólico, proporciona substratos y contribuye a la eliminación de los metabolitos de la córnea avascular y del cristalino. Además, tiene un papel fundamental en el mantenimiento de la presión intraocular. De hecho, es así su relevancia, que la fisiopatología del glaucoma gira en torno a la dinámica del humor acuoso. Hay distintas estructuras que también se encuentran involucradas en su dinámica, como son los cuerpos ciliares, el ángulo de la cámara anterior y el sistema de drenaje del humor acuoso.

- La morfología y la morfometría del ángulo camerular tiene un papel clave en el drenaje del humor acuoso, no solo porque varía entre individuos, sino porque puede favorecer el desarrollo de algunos tipos de glaucoma, como el glaucoma de ángulo cerrado.

- El sistema de drenaje del humor acuoso está formado por la malla trabecular, el canal de Schlemm, los canales colectores y las venas epiesclerales.
    - La malla trabecular es una estructura esponjosa en forma de tamiz por la que de forma mayoritaria el humor acuoso abandona el ojo. Está constituida por tres capas (mencionadas del exterior hacia el interior): malla yuxtacanalicular, corneoescleral y uveal.
    - El canal de Schlemm. Se trata de un canal ovalado recubierto de células endoteliales que presentan formas irregulares y contienen grandes vacuolas presentes en la pared interior. Las células endoteliales presentes en la parte exterior son lisas y planas y contienen aperturas con los canales colectores.
    - Los canales colectores o llamados también vasos acuosos intraesclerales abandonan el canal de Schlemm y terminan en las venas epiesclerales (1,9).

- El segmento posterior ocupa los 2/3 restantes del ojo e incluye las estructuras posteriores al cristalino: la retina, la coroides y el disco óptico (anteriormente mencionadas), además del humor vítreo (1).
    - El humor vítreo ocupa alrededor de 4/5 del volumen total de la cavidad del globo ocular, con un volumen aproximado de 4 mL. Se trata de un líquido transparente, viscoso e inerte cuyas funciones principales son las de mantener la estructura del globo ocular y proporcionar una superficie uniforme en la retina para una recepción nítida de las imágenes. Al contrario que el humor acuoso, el humor vítreo no se renueva constantemente. Está formado fundamentalmente por agua (98-99,7%) y por proteínas fibrilares (principalmente el colágeno) que proporcionan flexibilidad, resistencia y viscosidad; además, contiene glicosaminoglicanos, fundamentalmente el ácido hialurónico y el condroitín sulfato, que se disponen entre las fibras de colágeno y atraen iones y agua, hinchando y espaciando la matriz. El humor vítreo es prácticamente acelular y en él se pueden encontrar únicamente células fagocíticas, llamadas hialocitos, que eliminan los desechos y se sitúan en la periferia (1,4,10).

2. Patologías neurodegenerativas más relevantes que afectan al segmento posterior del ojo: etiología y mecanismos fisiopatológicos.

Las enfermedades neurodegenerativas representan un grupo heterogéneo de enfermedades que se caracterizan por una degeneración progresiva estructural y funcional del sistema nervioso central y periférico. La retina es una unidad funcional del sistema nervioso central que está conectada físicamente con el cerebro a través de los axones del nervio óptico. Es por ello, que las enfermedades que afectan a la retina se encuentran dentro de esta clasificación.

Entre ellas, ordenadas de mayor a menor prevalencia en mayores de 50 años, se sitúan el glaucoma, la degeneración macular asociada a la edad (DMAE) y la retinopatía diabética (RD). Hay que señalar que la prevalencia varía con la edad, siendo la DMAE más común en las personas mayores, y la retinopatía diabética en los jóvenes. A este grupo también pertenecen la retinosis pigmentaria (RP) y la neuropatía óptica hereditaria de Leber (NOHL), cursando ambas por mutaciones genéticas que se detallan a continuación (11,12).

2.1. Glaucoma.

En 2020, el glaucoma presentó una prevalencia global de 2,29 personas por cada 1000 en discapacidad visual, y de 2,04 personas por cada 1000 en lo que respecta a pérdida de visión. Se sitúa como la segunda causa de pérdida de visión mundial por detrás de las cataratas (11% vs 45,4%, respectivamente). Por lo tanto, es la primera causa de pérdida de visión irreversible por enfermedades neurodegenerativas (13).

El glaucoma se define como un grupo de enfermedades heterogéneas que se caracterizan por la muerte progresiva de las células ganglionares de la retina (RGCs), la disminución en espesor de la capa de fibras nerviosas de la retina y una neuropatía del nervio óptico. Desde la perspectiva del tratamiento y la fisiopatología, el incremento de la presión intraocular (PIO) es el principal factor de riesgo modificable. En general se considera que la disminución de PIO entre un 30 y un 50%, frena el progreso de esta enfermedad (14). Los valores de PIO considerados normales se sitúan entre los 10 y 21 mmHg, considerándose valores superiores a 21 mmHg como hipertensión ocular (15).

El glaucoma se puede clasificar en dos grupos en función de la morfología de la cámara anterior, si el ángulo que forman el iris y la córnea está adecuadamente abierto para el drenaje del humor acuoso: glaucoma de ángulo abierto o de ángulo cerrado. En este último caso, se produce una obstrucción que impide el correcto drenaje, causando la elevación en la PIO (14).

El aumento de la PIO produce un daño en las fibras nerviosas ópticas de la lámina cribosa, situada en la base del nervio óptico, que causa estrés y presión en su estructura. Esta diferencia de presión finalmente conduce a la compresión, deformación y remodelado de la lámina cribosa, impidiendo el transporte axonal dentro de las fibras del nervio óptico e iniciando, por último, la apoptosis de las RGCs (14,16).

Sin embargo, también se puede dar en pacientes con glaucoma que no presentan una elevación de la PIO, pero sí una degeneración de las neuronas de la retina. Este tipo de glaucoma se denomina “glaucoma normotensivo”. Existen distintas teorías para explicar esta patología, como podría ser una sensibilidad mayor a la presión intraocular normal, una desregulación vascular o un proceso neurodegenerativo, entre otros. Sin embargo, la conclusión que puede sacarse es que su fisiopatología no es del todo conocida y que se trata de una enfermedad multifactorial, existiendo varios mecanismos que la pueden explicar (17).

Independientemente de la PIO, en el glaucoma existen otros factores que pueden causarlo. Estos pueden ser un anormal flujo sanguíneo ocular, una estructura anormal de la lámina cribosa, presión intracraneal baja, autoinmunidad y una disfunción mitocondrial (18). Además, se está investigando la implicación de las alteraciones de la perfusión ocular con el desarrollo de glaucoma (19,20).

Además, otros mecanismos patogénicos que inducen los procesos neurogenerativos, son isquemia/hipoxia, estrés oxidativo crónico, excitotoxicidad, estrés metabólico, descenso en los niveles de nicotinamida, deprivación de neurotrofinas y neuroinflamación. Entre ellos, los que son considerados como principales factores de riesgo de glaucoma son el estrés oxidativo, la disfunción mitocondrial y la senescencia celular que, a la vez, incrementan con el envejecimiento.

El estrés oxidativo y la peroxidación lipídicas son las principales causas del estrés tisular que conllevan a la activación de la para-inflamación local. La para-inflamación se define como una respuesta adaptativa de los tejidos al estrés nocivo o una malfunción, y se considera como un estadio intermedio entre los estados normal o basal y los inflamatorios. Un nivel fisiológico es necesario para mantener la homeostasis de los tejidos y restablecer su funcionalidad, sin embargo, si el tejido es expuesto a estos estímulos durante un tiempo prolongado, la inflamación puede tener un efecto perjudicial y progresar la enfermedad (21).

Por todos estos factores, la terapia combinada con principios activos con diferentes mecanismos de acción y que posean una actividad neuroprotectora tiene una especial relevancia para el tratamiento del glaucoma (22).

2.2. Degeneración macular asociada a la edad (DMAE).

La DMAE representó un 5,6% de los casos de ceguera a nivel global en el 2020. Su prevalencia fue de unas 3,39 personas por cada 1000 cursando con una pérdida de visión y unas 1,03 personas por cada 1000 en ceguera (13). Es una enfermedad progresiva que afecta a las personas mayores. En su estado avanzado, se caracteriza por la degeneración de los fotorreceptores y del epitelio pigmentario de la retina (23).

El envejecimiento ocular a menudo se acompaña de la acumulación de desechos celulares no aclarados que se originan en el epitelio pigmentario de la retina (RPE) y se depositan en la zona donde el RPE interactúa con la membrana de Bruch y la retina neurosensorial. Estos depósitos, denominados drusas, están formados principalmente por lípidos, pero también por proteínas e hidratos de carbono. Las drusas junto con otros cambios bioquímicos asociados a su patogénesis (como es la activación de la cascada del complemento o la inflamación) producen un engrosamiento y un descenso en la permeabilidad de la membrana. Esto conduce a la obstrucción del transporte de nutrientes a la retina y del intercambio de productos de desecho a la coroides, y el adelgazamiento de la vasculatura coroidal. Estas circunstancias, combinadas con los cambios neurodegenerativos en el complejo fotorreceptores-RPE, produce anormalidades pigmentarias en los RPE y, finalmente, daños que afectan a las funciones de las RPE y los fotorreceptores (24).

Se han descrito dos tipos de DMAE: seca o atrófica y húmeda o exudativa (Figura 5). Recientemente, los criterios para clasificar esta enfermedad se han unificado, estableciendo tres estadios de la enfermedad: precoz, intermedio y avanzado, en función de la severidad de las lesiones. La DMAE avanzada puede evolucionar hacia una DMAE exudativa o húmeda (25).

DMAE atrófica o seca, se caracteriza por una lenta y progresiva pérdida de la visión, que cursa con la acumulación de drusas de tamaño variable.

DMAE exudativa o húmeda, tiene un curso más rápido y presenta neovascularización. Es menos frecuente que la DMAE seca. Los nuevos vasos sanguíneos son producidos por el reclutamiento de células del sistema inmune a la mácula dañada y la secreción de citoquinas proinflamatorias y proangiogénicas, especialmente de VEGF. El VEGF estimula la proliferación y migración de células endoteliales, conduciendo a la angiogénesis y al incremento de la permeabilidad vascular. Estos nuevos vasos liberan líquido que produce la interrupción y el daño en la capa de fotorreceptores. Si no se trata, la exudación retiniana produce la fibrosis y atrofia de la mácula y, en pocos meses, la pérdida irreversible de visión central (24).

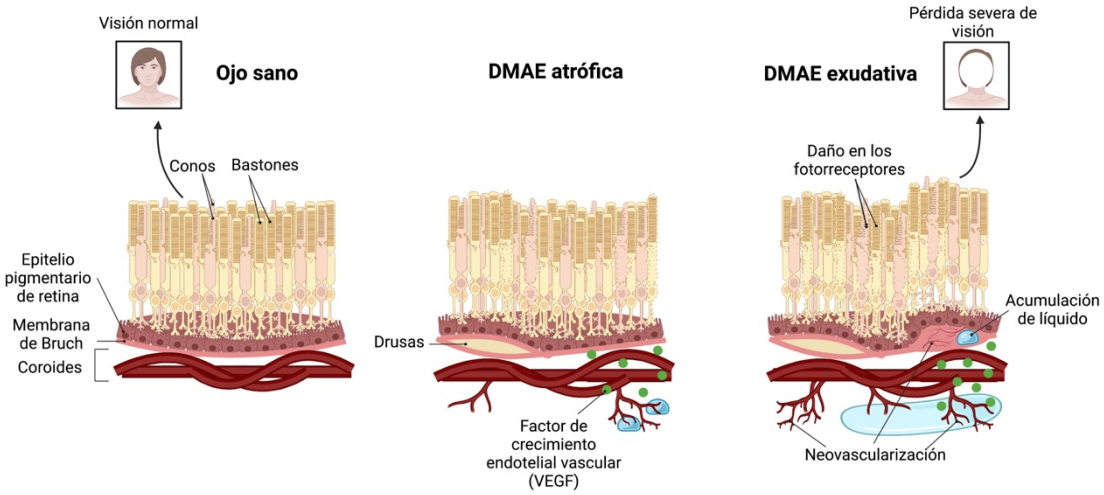

Figura 5. Esquema de la fisiopatología de la DMAE atrófica y exudativa. Imagen creada con BioRender.com

2.3. Retinopatía diabética (RD).

En 2020, la retinopatía diabética supuso el 2,5% de los casos de ceguera a nivel global. En ese mismo año, presentó una prevalencia de 1,59 personas por cada 1000 en casos de pérdida de visión y de unas 0,46 personas por cada 1000 en ceguera (13).

La RD es una de las principales complicaciones de la diabetes mellitus. Se puede dividir en no proliferativa y proliferativa. La forma no proliferativa se da en las primeras etapas de la enfermedad, cuando se produce un incremento de la permeabilidad vascular y la oclusión de los capilares en la vasculatura retiniana. En esta etapa, se puede observar microaneurismas, hemorragias y exudados. La forma proliferativa es un estado avanzado de esta enfermedad y se caracteriza por una neovascularización. Es en esta etapa cuando los pacientes pueden presentar pérdidas de visión debidas a hemorragias en el vítreo de los nuevos vasos sanguíneos formados o debido a un desprendimiento de retina (26).

La causa más común de pérdida de visión en la RD es el edema macular diabético (EMD), que se produce por un hinchamiento o engrosamiento de la mácula debido a la acumulación de líquido sub o intra-retinal. Esta acumulación se produce por la ruptura de la barrera hemato-retiniana.

La RD se ha considerado tradicionalmente una enfermedad microvascular, sin embargo, hay evidencias que sugieren que los procesos de inflamación y neurodegeneración retiniana están implicados. En lo que respecta a la inflamación, se ha detectado leucostasis y monocitos y granulocitos en la vasculatura retiniana. Además, se ha visto que estos pacientes también presentan niveles incrementados de moléculas de adhesión endotelial celular como son la molécula de adhesión intercelular (ICAM-1), molécula de adhesión celular vascular (VCAM-1) y selectinas (selectina-E), además de la presencia de quimiocinas. Tampoco hay que olvidar que bajo condiciones de estrés hiperglucémico se ha visto que la microglía se encuentra activada, secretando TNF-α, IL-6, MCP-1 y VEGF, para después activarse las células de Müller y los astrocitos que amplifican la respuesta a la inflamación y producen citoquinas proinflamatorias (26).

En cuanto a la neurodegeneración retiniana, se ha observado que ocurre en las primeras fases de la enfermedad durante la progresión de esta. La apoptosis de las neuronas retinianas se produce por la mayor expresión de moléculas pro-apoptóticas, la disfunción mitocondrial y el estrés oxidativo, ya que, en estas condiciones, se incrementan la producción de especies reactivas a oxígeno (ROS) (26).

La primera línea de tratamiento, tanto para la RD como para la EMD, es la inyección intravítrea de agentes anti-VEGF. La fotocoagulación con láser tiene un papel importante como terapia adyuvante. Sin embargo, en pacientes que no responden a la terapia anti-VEGF, la terapia antiinflamatoria con corticosteroides ha mostrado ser de gran utilidad. Debido a la implicación de un proceso neurodegenerativo, hay otros tratamientos que están siendo evaluados como podría ser el uso de antioxidantes (luteína), antioxidantes específicos de la mitocondria (ácido α-lipoico) o un inhibidor de la cardiolipina, fosfolípido de la membrana interna de la mitocondria implicado en la apoptosis celular, (MTP-131) (26).

2.4. Retinitis pigmentaria (RP)

El término retinitis o retinosis pigmentaria se refiere a un conjunto de desórdenes genéticos que afectan la capacidad de la retina para responder a la luz, y que cursa con la degeneración de los conos y de los bastones. La prevalencia global de la RP es 1 persona por cada 4000. Puede ser heredada por gen autosómico-dominante, autosómico recesivo o ligado al cromosoma X. Además, existe una forma sindrómica y otra no sindrómica. La afección sindrómica afecta a un 20-30% de los pacientes, provocando síntomas en otras partes del cuerpo (27,28).

Muchos de los casos son monogénicos, sin embargo, está enfermedad es genéticamente heterogénea. Esto queda demostrado en que, hasta la fecha, se han identificado al menos 45 loci cuyas mutaciones pueden causar la enfermedad. Las mutaciones principales son las que afectan al gen de la rodopsina (RHO), el gen USH2A y el gen RPGR, que causan alrededor del 30% de los casos de RP (28).

Algunos de estos genes afectados codifican para proteínas que intervienen en la cascada de los bastones, por lo que afectan a su función y, posteriormente, producen su muerte. Las mutaciones solo afectan a los bastones, pero también se ha visto que se

produce la muerte de los conos. Esta muerte secundaria de los conos, aunque todavía no ha sido explicada, podría deberse a una interacción entre conos y bastones, por lo que resulta de gran importancia comprender esta interacción además de los factores que pueden estar involucrados (28).

En cuanto al tratamiento de esta patología, se han publicado varios estudios sobre el uso de suplementos nutricionales en estos pacientes, en los que se ha visto que la administración de vitamina A enlentece la pérdida de campo, así como el posible beneficio de la suplementación con DHA (ácido docohexanoico), un ácido graso omega-3. Además, hay tratamientos prometedores en estudio como el uso del factor neurotrófico ciliar (CNTF), la terapia génica, tratamientos neuroprotectores o el trasplante de células para reemplazar el tejido retiniano perdido (27,28).

2.5. Neuropatía óptica hereditaria de Leber (NOHL)

La neuropatía óptica hereditaria de Leber es una enfermedad mitocondrial de herencia materna en la que el ADN mitocondrial se encuentra mutado. Esto provoca la muerte de las RGCs debido a una producción de energía celular defectuosa por parte de estas (29). Tiene una prevalencia de entre 1/31000 y 1/54000, variando según las regiones (30).

Las RGCs obtienen energía gracias a la fosforilación oxidativa de los nutrientes que ocurre en la mitocondria y produce ATP. El mecanismo patológico que produce la muerte de las RGCs no está todavía claro. Sin embargo, como posibles mecanismos se han propuesto una disfunción en la cadena respiratoria mitocondrial y en la producción del ATP, el incremento de las especies reactivas de oxígeno (ROS) mitocondriales y la excitotoxicidad por glutamato. Es probable que haya una sinergia entre el descenso de la fosforilación oxidativa mitocondrial y el aumento de ROS, provocando la muerte de las RGCs y la degeneración del nervio óptico. Esto produce la pérdida de la visión central bilateral en los pacientes, aunque en los casos más severos se puede producir la pérdida completa del campo visual (29,30).

El objetivo principal del tratamiento es incrementar la respiración mitocondrial y reducir las ROS. Para ello, se están evaluando distintas estrategias como el uso de sustancias activas con actividades antioxidantes, la terapia génica o la medicina

regenerativa. Entre los compuestos utilizados, destacan diferentes combinaciones de vitaminas (B2, B3, B12, C, E y ácido fólico), ubiquinona y otros suplementos (ácido α-lipoico, carnitina, creatina, L-arginina o glutation). Con respecto a la terapia génica, se han realizado ensayos clínicos con resultados promotedores. Al tratarse de una enfermedad genética, la ausencia o la mutación de un gen produce la ausencia de una proteína. Por ello, la terapia genética permitiría la producción de la proteína funcional debido a la liberación en la célula diana, en este caso las RGCs, de una copia del gen que no incluye esa mutación. La medicina regenerativa también es muy prometedora, pero se encuentra en fases iniciales de desarrollo. Asimismo, se está desarrollando la terapia de reemplazamiento mitocondrial, la cual está siendo intensamente debatida por la comunidad científica debido a las cuestiones legales y éticas que la alteración de genes de la línea germinal conlleva (29,30).

3. Vías de administración de sustancias activas para el tratamiento de las patologías que afectan al segmento posterior.

Una de las principales claves del tratamiento de las patologías crónicas oftálmicas es mantener las concentraciones terapéuticas de los principios activos en el lugar de acción y reducir la frecuencia de las administraciones. Sin embargo, la administración de principios activos por vía ocular siempre ha sido un reto debido a la presencia de barreras anatómicas y fisiológicas que sirven como protección contra la entrada se sustancias químicas tóxicas (Figura 6) (31).

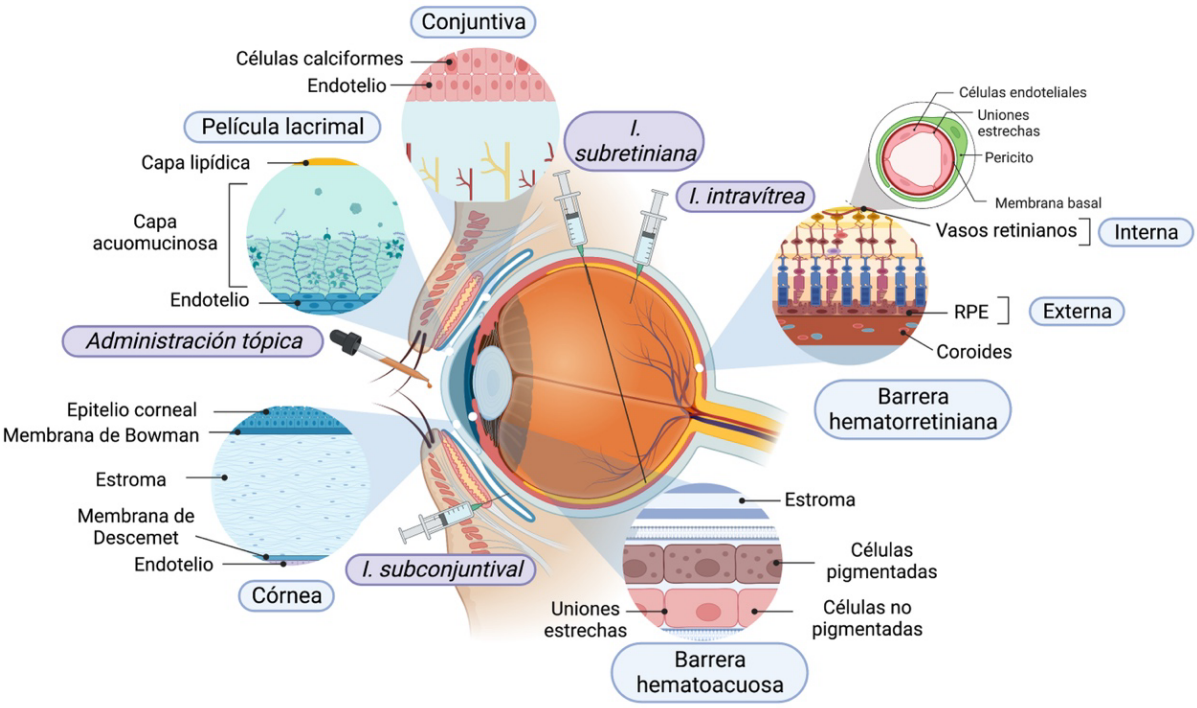

Figura 6. Principales barreras anatómicas y fisiológicas oculares en el paso de sustancias junto con algunas de las principales rutas de administración de fármacos por vía ocular. Imagen creada con BioRender.com

En el **segmento anterior** nos encontramos:

Los párpados y la película lacrimal. Los párpados son una barrera mecánica para la penetración de patógenos, cuerpos extraños y otras agresiones externas. El parpadeo reflejo es el principal factor que interviene en la eliminación de las gotas instiladas en la superficie ocular. Asimismo, gracias a su composición, la película lacrimal evita la adhesión y favorece la eliminación de patógenos. De acuerdo con estudios recientes, la

película lacrimal está compuesta de una capa acuo-mucinosa, en la que existe un gradiente de concentración de mucinas, recubierta por una capa lipídica. Esto hace que sea un fluido ligeramente viscoso con una estructura muy compleja (32). Además de lo anteriormente descrito, tras la instilación de cualquier producto en la superficie ocular se produce un lagrimeo reflejo que también contribuye a la eliminación rápida de los compuestos instilados por el conducto nasolacrimal (33).

La córnea es una capa transparente que está formada, a su vez, por distintas capas tal y como queda recogido en el apartado 1 (Anatomofisiología ocular). El epitelio corneal es la estructura más externa, tiene carácter lipófilo y contribuye en primera instancia a la resistencia del paso de moléculas hidrofílicas a través de la córnea. Las células del epitelio corneal se encuentran fuertemente unidas mediante uniones intercelulares muy estrechas, que también limitan la entrada de moléculas polares por la ruta paracelular (34).

La conjuntiva es una membrana mucosa que está dividida en varias capas. El epitelio conjuntival, al igual que el de la córnea, sirve de barrera para el paso de sustancias debido a las uniones muy estrechas que poseen sus células, impidiendo el paso de compuestos hidrófilos (34). Es importante tener en cuenta que el epitelio corneal y conjuntival son ligeramente diferentes, y que la conjuntiva es más permeable y menos restrictiva que la córnea debido, entre otras cosas, a que el espacio paracelular es superior en la conjuntiva que en la córnea (35). Además, en el epitelio conjuntival también se expresan bombas de eflujo o expulsoras que limitan la absorción de los compuestos lipófilos (34).

La barrera hematoacuosa está formada por el epitelio no pigmentado del epitelio del cuerpo ciliar y el endotelio de los vasos sanguíneos del iris. Además de formar una barrera física, también posee transportadores y bombas de flujo por lo que reducen la biodisponibilidad de los compuestos, además de participar en la eliminación activa de estos del humor acuoso (32).

En el **segmento posterior** nos encontramos con:

La barrera hematorretiniana que protege a la retina y al vítreo de la entrada de sustancias tóxicas y mantiene la homeostasis (36). Se divide a su vez en barrera

hematorretiniana interna y externa. La interna está formada por los capilares retinianos, en concreto, son las uniones estrechas entre las células endoteliales retinianas las que restringen la difusión por permeabilidad de las sustancias. La barrera hematorretiniana externa está formada por las uniones estrechas de las RPE, que forman una única capa que descansa sobre la membrana de Bruch, separando la retina neural de los capilares de la coroides y, por tanto, tiene un papel fundamental en la regulación del paso de los nutrientes de la sangre a los fotorreceptores y la eliminación de sustancias de desecho (37).

La coroides es un tejido vascular con mayor flujo por lo que produce una considerable pérdida de los principios activos (36).

3.1. Administración tópica ocular

La administración de principios activos por vía tópica ocular es una de las menos invasivas y más cómodas para para el paciente. Sin embargo, presenta algunas desventajas como son la limitada biodisponibilidad (<5%) debido a las barreras físicas y bioquímicas que protegen al ojo que ya han sido mencionadas anteriormente (película lacrimal, córnea, drenaje lacrimal, parpadeo reflejo), la circulación de humor acuoso dentro del ojo y el limitado volumen que puede ser administrado en el *cul-de-sac*.

La gran mayoría de los tratamientos administrados por vía tópica ocular son administrados por los propios pacientes. Y la administración tópica es el principal tratamiento para las patologías del segmento anterior del ojo (36). Sin embargo, cuando se trata de enfermedades crónicas, el tratamiento conlleva varias administraciones al día y va asociado a efectos no deseados en la superficie ocular (asociados al propio fármaco o a algunos excipientes, como los conservantes), que conducen generalmente a la baja adherencia al tratamiento por parte de los pacientes.

3.2. Administración por vías que impliquen efecto sistémico

La vía oral ha sido estudiada como una posible vía no invasiva y preferida por los pacientes para el tratamiento de las patologías crónicas oftálmicas frente a la vía inyectable. Sin embargo, esta vía requiere de altas dosis de los principios activos para tener una eficacia terapéutica a nivel ocular, produciendo efectos adversos sistémicos. Por ello, la vía oral está destinada solo a unos pocos medicamentos como puede ser

analgésicos, antibióticos o antineoplásicos. Además, para poder ser administrados por vía oral, estos fármacos han de presentar una alta biodisponibilidad oral y ser capaces de atravesar las barreras hematorretiniana y hematoacuosa, muy limitantes al paso de sustancias al interior del ojo (38).

La administración por vía parenteral sistémica también se enfrenta a las barreras hematoacuosa y hematorretiniana como principales obstáculos. El paso de los principios activos a la coroides es relativamente fácil debido a su elevada vascularización, sin embargo, no pueden pasar de esta capa a la retina debido al RPE, que forma parte de la barrera hematorretiniana (38).

Tampoco hay que olvidar que frecuentemente la población a tratar la componen personas de edad avanzada que son más susceptibles de presentar efectos adversos, debido, entre otros factores, a que la excreción de fármacos a través de la orina y la capacidad del hígado para metabolizar los fármacos es menor. Por lo que a pesar de necesitarse menos dosis de fármaco la toxicidad sistémica puede presentar algún problema. Además, es muy probable que se trate de pacientes polimedicados, pudiéndose producir interacciones entre los distintos principios activos (36).

3.3. Administración intraocular

La administración intraocular permite la administración de fármacos en el interior del globo ocular. Esta vía de administración engloba la administración intracameral, intravítrea y subretiniana.

La administración intracameral se realiza por inyección directa del principio activo en la cámara anterior del ojo. Esta vía de administración se utiliza frecuentemente para administrar antibióticos en el tratamiento de las infecciones de ojo o endoftalmitis tras la cirugía de cataratas. A pesar de que el tratamiento de primera elección para reducir la PIO en glaucoma emplea formulaciones administradas por vía tópica, las barreras comentadas anteriormente han llevado a investigar la administración intracameral para mejorar los resultados de los pacientes (39).

En la inyección intravítrea la administración del principio activo se realiza directamente en el segmento posterior del ojo, concretamente en el humor vítreo, por lo que resulta de interés en la liberación de fármacos para el tratamiento de patologías

retinianas, al permitir la administración de fármacos en las proximidades de las RGCs, los fotorreceptores y la cabeza del nervio óptico (39). En la actualidad, la administración de fármacos con actividad anti-VEGF (36) por esta vía está muy extendida en la clínica.

Tras la administración del compuesto, su eliminación se puede realizar por la ruta anterior o posterior. La ruta anterior puede ser utilizada por todos los compuestos, que difunden a través del vítreo hacia la cámara posterior para ser eliminados a través del drenaje del humor acuoso. La eliminación posterior se produce por difusión pasiva o transporte activo a través de las barreras hemato-oculares hacia la sangre. Es por ello, que las moléculas de alto peso molecular o solubles en agua, que tienen dificultado su paso a través de estas barreras, poseen un menor aclaramiento, lo que permite que su tiempo de semivida en el vítreo sea más prolongado (33).

Sin embargo, la administración intravítrea de fármacos no está exenta de riesgos, como el desarrollo de cataratas, infecciones o desprendimiento de retina, entre otros, por lo que las tendencias actuales se enfocan en prologar el efecto de las terapias para reducir la frecuencia de las administraciones (36).

La zona de inyección en la vía subretiniana es el espacio subretiniano, que es aquel que se encuentra entre las células del RPE y los fotorreceptores. Por lo que, con esta vía, las moléculas están en contacto directo con las membranas plasmáticas de los fotorreceptores y las células del RPE. Su uso está siendo estudiado para la terapia génica y celular para enfermedades degenerativas como DMAE o RP, entre otras. Sin embargo, esta vía también puede presentar complicaciones como el desprendimiento de retina o hemorragia en el vítreo (40).

3.4. Administración periocular

Esta vía de administración permite la liberación de los principios activos en el área que rodea inmediatamente al ojo, siendo una ruta más eficiente para el tratamiento de la parte más externa de la retina. Con este tipo de administración existe menos riesgo de que se produzcan complicaciones asociadas a las inyecciones intravítreas. En función de la zona en la que se produce la inyección ésta puede dividirse en: subconjuntival, retrobulbar, peribulbar, sub-tenoniana y juxtascleral posterior (41).

4. Tratamientos farmacológicos actuales de las patologías neurodegenerativas del segmento posterior del ojo.

Como se ha comentado anteriormente, las patologías neurodegenerativas se caracterizan por tener una etiología multifactorial, por lo que son varios los mecanismos los causantes de las mismas.

4.1. Agentes hipotensores

En el glaucoma, la PIO elevada es el principal factor de riesgo para su desarrollo y progresión, y el único que puede ser tratado mediante el empleo de agentes hipotensores por vía tópica, dada su comodidad de administración. Estos agentes se clasifican en 5 grupos en función de su mecanismo de acción: agonistas α-adrenérgicos, antagonistas β-adrenérgicos, agonistas colinérgicos, inhibidores de la anhidrasa carbónica y análogos de prostaglandinas (42).

- Agonistas adrenérgicos α-2

Los principales agonistas α-adrenérgicos son la brimonidina y la apraclonidina. Estos disminuyen la PIO mediante dos mecanismos:

- La disminución de la producción de humor acuoso en los cuerpos ciliares debido a la activación de los receptores presinápticos α-2 que produce un descenso en la liberación de las catecolaminas y un descenso en el AMPc. También se ha visto que pueden activar nominalmente los receptores α-1 que producen una vasoconstricción en los cuerpos ciliares y, por tanto, un descenso también en la producción (43).
- Modulan la expresión y actividad enzimática de metaloproteinasas e inhibidores de metaloproteinasas tisulares. Esto produce un incremento en la degradación de la matriz extracelular y, en consecuencia, una disminución de la resistencia del drenaje del humor acuoso por vía uveoescleral (43).

Han varias formulaciones comercializadas de brimonidina, la más conocida es Alphagan™ y también existe en combinación con timolol, Combigan ™, y con brinzolamida, Simbrinza ™ (43). La reducción de PIO que produce la brimonidina

instalada dos veces al día en concentraciones entre el 0,2 y el 0,1% se sitúo entre un 20-25% aproximadamente (44).

- Antagonistas β-adrenérgicos o bloqueantes β-adrenérgicos

Son los más usados en el tratamiento del glaucoma. Estos agentes producen la disminución del humor acuoso a nivel de los procesos ciliares. Se dividen en no selectivos (bloquean los receptores β1 y β2) y selectivos, que actúan en los receptores β1 (también son llamados bloqueantes β-adrenérgicos cardioselectivos). Son relativamente bien tolerados, sin embargo, los β-bloqueantes no selectivos pueden producir efectos adversos como broncoespasmo, bloqueo cardíaco o bradicardia. Por lo general se administran entre 1 y 2 veces al día y producen un descenso del 20-25% de la PIO. El maleato de timolol es uno de estos antagonistas más utilizado (42,45).

- Agonistas colinérgicos

Producen la liberación de acetilcolina ya sea por la estimulación de los receptores nicotínicos o muscarínicos o por la inhibición de la acetilcolinesterasa. Esto produce un aumento en el drenaje del humor acuoso debido a la contracción de la musculatura lisa de los cuerpos ciliares y a una apertura de la malla trabecular. Dentro de este grupo, la pilocarpina es el que más se ha utilizado y ha demostrado reducir la PIO en un 20-25% (42,45).

- Inhibidores de la anhidrasa carbónica

La anhidrasa carbónica es una enzima que cataliza la hidratación del monóxido de carbono, formando bicarbonato (HCO_3) y protones. Los inhibidores de esta enzima suprimen su actividad. Hay diferentes isozimas en los humanos, pero la inhibición de la isozima presente en los cuerpos ciliares disminuye la secreción de bicarbonato en la cámara posterior por las células epiteliales ciliares, disminuyendo la producción del humor acuoso. Actualmente los más usados son la dorzolamida y la brinzolamida (46).

- Análogos de prostaglandinas

Los análogos de prostaglandinas disminuyen la PIO mediante la disminución de la resistencia intrínseca del drenaje del humor acuoso por la vía uveoescleral. Puede ser debido a los efectos que tienen estos compuestos en los cuerpos ciliares, remodelando

la matriz extracelular y mejorando el drenaje del humor acuoso por esta vía. Debido a su eficacia, tolerancia y que solo requiere de una administración al día, son usados como tratamiento de primera línea para el glaucoma de ángulo abierto e hipertensión ocular. Han mostrado un descenso de la PIO de entre un 20 y un 35% y presentan pocos efectos adversos sistémicos, siendo el dolor de cabeza el más frecuente. Los análogos de prostaglandinas incluyen al bimatoprost, latanoprost, tafluprost y travoprost (42).

- Tratamientos aprobados recientemente

- Inhibidores de la Rho quinasa. Las rho quinasas son unas proteínas serina/treonina quinasas involucradas en la regulación y modulación de la forma y del tamaño celular por medio del citoesqueleto, además de la proliferación, adhesión y contracción del músculo liso (47). Al bloquear la vía de las rho quinasas con estos agentes, se producen cambios en el citoesqueleto de la malla trabecular y el canal de Schlemm, que conduce a una modificación de la morfología celular en la malla trabecular y cambios en la permeabilidad de las células endoteliales del canal de Schlemm. Tiene como consecuencia final un incremento en el drenaje del humor acuoso por esta vía. En el caso de netarsudil también disminuiría la producción del humor acuoso y la presión venosa epiescleral. Otro compuesto perteneciente a este grupo es el ripasudil (42,48).
- Prostaglandinas donadoras de óxido nítrico (NO). En este grupo se encuentra Latanoprosteno bunod, un análogo F2α prostaglandinas donadora de NO, por lo que disminuye la PIO por dos mecanismos: aumentando el drenaje del humor acuoso por vía uveoescleral (mediado por latanoprost) y trabecular (mediado por NO). El NO interviene en la relajación de la musculatura lisa en los tejidos oculares (42,49).

Hay que destacar que se han desarrollado combinaciones fijas de los fármacos anteriormente mencionados para facilitar la administración de los mismos, reduciendo la carga de la medicación, la complejidad de su administración, la falta de adherencia por parte de los pacientes, así como la exposición a los conservantes, cuya exposición crónica está asociada a alteraciones en la superficie ocular. En este último punto hay que mencionar que el cloruro de benzalconio (BAK) es el conservante más usado en colirios y ha mostrado tener efectos adversos en la superficie ocular, por lo que su

reducción o sustitución por otras alternativas supone un gran avance (42). Además, para aumentar el cumplimiento de los pacientes también se han desarrollado sistemas de liberación controlada de hipotensores oculares inyectables, encontrándose por el momento únicamente aprobado por la FDA y comercializado, un implante intracameral de Bimatoprost SR (DURYSTA™). Existen otros sistemas de este tipo en ensayos clínicos como son Durasert (implante subconjuntival de latanoprost), un implante de travoprost intracameral y iDose® y ENV515, ambos también de travoprost, el primero se coloca en la malla trabecular y el segundo en la cámara anterior (42). Estos dos últimos recientemente han terminado ensayos clínicos de fase 3 (NCT03519386) y 2 (NCT02371746), respectivamente. Se espera que iDose® sea aprobado por la FDA en 2023 (50).

4.2. Antiangiogénicos

El importante papel que tiene el VEGF en la angiogénesis tanto en la DMAE como RD, ha conducido al desarrollo de tratamientos que bloqueen esta molécula. Los anti-VEGF son normalmente administrados por vía intravítrea. Entre ellos, actualmente se emplean tanto para DMAE como para RD: Pegaptinib (Macugen®), ranibizumab (Lucentis®), bevacizumab (Avastin®) y afliberept (EYLEA®). Su uso ha supuesto una revolución en el tratamiento de estas patologías, sin embargo, presentan limitaciones y efectos adversos ya que su corto tiempo de semivida requiere inyecciones mensuales o bimensuales para asegurar su eficacia. Debido al aumento del número de inyecciones, la incidencia de endoftalmitis puede aumentar (26,51).

4.3. Antiinflamatorios

La inyección intravítrea de corticosteroides se ha convertido en un tratamiento muy importante en el edema macular y en los casos en los que no se produce respuesta a la terapia anti-VEGF. Debido a su gran potencia antiinflamatoria, los corticosteroides actúan en varios de los mediadores envueltos en la patogénesis del edema macular como son el VEGF, TNF-α, quimiocinas o leucoestasis. Actualmente, se utilizan para el tratamiento del edema macular la triamcinolona como medicamento off-label, un implante intravítreo de dexametasona (Ozurdex®) y un implante intravítreo de acetónido de fluocinolona (Iluvien®), ambos aprobados por la FDA (26).

En el caso de la DMAE, la inflamación también está involucrada en el progreso de la enfermedad. Tanto la dexametasona como el acetónido de triamcinolona han sido usados para esta patología. La administración oral de espironolactona ha demostrado efectos beneficiosos en la neovascularización coroidal (52).

En cuanto a los AINES (antiinflamatorios no esteroides), estos inhiben la síntesis de prostaglandinas inactivando las ciclooxigenasas. En el tratamiento de la DMAE, se han usado de forma tópica la aspirina y el nepafenaco y a nivel intravítreo en un modelo animal se ha visto que el diclofenaco y el ketorolaco presentan efectos beneficiosos (52).

5. Potenciales estrategias neuroprotectoras para el desarrollo de nuevos tratamientos contra el glaucoma.

Como se ha comentado anteriormente, el glaucoma es una enfermedad crónica neurodegenerativa progresiva. Por lo que además de los tratamientos anteriormente mencionados, enfocados prácticamente en su totalidad en descender la PIO, otra estrategia que sería interesante es la neuroprotección. La neuroprotección busca incrementar la supervivencia de las neuronas preservando su estructura y función, retrasando o evitando, en el caso del ojo, la pérdida de la visión. Una terapia exitosa de este tipo podría proporcionar meses o incluso años de visión útil que permitiría al paciente mantener su independencia y calidad de vida (53).

Existen varias estrategias, detallándose a continuación las más importantes (Figura 7).

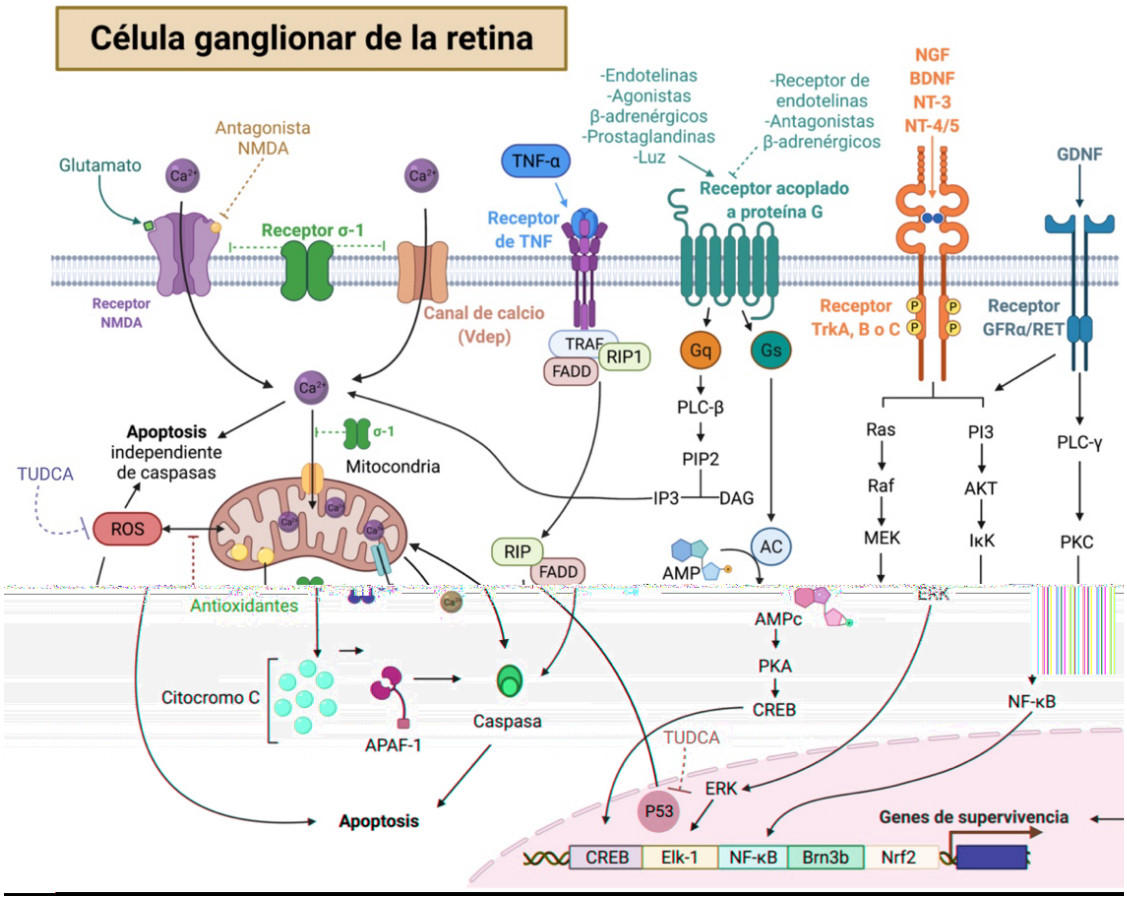

Figura 7. Principales estrategias moleculares neuroprotectoras en el glaucoma. Imagen extraída y adaptada de García-Herranz, D (2022). Microesferas biodegradables en el desarrollo de modelos animales de glaucoma y como plataformas híbridas neuroprotectoras. [Tesis doctoral] Universidad Complutense de Madrid. Imagen creada con Biorender.com.

5.1. Activación o bloqueo de receptores

Receptores de glutamato.

Se dividen en ionotrópicos (canales iónicos asociados a un ligando) y metabotrópicos (asociados a un segundo mensajero). Los receptores ionotrópicos al activarse con el glutamato producen un influjo de cationes extracelulares, como el calcio (Ca^{2+}), al interior de la célula y activan actividades neurofisiológicas importantes. Sin embargo, cuando hay una gran cantidad de glutamato, se sobreestimulan estos receptores, entrando un exceso de Ca^{2+} y causando una desregulación celular y, finalmente, la muerte apoptótica (excitotoxicidad por glutamato) (54,55).

El receptor de NMDA (N-metil-D-aspartato) es un receptor ionotrópico y ha sido evaluado como posible diana neuroprotectora. El glutamato utiliza este tipo de receptores, sin embargo, altos niveles de este neurotransmisor están asociados a excitotoxicidad y, por tanto, al desarrollo de enfermedades neurodegenerativas. Un antagonista de este neurotransmisor, como es por ejemplo la memantina, podría ser interesante para el tratamiento del glaucoma (54). Desafortunadamente, los ensayos clínicos no han mostrado la capacidad de la memantina para detener la progresión del glaucoma, aunque esta molécula sí que resulta beneficiosa en otras patologías neurodegenerativas como son el Alzheimer y el Parkinson (56).

También existen en este grupo, los receptores de AMPA (ácido α-amino-3-hidroxi-5-metil-4-isoxazolapropiónico) que son receptores ionotrópicos de glutamato. Se ha visto que están implicados en la neurodegeneración y que los cambios que se producen en este tipo de receptores en condiciones de enfermedad pueden incrementar la susceptibilidad de las neuronas a la excitotoxicidad. Sin embargo, se necesitan más estudios acerca de estos receptores (54,57,58).

Receptores sigma (σ-1-r)

En la retina, se ha visto una mayor expresión de estos receptores en la capa de RGC. Se sugiere que su mecanismo es la interacción con canales de Ca^{2+} para regular las concentraciones intracelulares neuronales de Ca^{2+}. Cuando las RGCs están en condiciones de excitotoxicidad o isquemia, estos receptores confieren protección a las células. También regulan la función mitocondrial, ya que un exceso de Ca^{2+} en este

orgánulo produce apoptosis por la generación de ROS. De hecho, se ha visto que el agonista (+)-pentazocina previene la muerte de las RGCs. Estos resultados son muy prometedores y, recientemente, se han realizado algunos estudios en modelos animales de glaucoma sobre el papel de estos receptores y de este agonista, aunque se necesitan más para explicar completamente los efectos neuroprotectores de esta estrategia (54,59,60).

Endotelinas

Las endotelinas son péptidos vasoconstrictores. Existen 3 isoformas y se ha visto que la 1 (ET-1) está aumentada en el humor acuoso de pacientes con glaucoma de ángulo abierto y en modelos animales de glaucoma. La administración de dosis bajas de este compuesto produce la pérdida de RGCs pero no produce ningún efecto vascular en el nervio óptico, demostrando su acción directa en las RGCs. Los estudios sugieren que los antagonistas de endotelinas podrían ser un tratamiento potencial para el glaucoma (54,61,62).

Factor de necrosis tumoral alfa

Existen evidencias que apoyan el papel del TFN-α como un mediador en la neurodegeneración en el glaucoma. Esto podría deberse a diversos mecanismos. Los ojos glaucomatosos presentan niveles aumentados de esta citoquina. Esta se une a sus receptores y produce la muerte de las RGCs y los axones del nervio óptico. También, puede producir la muerte de las RGCs mediante la activación de receptores de caspasa, disfunción mitocondrial o estrés oxidativo. Además, también se ha relacionado que este factor pueda promover la liberación de ET-1. De hecho, la administración de etanercept, un antagonista de TNF-α, inhibe la respuesta inflamatoria de la microglía y previene la degeneración axonal y la pérdida de las RGCs, postulando a estos antagonistas como una posible estrategia neuroprotectora (54,63,64).

5.2. Sustancias antioxidantes

El estrés oxidativo está involucrado en la muerte de las RGCs debido a una generación de ROS que excede las capacidades antioxidantes de las células. Por ello, el tratamiento con moléculas antioxidantes, capaces de captar los radicales libres, podría ser una buena estrategia (65).

Se puede recurrir a la administración directa de moléculas antioxidantes que son capaces de neutralizar las ROS. Hay varios estudios tanto en animales como clínicos en los que se administran vitamina C, vitamina E, luteína, coenzima Q10, flavonoides o ácido lipoico, entre otros.

La administración de vitamina B3, aunque no disminuye la PIO, se ha visto que previene la muerte de las RGCs, la pérdida de axones, el daño mitocondrial y el fallo en el transporte axonal en ratones. Se necesitan más estudios sobre los efectos a largo plazo de la suplementación con esta vitamina (54,66).

En un metaanálisis también se han evaluado otras vitaminas como es la vitamina A, relacionando una alta ingesta de esta con una baja prevalencia de glaucoma. En el caso de las vitaminas C, D y E, los resultados son controvertidos y no se pueden relacionar con una baja prevalencia de esta patología. Sin embargo, se necesitan más estudios para entender el mecanismo biológico de estas vitaminas y su papel en la fisiopatología del glaucoma (67).

Los flavonoides son unos compuestos ubicuos en la naturaleza, entre ellos se encuentran los extractos de *Ginkgo biloba* y *Erigeron Breviscapus Hand Mazz*. Los flavonoides han mostrado tener efectos antiinflamatorios y neuroprotectores, pudiendo reducir el estrés oxidativo, además de mejorar la circulación sanguínea. Por estos efectos, su papel en el tratamiento del glaucoma está siendo evaluado con resultados favorables en el campo visual. Son necesarios más estudios sobre el mecanismo molecular en las RGCs, la administración directa de estos compuestos a nivel ocular en lugar de por vía oral, así como estudios clínicos que evalúen su eficacia y tolerancia a largo plazo debido a la naturaleza de esta patología (68).

La Coenzima Q10 es un antioxidante a nivel mitocondrial con propiedades neuroprotectoras (21). Ha mostrado proteger las RGCs de la apoptosis inducida por glutamato en condiciones experimentales de elevación de la PIO inducida por isquemia (69). También se ha evaluado su combinación con vitamina E, mostrando efectos beneficiosos en pacientes con glaucoma de ángulo abierto. Estos efectos se reflejaron en una mejora de las respuestas visuales además de en la función retiniana (70).

Además, no hay que dejar de mencionar que en el propio cuerpo existen mecanismos de defensa contra el estrés oxidativo como son las enzimas antioxidantes, entre las que se encuentran la superóxido dismutasa (SOD) y las catalasas. Las mutaciones en estas enzimas modifican su actividad y desequilibrarían las condiciones de producción y eliminación de ROS y, por tanto, conllevan a condiciones de estrés oxidativo. La deficiencia en SOD1 en animales ha mostrado una pérdida de RGCs, poniendo de manifiesto el papel protector de dicha enzima (54,71,72).

5.3. Factores neurotróficos

La secreción de factores neurotróficos por el sistema nervioso central y periférico produce la diferenciación, desarrollo y supervivencia de las neuronas, entre ellas, las RGCs. Son compuestos que pueden ser secretados por el sistema nervioso a nivel sistémico y por la retina a nivel local. De entre todos ellos, los más relevantes en la patología del glaucoma son los que pertenecen a las familias del factor de crecimiento nervioso y la glicoproteína GP130 (73). Se ha visto que su carencia o ausencia está involucrada en la fisiopatología del glaucoma (74).

Factor neurotrófico ciliar (CNTF). Este factor y sus receptores se expresan en la retina neural, RPE y en la cabeza del nervio óptico. Pertenece a la familia de la glicoproteína GP130 (73). Inyecciones intravítreas de CNTF han mostrado un efecto beneficioso en la supervivencia de los fotorreceptores en modelos animales de retinitis pigmentosa y de degeneración retiniana (75,76). Además, se ha desarrollado un implante que ha permitido la liberación sostenida de CNTF en la retina durante 7 semanas. Dicho implante contenía células secretoras de CNTF, y posibilitó la liberación continua y del orden de nanogramos del factor neurotrófico, demostrándose que la liberación sostenida a bajas dosis tenía un efecto terapéutico mayor que una inyección en bolus de altas dosis de CNTF (77).

Factor neurotrófico derivado del cerebro (BDNF). Es producido fundamentalmente en la retina por las RGCs y astrocitos, y también en el cerebro, siendo transportado a la retina por los axones de las RGCs (73). Está involucrado en la formación adecuada de la estructura retiniana. El BDNF endógeno posee efectos neuroprotectores ya sea disminuyendo la pérdida de visión después de producirse una lesión inducida por

hipertensión o protegiendo a las células retinianas de los daños causados por la hipoxia y la privación de glucosa (78). *In vitro,* la administración de microesferas cargadas con este agente evitó la apoptosis de las células de retina (79). *In vivo*, la inyección intravítrea de BDNF se ha probado en modelos animales de glaucoma, mostrando efectos beneficiosos, pero limitados en el tiempo debido a la regulación negativa de sus receptores (TrkB) tras su administración (80,81). Para solventar este efecto, se ha desarrollado una terapia génica en la que se libera BDNF y el gen de TrkB para aumentar la supervivencia a largo plazo de RGCs en un modelo murino de daño en el nervio óptico. Este estudio ha mostrado resultados prometedores (82).

Factor derivado del epitelio pigmentario (PEDF). Es producido por las células epiteliales y posee actividades antiangiogénicas, neurotróficas y antiinflamatorias. En la retina produce la diferenciación de las células precursoras en células con fenotipos neuronales y reduce la activación de las células de Müller (activadas estas por factores estresantes relacionados con el glaucoma). Además, se ha visto que es expresado en altas concentraciones en las células de Müller (83). También ha demostrado propiedades neuroprotectoras en condiciones de degeneración retiniana, estrés oxidativo o excitotoxicidad por glutamato (84). De hecho, se ha evaluado la administración diaria de un colirio con PEDF frente a inyecciones intravítreas semanales en un modelo de aplastamiento de nervio óptico. Este estudio ha mostrado una mayor efectividad en la supervivencia de RGCs en los animales inyectados que los que recibieron el colirio diariamente (85). También existen estrategias de terapia génica con este factor (86).

Factor neurotrófico derivado de la glía (GDNF). Es una neurotrofina secretada por las células gliales que se une a sus receptores expresados en las RGCs, células de Müller y amacrinas (73). Ha mostrado retrasar la muerte de las RGCs después de sufrir axotomia y en retrasar la degeneración retiniana en un modelo de retinitis pigmentaria en ratones rd1 (87,88). Se han realizado estudios *in vivo* en los que se administraba mediante inyección intravítrea este factor encapsulado dentro de microesferas y han demostró el papel neuroprotector del GDNF, incrementando la supervivencia de las RGCs y disminuyendo la activación glial en modelos de glaucoma (89–91).

5.4. Otros agentes neuroprotectores

Agentes antiapoptóticos.

En este grupo nos encontramos el ácido ursodesoxicólico (UDCA) y su conjugado derivado de taurina, el ácido tauroursodeoxicólico (TUDCA), ambos se encuentran naturalmente en el ácido biliar de los osos. El TUDCA posee beneficios en un amplio rango de enfermedades en el riñón, en el hígado o cardiovasculares, mostrando también efectos neuroprotectores en enfermedades neurodegenerativas como el Parkinson o el Huntington (53).

El TUDCA previene la apoptosis por diferentes mecanismos: estabiliza la membrana mitocondrial, suprime la proteína pro-apoptótica P53 y disminuye las ROS. También ha mostrado efectos antiinflamatorios reduciendo la activación de las células gliales. Se sugiere que el TUDCA al escindirse libera taurina, la cual ha mostrado también efectos neuroprotectores en los fotorreceptores y en las RGCs (53).

A nivel de la retina, ha mostrado efectos neuroprotectores en modelos de enfermedad: es capaz de proteger contra la degeneración de los fotorreceptores en distintos modelos animales de degeneración de fotorreceptores y retinitis pigmentosa (92–94), preservar la función visual o disminuir la muerte celular en las células de retina en modelos de retinopatía diabética (95,96), proteger las RGCs tras la degeneración inducida por NMDA (97) o incluso en RGCs sanas, mejorando la respuesta visual de estas (98). El UDCA también ha mostrado efectos neuroprotectores en la retina, protegiendo a los fotorreceptores de la apoptosis (99). Esto hace que ambas moléculas sean buenas candidatas para el tratamiento del glaucoma.

Antiinflamatorios

Aunque se ha hablado anteriormente de los antiinflamatorios, se ha hecho desde un punto de visto del tratamiento de la inflamación que se produce en la DMAE o en el edema macular asociado a la RD. Recientemente se ha señalado la neuroinflamación como un proceso clave en el glaucoma, por ello, la modulación de esta inflamación podría ser usada como terapia para limitar el daño en el nervio óptico y la muerte de las RGCs asociadas al glaucoma (21,100). Aunque todavía no hay muchos estudios que corroboren esta neuroprotección, es cuestión de tiempo, ya que muchos autores

señalan esta estrategia como una nueva terapia para las enfermedades neurodegenerativas (21,100–102). El tratamiento de la neuroinflamación se podría abordar a través de la supresión de la actividad de las células de la glía, suprimiendo el estrés oxidativo con el uso de antioxidantes (como ya se ha mencionado anteriormente) o mediante el uso de antiinflamatorios.

El ketorolaco es un antiinflamatorio no esteroideo (AINE) inhibidor no selectivo de la ciclooxigenasa (21). En un estudio clínico se ha usado este compuesto asociado a un análogo de prostaglandinas, mostrando una mejoría en la acción hipotensora de estos análogos (103). Por su efecto antiinflamatorio ha sido usado en el edema macular diabético como adyuvante al tratamiento con un anti-VEGF mostrando una mejoría del tratamiento con el anti-VEGF (104). Otro estudio, esta vez con el AINE nepafenaco, indica el posible efecto beneficioso en el tratamiento del edema macular diabético, aunque son necesarios estudios con un número más elevado de pacientes para evaluar el papel del nepafenaco en prevenir la pérdida de visión en esta enfermedad (105).

Los corticosteroides, y entre ellos, la dexametasona y el acetónido de fluocinolona, han sido usados en el tratamiento de la inflamación ocular tanto en el edema macular diabético como otras patologías que cursan con inflamación, como ya se ha mencionado anteriormente (106). Particularmente existe un implante intravítreo comercializado cargado con dexametasona (Ozurdex®) (107). Además, se han estudiado sus efectos neuroprotectores por ejemplo en el daño isquémico. En este estudio, se mostró que la administración de dexametasona inhibía la inflamación mediada por la vía NFkB p65 y reducía la expresión de óxido nítrico sintasa inducible, ciclooxigenasa (COX2), TNF-α y de la IL-1β (108). A nivel ocular, en condiciones de hiperglucemia, la dexametasona disminuyó a niveles basales las interleucinas IL-1β, IL-6 y TNF-α, asociadas con la muerte de RGCs y cuyos niveles se encontraban aumentados en estas condiciones (109). Por ello, los corticosteroides, incluida la dexametasona, son una estrategia neuroprotectora prometedora para el glaucoma y otras enfermedades que cursen con neurodegeneración.

Agentes hipotensores.

Agentes hipotensores como la brimonidina, han mostrado tener un papel neuroprotector. La aplicación sistémica de este hipotensor produjo una prevención en la pérdida celular que se mostró independiente a su efecto en la PIO (110). Este efecto se cree que pueda ser debido a diversos mecanismos como la inhibición de la cascada apoptótica, la reducción de la excitotoxicidad por glutamato, la inhibición de la actividad glial, la inhibición de la NO sintasa o por el aumento de la expresión de BDNF (111,112).

5.5. Neuroregeneración y terapia celular

Lo que se pretende con la neuroregeneración es revertir el proceso de muerte de las RGCs mediante la regeneración de axones funcionales y la restauración o recuperación de la visión funcional. Esta estrategia de tratamiento se ha estudiado en modelos animales experimentales en los que se han administrado células madre para remplazar las RGCs y sus axones, aunque aún no ha sido posible su evaluación en humanos (113). Recientemente, se ha publicado un trabajo realizado en roedores en los que se produce la diferenciación de células madre embrionarias (hESCs) a neuronas tipo RGC, y su migración, con éxito, hacia la capa celular ganglionar, transcurrida 1 semana desde su inyección intravítrea (114).

En cuanto a la terapia celular, existe un implante que contiene en su interior células modificadas genéticamente para liberar CNTF, que ha sido comentado anteriormente. El dispositivo es implantado en el vítreo produciendo un efecto protector en los fotorreceptores en términos de reducción de muerte celular (77) y disminuyendo la progresión de la degeneración retiniana (115).

5.6. Terapia génica

Existen, al menos una veintena de estudios sobre terapia génica con propiedades neuroprotectoras en las RGCs. Algunos de ellos utilizan un vector viral que codifica para BDNF o para eritropoyetina, vectores virales que codifican genes o terapias basadas en genes de microARN. Basándonos los resultados *in vivo* e *in vitro* publicados, esta estrategia podría ser muy prometedora, aunque son necesarios muchos más estudios para llegar a la clínica (116). En cuanto a esto, se ha comercializado un vector voretigén neparvovec que contiene una copia del gen RPE65 (Luxturna®) para el tratamiento de distrofia retiniana hereditaria causada por mutaciones en dicho gen (117).

6. Nuevos sistemas de administración de fármacos para las patologías neurodegenerativas de la retina.

Como se ha comentado anteriormente, existen distintas vías para la administración de los principios activos en el segmento posterior del ojo con sus ventajas y sus inconvenientes. Sin embargo, en muchos casos hay que recurrir a la administración intravítrea directamente para alcanzar concentraciones terapéuticas eficaces y obtener así un tratamiento efectivo. Al tratarse en la mayoría de los casos de enfermedades crónicas, se requiere la inyección repetida en el globo ocular, con los inconvenientes asociados a esta vía de administración y el malestar que eso conlleva en los pacientes. Para evitar esto, se puede recurrir al uso de sistemas de liberación controlada (118) que permiten aumentar el tiempo entre administraciones, reduciendo los efectos no deseados asociados a esta vía. Actualmente, la administración de fármacos por vía intravítrea mediante inyecciones o implantes es una de las más utilizadas para el tratamiento de patologías oculares neurodegenerativas (119).

6.1. Implantes

Los implantes intravítreos evitan la necesidad de las administraciones repetidas ya que permiten la liberación de sustancias activas durante tiempos prolongados (120). Tienen un tamaño superior a 1 mm y pueden estar hechos con materiales biodegradables o no biodegradables. Para su administración, algunos necesitan cirugía y los implantes no biodegradables tienen que ser retirados del lugar de acción una vez realizado el efecto (121).

El primer implante aprobado por la FDA fue de ganciclovir (Vitrasert®) usado para el tratamiento de la retinitis por citomegalovirus. Se trata de un implante no biodegradable compuesto por acetato de etilen-vinilo recubierto con alcohol polivinílico (PVA). Tras su éxito, se desarrollaron numerosos implantes (120,122).

Durasert™ es un implante que puede liberar sustancias activas hasta 3 años y puede ser inyectado por agujas de pequeño calibre. La tecnología de este inserto fue aprobada por la FDA y dio lugar a los siguientes implantes: Retisert® (acetónido de fluocinolona, implante intravítreo no biodegradable, formado por silicona y PVA, para el tratamiento de la uveítis posterior crónica no infecciosa), Iluvien® (acetónido de fluocinolona,

implante intravítreo no biodegradable, formado por poliamida y PVA, para el tratamiento el EMD) y Vitrasert®, que se acaba de describir en el párrafo anterior (120).

También existe un implante de dexametasona, Ozurdex®, indicado para el tratamiento del edema macular por oclusión venosa retiniana, uveítis no infecciosa y EMD. Se trata de un implante biodegradable formado por PLGA (120).

Además, entre otros implantes, existen implantes biodegradables de brimonidina (Brimo DDS), de bevacizumab (ENV705) y de ranibizumab (Zordera), todos ellos se encuentran en fases preclínicas (123).

6.2. Micropartículas

Las micropartículas son sistemas farmacéuticos con un tamaño de entre 1 y 1000 µm y son capaces de encapsular y liberar principios activos durante periodos de tiempo prolongados que oscilan de semanas a meses en función del material utilizado y de las características del fármaco que contienen. Pueden estar formadas por distintos materiales, siendo las micropartículas poliméricas las que más se utilizan (121,124). Según su estructura interna, se pueden clasificar en microcápsulas, si el principio activo está en forma de reservorio rodeado de una capa continua de polímero, o microesferas, si la sustancia activa está dispersada en una matriz polimérica (Figura 8). Entre sus ventajas, se encuentran que su administración se puede llevar a cabo en forma de suspensión utilizando agujas de bajo calibre y se puede personalizar la terapia dependiendo de la cantidad de micropartículas que se inyecten (121). Como los implantes, las microesferas biodegradables son preferibles ya que desaparecen de su lugar de administración tras su degradación. Entre los distintos polímeros biodegradables, los más utilizados son el ácido poli-láctico, el ácido poli-glicólico y el PLGA, ya que estos se encuentran aprobados para su empleo en dispositivos oculares (121). Además, sus características pueden ser adaptadas para un determinado uso, ya que se puede modificar la composición y las proporciones del polímero, el grupo terminal del polímero, el peso molecular o modificar la superficie las micropartículas. Se pueden encapsular moléculas de distinta naturaleza como hidrófilas e hidrofóbicas, proteínas, péptidos, vacunas o macromoléculas biológicas. Sin embargo, uno de los principales retos de estos microsistemas es la encapsulación de proteínas y las altas

liberaciones iniciales que pueden ocurrir en los primeros estadíos tras su administración (120).

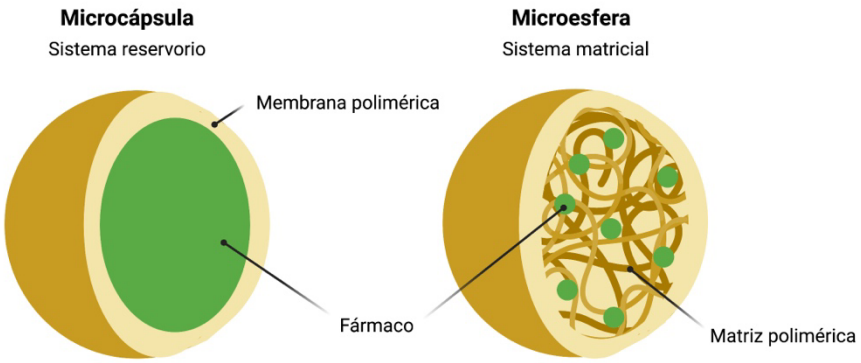

Figura 8. Estructura interna de las micropartículas. Imagen creada con BioRender.com

Existen numerosos ejemplos de formulaciones microparticulares en fase de investigación para el tratamiento de patologías oculares, siendo, además, una de las principales líneas de nuestro grupo de investigación "InnOftal: Innovación, terapia y desarrollo farmacéutico en oftalmología, UCM-920415" (90,91,125–128).

Teniendo en cuenta la multifactorialidad de las enfermedades neurodegenerativas, las microesferas presentan otra ventaja importante, ya que pueden encapsular más de un principio activo en su interior y liberarlos durante largos periodos de tiempo de una forma controlada. Esta es una de las recientes estrategias de nuestro grupo de investigación (79,129–131).

6.3. Hidrogeles

Los hidrogeles son redes tridimensionales de cadenas poliméricas capaces de retener agua. Pueden estar formados por polímeros naturales, sintéticos o semisintéticos. En los últimos años, este tipo de sistemas de liberación contralada están en auge y son muy interesantes desde el punto de vista de la liberación de los principios activos, ya que pueden ser diseñados para controlar o sostener la liberación de estos (132,133). Entre los distintos tipos de hidrogeles (Figura 9), hay que destacar los denominados hidrogeles "inteligentes" o sensibles a estímulos, llamados así porque desencadenantes externos como pueden ser el cambio en el pH, la temperatura, la luz o biomoléculas, entre otros, producen un cambio en las propiedades físicas de estos hidrogeles, pasando de un estado sol o líquido a un estado gel ante la presencia de dicho estímulo (132).

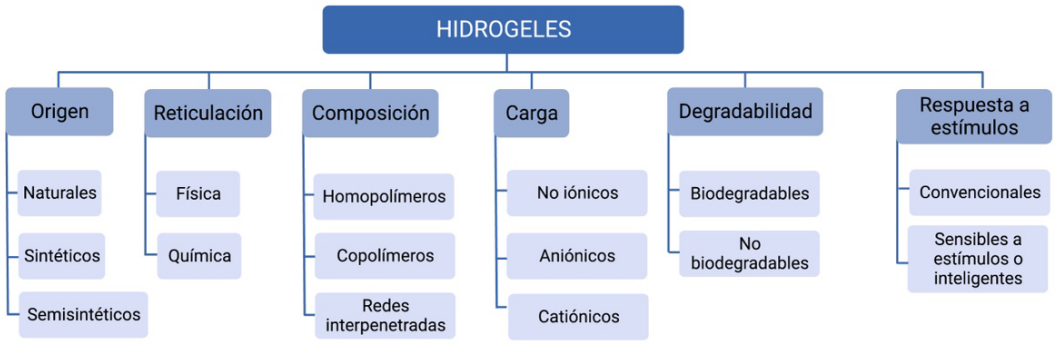

Figura 9. Clasificación de los hidrogeles, adaptada de "Ali, F., Khan, I., Chen, J., Akhtar, K., Bakhsh, E. M., & Khan, S. B. (2022). Emerging Fabrication Strategies of Hydrogels and Its Applications. Gels, 8(4), 205. MDPI AG. doi: 10.3390/gels8040205". Imagen creada con BioRender.com

Los hidrogeles reticulados químicamente producen el hidrogel debido a interacciones covalentes entre el polímero y el agente reticulante (134). Los hidrogeles formados a partir de ácido hialurónico (HA) resultan interesantes debido a su biocompatibilidad y a su biodegradabilidad. Además, sus propiedades pueden ser modificadas, por ejemplo, mediante la funcionalización de esta molécula con distintos grupos químicos y la cantidad de polímero que lo forma (135,136). Una de las características más llamativas de estos geles es su capacidad de "autocuración", haciendo que incluso una vez hayan gelificado, sean unos buenos candidatos como sistema de liberación controlada inyectable, ya que serían capaces de fluir por la aguja para su administración (137,138). El HA funcionalizado se puede unir a otros polímeros para formar hidrogeles. Un ejemplo de ello es el hidrogel formado por HA funcionalizado con dextrano tiolado, para formar un hidrogel *in situ* que fue capaz de liberar de forma controlada bevacizumab durante al menos 6 meses (139). Además, se pueden crear hidrogeles de HA funcionalizado con N-isopropilacrilamida o con gelatina funcionalizada, entre otros compuestos (135).

Entre los hidrogeles sensibles a estímulos, resultan interesantes los hidrogeles sensibles a la temperatura para la aplicación oftálmica. Estos hidrogeles están diseñados para estar en forma "sol" a temperatura ambiente y cuando esta cambia, formar el hidrogel (pasar a estado "gel"). En este sentido, por ejemplo, hay hidrogeles formados por la combinación de quitosano y gelatina, de quitosano, gelatina y glicerol o formados por bloques de copolímeros como puede ser PLGA-PEG-PLGA (134). También se han desarrollado este tipo de hidrogeles a base de poli(N-isopropilacrilamida) (PNIPAAm)

(120). Todos ellos diseñados para aplicaciones oftálmicas y presentando una liberación sostenida de los principios activos (134). De hecho, el copolímero PLGA-PEG-PLGA ha mostrado ser un candidato prometedor para su aplicación oftálmica al ser cargado con una sustancia anti-VEGF (Avastin®), mostrando ser segura su aplicación (al no mostrar toxicidad ni afectar a la función retiniana) y una liberación sostenida del principio activo (140).

6.4. Nanopartículas poliméricas

Las nanopartículas presentan un tamaño de entre 1 y 1000 nm y se pueden clasificar también, como las micropartículas, en nanocápsulas y nanoesferas, presentando las mismas características anteriormente citadas. Los polímeros usados más comunes son el ácido poliláctico y el PLGA. Son capaces de liberar progresivamente los compuestos activos que contienen, pero su elevada superficie específica las provee de una menor capacidad para controlar la cesión durante largos periodos de tiempo. Sin embargo, presentan la ventaja de que pueden ser internalizadas por las células por lo que resultan muy útiles para la terapia génica (121,141). Un ejemplo de ello es el desarrollo de nanopartículas cargadas con dexametasona para el tratamiento de la uveítis no infecciosa, demostrando su eficacia en estudios *in vivo* al reducir la inflamación ocular y proteger la función retiniana (142).

6.5. Liposomas

Los liposomas son vesículas esféricas de un tamaño de entre 10 nm y 10 µm formadas por bicapas lipídicas. Esta estructura de bicapa está rodeada de un núcleo acuoso, permitiendo la incorporación tanto de sustancias lipófilas como hidrófilas. Estas últimas pueden ser incorporadas dentro del núcleo acuoso o disueltas en el vehículo acuoso donde se dispersan las vesículas. En cambio, las sustancias lipófilas son incorporadas en la bicapa lipídica. Su aplicación en enfermedades oftálmicas ha sido muy estudiada debido a su buena tolerancia y a su capacidad de incrementar la penetración de sustancias activas tanto lipófilas como hidrófilas al ser aplicados por vía tópica. Estos sistemas pueden ser usados para incrementar el tiempo de retención de los principios activos en la superficie ocular además de producir una liberación sostenida de estos. Las dispersiones acuosas liposomales se pueden usar también como lágrimas artificiales ya que han demostrado su capacidad de restaurar la capa lipídica de la película lacrimal,

que se encuentra alterada en ciertas patologías de la superficie ocular como la enfermedad de ojo seco. Otra ventaja que presentan es su aplicación por vía tópica sobre la superficie ocular mediante colirios, por lo que no requiere el uso de técnicas invasivas (143).

6.6. Otros nanosistemas

Dendrímeros. Se trata de nanoestructuras poliméricas ramificadas con forma globular que se forman a partir de un núcleo central. Los principios activos pueden ser atrapados en su interior mediante interacciones iónicas, hidrofóbicas, puentes de hidrógeno o enlaces covalentes. Los más estudiados son los formados por poli(amidoamina) (PAMAM) (141). Entre algunos ejemplos de su utilidad para el tratamiento de patologías oculares, destaca el uso de dendrímeros cargados con acetónido de fluocinolona, que han mostrado su efectividad en reducir la neuroinflamación en un modelo de degeneración retiniana (144).

Niosomas. Su estructura es muy similar a la de los liposomas. Son vesículas de un tamaño de entre 10 nm y 1 µm, formados también por bicapas, pero en lugar de fosfolípidos, estas están formadas por surfactantes no iónicos. Presentan ventajas frente a los liposomas como son sus menores costes de producción además de su almacenaje, ya que no necesitan condiciones especiales. También poseen la característica de promover la penetración de los principios activos modificando la permeabilidad de la membrana conjuntival y la esclera (145).

6.7. Sistemas híbridos

Los sistemas que se han visto hasta ahora en ocasiones pueden combinarse constituyendo lo que se conoce como sistema híbrido. Con ello, se unirían las ventajas que poseen cada uno de los sistemas, por ejemplo, de los microsistemas en liberar los compuestos encapsulados durante largos periodos después de ser inyectados de forma intravítrea, y de los nanosistemas la protección del principio activo del ambiente externo y ser dirigido al tejido diana (146). En este sentido, existen tantas combinaciones como sistemas existen, pudiéndose combinar micro- y nanosistemas, pero también varios nanosistemas en la misma formulación, de los cuales se van a exponer unos ejemplos.

Se ha utilizado la combinación de microesferas de PLGA o de alginato en hidrogeles termorrespuesta de PLGA-PEG-PLGA. La combinación de estos dos sistemas proporciona un mayor control de la liberación rápida inicial, además de poder aportar un efecto protector de las enzimas y de la degradación celular *in vivo* de las microesferas y de agregarlas en el momento de la inyección (147–149). También en estos hidrogeles se han incorporado nanopartículas de quitosano mostrando su efectividad en el tratamiento de la retinopatía diabética (150) y liposomas, aunque este sistema fue diseñado para el tratamiento de cáncer de mama, también fue evidente el descenso de la liberación inicial en la formulación híbrida frente a la liberación del mismo principio activo desde el hidrogel (151). El control sobre la liberación inicial es importante ya que un exceso de esta liberación puede provocar un acortamiento de la duración total del efecto terapéutico del principio activo o incluso producir problemas de toxicidad, si la liberación en este corto periodo de tiempo es excesiva (152).

Recientemente, se ha desarrollado un hidrogel *in situ* formado por el entrecruzamiento de PVA y quitosano que contiene microesferas cargadas con 5-fluorouracilo como un sustituto del vítreo para la vitreoretinopatía proliferativa (153).

También existen numerosos trabajos sobre la encapsulación de nanopartículas en micropartículas. En estos, la técnica más utilizada es la encapsulación por doble emulsión acuo-oleo-acuosa ($A_1/O/A_2$) (154–156), método que se explicará en el siguiente apartado. Con esta estrategia se pretende aprovechar las ventajas de las nanopartículas, como son su fácil difusión en los tejidos e incluso su penetración en las células de dichos tejidos, y las de las microesferas, como su mayor tiempo de retención, ya que no son eliminadas rápidamente después de su administración intraocular (157). Las microesferas liberarían al medio las nanopartículas encapsuladas en su interior y estas liberarían el principio activo con el que están cargadas en las células diana (157). Sun et al. observaron que la liberación inicial de N_3-O-toluil-5-fluorouracilo (TFu) en el sistema híbrido era más baja y poseía una liberación más controlada que el sistema nanoparticular también cargado con ese compuesto (158).

7. Métodos de microencapsulación de sustancias activas para administración intravítrea

Merece la pena destacar los métodos de microencapsulación de las sustancias activas. Para la preparación de las microesferas, se pueden utilizar distintos métodos como son: electrospray, por atomización o por emulsificación. La tecnología microfluídica ha emergido recientemente como una estrategia de producción de microesferas a gran escala más controladas y uniformes (159).

El método de emulsificación (también llamado extracción-evaporación del solvente) es el que más se utiliza y es un proceso sencillo que permite controlar el tamaño de partículas hasta un cierto grado. Además, en función de las características físicas y químicas de los principios activos, se pueden elegir diferentes métodos como son la emulsión simple óleo-acuosa (O/A) o la doble emulsión de la cual hay distintos tipos: acuo-óleo-acuosa ($A_1/O/A_2$), sólido-óleo-acuosa (S/O/A) y sólido-óleo-oleosa (S/O/O) (159).

7.1. Extracción-evaporación del disolvente previa formación de una emulsión simple

7.1.1. Extracción-evaporación del disolvente a partir de una emulsión óleo-acuosa (O/A)

Este método es adecuado para la encapsulación de moléculas hidrofóbicas. Tanto el principio activo como el polímero son disueltos en un disolvente orgánico. Esta mezcla se añade a una fase acuosa que contiene un surfactante que permite formar la emulsión mediante fuerzas mecánicas. El disolvente orgánico es extraído y evaporado y esto permite que las gotículas se reduzcan en tamaño y solidifiquen. Tras la formación de las micropartículas poliméricas se procede a la recogida, lavado, separación por filtración o centrifugación y secado para obtener un polvo fino (Figura 10). A veces, para conseguir una encapsulación más alta de las moléculas, se puede recurrir a la incorporación en la fase orgánica de cosolventes solubles en agua como es el caso de la acetona o el etanol (159). Una gran limitación de este método es la encapsulación de sustancias hidrosolubles ya que pueden migrar a la fase acuosa de la emulsión y producir cristales en su superficie. Esto provocaría una liberación inicial muy rápida a la hora de

administrar estas formulaciones. Esto podría evitarse si se modifica el principio activo a un profármaco más lipófilo o utilizando una doble emulsión, como se describe a continuación. También se podría usar una emulsión óleo-oleosa (O/O), sin embargo, esta estrategia es más complicada de llevar a cabo dada la dificultad de eliminar el aceite mineral o vegetal (usado en la fase externa oleosa) de las microesferas (160).

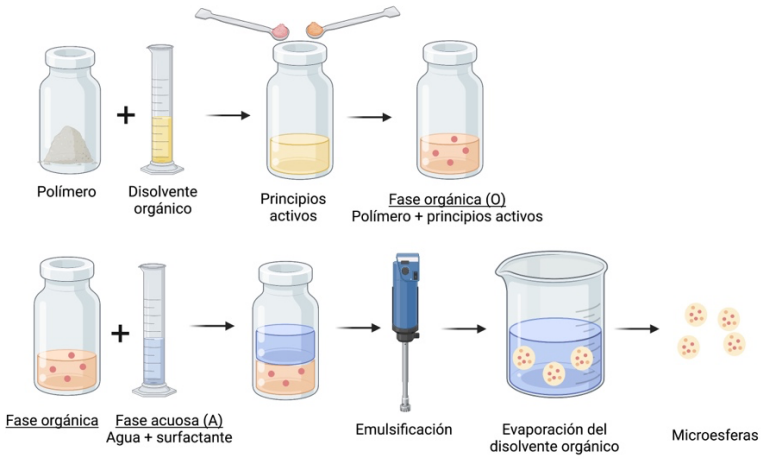

Figura 10. Representación esquemática de la elaboración de microesferas a través de la técnica de extracción-evaporación del solvente a partir de una emulsión O/A. Imagen creada con BioRender.com

7.1.2. Extracción-evaporación del disolvente a partir de una emulsión sólido-óleo-acuosa (S/O/A)

El método más común para preparar microesferas por doble emulsión es el que se acaba de mencionar ($A_1/O/A_2$), sin embargo, en cuanto respecta a la encapsulación de proteínas, este método puede presentar algunos inconvenientes como son la inactivación y agregación de proteínas debido a la adsorción de estas en la interfase óleo-acuosa que se forma cuando la proteína disuelta en la solución acuosa es emulsificada en el disolvente orgánico. Por ello, la técnica de emulsión sólido-oleo-acuosa ha ganado reconocimiento ya que permite mantener la estabilidad de la proteína durante la encapsulación. Esta sería incluida en estado sólido en la fase interna que se incorpora a la fase orgánica, formando la primera emulsión (Figura 12). Después se produciría la emulsificación en una fase acuosa que contiene el agente emulfisicante (160).

Este método fue utilizado para el desarrollo y optimización de las microesferas desarrolladas en los capítulos II y IV de la presente Tesis Doctoral.

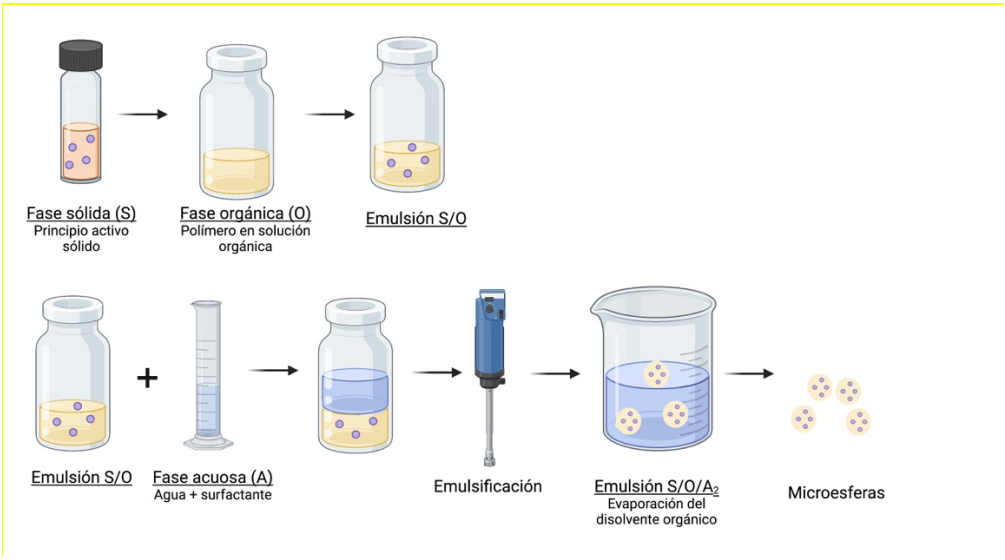

Figura 11. Representación esquemática de la elaboración de microesferas a través de la técnica de extracción-evaporación del solvente a partir de una doble emulsión S/O/A. Imagen creada con BioRender.com

7.1.3. Extracción-evaporación del disolvente a partir de una emulsión sólido-óleo-oleosa (S/O/O)

Este método es similar al anterior, se incorpora la proteína en estado sólido a una solución orgánica polimérica para formar la primera emulsión. A continuación, se emulsiona con una fase externa orgánica. Aunque confiere una gran ventaja ya que la ausencia de una fase externa acuosa permite mayores eficacias de encapsulación, existe el inconveniente de utilizar grandes volúmenes de solventes orgánicos y oleosos lo que pueden casuar problemas de toxicidad y contaminación ambiental (160,162). Entre los disolventes utilizados en la fase orgánica externa se pueden encontrar el aceite de semillas de algodón y los heptanos, entre otros.

7.2. Extracción-evaporación del disolvente previa formación de una doble emulsión acuo-óleo-acuosa ($A_1/O/A_2$).

Es una estrategia utilizada para encapsular sustancias hidrosolubles, aunque se pueden incorporar tanto sustancias hidrosolubles como liposolubles. El principio activo es disuelto en la fase acuosa interna (A_1) y se emulsiona con la disolución de polímero en la fase orgánica (y principio activo liposoluble en el caso de que lo incorpore), para formar así la primera emulsión A_1/O. A continuación, se realiza el mismo proceso que en la emulsión simple, se añade a una fase acuosa (en este caso es la A_2) que contiene el surfactante. Finalmente, se emulsifica y se forma la emulsión $A_1/O/A_2$. Una vez el

disolvente orgánico se haya eliminado, las partículas resultantes serán lavadas, filtradas o centrifugadas para su separación y secadas (Figura 11). Las microesferas preparadas a partir de este método pueden presentar una encapsulación baja del principio activo y una rápida liberación inicial debido a la alta solubilidad en agua que presenta la sustancia activa, produciendo una difusión de esta a la fase externa acuosa antes de la solidificación del polímero (159,161). La estabilidad de las gotículas de la fase interna en la primera emulsión es importante para la estabilidad final, pudiendo mejorarse cambiando las proporciones en volumen de las dos fases o añadiendo estabilizantes a la fase acuosa interna.

Este método de encapsulación de sustancias activas fue utilizado para la encapsulación de los principios activos del capítulo I de la presente Tesis Doctoral.

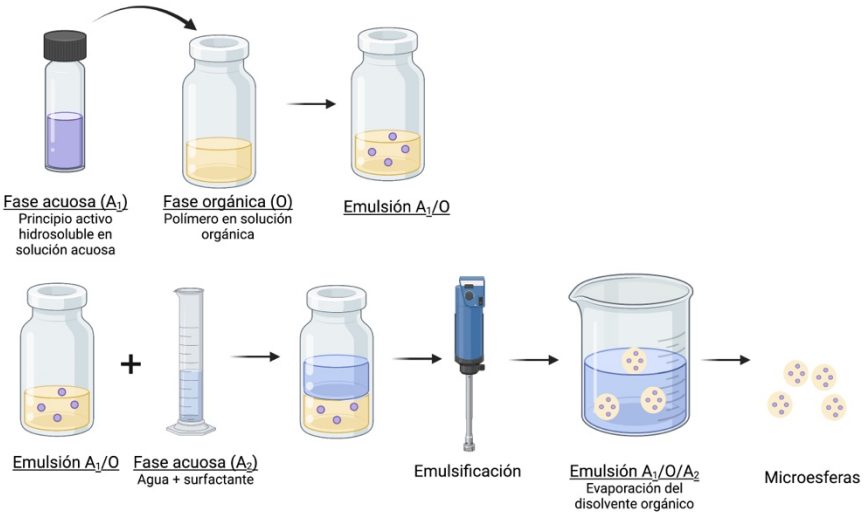

Figura 12. Representación esquemática de la elaboración de microesferas a través de la técnica de extracción-evaporación del solvente a partir de una doble emulsión A_1/O/A_2. Imagen creada con BioRender.com

8. Modelos de glaucoma en roedores para la evaluación y estudio de tratamientos.

Algunos de los mecanismos fisiopatológicos que desencadenan la patología de glaucoma son todavía un misterio a pesar de la gran prevalencia de la enfermedad (155). Por ello, el desarrollo de modelos animales de glaucoma es de gran importancia ya que pueden aportar información muy útil tanto en su patogénesis como las potenciales dianas terapéuticas en las que se puede actuar (163). Los estudios en humanos son muy complejos, debido a la dificultad en acceder a ojos de donantes humanos con historial de glaucoma claramente definido, a la conservación de estos y a que, aun superando estas dificultades, la mayoría de los ojos de donantes se encuentran en estadios avanzados de la enfermedad. Por ello, el desarrollo de modelos animales que simulen las condiciones del glaucoma en humanos es sumamente importante (164).

Se han desarrollado modelos en primates no humanos ya que su estructura anatómica es la más cercana a la del ojo humano, sin embargo, el alto coste de mantenimiento hace que se busquen otras alternativas. En esta dirección, el uso de animales de origen murino ha sufrido un auge. Esto se debe a sus bajos costes y, en consecuencia, a la posibilidad de aumentar el número de animales en los estudios y así obtener datos estadísticamente más significativos. Además, su estructura anatómica posee similitudes con la humana. Otra ventaja de estos animales es la facilidad de modificación genética. Sin embargo, un problema de estos modelos animales es la oclusión artificial de la salida del humor acuoso que produce una elevación aguda de la PIO, porque a pesar de que produce un daño en el nervio óptico y la retina, no simula las condiciones del glaucoma humano donde se produce una neurodegeneración progresiva. Por ello, se han desarrollado varios modelos animales de glaucoma mediante distintos mecanismos para estudiar las distintas rutas patológicas que lo pueden producir, clasificándose principalmente en modelos dependientes de la PIO o independientes de la PIO (164).

No hay que olvidar que para que un modelo animal sea ideal tiene que cumplir las siguientes características (165,166):

- Fácil de inducir y ser reproducible con los mínimos efectos secundarios posibles.

- Ser predecible de principio a fin.
- Simular las condiciones fisiopatológicas de la patología en humanos, en el caso del glaucoma, tiene que presentar remodelado de la cabeza del nervio óptico, adelgazamiento de la capa de fibras nerviosas retiniana, remodelación de la lámina glial y degeneración progresiva de las RGCs.
- Tener un bajo coste.

8.1. Modelos dependientes de la PIO

El principal y más importante factor de riesgo en el glaucoma es la elevación de la PIO, por eso, la mayoría de los modelos dependientes de glaucoma se centran en su aumento (Figura 13) (164). La duración y la elevación de la PIO depende del tipo de glaucoma, pudiéndose desarrollar modelos agudos en los que la PIO es elevada rápidamente durante un corto periodo de tiempo o modelos crónicos donde esta se incrementa de forma moderada y más sostenida (165).

La mayoría de los modelos desarrollados con un aumento de la PIO son modelos agudos en los que se produce un aumento por el bloqueo de la salida del humor acuoso, ya sea por la inyección intracameral de sustancias que obstruyen o por el daño esclerótico de las estructuras o de la vasculatura de salida (164).

Por último, es bien conocido que la PIO presenta un ritmo circadiano y esta es una característica que hay que tener en cuenta a la hora de desarrollar estos modelos en roedores. Los roedores son más activos durante la noche y su producción de humor acuoso y PIO son más altas durante la noche también. Por lo que, si se produce un daño en la salida del humor acuoso, las PIOs serán más altas durante la noche. Sin embargo, muchos de los estudios miden la PIO durante las horas de luz, por lo que se produce una subestimación del pico de la PIO (164,167,168).

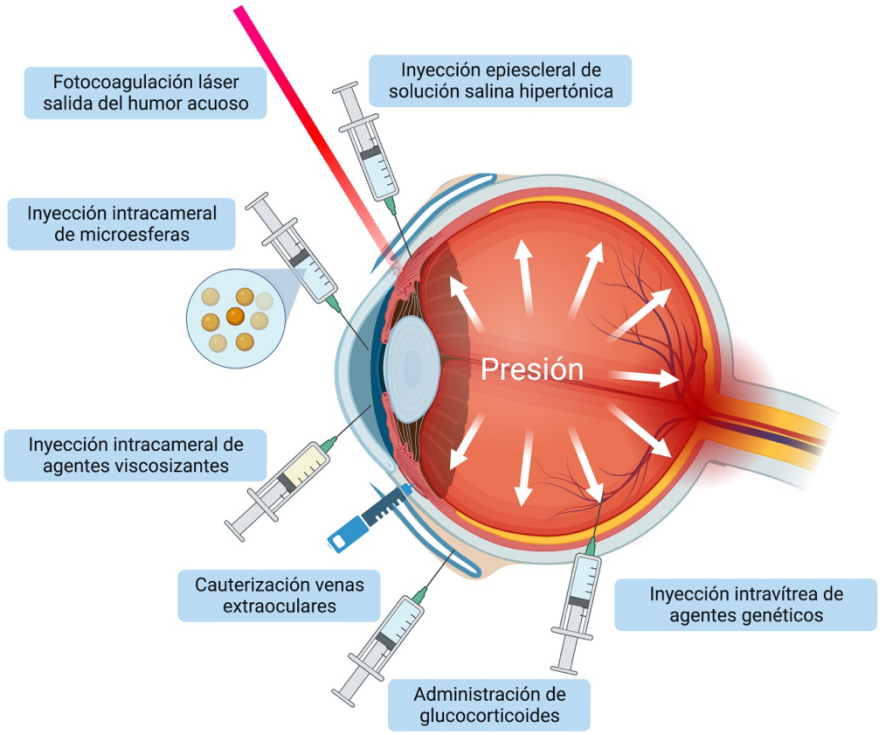

Figura 13. Representación esquemática de las principales vías de inducción de modelos murinos de glaucoma dependientes de la PIO. Imagen creada con BioRender.com

8.1.1. Modelos basados en la oclusión de la malla trabecular por la presencia de microesferas

Hay distintas variantes de la oclusión que utilizan microesferas y parecen funcionar bien en investigación, además de producir una evolución de la PIO con el tiempo. Sin embargo, no se ha realizado una comparación entre los mismos que permita determinar cuál sería el método óptimo. Entre estos modelos se encuentran los siguientes:

- Inyección intracameral de microesferas no biodegradables.

Este método primero fue desarrollado en mamíferos más grandes como los primates mediante la inyección de microesferas de látex (166). Más tarde, este se adaptó y optimizó para roedores inyectando microesferas no biodegradables de látex o poliestireno. La inyección en la cámara anterior de las microesferas produce un bloqueo físico de la salida del humor acuoso y, en consecuencia, una subida de la PIO, ya que las microesferas se acumulan en la malla trabecular y en el canal de Schlemm (169,170).

Es importante tener en cuenta el pequeño tamaño de los ojos de los roedores. Esto limita el volumen de inyección, ya que la inyección de un fluido en la cámara anterior

per se ya es suficiente para producir una elevación de la PIO. La inyección de un volumen excesivo puede incrementar tanto la PIO que puede reducir de forma temporal la circulación retiniana o conducir a otro tipo de daños oculares no esperados. Por ello, los volúmenes máximos establecidos en la inyección ocular son de 2 µL en el ratón y 10 µL en la rata, aunque también se han reportado volúmenes más altos (164).

También se ha evaluado la influencia del tamaño y el número de microesferas inyectadas. En ratones, se demostró que usando microesferas más pequeñas (10 µm vs 15 µm) la elevación de PIO producida era mayor y más duradera, y que una segunda inyección prolongaba el efecto hasta las 8 semanas (171). En ratas, Sappington et al. concluyeron que tras la inyección de 5 x 10^3 microesferas de poliestireno de 15 µm en un volumen de 5 µL producía un aumento consistente de la PIO y se alargaba hasta las 8 semanas con una reinyección (170). Urcola et al. inyectaron semanalmente 2-4 x 10^5 microesferas de látex en un volumen de 20 µL, produciendo una elevación de la PIO durante 30 semanas (172).

- Inyección intracameral de microesferas combinadas con agentes viscosizantes

Las microesferas se pueden suspender en un agente viscosizante como el hialuronato sódico o la hidroxipropilmetilcelulosa para su inyección. La adición de esta solución tendría como principal ventaja minimizar la fuga o salida de las microesferas cuando la aguja es retirada, además de que, por sus propiedades físicas, también puede contribuir adicionalmente a bloquear la salida del humor acuoso (164,172,173).

En ambos tipos de inyección, ya sean micropartículas suspendidas en un medio acuoso o con un agente viscosizante, se tuvo que recurrir a la reinyección para mantener elevada la PIO durante largos periodos (165).

- Inyección intracameral de microesferas magnéticas

Los anteriores métodos fueron optimizados con la inyección de microesferas magnéticas. El principal inconveniente de la inyección de microesferas es la variabilidad en la elevación de la PIO debido a la dificultad de retener las micropartículas en la cámara anterior y su localización en esta zona es impredecible (165). Para solventar este

problema, se desarrollaron microesferas magnéticas que, tras ser inyectadas, son retenidas por el uso un imán para evitar su fuga del lugar de inyección al retirar la jeringa y son dirigidas al ángulo iridocorneal (174). Este método fue optimizado mediante la utilización de un imán cilíndrico situado en el segmento anterior. Esto dirigiría de forma rápida a las microesferas magnéticas hacia la malla trabecular, sin embargo, también produce unas elevaciones excesivas de la PIO que pueden provocar unos daños muy agresivos en los tejidos retinianos (175).

- Inyección intracameral de microesferas biodegradables

Recientemente, nuestro grupo de investigación ha desarrollado distintos modelos murinos mediante la inyección de microesferas biodegradables de PLGA, siendo hasta el momento, los únicos modelos producidos con microesferas de esta naturaleza. En un primer trabajo se evaluó la inyección de microesferas de distinto tamaño (fracciones 38-20 µm vs 20-10 µm), concluyendo que la inyección de las microesferas más pequeñas producía menos fluctuaciones en la subida de la PIO tras 8 semanas de estudio (176). Posteriormente, se desarrolló un modelo de glaucoma crónico mediante la inyección de microesferas blanco de entre 20-10 µm, mostrando una elevación de la PIO durante 24 semanas mediante 7 inyecciones intracamerales (177). Además, a partir de este modelo animal se desarrolló otro modelo mediante la inyección de microesferas cargadas con un principio activo (dexametasona), produciendo, por tanto, un bloqueo físico y farmacológico (178). En este modelo, se recurrió a una inyección adicional para mantener la PIO elevada durante 24 semanas (178). En cuanto cuál es el óptimo, cada uno de los modelos animales desarrollados presentaron características individuales y específicas con distintas tendencias en la elevación de la PIO, siendo esta una elevación progresiva, y presentando todos ellos daño retiniano. De este modo, la elección del modelo se podría hacer en función de lo que se desee estudiar (179).

Todos los modelos inducidos por la inyección de microesferas en roedores mostraron cambios patológicos similares a los ocurridos en la retinopatía glaucomatosa y neuropatía del nervio óptico (169–172,176–178,180).

8.1.2. Inyección intracameral de agentes viscosizantes

Además de la oclusión por microesferas, la elevación de la PIO también se puede realizar inyectando sustancias viscosizantes en la cámara anterior como, por ejemplo, el polímero hidrosoluble ácido hialurónico. La presencia de ácido hialurónico impide la salida normal del humor acuoso ya que actúa reduciendo el diámetro del espacio corneoescleral e intertrabecular y/o regulando el paso del humor acuoso a través de la malla trabecular. Sin embargo, el inconveniente que presentan estos modelos es la necesidad de inyecciones repetidas con los riesgos que ello conlleva (cataratas, edema corneal transitorio, etc.) (164,165). En ese sentido, con una primera inyección se consiguió una elevación de la PIO de más de una semana en ratas, que se mantuvo hasta las 10 semanas con inyecciones semanales (181).

8.1.3. Esclerosis de la vía de salida del humor acuoso

- Inyección epiescleral de solución salina hipertónica

Fue descrito por primera vez por Morrison et al. y consiste en la inyección en una de las venas epiesclerales de una solución salina hipertónica (concentración 1,75M) mientras que el resto de las venas epiesclerales son oprimidas por un anillo colocado en la circunferencia del globo ocular. Con este método se produce una esclerosis ya que la solución salina pasa de forma retrógrada por el canal de Schlemm y las estructuras relacionadas con la salida del humor acuoso. La elevación de la PIO normalmente tarda en manifestarse un par de días después de la inyección (182–185). Los cambios patológicos que se producen con estos modelos en la retina, nervio óptico y cabeza del nervio óptico son similares a los descritos en los pacientes humanos de glaucoma (164). Los inconvenientes de este método es que no todos los ojos inyectados sufren una elevación de la PIO y esta puede ser variable entre los ojos, el procedimiento es técnicamente difícil y en ratones no se puede realizar (164).

- Fotocoagulación laser de la salida del humor acuoso.

Se cree que la fotocoagulación láser de la malla trabecular, el plexo limbal y las venas epiesclerales incrementa la resistencia de las vías de salida del humor acuoso debido al cierre del ángulo, la destrucción del canal de Schlemm y la cicatrización de la malla trabecular (186). Este procedimiento produce la muerte apoptótica de las RGCs y la

pérdida de axones del nervio óptico, sin embargo, para prolongar el incremento de la PIO se necesita repetir varias veces el procedimiento (164). Aunque este método es efectivo y produce resultados similares a los encontrados en el glaucoma humano, es difícil de realizar en los ojos de roedores y requiere numerosas y precisas quemaduras láser (164).

8.1.4. Cauterización de las venas extraoculares

Es un método relativamente fácil de realizar en las ratas, sin embargo, durante el proceso de cauterización hay que tener especial cuidado en no confundir las venas epiesclerales con las venas vorticosas, ya que la cauterización de estas produce otros efectos además de la subida de la PIO. Aunque también es un método efectivo en subir de la PIO, se ha observado que en algunas ocasiones la PIO vuelve a valores basales después de unas semanas debido al crecimiento de nuevos vasos sanguíneos (164).

8.1.5. Elevación transitoria o intermitente de la PIO

En las primeras fases del glaucoma, se producen fluctuaciones repetidas de la PIO. Algunas de las modificaciones biológicas producidas por las elevaciones agudas de la PIO no pueden ser conseguidas con los modelos crónicos. Por ello, se han desarrollado estos modelos de glaucoma sin una isquemia retiniana significante. Hay modelos que producen una elevación de 45 mmHg hasta 7 horas por compresión del limbo conjuntival (187), otros elevan la PIO a 50 mmHg durante 30 minutos por la canulación de la cámara anterior (188), la elevación a 60 mmHg durante 8 horas (188) o la elevación a 70 mmHg repetidamente hasta un total de 4 veces durante 15 minutos mediante la canulación de la cámara anterior (189). En todos los trabajos se observó afectación en el nervio óptico y/o pérdida de RGCs. Como se puede observar, no hay un criterio único en los niveles de elevación de PIO, las duraciones o las técnicas, haciendo muy difícil la comparación entre estudios (164).

8.1.6. Modificación genética de la malla trabecular mediante genes relacionados con el glaucoma

Entre los factores de riesgo, los antecedentes familiares también son importantes en el desarrollo de glaucoma. Para estudiar mejor el daño en la malla trabecular, se han utilizado vectores virales con factores ligados al glaucoma, que son capaces de producir

una modificación en la malla trabecular. Como vector viral se suele utilizar el adenovirus 5 (Ad5) ya que se ha visto que es capaz de modificar la malla trabecular en los ojos de ratón. En cuanto a la forma de administración, se ha visto que es más efectivo por administración intravítrea que intracameral, posiblemente debido a la liberación más lenta desde el humor vítreo. Los principales problemas de este método son la corta duración del Ad5, ya que solo dura entre 3 y 6 semanas, y los efectos adversos. Los principales genes implicados confirmados en ratones son MYOC, TGFβ2, CTGF, GREM1, SFRP1 y CD44.

8.1.7. Hipertensión ocular inducida por glucocorticoides

Los glucocorticoides se utilizan ampliamente para diversas dolencias por su actividad antiinflamatoria e inmunosupresora, incluso para la inflamación ocular. Sin embargo, su uso prolongado produce en ciertos casos hipertensión ocular y glaucoma secundario que clínicamente es muy similar al glaucoma primario de ángulo abierto (190,191).

Aunque no está muy claro el mecanismo por el cual los glucocorticoides incrementan la PIO, se cree que produce una serie de cambios en la malla trabecular que causan una mayor resistencia en la salida del humor acuoso. Entre todos estos cambios están el incremento de la deposición de material en la matriz extracelular como pueden ser glicoproteínas como la fibronectina, la laminina y el colágeno tipo IV, inhibición de la fagocitosis, inhibición de la actividad de enzimas como las metaloproteinasas (encargadas de la renovación de la matriz extracelular) o modificaciones en el citoesqueleto de la malla trabecular que produce un incremento de tamaño celular. La administración de glucocorticoides exógenos puede causar hipertensión ocular en el 40% de la población general aproximadamente, refiriéndose a estas personas como “respondedoras a corticosteroides” (191).

El primer modelo descrito utilizaba dexametasona por vía sistémica en ratones. Un 60% de los animales sufrieron un incremento de la PIO, pero este método también causó efectos secundarios (192). Para solventar estos problemas, se recurrió a la administración tópica de dexametasona (0.1%) tres veces al día con resultados en elevación de la PIO y daño glaucomatoso en el nervio óptico y RGCs (193). Sin embargo, la administración 3 veces al día durante varias semanas es muy exigente, por lo que se ha recurrido a formulaciones con liberación más lenta como las inyecciones perioculares

de una suspensión de dexametasona, administrada semanalmente. Se consiguió una elevación de la PIO de hasta 70 días (168).

También se han utilizado sistemas de liberación modificada como son las nanopartículas de PGA−PCL−PEG−PCL−PGA cargadas con dexametasona y administradas por vía subconjuntival/periocular cada 1 o 2 semanas. Este modelo consiguió una elevación de la PIO de hasta 60 días con cambios en la malla trabecular y el canal de Schlemm (194,195). Recientemente, también se ha administrado microesferas de PLGA cargadas con dexametasona mediante inyección intracameral. Este trabajo ya ha sido comentado también en los modelos creados por la inyección de microesferas ya que se produce por un bloqueo físico, debido a las microesferas, y farmacológico por encapsulación de dexametasona. La encapsulación de la dexametasona permitió reducir el número de inyecciones en comparación a la inyección de microesferas blanco, de 7 intervenciones a 2. La elevación de la PIO duró hasta las 24 semanas con hallazgos patológicos similares a los del glaucoma humano (178,179).

8.2. Modelos independientes de la PIO

El papel de la PIO en la progresión del glaucoma es indiscutible, sin embargo, no todos los individuos que desarrollan glaucoma presentan una PIO elevada ni todos los que presentan PIO elevada, desarrollan glaucoma. Por ello, se han desarrollado modelos animales en los que no está implicada la elevación de la PIO (Figura 14) que, aunque no necesariamente imiten las mismas características del glaucoma, permiten el estudio de otras vías y mecanismos implicados en el daño de las RGCs y el nervio óptico (164).

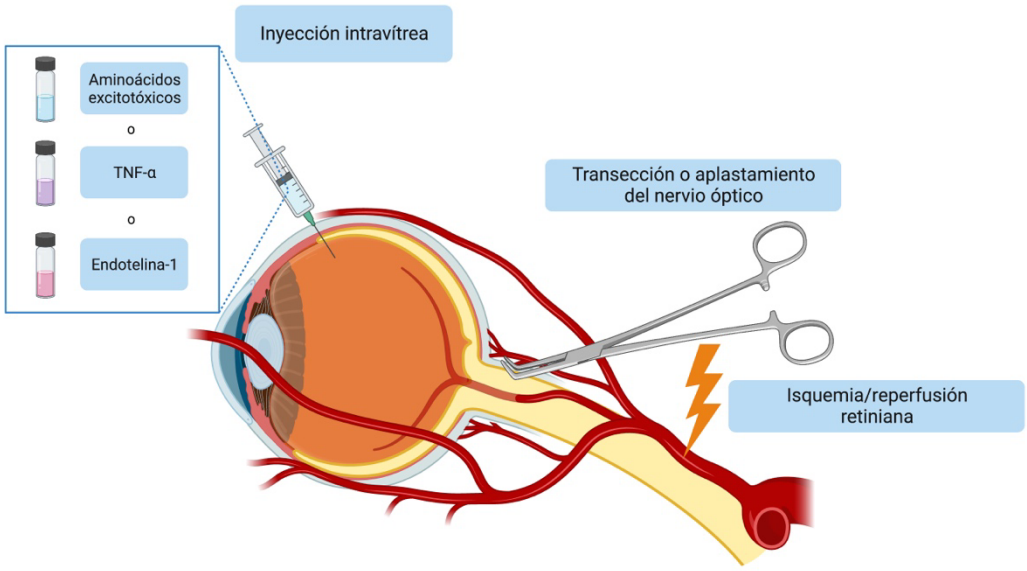

Figura 14. Representación esquemática de las principales vías de inducción de modelos murinos de glaucoma no dependientes de la PIO. Imagen creada con BioRender.com

8.2.1. Transección o aplastamiento del nervio óptico.

Howell et al. demostraron que el primer lugar afectado cuando se produce un daño glaucomatoso son los axones del nervio óptico tras un daño local (196). Estos hallazgos concordaban con otros anteriores en humanos y primates no humanos (197–199).

La transección o aplastamiento del nervio óptico en los roedores produce un daño en este nervio. En las ratas causa una ruptura completa de los axones del nervio y, por tanto, una pérdida de las RGCs por apoptosis en aproximadamente 2 semanas (200). En los ratones se han reportado resultados similares, a las dos semanas, la mayoría de las RGCs se han perdido (201).

Sin embargo, algunos autores argumentan que el daño que se produce en los axones es tan severo que no representa los cambios del glaucoma. Por ello, se han desarrollado modelos con una transección parcial (por ejemplo, cortando un tercio del nervio óptico). Esto permitiría el estudio de los cambios que se producen tanto por la axotomía como el daño secundario que se produce en los axones no cortados del nervio óptico y en las RGCs (202). Este daño secundario como se ha comentado anteriormente tiene un papel importante en la patología del glaucoma.

Otra técnica para aplastar el nervio óptico es mediante pinzas o fórceps, produciendo un daño en éste y la muerte de las RGCs (203). Sin embargo, los resultados varían dependiendo de la fuerza con las que se aplaste el nervio óptico (164,204–206).

8.2.2. Isquemia/reperfusión retiniana

En muchos estudios se ha relacionado la reducción del flujo sanguíneo con el glaucoma, ya que produce una elevación de la PIO, desregulación vascular e hipotensión sistémica, entre otros desórdenes vasculares. Por lo que la anormalidad del flujo sanguíneo se postula como uno de los mecanismos fisiopatológicos del glaucoma (164,207,208). Se puede hacer por diversos métodos:

Canulación ocular. Es un método muy común, consiste en colocar una cánula conectada a un reservorio, esto genera una presión hidrostática sobre la presión sanguínea sistólica que para el flujo sanguíneo en el ojo (209). El blanqueamiento del iris y la retina confirma el éxito de esta técnica. La isquemia transitoria durante 60 minutos seguida de reperfusión es un método muy utilizado (164). Produce una pérdida de RGCs apoptótica (210), daño en el nervio óptico (211) e incluso daño panretiniano y en los fotorreceptores (164).

Fototombrosis. Se realiza mediante la inyección de rosa de bengala en la arteria central retiniana junto con la posterior irradiación de luz verde. Tras la irradiación, el rosa de bengala libera oxígeno molecular que inicia la activación plaquetaria y consecuentemente, un trombo localmente (212). Se puede producir la posterior reperfusión mediante la disolución del trombo. Aunque produce la muerte de las RGCs, no se descarta que la fototoxicidad contribuya en los daños encontrados (213).

Ligación del nervio óptico. Es un procedimiento mucho más invasivo. Consiste en la sutura del nervio óptico mediante un procedimiento quirúrgico para impedir el flujo sanguíneo en la arteria retiniana central y otros vasos adyacentes. Al retirar la sutura se produce la reperfusión (214). Sin embargo, esta técnica además de producir isquemia genera un daño mecánico en el nervio óptico. Para solventar esto, se ha descrito una técnica que consiste en la sutura selectiva de venas oftálmicas mediante suturas de nylon (215).

8.2.3. Inyección intravítrea de aminoácidos excitotóxicos

El glutamato es el principal neurotransmisor excitatorio en la retina de los vertebrados y la sobreestimulación de sus receptores, receptores NMDA, produce una entrada excesiva de Ca^{2+} en las neuronas, como se ha comentado anteriormente. Con esta idea en mente, se ha administrado por inyección intravítrea NMDA o glutamato, produciendo una apoptosis de las RGCs dosis-dependiente (216). Sin embargo, no solo afecta a las RGCs y se han reportado efectos en las células amacrinas (217).

Esta técnica es relativamente fácil de realizar y los efectos pueden ser evaluados en pocos días, sin embargo, debido al poco conocimiento de la relación entre la excitotoxicidad y la fisiopatología de la enfermedad, es una técnica que presenta controversias para el estudio del glaucoma (164).

8.2.4. Inyección intravítrea de TNF-α

También se ha hablado anteriormente del papel del TNF-α en la neurodegeneración glaucomatosa. Aunque la concentración en el humor acuoso está por debajo de los límites de sensibilidad de los inmunoensayos, se ha conseguido detectar que la concentración de esta citoquina era superior en las muestras de pacientes glaucomatosos que en los controles (218).

La inyección intravítrea de TNF-α disminuye la supervivencia de las RGCs, los oligodendrocitos y la degeneración y pérdida de los axones del nervio óptico (219,220).

8.2.5. Inyección intravítrea de endotelina-1

La endotelina 1 (ET-1) se ha visto también implicada en la patogénesis del glaucoma (221). Inicialmente era usada por su acción vasoconstrictora para inducir una isquemia crónica en el nervio óptico (222). Sin embargo, se ha descubierto que causa daño directamente en las RGCs y en el nervio óptico, sin relación alguna con su acción en la circulación (223,224). Por ello, el modelo inducido por endotelina-1 podría ser interesante en la investigación de esta patología (225).

HIPÓTESIS DE TRABAJO

El desarrollo de sistemas de liberación controlada multicargados permitirá la creación de un modelo animal de glaucoma crónico y también de una plataforma neuroprotectora para el tratamiento de dicha enfermedad. Además, la formación de sistemas híbridos mediante la dispersión de las microesferas en hidrogeles termosensibles facilitará su inyección, así como el control de la liberación inicial de los agentes neuroprotectores a partir de las microesferas.

OBJETIVOS Y PLANTEAMIENTO

<u>Primer objetivo</u>. Desarrollo y caracterización de microesferas de PLGA cargadas con dexametasona y fibronectina para la creación de un modelo animal de glaucoma crónico tras su inyección en cámara anterior.

Para el cumplimiento de este objetivo, se realizaron las siguientes actividades:

- ✓ Desarrollo de microesferas de PLGA cargadas con dexametasona y fibronectina empleando el método de extracción-evaporación del solvente a partir de una doble emulsión acuo-óleo-acuosa (A/O/A).
- ✓ Caracterización *in vitro* de las microesferas desarrolladas mediante el estudio de su morfología, tamaño, eficacia de encapsulación y perfiles de liberación de las sustancias activas.
- ✓ Creación del modelo en animales de experimentación (ratas Long-Evans) mediante inyección de las microesferas en cámara anterior.
- ✓ Monitorización de la presión intraocular de los animales tratados y evaluación de los cambios en la retina mediante técnicas no invasivas (ERG y OCT) y estudios histopatológicos.

Las dos últimas actividades se realizaron en colaboración con el Grupo de Investigación e Innovación Miguel Servet Oftalmología (GIMSO) de Zaragoza.

<u>Segundo objetivo</u>. Desarrollo de plataformas neuroprotectoras de liberación sostenida cargadas con varios principios activos para el tratamiento del glaucoma.

Este objetivo, se puede subdividir a su vez en los siguientes:

1- **Desarrollo y optimización de un sistema microparticular cargado con una combinación de tres agentes neuroprotectores (dexametasona, ácido ursodesoxicólico y factor neurotrófico derivado de la glía) para el tratamiento del glaucoma**.

Para el cumplimiento de este objetivo, se realizaron las siguientes actividades:

- ✓ Desarrollo y optimización de la formulación cargada con dexametasona y ácido ursodesoxicólico elaborada mediante el método de extracción-evaporación del solvente a partir de una emulsión sólido-oleo-acuosa (S/O/A).
- ✓ Caracterización *in vitro* de la formulación desarrollada mediante el estudio de su morfología, tamaño, DSC, difracción de rayos X, cromatografía de gases, eficacias de encapsulación y perfiles de liberación de las sustancias activas.
- ✓ Inclusión de la proteína (GDNF) en la formulación optimizada cargada con dos principios activos de bajo peso molecular (dexametasona y ácido ursodesoxicólico).
- ✓ Caracterización *in vitro* de la formulación cargada con los tres compuestos neuroprotectores mediante el estudio de su morfología, tamaños, eficacias de encapsulación, perfiles y cinéticas de liberación de las sustancias activas y estudios de degradación.

2- Desarrollo de hidrogeles "inteligentes" biodegradables como plataformas inyectables para el tratamiento de enfermedades neurodegenerativas de la retina.

Para su cumplimiento, se realizaron las siguientes actividades:

- ✓ Desarrollo y optimización de hidrogeles formados por ácido hialurónico funcionalizado. Esta actividad se realizó en colaboración con el grupo de Dr. Wenxin Wang en Irlanda (UCD Charles Institute of Dermatology, Blafar Ltd).
- ✓ Síntesis y caracterización del polímero PLGA-PEG-PLGA para la elaboración de hidrogeles termosensibles.
- ✓ Caracterización de los hidrogeles elaborados a partir de ácido hialurónico en función del pH final y análisis de las propiedades reológicas para la selección de un candidato final.
- ✓ Caracterización y optimización de los hidrogeles termorrespuesta mediante el estudio de los tiempos de disolución, pH, propiedades reológicas, tamaño de micelas y duración de la gelificación, para la selección de los candidatos finales.
- ✓ Evaluación de los hidrogeles formados por ácido hialurónico y de los hidrogeles formados con PLGA-PEG-PLGA en función del hinchamiento, degradación y liberación *in vitro* de sustancias antiinflamatorias para su aplicación en enfermedades oftalmológicas.
- ✓ Estudios de tolerancia y cicatrización en células de epitelio pigmentario de la retina (RPE-1) de los hidrogeles finales seleccionados como candidatos para el tratamiento de patologías crónicas oculares.

3- Desarrollo de sistemas híbridos compuestos por microesferas multicargadas e hidrogeles inteligentes cargados de un antiinflamatorio para el tratamiento de enfermedades neurodegenerativas de la retina.

Para su cumplimiento se realizaron las siguientes actividades:

- ✓ Elaboración y caracterización de los hidrogeles termorrespuesta mediante la evaluación del comportamiento reológico, tamaños, pH, morfología de las micelas, densidad, degradación y concentración crítica micelar.
- ✓ Incorporación de las microesferas cargadas con tres principios activos con actividades neuroprotectoras en los hidrogeles termorrespuesta y caracterización *in vitro* del sistema híbrido: prueba del "frasco invertido", hinchamiento, inyectabilidad y perfiles y cinéticas de liberación.
- ✓ Estudios de tolerancia en células de epitelio pigmentario de la retina (RPE-1) de las microesferas y de las formulaciones finales incorporando las microesferas en el hidrogel.
- ✓ Estudios preliminares de agregación de las microesferas incluidas en el sistema híbrido tras su inyección.

CAPÍTULO I – CHAPTER I. Mimicking chronic glaucoma over 6 months with a single intracameral injection of dexamethasone/fibronectin-loaded PLGA microspheres

Mimicking chronic glaucoma over 6 months with a single intracameral injection of dexamethasone/fibronectin-loaded PLGA microspheres

Alba Aragón-Navas[a,e#]; María J. Rodrigo[b,c#]; David Garcia-Herranz D[a,e], Teresa Martinez[b]; Manuel Subias[b]; Silvia Mendez[b]; Jesús Ruberte[d]; Judit Pampalona[d]; Irene Bravo-Osuna[a,c,e]; Luis E. Pablo[b,c]; Elena Garcia-Martin[b,c*]; Rocío Herrero-Vanrell[a,c,e*].

a: Complutense University, Innovation, Therapy and Pharmaceutical Development in Ophthalmology (InnOftal) Research Group, UCM 920415, Department of Pharmaceutics and Food Technology, Faculty of Pharmacy, Complutense University of Madrid Spain. Health Research Institute of the San Carlos Clinical Hospital (IdISSC), Madrid, Spain.

b: Department of Ophthalmology, Miguel Servet University Hospital, Zaragoza, Spain. Miguel Servet Ophthalmology Research Group (GIMSO), Aragon Health Research Institute (IIS Aragon), University of Zaragoza, Spain.

c: Thematic Research Network in Ophthalmology (Oftared), Carlos III National Institute of Health, Spain

d: Center of Animal Biotechnology and Gene Therapy (CBATEG), Universitat Autònoma de Barcelona, Bellaterra, Spain. CIBER de Diabetes y Enfermedades Metabólicas Asociadas (CIBERDEM), Madrid, Spain. Department of Animal Health and Anatomy, School of Veterinary Medicine, Universitat Autònoma de Barcelona, Bellaterra, Spain.

e: Department of Pharmaceutics and Food Technology, Faculty of Pharmacy, Complutense University of Madrid, Plaza Ramón y Cajal s/n, 28040, Madrid, Spain; Research Institute of the San Carlos Clinical Hospital (IdISSC), Grupo de Investigación Innovación Farmacéutica en Oftalmología, Profesor Martín Lagos s/n, 28040, Madrid, Spain.

Artículo publicado en: Drug Delivery 2022, vol. 29, NO. 1, 2357–237

ABSTRACT

To create a chronic glaucoma animal model by a single intracameral injection of biodegradable poly lactic-co-glycolic acid (PLGA) microspheres (MSs) co-loaded with dexamethasone and fibronectin (MSsDexaFibro). MSsDexaFibro were prepared by a water-in-oil-in-water emulsion method including dexamethasone in the organic phase and fibronectin in the inner aqueous phase. To create the chronic glaucoma model, an interventionist and longitudinal animal study was performed using forty-five Long Evans rats (4-week-old). Rats received a single intracameral injection of MSsDexafibro suspension (10 % w/v) in the right eye. Ophthalmological parameters such as clinical signs, intraocular pressure (IOP), neuro-retinal functionality by electroretinography (ERG), retinal structural analysis by optical coherence tomography (OCT), and histology were evaluated up to six months. According to the results obtained, the model proposed was able to induce IOP increasing in both eyes over the study, higher in the injected eyes up to 6 weeks ($p < 0.05$), while preserving the ocular surface. OCT quantified progressive neuro-retinal degeneration (mainly in the retinal nerve fiber layer) in both eyes but higher in the injected eye. Ganglion cell functionality decreased in injected eyes, thus smaller amplitudes in PhNR were detected by ERG. In conclusion, a new chronic glaucoma animal model was created by a single injection of MSsDexaFibro very similar to open-angle glaucoma occurring in humans. This model would impact in different fields such as ophthalmology, allowing long period of study of this pathology; pharmacology, evaluating the neuroprotective activity of active compounds; and pharmaceutical technology, allowing the correct evaluation of the efficacy of long-term sustained ocular drug delivery systems.

1. Introduction

Glaucoma is a multifactorial neurodegenerative disorder, leading cause of blindness with an estimated 60 million people worldwide currently suffering and it will be around 118 millions in 2040 (Quigley & Broman, 2006; Tham et al., 2014). It is produced by the gradual death of retinal ganglion cells (RGC) which leads to irreversible vision loss, although recent studies have also suggested the involvement of other retinal cells as photoreceptors or activated glia (Asaoka et al., 2017; Ramirez et al., 2017; Ashimatey et al., 2018). Intraocular pressure (IOP) is the major modifiable risk factor strongly associated with the onset and progression of the disease (Gaasterland et al., 2000). For this reason, the usual treatment of glaucoma consists in the frequent instillation of hypotensive drugs (Conlon et al., 2017); however, it is important to remark that the return to normal intraocular pressure values does not always stop the retinal degeneration (Pascale et al., 2012) and that, in addition, in many other cases these same failures in the retina and optic nerve occur in normotensive patients (Anderson, 2003; Lestak et al., 2018). Sadly, there is not yet any optimal treatment for this and any other retinal neurodegenerative diseases.

Degenerative diseases of the retina begin with primary damage, for example of the axons of retinal ganglion cells in the case of glaucoma. When the damaged cell dies, it releases neurotoxic compounds in the vicinity that damage the adjacent neurons that also end up dying in what is known as “secondary neurodegeneration” (Ritch, 2000). Several decades ago, some researchers postulated the idea of “neuroprotection” as a complementary treatment in degenerative diseases (Weinreb & Levin, 1999). At the level of the retina neuroprotection can be defined as: “Prevention or slowing down of the loss of functional integrity of the cells of the retina, their axons and their axonal connections to maintain and stabilize the vision of patients as much as possible” (Ritch, 2000). Pardue et al. describe this neurodegeneration of the retina in 3 stages: an adaptive first step where there is only oxidative stress and neuronal dysfunction, a second stage, the “early pathology”, where retinal structures begin to damage but still reversibly, and a third stage of "late pathology" where blindness appears and where the damage is already irreversible. According to those authors, “starting neuroprotective

treatments at the first signs of the retinal disease would provide the most benefit in preserving vision" (Pardue & Allen, 2018).

In recent decades, different neuroprotective pharmacological strategies have been explored (Thanos & Emerich, 2005; Masuda et al., 2017; Avotri et al., 2019; Fernández-Albarral et al., 2019; Stankowska et al., 2019; Naik et al., 2020). However, one of the main problems to evaluate the efficacy of neuroprotective treatments resides in the absence of a chronic and slow degeneration glaucoma animal model that simulates the conditions found in the human glaucomatous eyes (Pang & Clark, 2020). In general, it is very difficult to obtain optimal animal models of retinal pathologies. For example, in the case of glaucoma, there are the so-called "acute models", in which a fast retinal degeneration occurs, either due to genetic failures (Schlamp et al., 2006), to the direct intravitreal injection of toxic compounds (Kitaoka et al., 2006), or to the direct damage of the optic nerve for example by crushing it (Sharma et al., 2014). Despite their utility for neuroprotective studies, these acute models: (1) Do not reproduce the reality of retinal chronic pathologies in human beings; (2) Do not allow testing the long term efficacy of new therapies because the retina is almost directly in the last step of the diseases from the very beginning of the study; and (3) It is difficult to assess the potential of modified release systems so in a few days or weeks the retina is completely ruined (Cuenca et al., 2014; Smedowski et al., 2014; Pang & Clark, 2020). There are also the so-called "chronic models", which present a more progressive retinal degradation based on the increase in IOP secondary to a limitation of aqueous humor outflow. In rodent models, the reduction in aqueous humor drainage is typically obtained, either through cauterization, ligature and/or sclerosis of episcleral veins (Morrison et al., 1997; Morgan & Tribble, 2015; Dey et al., 2018) either by mechanical blockage of the trabecular meshwork (TM) with non-biodegradable particles injected in the anterior chamber (Urcola et al., 2006), through the use of corticoids which reduce aqueous humor outflow when inhibiting cellular phagocytosis thus avoiding cleaning the waste channels in the TM (Clark & Wordinger, 2009; Patel et al., 2017), or by fibronectin expression in a genetically modified mouse model altering the extracellular matrix of the TM (Roberts et al., 2020). All the previous need repeated interventions on the animal, damage aggressively or even modify their nature.

Thus far, no research group has achieved the creation of an animal model which simulates open-angle glaucoma combining the last three different strategies. With this idea in mind, we recently proposed an initial animal model of glaucoma by using intracameral injections of non-loaded PLGA microspheres. The weekly injection of blank microspheres produced a sustained and prolonged ocular hypertension (OHT) over six months due to a progressive physical blockage of the trabecular meshwork. This maintained OHT produced a very progressive degeneration of the retina (Garcia-Herranz et al., 2021; Rodrigo et al., 2021). In a second study, dexamethasone loaded PLGA microspheres also generated OHT and neuroretinal degeneration by only two times injections (Rodrigo et al., 2021). After those initial approaches, in the present work, we propose a new model of chronic glaucoma produced by intracameral injection of dexamethasone/fibronectin co-loaded PLGA microspheres. This study aims to establish whether lower quantities of sustained and simultaneous co-release of those two active compounds from PLGA microspheres in the anterior segment of the eye, combined with the mechanical blockage produced by PLGA microspheres themselves, would promote a progressive OHT and subsequent retinal chronic degradation, only using a single injection. The follow up of animals in terms of retinal structure and function is performed for six months.

2. Materials

Dexamethasone (DX) was supplied by Sigma-Aldrich (St. Louis Mo., USA) (purity >98%). Poly(D,L-lactide-co-glycolide) (PLGA) 50:50 (Inherent viscosity: 0.16–0.24 dL/g) was purchased from Evonik Industries (Essen, Germany). Polyvinyl alcohol 67,000 g/mol (PVA) was obtained from Merck KGaA (Darmstadt, Germany) and methylene chloride from PanReac AppliChem (Barcelona, Spain). Fibronectin (FN), fibronectin ELISA and reactants (Reagent Diluent DY995, Wash Buffer WA126, Stop Solution DY994 and Substrate Reagent Pack DY999) were purchased from R&D Systems (Minneapolis, MN, USA).

2.1. Manufacture of dexamethasone/fibronectin-loaded PLGA microspheres

The water-in-oil-in-water (W/O/W) double emulsion solvent followed by extraction-evaporation technique was employed for dexamethasone/fibronectin-loaded PLGA microspheres elaboration. In brief, micronized DX (40 mg) was added to a polymeric organic solution (400 mg of PLGA dissolved in 2 mL of methylene chloride). The suspension was homogenized by ultrasonication in an ice-water bath (Ultrasons; J.P. Selecta, Barcelona, Spain) for 5 minutes and sonication (Sonicator XL; Heat Systems, Inc., Farmingdale, NY, USA) for 1 additional minute in an ice-water bath. The inner aqueous phase composed of 20 µL of FN aqueous solution (containing 42.8 µg of fibronectin) was added to this organic phase and emulsified by sonication (Sonicator XL; Heat Systems, Inc., Farmingdale, NY, USA) for 30 seconds at 4 °C to create the initial W_1/O emulsion. Afterwards, 5 mL of PVA solution 1% (w/v) were added to the mentioned W_1/O emulsion and the mixture was emulsified (Polytron®RECO, Kinematica, GmbHT PT3000, Lucerna, Switzerland) at 7,000 rpm for 1 minute to form the final $W_1/O/W_2$ emulsion that was finally added to 100 mL of PVA solution 0.1% (w/v) to get droplets hardening by organic solvent evaporation under stirring at room temperature for 3 hours. After that, MSs were washed with MilliQ® water to remove surface PVA. The desired granulometric size fraction (20–10 µm) was collected by sieving, freeze-dried (Freezing: −60 °C/15 min, drying: −60 °C/12h/0.1 mBar) and storage at −30 °C in dry conditions (Figure 1).

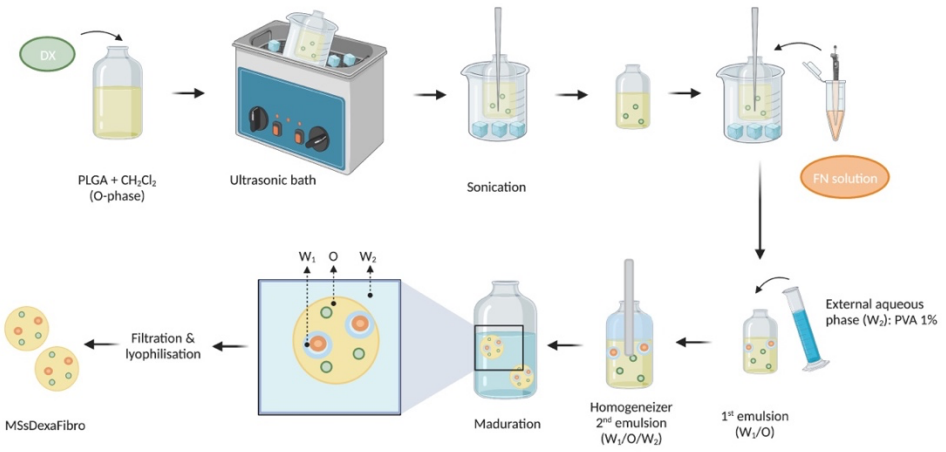

Figure 1. Elaboration scheme of dexamethasone-fibronectin co-loaded PLGA microspheres. Created with BioRender.com

2.2. Dexamethasone/fibronectin-loaded PLGA microspheres characterization

2.2.1. Production yield percentage (PY %)

The production yield percentage of the chosen granulometric fraction was calculated according to the following Eq. (1):

$$PY\% = \frac{Weight\ of\ MSs\ (W_1)}{weight\ of\ polymer\ (W_2) + weight\ of\ DX\ (W_3) + weight\ of\ FN\ (W_4)} x100$$

Equation 1. Production yield percentage.

2.2.2. Morphological evaluation

Scanning electron microscopy (SEM, Jeol, JSM-6335F, Tokyo, Japan) was employed for the observation of the external surface of dexamethasone/fibronectin-loaded PLGA microspheres after gold sputter-coating.

Transmission electron microscopy (TEM, Jeol 1010, Tokyo, Japan) was used for the assessment of the internal structure. MSs were embedded in a synthetic resin medium (Spurr Low Viscosity Embedding Kit) and cut in slides (50–70 nm) by Reichert Ultracut S ultramicrotome (Leica Microsystems Inc, Wetzlar, Germany).

2.2.3. Mean particle size and particle size distribution

Dual light scattering (Microtrac® S3500 Series Particle Size Analyzer, Montgomeryville, PA, USA) was the technique employed to analyze particle size and particle size distribution. The volume mean diameters (± standard deviation) obtained from 3 measurements were calculated and expressed as mean particle size.

2.2.4. Dexamethasone quantification by HPLC/MS

Dexamethasone was quantified using a HPLC/MS system consisting of a liquid chromatography instrument (Waters 1525 binary HPLC pump and Waters 2707 autosampler) connected to a MS detector (Waters 3100 single quadrupole mass spectrometer). A guard column (4 µm, 3.9 mm x 20 mm) and a Nova-Pak C18 column (4 µm, ID 2.1 mm x 150 mm) were used in-line at 45 °C in the HPLC instrument. The MS detector was connected to the system via Empower 2 (Waters, Milford, USA). For DX detection, the positive ion mode was chosen for the ESI source. Selected ion recording (SIR) DX mass (m/z) 393.40 was obtained under mass spectrometer source conditions of

3.5 kV electrospray voltage. The conditions for nebulization were 150 L/h flow rate, 120 °C source temperature, 3 V extractor voltage and for desolvation were 500 L/h flow rate, 350 °C desolvation temperature. Nitrogen gas (> 99.999%) was employed in nebulization and desolvation. For encapsulation efficiency and release from MSs, an isocratic method was developed which was composed of 50% ammonium acetate 15 mM/1 mL formic acid in MilliQ® water and 50% acetonitrile (flow rate: 0.3 mL/min).

2.2.5. Fibronectin quantification by enzyme-linked immunosorbent assay (ELISA)

Fibronectin quantification was performed by ELISA technique using a Fibronectin ELISA Kit (DuoSet® Human Fibronectin DY1918-05, R&D Systems, Minneapolis, MN, USA).

2.2.6. Dexamethasone encapsulation efficiency from dexamethasone/fibronectin-loaded PLGA microspheres

1 mg of dexamethasone/fibronectin-loaded PLGA MSs was dissolved in 2.5 mL of methylene chloride. Afterwards, 6 mL of methanol (MeOH) was added to cause the polymer precipitation, remaining the drug dissolved in the methylene chloride:methanol mixture. This organic solution was isolated from the solid polymer by centrifugation (5,000 rpm, 5 minutes, 20 °C). The supernatant was collected, filtered (0.22 µm) and analyzed by the HPLC/MS method previously described.

2.2.7. Dexamethasone and fibronectin *in vitro* release studies from dexamethasone/fibronectin-loaded PLGA microspheres

2.5 mg of dexamethasone/fibronectin-loaded PLGA MSs were incubated in 1 mL of release media composed by a phosphate-buffered saline (PBS, pH 7.4) solution including sodium azide (0.02% (w/v) (n = 4). The so-prepared samples were located in a water shaker bath (100 rpm, 37 °C, Memmert Shaking Bath, Memmert, Schwabach, Germany). At pre-set times samples were gently centrifugated (5,000 rpm for 5 min, 20 °C). The supernatant was extracted, filtered (0.22 µm) and used for dexamethasone quantification by HPLC/MS employing the method previously mentioned. The formed pellet was resuspended in the same volume of fresh release media to continue the study until the following sampling time-point.

In parallel, the same amount of dexamethasone/fibronectin-loaded PLGA MSs was suspended in phosphate-buffered saline (1 ml, PBS, pH 7.4) including sodium azide (0.02% (w/v) and bovine serum albumin (BSA) (1% (w/v)). The suspension was placed in a water shaker bath (100 rpm, 37 °C, Memmert Shaking Bath, Memmert Schwabach, Germany) (n = 2). Similarly, at pre-set times, the so-prepared samples were centrifuged (5,000 rpm, 5 minutes, 20 °C), the supernatants removed for FN quantification by ELISA and the remaining microspheres refilled with fresh PBS/azide/BSA media.

2.3. Animal's welfare and anesthesia

The work with animals was carried out in the experimental surgery service department of the Biomedical Research Center of Aragon (CIBA). The experiment was previously approved by the Ethics Committee for Animal Research (PI34/17) and carried out in strict accordance with the ARVO Statement for the Use of Animals in Ophthalmic and Vision Research.

The study was carried out in 45 (40% males, 60% females) Long-Evans rats with 4-week-old of age and weights ranged from 50 to 100 grams at the beginning of the study. Animals were housed in standard cages with water and food ad libitum, in 12-hours dark-light cycled rooms with temperature (22 °C) and relative humidity (55%) controlled conditions. IOP measurements were recorded under gas anesthesia with a mixture of 3% sevoflurane gas and 1.5% oxygen and the same gas anesthesia with subcutaneous analgesia (dilution 1/10 of buprenorphine (0.05 mg/kg)) was used for performing OHT injections. General anesthesia by intraperitoneal injections (60 mg/Kg of Ketamine + 0.25 mg/Kg of Dexmedetomidine) was used for electroretinogram (ERG) and optical coherence tomography (OCT) and mydriatic eye drops with tropicamide 10 mg/ml and phenylephrine 100 mg/ml, (Alcon Cusí® SA, Barcelona, Spain) to fully dilate. Surgical and sedative procedures were realized under temperature control with warm pads, antisepsia conditions, topical anesthesia with tetracaine 1 mg/ml + oxibuprocaine 4 mg/ml (Anestesico doble Colircusi®, Alcon Cusí® SA, Barcelona, Spain) and antibiotic with ofloxacin 3 mg/ml (Exocin Colircusi®, Alcon Cusí® SA, Barcelona, Spain) eye drops and lubrication on eyes with hypromellose 2% (Methocel® OmniVision, Germany) or erythromycin 5 mg/g (Oftalmolosa Cusí® eritromicina, Alcon Cusí® SA, Barcelona, Spain) and after procedures animals were let recovering in enriched 2.5% oxygen atmosphere.

2.4. Injection procedure for ocular hypertension induction

Forty-five rats received 2 microliters PLGA MSsDexaFibro suspension (10% w/v) into the anterior chamber of the right eye (RE) using a 10-µl-Hamilton® syringe and glass micropipette by a corneal superotemporal puncture at baseline. To avoid reflux it is recommended placing the rat on its left side and covering the eye puncture with a surgical sponge.

2.5. Clinical signs and intraocular pressure measurements

Ophthalmological clinical signs such as ocular hyperemia, cornea alteration, infection or intraocular inflammation were weekly evaluated; as well as IOP measured with the rebound tonometer Tonolab® (Tonolab; Tiolat Oy Helsinki, Finland). The value of the IOP was the average of three consecutive measurements, which resulted from the average of 6 rebounds. IOP was always recorded in the mornings (9 to 13 am).

2.6. *In vivo* neuro-retinal examination

2.6.1. Electroretinography

Functionality of neuro-retinal structures was studied using electroretinography (ERG) (Roland consult® RETIanimal ERG, Germany) by full-field scotopic ERG and Photopic Negative Response (PhNR) protocols at baseline, 12 and 24 weeks. To perform the scotopic ERG test animals were dark-adapted for 12 hours and pupils fully dilated. Active electrodes were placed on the cornea, references at both sides under the skin and the ground electrode nearby its tail. Electrode impedance was accepted with a difference <2kΩ between electrodes. Both eyes were simultaneously tested by a Ganzfeld Q450 SC sphere with white LEDs flashes for stimuli and seven steps with increasing intensity of luminance and intervals were performed. Scotopic test examined rod response: step 1: −40 dB, 0.0003 cds/m^2, 0.2 Hz [20 recordings averaged]; step 2: −30 dB, 0.003 cds/m^2, 0.125 Hz [18 recordings averaged]; step 3: −20 dB, 0.03 cds/m^2, 8.929 Hz [14 recordings averaged]; step 4: −20 dB, 0.03 cds/m^2, 0.111 Hz [15 recordings averaged]; step 5: −10 dB, 0.3 cds/m^2, 0.077 Hz [15 recordings averaged]; mixed rod–cone response: step 6: 0 dB, 3.0 cds/m^2, 0.067 Hz [12 recordings averaged]; and oscillatory potentials: step 7: 0 dB, 3.0 cds/m^2, 29.412 Hz [10 recordings averaged]). The PhNR protocol was performed after light adaptation to blue background (470 nm, 25 cds/m^2), and a red LED flash (625 nm, −10 dB, 0.30 cds/m^2, 1.199 Hz [20 recordings averaged]) was used as

stimuli. Latency (in milliseconds) and amplitude (in microvolts) were studied in a, b and PhNR waves.

2.6.2. Optical coherence tomography

Neuro-retinal structures were studied with the Spectralis OCT device (Heidelberg® Engineering, Germany) and with a contact lens adapted on the rat cornea to get higher quality acquisitions. It was performed at baseline and at 2, 4, 6, 8, 12, 18 and 24 weeks after the OHT injection. Protocols such as full Retina thickness posterior pole (R), Retina Nerve Fiber Layer (RNFL) and Ganglion Cells Layer (GCL) with automatic segmentation were used. These protocols analyzed an area of 3 mm around the center of the optic disk by 61 b-scans and subsequent follow-up examinations were acquired at this same location using the eye tracking software and follow-up application. The Retina and GCL were analyzed by mimicking the 9 ETDRS areas which included a central (C) 1 mm circle centered in the optic disk, (though no fovea exists in rats) and inner (inferior -II-, superior -IS-, nasal -IN-, temporal -IT-) and outer (inferior -OI-, superior -OS, nasal -ON-, temporal -OT-) rings measuring 2 and 3 mm in diameter, respectively, as well as total volume (TV). The RNFL protocol provides measurements of the 6 peripapillary sectors (inferotemporal -IT-, inferonasal -IN-, superotemporal -ST-, superonasal -SN-, nasal -N- and temporal -T-). Full retinal thickness posterior pole (R) comprises from the inner limiting membrane to the retinal pigment epithelium; RNFL from the inner limiting membrane to the GCL boundaries; and GCL from RNFL to the inner nuclear layer boundaries.

Biased examinations were rejected or manually corrected if the algorithm had obviously failed.

2.7. Histology

Animals were euthanized under humanity conditions with an intracardiac injection of sodium thiopental (25 mg/ml) under general anesthesia and eyes were immediately enucleated. Paraffin-embedded eyes were sectioned (5 µm) along the eye axis, deparaffinized and rehydrated. After several washes in phosphate-buffered saline (PBS), sections were incubated overnight at 4 °C with mouse anti-Brn3a (Santa Cruz Biotechnology, Heidelberg, Germany) at 1:50 dilution. After washing the sections in PBS,

slides were incubated for 2 hours at room temperature with biotinylated horse anti-mouse at 1:50 dilution (Vector Laboratories, Burlingame, CA, USA). Then, incubation with ABC-HRP (Thermo Fisher Scientific, Waltham Massachusetts, USA) at 1:50 dilution at room temperature was performed. Finally, sections were stained with DAB (Sigma-Aldrich) for 3 minutes and counterstained with Harrys Hematoxylin (Sigma-Aldrich) for 20 minutes at room temperature. Ganglion cells were counted in radial sections of the retina, along 2 mm of a linear region of the ganglion cell layer, at four areas, two in both sides of the optic nerve head. Images were analyzed by an operator blinded to treatment groups. Statistical analysis of the number of ganglion cells was conducted in R (v. 3.6.0) using a paired t-test. The results are shown as mean ± SEM. Values of $p < 0.05$ were considered statistically significant. Procedural immunohistochemistry controls were carried out by omitting the primary antibody in a sequential tissue section.

To analyze the anterior segment of the eye and the location of the microspheres, sections were deparaffinized and stained with Hematoxylin/Eosin or only with Harris Hematoxylin and then observed by differential interference contrast (Nomarski) microscopy. In addition, paraffin sections were stained with the fluorescent dye BODIPY (Invitrogen, Carlsbad, CA, USA) at 1:50 dilution and nuclear counterstained using Hoechst (Sigma-Aldrich) at 1:100 were assessed. For fluorescence image acquisition, a laser scanning confocal microscope (TCS SP5; Leica Microsystems GmbH, Heidelberg, Germany) was used. Image analyses were performed with Fiji (Schindelin et al., 2012).

2.8. Statistical analysis

Data were recorded in an Excel database and statistical analysis was performed using SPSS software version 20.0 (SPSS Inc., Chicago, IL). The Kolmogorov-Smirnov test was used to assess sample distribution. Given the parametric distribution of the data, Student's t-test was used to evaluate the differences between eyes, and a paired Student's t-test was used to compare the changes recorded in each eye over the study period. All values were expressed as means ± standard deviations. Values of $p < 0.05$ (expressed as *) were considered to indicate statistical significance. The Bonferroni correction for multiple comparisons was also calculated to avoid a high false-positive rate. The level of significance for each variable was established according to Bonferroni calculations (expressed as $^{\#}$).

3. Results

3.1. Production yield

MSs showed a production yield of 55.14% for the selected 20–10 µm fraction. The particle size distribution resulted unimodal with a mean particle size value of 14.81 ± 0.30 µm.

3.2. Encapsulation efficiency

The dexamethasone encapsulation efficiency measurements lead to 79.13 ± 2.64% of the initial drug included during the preparation procedure (71.94 ± 2.40 µg DX/mg MSs). Unfortunately, the fibronectin lability made impossible the real quantification of the loaded protein.

3.3. Morphological evaluation

SEM images evidenced the presence of spherical and regular-sized MSs with surficial porous and slightly rough surfaces. Moreover, the presence of internal porous was confirmed by TEM images, typically due to the double emulsion method employed for MSs elaboration (Figure 2).

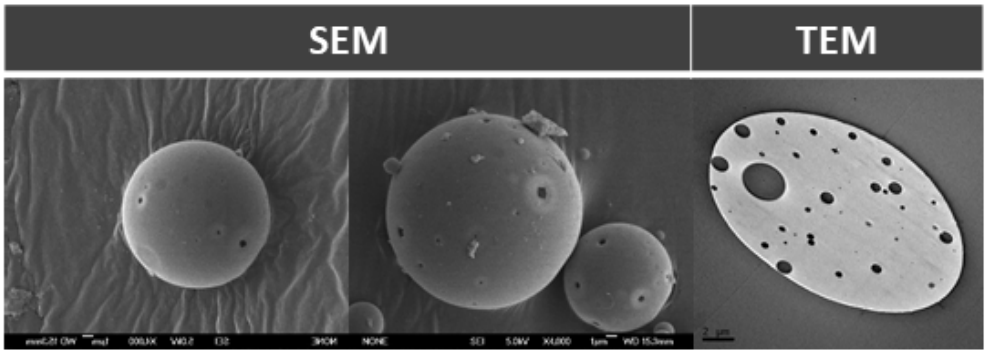

Figure 2. Dexamethasone-fibronectin co-loaded PLGA microspheres morphology. Scanning (left and centre) and transmission (right) electron microscopy images.

3.4. *In vitro* release studies

Both dexamethasone and fibronectin *in vitro* release profiles showed a multiphasic shape typically observed for PLGA microspheres.

Figures 3 and 4 show the cumulative amount of both fibronectin and dexamethasone per mg of MSs released versus time. In addition, to offer more complete information,

values of the accumulated percentage of transfer are also provided throughout the graph.

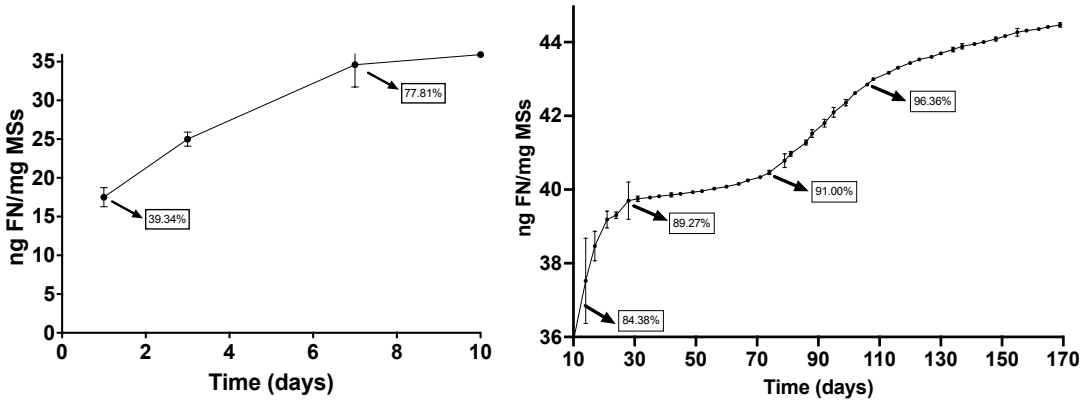

Figure 3. Cumulative *in vitro* release of fibronectin from dexamethasone-fibronectin co-loaded PLGA microspheres.

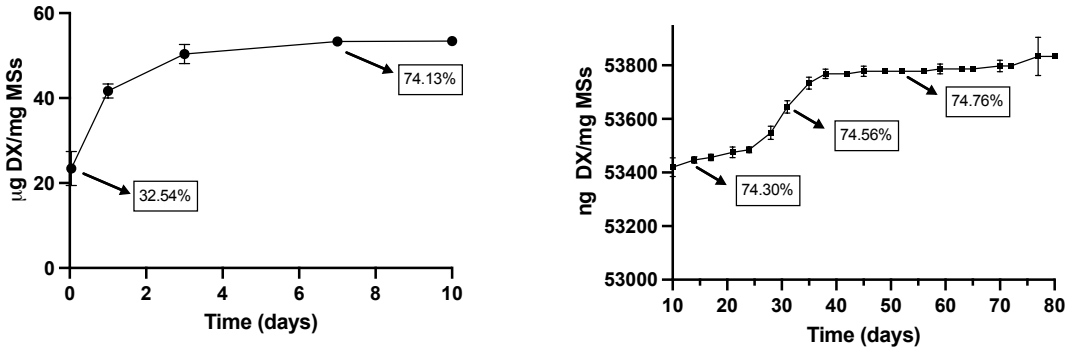

Figure 4. Cumulative *in vitro* release of dexamethasone from dexamethasone-fibronectin co-loaded PLGA microspheres.

Fibronectin underwent an initial rapid release of 35.90 ng/mg MSs in the first 10 days. After that, a sequence of rapid and slow-release profiles was detected: from day 10 to day 28, the profile shows a release of 0.211 ng FN/mg MSs/day, followed by a slower release of 0.017 ng FN/mg MSs/day from day 28 to 74. Next, from day 74 to 108, a second faster release of 0.074 ng FN/mg MSs/day was found and finally from day 108 to the end of the study the release rate was 0.024 ng FN/mg MSs/day.

Dexamethasone also showed a high initial release of 53.42 µg/mg MSs in the first 10 days and, as mentioned before, a subsequent slow but continuous release of

different releases rates, characteristic of PLGA microspheres. From day 10 to 28, the *in vitro* release presented a slow phase with a rate of 7.22 ng DX/mg MSs/day, followed by a faster release of 22 ng DX/mg MSs/day from day 28 to 38 and the final release rate was slower, 1.54 ng DX/mg DX/day from day 38 to day 77. No dexamethasone was released from this time point.

3.5. Ophthalmological signs and intraocular pressure

Forty of 43 animals used, did not show infection, intraocular inflammation, cataract formation or retinal detachment and the ocular surface was well preserved. The MSsDexaFibro showed a tendency to localize at the superior iridocorneal angle, due to their lower density compared to aqueous humor and this disposition allowed a clear visual axis. One animal developed corneal leucoma and other an iridocorneal synechia that did not preclude proper testing and follow-up; however, another third rat developed a focus of vitreoretinitis so this animal was discarded and its results were not used.

This model caused a progressive IOP increase and ocular hypertensive (OHT) eyes (>20 mmHg) over the study. The injected right eye (RE) showed higher measurements than the non-injected left eye (LE) up to 6 weeks ($p < 0.05$), but then both eyes similarly increased up to 24 weeks. Both eyes reached OHT at week 11 and fluctuations were observed over the study (Figure 5a). The highest percentage (88.9%) of OHT eyes was reached at 20 weeks (Figure 5b). Most rats experienced an IOP increase (in average) according to a medium corticosteroid response (between 6 and 15 mmHg), (Figure 5c) with constant lineal tendency on corticosteroid response in the injected eyes. Very few animals were high corticosteroid responders (>15 mmHg increase).

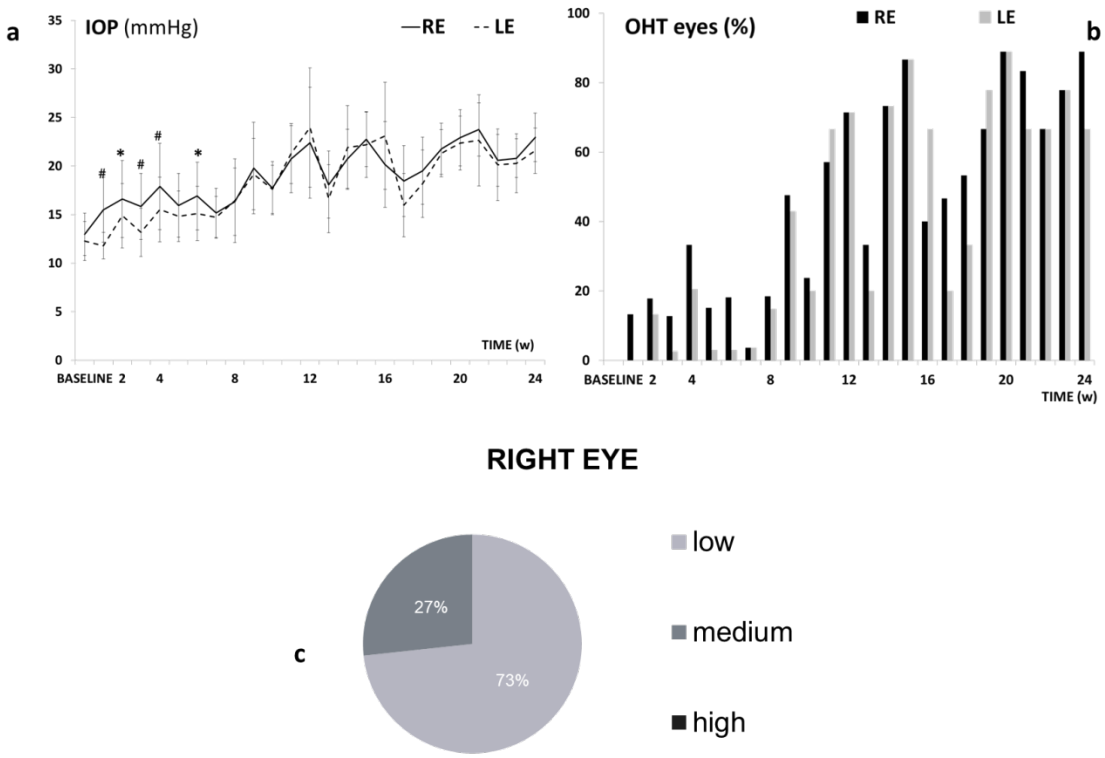

Figure 5. Intraocular pressure in the dexamethasone-fibronectin co-loaded microsphere (MSsDexaFibro) model. a: Intraocular pressure curve over 6 months. b: Percentage of ocular hypertensive eyes (>20mmHg). c: Percentage of corticosteroid response and tendency in right eyes over the study. d: Averaged percentage of corticosteroid response in right eyes. Low: <6 mmHg increase; medium: 6-15mmHg increase; high: >15mmHg increase. Abbreviations: IOP: intraocular pressure; RE: right eye; LE: left eye; w: week; OHT: ocular hypertension; %: percentage *: p<0.05; #: p<0.02 (Bonferroni Correction for multiple comparisons).

3.6. *In vivo* neuroretinal examination

3.6.1. Electroretinography

The induced RE showed a tendency to longer latency signals in bipolar cells (b-wave) and smaller amplitudes in photoreceptors (a-wave) and bipolar (b-wave) cells compared to LE and over the study, but did not reach statistical differences with scotopic ERG conditions. However, the light-adapted PhNR protocol that specifically measures the retinal ganglion cells (RGC) activity detected smaller amplitudes ($p < 0.05$) in the injected RE, which it involves lower number of functional RGC (Figure 6).

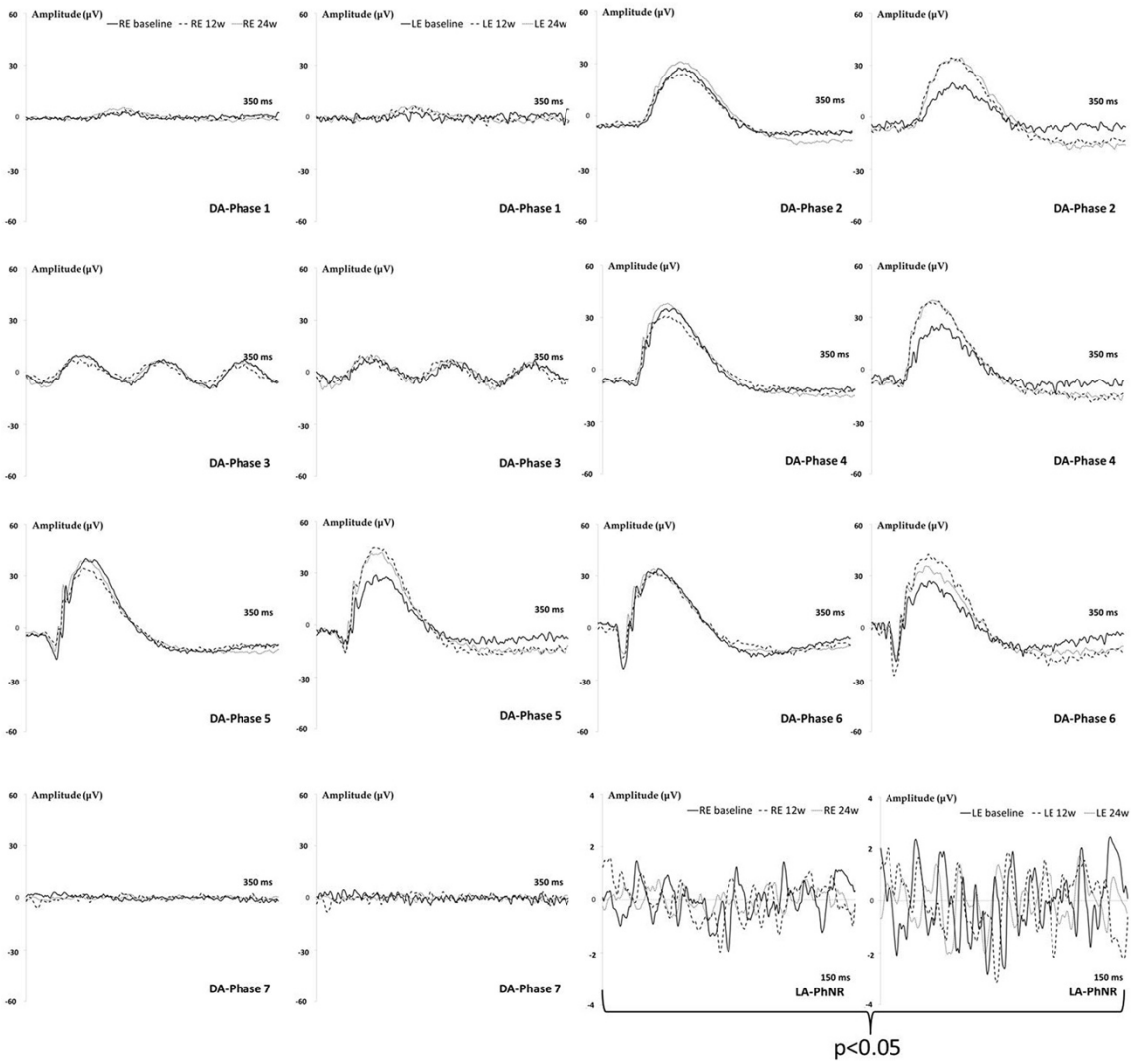

Figure 6. Neuroretina functionality, measured by dark- and light-adapted electroretinography (ERG), in the dexamethasone-fibronectin co-loaded microspheres (MSsDexaFibro) model over 6 months of follow-up. MSsDexafibro: microspheres loaded with dexamethasone and fibronectin; RE: right eye; LE: left eye; w: week; DA: dark-adapted; LA: light-adapted; μV: microvolts; ms: milliseconds.

3.6.2. Optical coherence tomography

All the three R, RNFL and GCL protocols showed a progressive decrease in neuroretinal thickness over the study, with very few OCT sectors showed statistical significance ($p < 0.05$) between RE and LE, a tendency to lower thickness measurements was detected in the injected RE. Full retinal thickness (R) experienced the highest decrease followed by RNFL and GCL and it occurred in both eyes. And an increasing fluctuation was detected at week 12 especially in injected RE (Figure 7a). However, when the percentage of thickness loss over time was analyzed, the RNFL parameter showed the highest percentage loss at every time point explored and on average. It was followed by the GCL and finally the full retinal thickness. Injected RE showed a lower percentage loss of thickness in RNFL and GCL than the non-injected LE (Figure 7b).

a

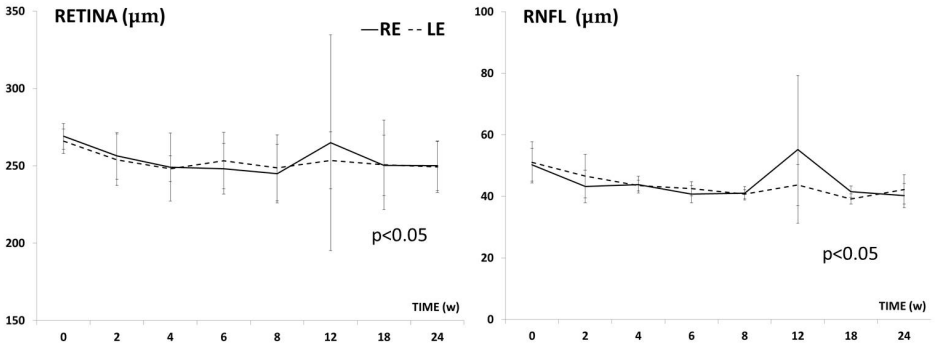

Ms Dexa Fibro (OCT µm)	RETINA		RNFL		GCL	
TIME (W)	RE	LE	RE	LE	RE	LE
0	269.05	265.89	50.26	51.04	26.27	26.42
2	256.40	253.96	43.23	46.59	25.94	24.98
4	249.20	248.20	43.81	43.54	24.83	25.53
6	248.14	253.35	40.69	42.49	23.64	24.66
8	244.96	248.77	41.00	40.69	22.99	24.14
12	265.00	253.57	55.26	43.66	24.72	23.01
18	250.35	250.66	41.54	39.16	23.70	23.63
24	250.02	249.26	40.23	42.27	22.02	22.50

b

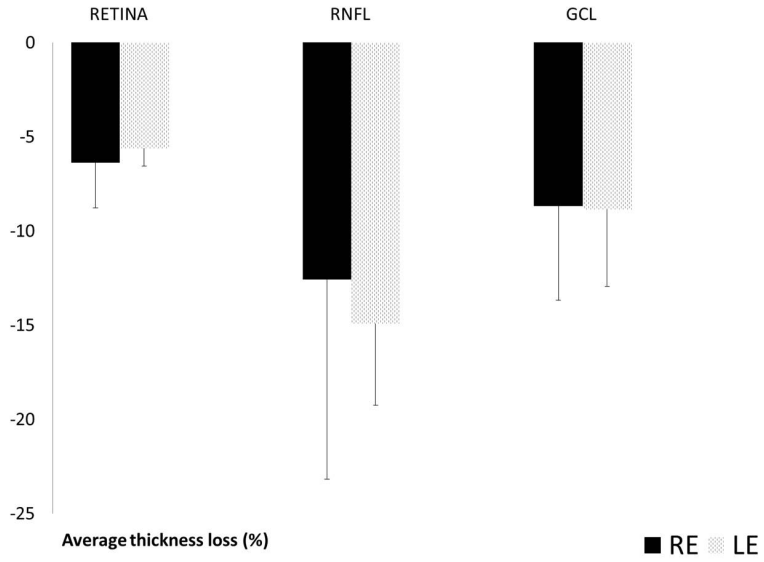

Figure 7. A. Neuro-retinal thickness in microns by OCT throughout 6-month follow-up. B. Average thickness percentage loss by OCT in microspheres co-loaded with dexamethasone and fibronectin (MSsDexaFibro) model up to 6-month follow-up. MSsDexaFibro: microspheres co-loaded with dexamethasone and fibronectin; RE: right eye; LE: left eye; OCT: optical coherence tomography; RNFL: Retinal Nerve Fiber Layer; GCL: Ganglion Cell Layer complex; average thickness in microns (µm); w: week; %: percentage.

The neuroretinal percentage loss by OCT sectors from RFNL, GCL and Retina was quantified, and the loss tendency was analyzed. The inferior sector in RNFL showed the most intense and frequent loss. In GCL the inner sectors showed bigger percentage loss

at any time explored in both eyes and the R experienced bigger loss in outer sectors with the STIN averaged loss trend (see Supplementary Figures S1–S3).

The average loss rate expressed in microns per mmHg and day extracted from all sectors was also quantified in both eyes and at all stages. Retina showed the highest loss rate followed by RNFL and finally GCL and the biggest loss rate occurred at early times. Moreover, both eyes lost similar quantity of microns in GCL thickness per every mmHg

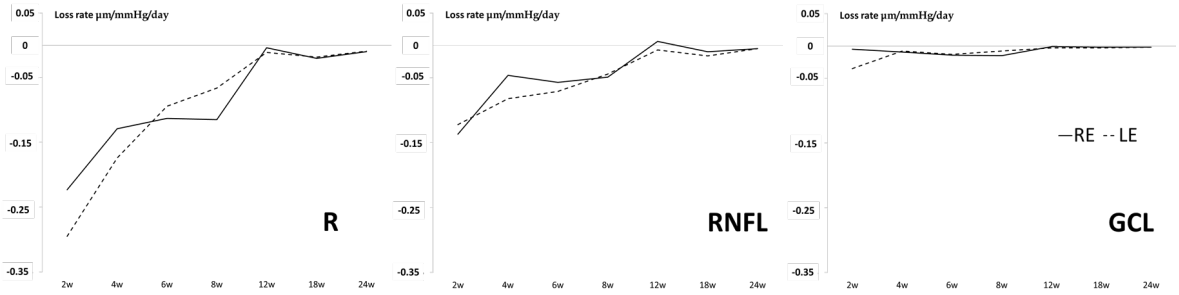

MsDexaFibro ALL SECTORS AVERAGE LOSS RATE (µm)/mmHg/day						
TIME	RETINA		RNFL		GCL	
	RE	LE	RE	LE	RE	LE
2w	-0.223	-0.295	-0.137	-0.122	-0.005	-0.035
4w	-0.129	-0.174	-0.046	-0.082	-0.0093	-0.008
6w	-0.113	-0.094	-0.057	-0.071	-0.014	-0.013
8w	-0.115	-0.066	-0.049	-0.044	-0.015	-0.008
12w	-0.004	-0.011	0.006	-0.007	-0.001	-0.003
18w	-0.020	-0.018	-0.010	-0.016	-0.002	-0.003
24w	-0.010	-0.009	-0.005	-0.005	-0.002	-0.002
AVERAGE	**-0.087**	**-0.095**	**-0.042**	**-0.049**	**-0.006**	**-0.010**

increased (Figure 8).

Figure 8. Neuro-retinal loss rate measured by optical coherence tomography (OCT) in the co-loaded with dexamethasone and fibronectin microspheres (MSsDexaFibro) model**.** MSsDexaFibro: microspheres co-loaded with dexamethasone and fibronectin; RE: right eye; LE: left eye; w: week; RNFL: Retinal Nerve Fiber Layer; GCL: Ganglion Cell Layer complex.

3.7. Pathological findings

The count of positive Brn3a cells along with four areas of the retina (Figure 9A), showed that the mean number of ganglion cells per linear mm of the retina was not significantly different in non-intervened left eyes in comparison to right eyes injected with dexamethasone-fibronectin microspheres ($p = 0.92$) (Figure 9B). However, fewer ganglion cells per linear mm of the retina were counted (10.12 ± 4.99) than in our previous model (12.16 ± 3.37) at 6 months (Rodrigo et al., 2021). In order to ascertain if the injected microspheres were located at the iridocorneal angle, they were analyzed using Hematoxylin/Eosin, Nomarski and fluorescent microscopy. The microspheres are

transparent, and they are not stained by Hematoxylin or Eosin, but its presence can be still appreciated in the sections (Figure 10A). The characteristic light refraction produced by the microspheres was used to readily identify them in paraffin sections using Normarski microscopy (Figure 10B). The staining of microspheres with the fluorescent BODIPY, that we previously have demonstrated is specific for PLGA (Garcia-Herranz et al., 2021), further confirmed that injected microspheres are hampered the iridocorneal angle and the trabecula meshwork (Figure 10C).

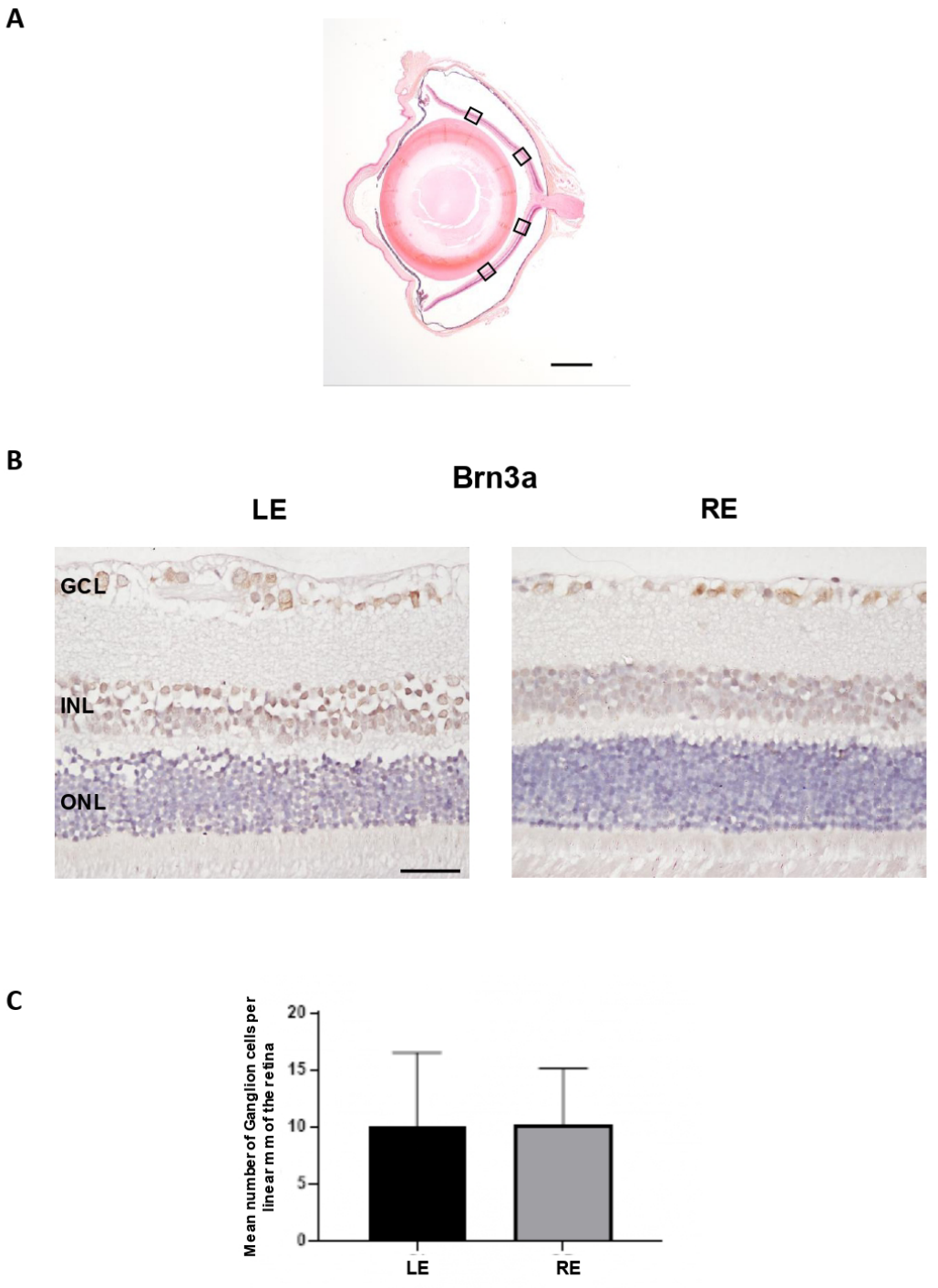

Figure 9. Ganglion cell analysis in glaucomatous eyes. A. Ganglion cells were counted in four areas (squares) of a radial section of the retina passing through the optic nerve. B. Two representative images of the retina marked with anti-Brn3a corresponding to a left non-intervened eye (LE) and a right eye (RE) injected with dexamethasone-fibronectin microspheres from the same animal. The mean number of ganglion cells per linear mm of retina was not different between non-intervened and injected eyes. GCL: Ganglion cell layer; INL: Inner nuclear layer; ONL: Outer nuclear layer. Scale bars: (A) 1mm, (B) 30 µm.

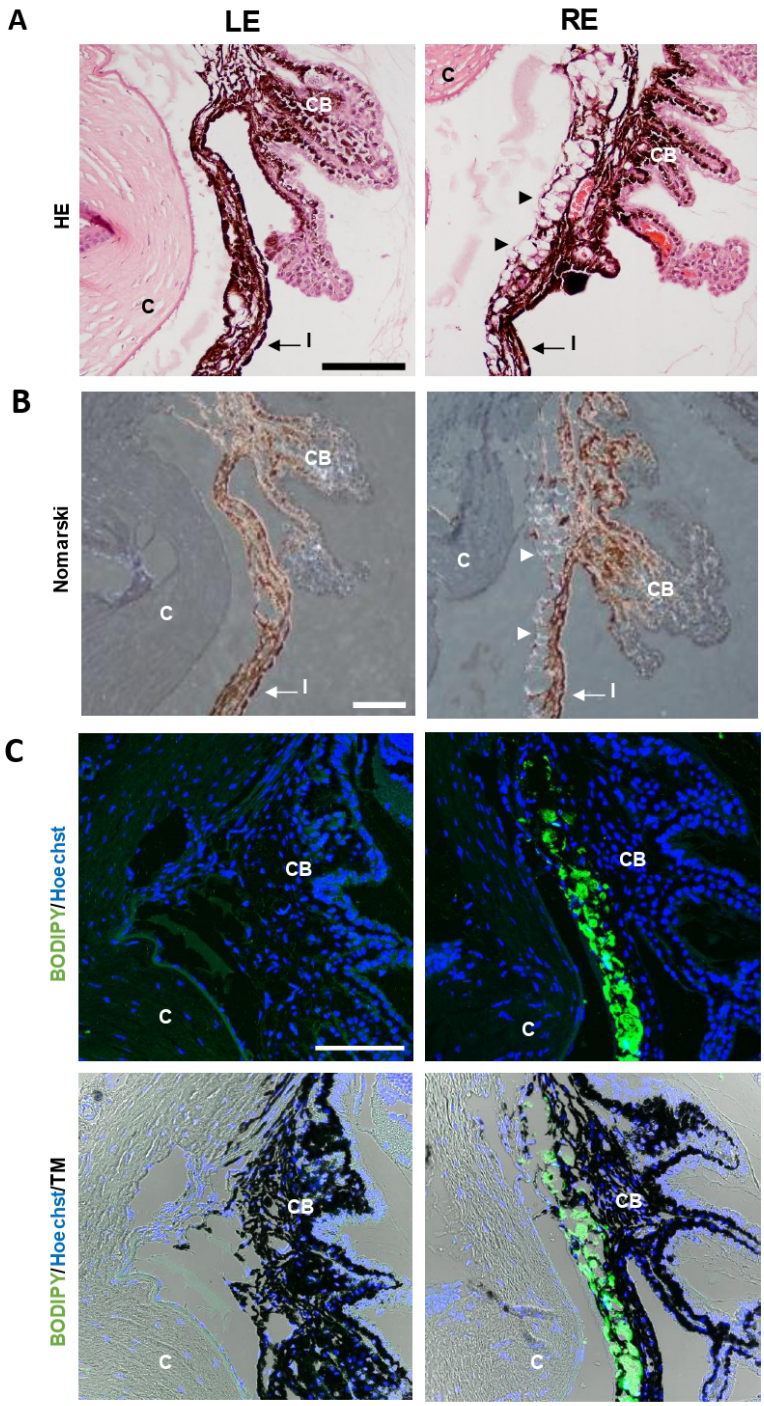

Figure 10. Detection of microspheres in injected eyes. A. Paraffin sections stained with Hematoxylin/Eosin exhibited the presence of the microspheres integrated into the iridocorneal angle (arrowheads), a finding never observed in the control ones. B. The characteristic light diffraction produced by microspheres using Nomarski microscopy (arrowheads) confirmed their presence in the iridocorneal angle of injected eyes. C. The Fluorescent Stain BODIPY (green) also showed the presence of microspheres hampering the iridocorneal angle and the trabecular meshwork. Nuclei were counterstained with Hoechst (blue). LE: left eye (non-intervened); RE: Right eye (dexamethasone-fibronectin microsphere injected). CB: Ciliary body; I: Iris; C: cornea; TM: Transmission mode. Scale bars: 100 µm.

Fibronectin plays a major role in the adhesion of many cell types, in fact, fibronectin is considered as the extracellular glue (Zollinger & Smith, 2017). Fibronectin has a RGD loop that is a promiscuous site for many cellular integrins, such as α5β1, α3β1, α8β1, and αvβ3 (Pankov & Yamada, 2002). This could explain how, unlike our other models where microspheres without fibronectin were injected (Garcia-Herranz et al., 2021; Rodrigo et al., 2021), focal adhesions were observed between the iris and the cornea (Figure 11). These synechiae are established through the fibronectin-containing microspheres and that would glue the iris and cornea (Figure 11). Obviously, these synechiae will modify the flow of the aqueous humor and therefore its reabsorption at the level of the trabecular meshwork.

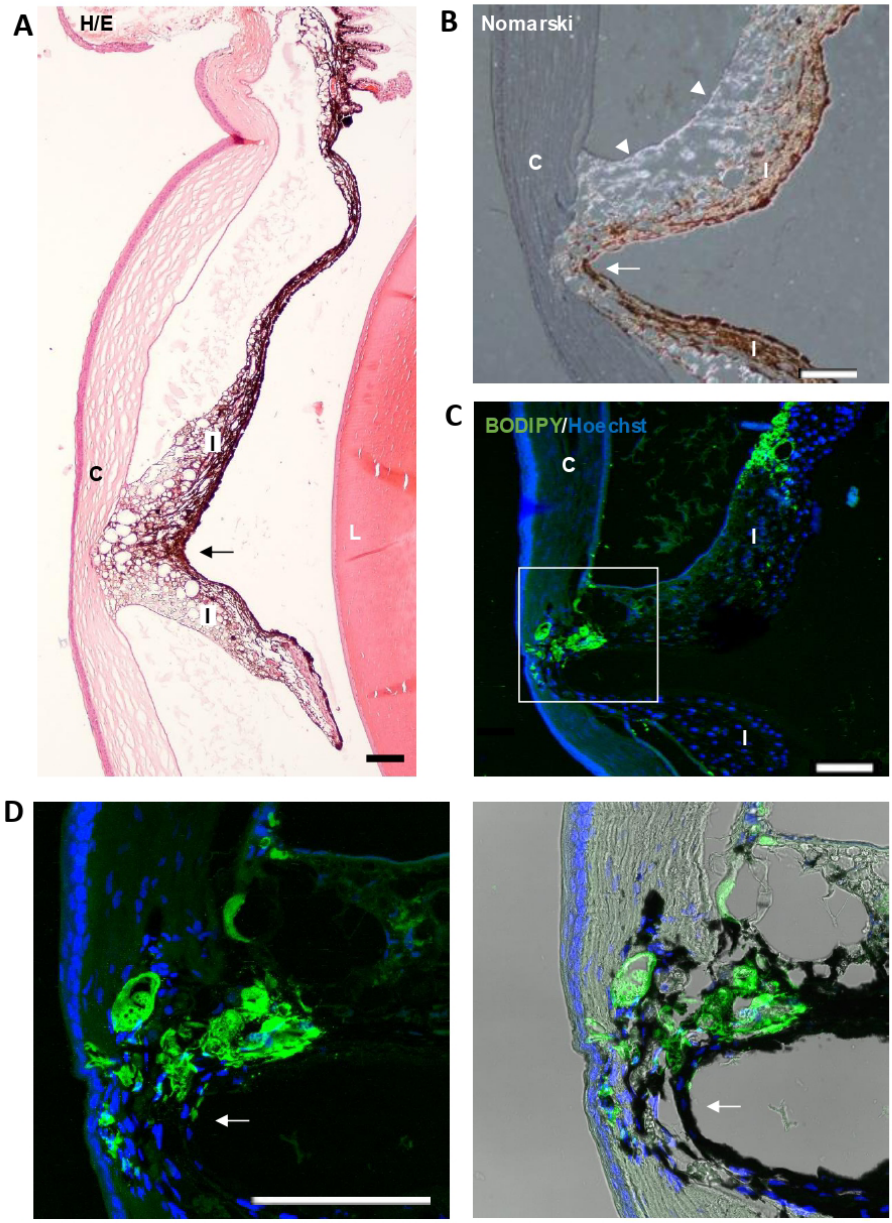

Figure 11. Iridocorneal synechias were observed in injected eyes (arrows). A. General view of a synechia between iris and the cornea. B. Using Nomarski microscopy, the diffracted light from the microspheres (arrowheads) was observed between the cornea and iris at the level of the focal contact between them. C. Staining with BODIPY (green) confirmed the presence of microspheres gluing the cornea and iris. Nuclei were counterstained with Hoechst (blue). C: cornea; I: Iris; L: lens; TM: Transmission mode. Scale bars: 100 µm.

4. Discussion

The model presented in this work combines some of the strategies previously used in other rodent models of glaucoma, such as physical blockage of the trabecular meshwork, the administration of corticosteroids or the increased deposition of the protein fibronectin in the extracellular matrix of the trabecular meshwork (Roberts et al., 2020; Rodrigo et al., 2021). It was decided to co-release dexamethasone and fibronectin as the former stimulates extracellular matrix production and inhibits debris clearance (Dismuke et al., 2016; Zeng et al., 2020) and on the other hand, fibronectin deposition has been associated with ocular aging and glaucoma progression by playing an important role in trabecular meshwork occlusion in human glaucoma (Babizhayev & Brodskaya, 1989; Kasetti et al., 2017). In the model that we present, a combination of dexamethasone with fibronectin in PLGA microspheres is performed. This model progressively increased IOP over 24 weeks, reaching ocular hypertension at 11 weeks. There was a slight initial increase in IOP after induction, coinciding with the physical blockade of MSs at the iridocorneal angle and the first release of the encapsulated substances. Thereafter, IOP slowly increased and was maintained, coinciding with lower load release. It was probably due to extracellular matrix production by the constant presence of dexamethasone and the deposition of the protein fibronectin.

Microencapsulation and subsequent simultaneous release of more than one compound in modified release systems represent a technological challenge that has been developed in recent years as a very interesting strategy, for example, to be able to diminish the amount of polymer injected (Arranz-Romera et al., 2019; 2019). In order to encapsulate both compounds in the same formulation, it was decided to include each of them in the emulsion phase in which they were more soluble, so the protein was incorporated into the internal aqueous phase while dexamethasone was incorporated into the organic phase. In the recent past, there have been some efforts to encapsulate two or more substances in particles for different therapies. Although studies of multiloaded nanoparticles are more frequent (Jamil et al., 2019; Sokol et al., 2019; Madani et al., 2020), multiloaded microencapsulation is also being explored (Dutt & Khuller, 2001; Román et al., 2014; Shi et al., 2014; Baek et al., 2017). The main challenge of incorporating several substances is to accomplish a controlled release from those

microsystems. In this sense, our research group has successfully achieved the microencapsulation and sustained release of more than one protein, the combination of proteins and low molecular weight compounds or even a tri-delivery of low molecular weight molecules using the single emulsion evaporation method (García-Caballero et al., 2018; Arranz-Romera et al., 2019; 2021). In the present work, we have achieved the release of both substances in a controlled and slow delivery for several months. Regarding double emulsions, works of co-encapsulation of two substances in the different phases of the emulsion are not very numerous. Qiao et al reported the co-microencapsulation of two antibiotics of different polarity by double emulsion, including each compound in the more soluble phase. They observed a slow release of both substances and suggested that the encapsulation of the hydrophilic compound may be enhanced with the addition of the hydrophobic one (Qiao et al., 2019). The same strategy has been successfully used in the present work; however, the potential benefit of the presence of the hydrophobic compound on the microencapsulation of the hydrophilic one has not been yet explored.

Obtaining models of neurodegenerative diseases of the retina is a challenge in the field of ophthalmology (Guidoboni et al., 2020). In the case of glaucoma, there are several animal models, among them, rodent animal models that are more convenient. Different mechanisms to create rat glaucoma models have been studied, as can be seen in Table 1, however, none of them achieves a slow and progressive degeneration of the retina as occurs when the disease develops in humans (Pang & Clark, 2020). In addition, neither of these rat models get an IOP increase for a long period of time. IOP-elevation induced glaucoma models (Dey et al., 2018) using non-biodegradable and biodegradable microspheres (Morgan & Tribble, 2015; Rodrigo et al., 2021) require periodic injections into the anterior chamber of the eye to maintain elevated pressures over prolonged study times. This fact increases the variability of results among different research groups, as well as the disadvantages derived from interventionism on the animal (Biswas & Wan, 2019). The present model, being single injection and technically simpler than other inducer models (Morrison et al., 2015; Dey et al., 2018), can be used by different research groups allowing for a more reliable comparison of treatments and therapies. It also improves animal welfare with reduced handling stress, reduces ocular

complications such as infections or PLGA toxicity (Dossarps et al., 2015; Park, 2017; Zhao et al., 2017); as well as is more cost-efficient and generates less environmental impact (Haines et al., 2017).

Table 1. Pressure dependent glaucoma rat models.

Authors group and publication date	Mechanism of model creation	Sample size	Control eye	Average time for IOP to rise	Average time length of IOP increase	Average magnitude of IOP elevation from baseline	Feature of histology for retina at the study end
Urcola et al. (2006)	Intracameral injection microbead	N = 6	Contralateral eye andControl group	5 weeks	25 weeks	15 mmHg IOP increase	23% RGC death
Urcola et al. (2006)	Intracameral injection microbead with viscoelastic material	N = 4	Contralateral eye and Control group	6 weeks	24 weeks	20 mmHg IOP increase	27% RGC death
Samsel et al. (2011)	Intracameral injection of magnetic microbead	N = 61	Contralateral eye	After injection	12.8–27 days.	6 mmHg IOP increase	36% RGC cell loss
Moreno et al. (2005)	Intracameral administration of viscous agents	N = 45	Contralateral eye	Not specified	10 weeks	8–10 mmHg IOP increase	Significant RGC loss and damage in ON axons. Decrease in scotopic ERG activity
Morrison et al (1997) and Jia et al (2000)	Sclerosis of the outflow pathway by episcleral injection of hypertonic saline	N = 20	Contralateral eye	10 days	7–36 days	7–28 mmHg IOP increase	10–100% ON axon loss
Ueda et al (1998), WoldeMussie et al., 2001)Levkovith-Verbin et al. (2002)	Sclerosis of the outflow pathway by laser photocoagulation of outflow pathway	N = 10	Control group	1 week	5 weeks	6–24 mmHg IOP increase	50–70% ON axon loss
Shareef et al. (1995) Laquis et al. (1998)	Cautery of extraocular veins	N = 18	Contralateral eye	After injection	6 weeks–2.5 months	13–47 mmHg IOP increase	4% RGC loss per week
Sun et al. (2011)	Transient/intermittent IOP elevation by corneal limbus compression	N = 31	Contralateral eye	After compression	7 hours	25 mmHg IOP increase	52% RGC loss at 28 days after the insult
Morrison et al (2016)	Transient/intermittent IOP elevation by controlled elevation of IOP (CEI)	N = 122	Naïve group	After the insult	10 days	48 mmHg IOP increase	lesions in 83% of ON
Shepard et al (2010)	Transduction of the TM with glaucoma related genes by TGFβ2	N = 7	Contralateral eye	5 days	12 days	10–15 mmHg IOP increase	Not reported any potential RGC and ON axon loss.

Our model showed that the most affected parameter by OCT was RNFL followed by inner sectors of GCL and finally full retina, which may reflect retrograde degeneration (Lawlor et al., 2018). Furthermore, when considering the GCL-RNFL component, the

greatest standardized loss per mmHg was suffered by RNFL, again showing that the hypertensive noxa exerts early and greater damage to axonal structure (Howell et al., 2007; Guo et al., 2010). At earlier times, the Inferior and Nasal sectors of RNFL seem to be the most vulnerable to damage, and at later times they become ISNT (INFERIOR > SUPERIOR > NASAL > TEMPORAL glaucoma rule) due to the possible influence of dynamic pathogenic changes. An example is the important fluctuation at 12 weeks of the study observed in this model of glaucoma as well as observed in our previous one and in healthy animals linked to neuroplasticity and glia involvement (Rodrigo et al., 2020; 2021; 2021). In the GCL, the sectors most affected on average were the inner sectors TSN (TEMPORAL > SUPERIOR > NASAL), which coincide with those with the highest density of retinal ganglion cells (RGC) (Salinas-Navarro et al., 2009; Guo et al., 2010). Glaucoma mainly affects the RGCs, and their decreased functionality has been detected in photopic conditions with the PhNR or pattern ERG tests, and scotopic conditions with pSTR (Porciatti, 2015; Wilsey et al., 2017). Furthermore, outer retinal cells changes have also been detected in scotopic conditions with reversible high IOP (approx. 35 mmHg) (Choh et al., 2016), and in patients with late glaucoma (Graham et al., 1995). In the present model, where the damage occurred gradually, RGC dysfunction with a statistically significant decrease in PhNR was detected early (12 weeks); and coinciding with mild hypertensive levels (20–22 mmHg) a limitation of outer retinal function was also found at early-intermediate stages.

A bilateral neurodegeneration after induction of unilateral OHT has been already observed in several animal models (Sapienza et al., 2016; de Hoz et al., 2018; Rodrigo et al., 2021; 2021). This can be explained because the glial activation, characteristic of glaucomatous eyes, spreads through the visual pathway, so the degenerative factors could, in turn, activate the glia of the contralateral eye (Howell et al., 2007), producing retrograde damage and also creating an imbalance in pressure at the optic nerve head (Jóhannesson et al., 2018). In addition, in other works a gradual increase in IOP in the non-induced contralateral eye has been also detected (Roubeix et al., 2015; Sapienza et al., 2016; Rodrigo et al., 2021; 2021), as in our case. In fact, the use of the contralateral eye as a control is not recommended in glaucoma animal models.

The present study shows a rat model of glaucoma with ocular hypertension that is easy to induce; with a high likelihood of being reproducible, since only one induction and nature-modifying intervention is performed; biologically plausible with minimal side effects, as the injected material is biocompatible as it degrades to CO_2 and H_2O in the Krebs cycle (Martins et al., 2018) and its trabecular meshwork modifying compounds (dexamethasone and fibronectin) are present features of steroid-induced glaucoma and primary open-angle glaucoma (Rozsíval et al., 1981; Babizhayev & Brodskaya, 1989; Kasimov & Aghaeva, 2017). This model tries to mimic then the pathophysiology of human glaucoma, with predictable IOP increase and progressive neuroretinal loss, by avoiding rapid increases in OHT and severe neuroretinal loss (Agarwal & Agarwal, 2017). All this fulfills the characteristics of an ideal model and allows for long-term studies (Biswas & Wan, 2019).

The animal model presented in this work is a clear example of how pharmaceutical technology can help other disciplines to achieve optimized results by joining forces. While the usual employ of controlled drug release systems is focused on the treatment of pathologies, we present in this paper another important utility of sustained-release systems, in this case not to correct damage to the body but to cause it. The use of modified-release systems to obtain animal models is very poorly developed yet but, as observed in this work, it presents enormous potential. Regarding this idea and consistent with a lower total dose of dexamethasone than that used in our previous model, mostly mild levels of corticoresponse were found. But, a similar % of rats (approx. 90%) developed OHT, and even fewer ganglion cells per linear mm of retina (10.12 ± 4.99 vs 12.16 ± 3.37) were counted at 6 months (Rodrigo et al., 2021). This supports the important role of fibronectin in the development of OHT.

Neuroprotective therapies aim to protect neurons from secondary degeneration, already described in the introduction, which is the true trigger for the amplification of neuronal degeneration in chronic retinopathies (Cheung et al., 2008). Therefore, in order to correctly evaluate neuroprotective therapies, it is necessary to start from experimental animals with healthy retinas and that these retinas slowly degenerate, as occurs in human retinal chronic pathologies (Morrison et al., 2011). The rat model that is presented in this work would allow this type of study since, by achieving a very

progressive ocular hypertension and sustained over time, the degeneration of the retina is also so. In addition, one of the main problems of the *in vivo* evaluation of intraocular drug delivery systems is that it is very difficult to demonstrate the potential of the system when applied on retinas as degenerated as those that appear in most animal models of glaucoma (Nadal-Nicolás et al., 2016; Rodrigo et al., 2021). In this sense, our animal model, by offering a prolonged degeneration of the retina over at least 6 months, would be a very useful candidate to evaluate this type of modified release system. In the present model, only an initial injection is needed to produce the sustained damage and, furthermore, this injection takes place in the anterior chamber of the eye, without any other structure of the eye being affected. Thus, the intravitreal space remains intact to test any modified release system for long periods.

Concerning the limitations of this work and future studies, (I) Due to the lability of fibronectin, encapsulation could not be quantified and therefore the actual amount of fibronectin injected is unknown. However, *in vitro* release was in the order of nanograms, much lower than *in vivo* results of fibronectin quantifications in the aqueous humor of glaucoma patients (Kim et al., 1992), which we did not perform in our study in order not to alter the model by adding other puncture and maintaining eye homeostasis as much as possible; (II) We have not analyzed the differences by sex, even when its involvement is linked to immune-mediated pathologies (Desai & Brinton, 2019; Rodrigo et al., 2021) and glaucoma; (III) It was neither evaluated the potential immune role of the protein fibronectin nor the anti-inflammatory effect of dexamethasone on it (Hernandez et al., 2020; Mzyk et al., 2022) and that it would be interesting to study in future works; (IV) Finally, glaucoma is an aged-link pathology, and the rats were in their childhood at the start of the study, so results could deviate from translational human interpretation.

In conclusion, a new chronic glaucoma animal model was created by a single injection of PLGA co-loaded MSsDexaFibro very similar to open-angle glaucoma. This chronic rat model would have an important impact in ophthalmology, so it allows long periods of study of this pathology, in pharmacology because it could be used to evaluate the neuroprotective activity of active compounds and also in pharmaceutical technology, so

it could allow the correct evaluation of the efficacy of sustained intraocular drug delivery systems.

Additional information

Funding

This work was supported by Rio Hortega Research Grant M17/00213, PI17/01726, PI17/01946 (Instituto de Salud Carlos III), Grants MAT2017-83858-C2-2 and MAT2017-83858-C2-1 funded by MCIN/AEI/10.13039/501100011033 and by 'ERDF A way of making Europe', Grants PID2020-113281RB-C21 and PID2020-113281RB-C22 funded by MCIN/AEI/10.13039/501100011033. A.A.N thanks for the grant PRE2018-083951 funded by MCIN/AEI/10.13039/501100011033 and by 'ESF Investing in your future'. D.G.H. acknowledges to UCM-Santander fellowship (CT17/17-CT17-18). The sponsor or funding organization had no role in the design or conduct of this research. This work was funded by Spanish Ministry of Science and Innovation.

Supplementary Materials

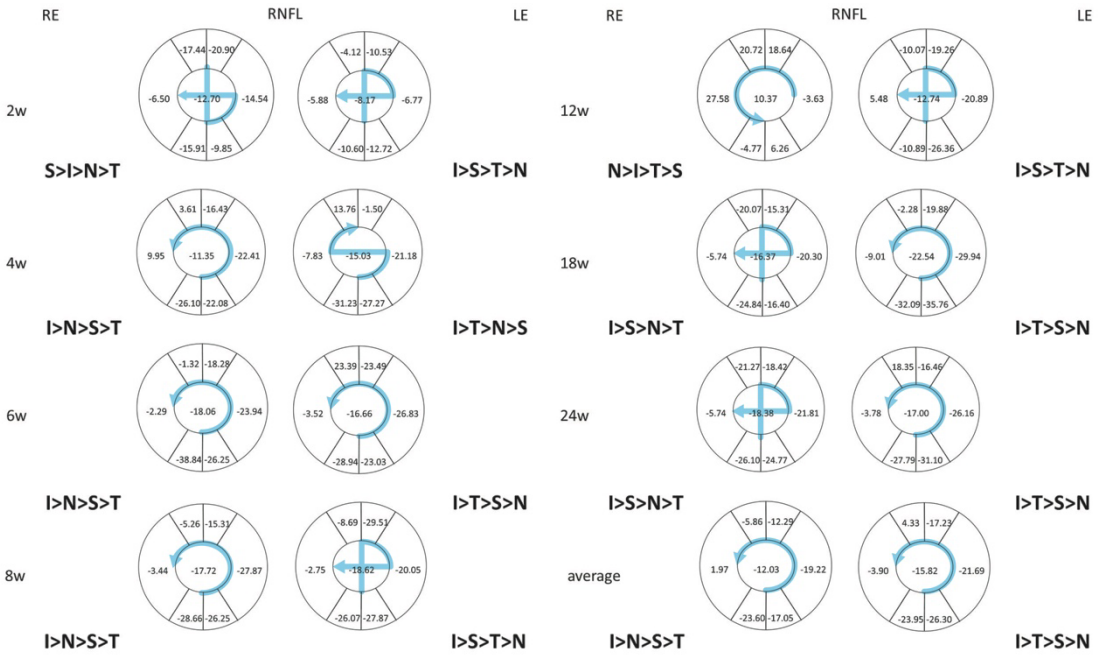

Supplementary figure 1. Retina nerve fiber layer (RNFL) percentage loss by optical coherence tomography (OCT) sectors and loss trend in MSsDexafibro model over 6 months. RE: right eye; LE: left eye; w: week; TV: total volume; S: superior; I: inferior; N: nasal; T: temporal.

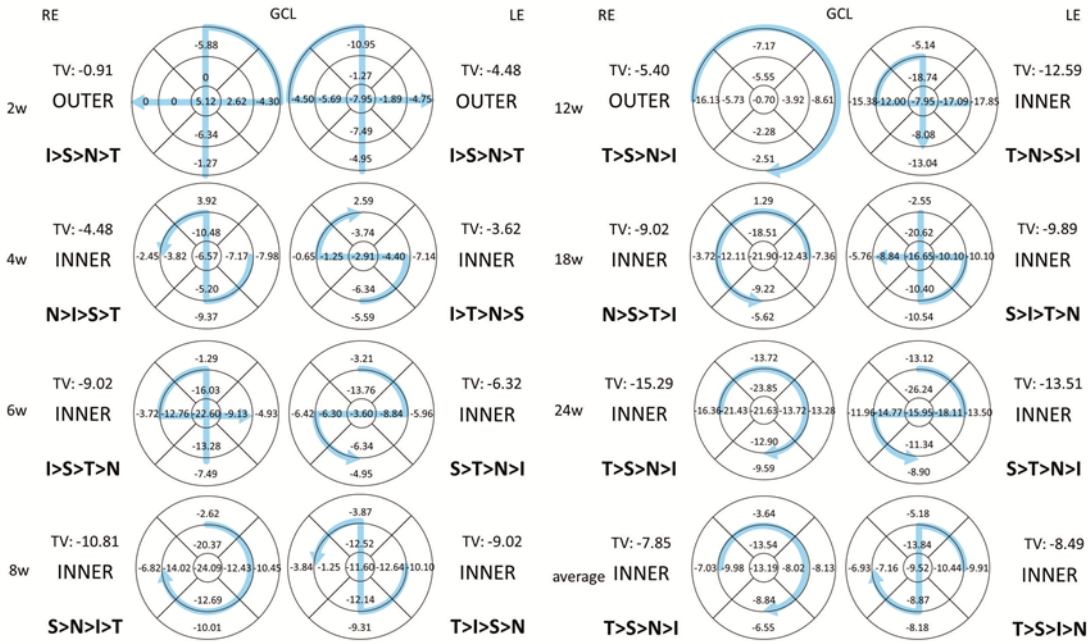

Supplementary figure 2. Ganglion cell layer (GCL) percentage loss by optical coherence tomography (OCT) sectors and loss trend in MSsDexafibro model over 6 months. RE: right eye; LE: left eye; w: week; TV: total volume; S: superior; I: inferior; N: nasal; T: temporal.

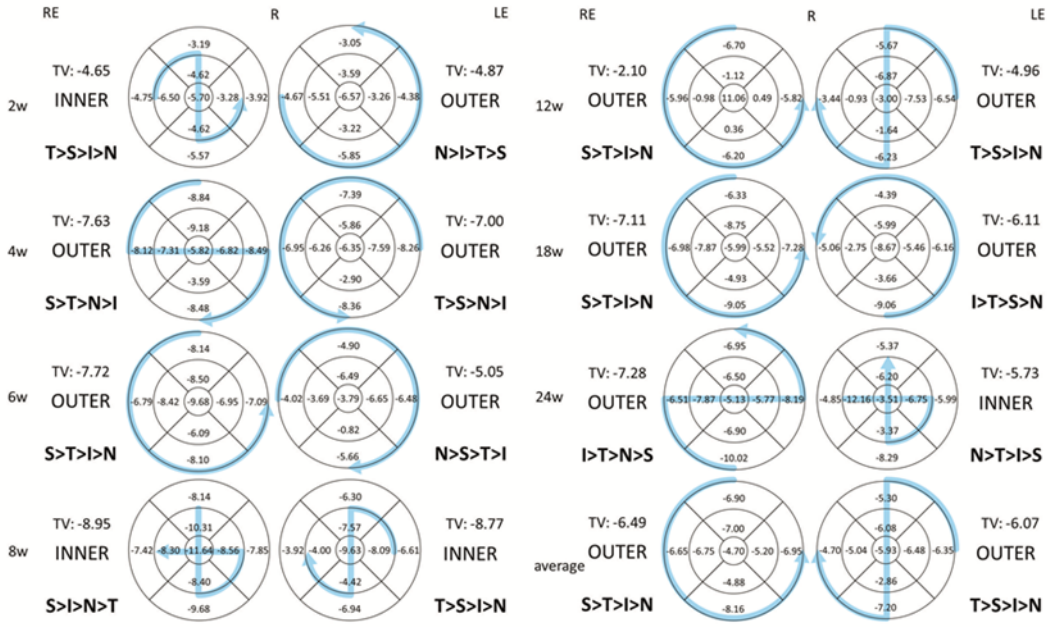

Supplementary figure 3. Retinal percentage loss by optical coherence tomography (OCT) sectors and loss trend in MSsDexafibro model over 6 months. RE: right eye; LE: left eye; w: week; TV: total volume; S: superior; I: inferior; N: nasal; T: temporal.

5. References

Agarwal R, Agarwal P. (2017). Rodent models of glaucoma and their applicability for drug discovery. Expert Opin Drug Discov 12:261–70. https://doi.org/10.1080/17460441.2017.1281244.

Anderson DR. (2003). Collaborative normal tension glaucoma study. Curr Opin Ophthalmol 14:86–90.

Arranz-Romera A, Davis BM, Bravo-Osuna I, et al. (2019). Simultaneous co-delivery of neuroprotective drugs from multi-loaded PLGA micro-spheres for the treatment of glaucoma. J Control Release 297:26–38.

Arranz-Romera A, Esteban-Pérez S, Garcia-Herranz D, et al. (2019). Combination therapy and co-delivery strategies to optimize treatment of posterior segment neurodegenerative diseases. Drug Discov Today 24:1644–53.

Arranz-Romera A, Hernandez M, Checa-Casalengua P, et al. (2021). A safe GDNF and GDNF/BDNF controlled delivery system improves migration in human retinal pigment epithelial cells and survival in retinal ganglion cells: potential usefulness in degenerative retinal pathologies. Pharmaceuticals 14:50.

Asaoka R, Murata H, Yanagisawa M, et al. (2017). The association between photoreceptor layer thickness measured by optical coherence tomography and visual sensitivity in glaucomatous eyes. PLoS One 12:e0184064.

Ashimatey BS, King BJ, Swanson WH. (2018). Retinal putative glial alterations: implication for glaucoma care. Ophthalmic Physiol Opt 38:56–65. https://doi.org/10.1111/opo.12425.

Avotri S, Eatman D, Russell-Randall K. (2019). Effects of resveratrol on inflammatory biomarkers in glaucomatous human trabecular meshwork cells. Nutrients 11:984.

Babizhayev MA, Brodskaya MW. (1989). Fibronectin detection in drainage outflow system of human eyes in ageing and progression of open-angle glaucoma. Mech Ageing Dev 47:145–57.

Baek JS, Choo CC, Tan NS, Loo SCJ. (2017). Sustained-releasing hollow microparticles with dual-anticancer drugs elicit greater shrinkage of tumor spheroids. Oncotarget 8:80841–52.

Biswas S, Wan KH. (2019). Review of rodent hypertensive glaucoma models. Acta Ophthalmol 97:e331–340.

Cheung W, Guo LI, Cordeiro MF. (2008). Neuroprotection in glaucoma: drug-based approaches. Optom Vis Sci 85:406–16.

Choh V, Gurdita A, Tan B, et al. (2016). Short-term moderately elevated intraocular pressure is associated with elevated scotopic electroretinogram responses. Invest Ophthalmol Vis Sci 57:2140–51.

Clark AF, Wordinger RJ. (2009). The role of steroids in outflow resistance. Exp Eye Res 88:752–9.

Conlon R, Saheb H, Ahmed IIK. (2017). Glaucoma treatment trends: a review. Can J Ophthalmol 52:114–24. https://doi.org/10.1016/j.jcjo.2016.07.013.

Cuenca N, Fernández-Sánchez L, Campello L, et al. (2014). Cellular responses following retinal injuries and therapeutic approaches for neurodegenerative diseases. Prog Retin Eye Res 43:17–75.

de Hoz R, Ramírez AI, González-Martín R, et al. (2018). Bilateral early activation of retinal microglial cells in a mouse model of unilateral laser-induced experimental ocular hypertension. Exp Eye Res 171:12–29.

Desai MK, Brinton RD. (2019). Autoimmune disease in women: endocrine transition and risk across the lifespan. Front Endocrinol (Lausanne) 10:265.

Dey A, Manthey AL, Chiu K, Do CW. (2018). Methods to induce chronic ocular hypertension: reliable rodent models as a platform for cell transplantation and other therapies. Cell Transplant 27:213–29.

Dismuke WM, Klingeborn M, Stamer WD. (2016). Mechanism of fibronec-tin binding to human trabecular meshwork exosomes and its modulation by dexamethasone. PLoS One 11:e0165326.

Dossarps D, Bron AM, Koehrer P, et al. (2015). Endophthalmitis after intravitreal injections: incidence, presentation, management, and visual outcome. Am J Ophthalmol 160:17–25.

Dutt MI, Khuller GK. (2001). Chemotherapy of mycobacterium tubercu-losis infections in mice with a combination of isoniazid and rifampicin entrapped in Poly(DL-lactide-co-glycolide) microparticles. J Antimicrob Chemother 47:829–35.

Fernández-Albarral JA, Ramírez AI, De Hoz R, et al. (2019). Neuroprotective and anti-inflammatory effects of a hydrophilic saffron extract in a model of glaucoma. IJMS 20:4110.

Gaasterland DE, Ederer F, Beck A, et al. (2000). The Advanced Glaucoma Intervention Study (AGIS): 7. The relationship between control of intraocular pressure and visual field deterioration. Am J Ophthalmol 130:429–40.

García-Caballero C, Lieppman B, Arranz-Romera A, et al. (2018). Photoreceptor preservation induced by intravitreal controlled delivery of gdnf and gdnf/melatonin in rhodopsin knockout mice. Mol Vis 24:733–45.

Garcia-Herranz D, Rodrigo MJ, Subias M, et al. (2021). Novel use of plga microspheres to create an animal model of glaucoma with progressive neuroretinal degeneration. Pharmaceutics 13:237.

Graham SL, Goldberg I, Buckland L, Hollows FC. (1995). Flash and pattern electroretinogram changes with optic atrophy and glaucoma. Exp Eye Res 60:697–706.

Guidoboni G, Sacco R, Szopos M, et al. (2020). Neurodegenerative disorders of the eye and of the brain: a perspective on their fluid-dynamical connections and the potential of mechanism-driven modeling. Front Neurosci 14:566428.

Guo L, Normando EM, Nizari S, et al. (2010). Tracking longitudinal retinal changes in experimental ocular hypertension using the cSLO and spectral domain-OCT. Invest Ophthalmol Vis Sci 51:6504–13.

Haines A, Harris F, Kasuga F, Machalaba C. (2017). Future Earth - Linking research on health and environmental sustainability. BMJ 357:j2358.

Hernandez H, Roberts AL, McDowell CM. (2020). Nuclear factor-kappa beta signaling is required for transforming growth factor Beta-2 induced ocular hypertension. Exp Eye Res 191:107920.

Howell GR, Libby RT, Jakobs TC, et al. (2007). Axons of retinal ganglion cells are insulted in the optic nerve early in DBA/2J glaucoma. J Cell Biol 179:1523–37. https://doi.org/10.1083/jcb.200706181.

Jamil A, Aamir Mirza M, Anwer MK, et al. (2019). Z. Iqbal, Co-delivery of gemcitabine and simvastatin through PLGA polymeric nanoparticles for the treatment of pancreatic cancer: in-vitro characterization, cellular uptake, and pharmacokinetic studies. Drug Dev Ind Pharm 45:745–53. https://doi.org/10.1080/03639045.2019.1569040.

Jóhannesson G, Eklund A, Lindén C. (2018). Intracranial and intraocular pressure at the lamina cribrosa: gradient effects. Curr Neurol Neurosci Rep 18:25.

Kasetti RB, Maddineni P, Millar JC, et al. (2017). Increased synthesis and deposition of extracellular matrix proteins leads to endoplasmic reticulum stress in the trabecular meshwork. Sci Rep 7:14951. https://doi.org/10.1038/s41598-017-14938-0.

Kasimov EM, Aghaeva FA. (2017). Cortisol levels in plasma and aqueous humour of patients with steroid induced and other glaucomas. Vestn Oftalmol 133:39–45.

Kim KS, Lee BH, Kim IS. (1992). The measurement of fibronectin concentrations in human aqueous humor. Korean J Ophthalmol 6:1–5.

Kitaoka Y, Kitaoka Y, Kwong JMK, et al. (2006). TNF-α-induced optic nerve degeneration and nuclear factor-κB p65. Investig Ophthalmol Vis Sci 47:1448–57.

L. Jia, Cepurna WO, Johnson EC, Morrison JC, Patterns of intraocular pressure elevation after aqueous humor outflow obstruction in rats. Invest Ophthalmol Vis Sci. 41 (2000) 1380–1385

Laquis S, Chaudhary P, Sharma SC. (1998). The patterns of retinal ganglion cell death in hypertensive eyes. Brain Res 784:100–4.

Lawlor M, Danesh-Meyer H, Levin LA, et al. (2018). Glaucoma and the brain: trans-synaptic degeneration, structural change, and implications for neuroprotection. Surv Ophthalmol 63:296–306.

Lestak J, Jiraskova N, Zakova M, et al. (2018). Normotensive glaucoma. Biomed Pap 164. https://doi.org/10.5507/bp.2018.039

Levkovith-Verbin H, Quigley HA, Martin KRG, Valenta D, Baumrind LA. (2002). Translimbal laser photocoagulation to the trabecular meshwork as a model of glaucoma in rats. Invest Ophthalmol Vis Sci 43:402–10. https://iovs.arvojournals.org/article.aspx?articleid=2162526.

Madani F, Esnaashari SS, Bergonzi MC, et al. (2020). Paclitaxel/metho-trexate co-loaded PLGA nanoparticles in glioblastoma treatment: formulation development and in vitro antitumor activity evaluation. Life Sci 256:117943.

Martins C, Sousa F, Araújo F, Sarmento B. (2018). Functionalizing PLGA and PLGA derivatives for drug delivery and tissue regeneration applications. Adv Healthcare Mater 7:1701035.

Masuda T, Shimazawa M, Hara H. (2017). Retinal diseases associated with oxidative stress and the effects of a free radical scavenger (edaravone). Oxid Med Cell Longev 2017:9208489.

Moreno MC, Aldana Marcos HJ, Croxatto JO, et al. (2005). A new experimental model of glaucoma in rats through intracameral injections of hyaluronic acid. Exp Eye Res 81:71–80.

Morgan JE, Tribble JR. (2015). Microbead models in glaucoma. Exp Eye Res 141:9–14. https://doi.org/10.1016/j.exer.2015.06.020.

Morrison JC, Cepurna WO, Johnson EC. (2015). Modeling glaucoma in rats by sclerosing aqueous outflow pathways to elevate intraocular pressure. Exp Eye Res 141:23–32.

Morrison JC, Cepurna WO, Tehrani S, et al. (2016). A period of controlled elevation of IOP (CEI) produces the specific gene expression responses and focal injury pattern of experimental rat glaucoma. Invest Ophthalmol Vis Sci 57:6700–11.

Morrison JC, Cepurna Ying Guo WO, Johnson EC. (2011). Pathophysiology of human glaucomatous optic nerve damage: insights from rodent models of glaucoma. Exp Eye Res 93:156–64.

Morrison JC, Moore CG, Deppmeier LMH, et al. (1997). A rat model of chronic pressure-induced optic nerve damage. Exp Eye Res 64:85–96.

Mzyk P, Zalog EG, McDowell CM. (2022). A20 attenuates the fibrotic response in the trabecular meshwork. IJMS 23:1928.

Nadal-Nicolás FM, Rodriguez-Villagra E, Bravo-Osuna I, et al. (2016). Ketorolac administration attenuates retinal ganglion cell death after axonal injury. Investig Ophthalmol Vis Sci 57:1183–92. https://doi.org/10.1167/iovs.15-18213.

Naik S, Pandey A, Lewis SA, et al. (2020). Neuroprotection: a versatile approach to combat glaucoma. Eur J Pharmacol 881:173208.

Pang IH, Clark AF. (2020). Inducible rodent models of glaucoma. Prog Retin Eye Res 75:100799.

Pankov R, Yamada KM. (2002). Fibronectin at a glance. J Cell Sci 115:3861–3.

Pardue MT, Allen RS. (2018). Neuroprotective strategies for retinal disease. Prog Retin Eye Res 65:50–76.

Park K. (2017). Tolerance levels of PLGA microspheres in the eyes. J Control Release 266:365.Pascale A, Drago F, Govoni S. (2012). Protecting the retinal neurons from glaucoma: lowering ocular pressure is not enough. Pharmacol Res 66:19–32. https://doi.org/10.1016/j.phrs.2012.03.002.

Patel GC, Phan TN, Maddineni P, et al. (2017). Dexamethasone-induced ocular hypertension in mice: effects of myocilin and route of administration. Am J Pathol 187:713–23. https://doi.org/10.1016/j.ajpath.2016.12.003.

Porciatti V. (2015). Electrophysiological assessment of retinal ganglion cell function. Exp Eye Res 141:164–70. (2014).

Qiao ZW, Yuan Z, Zhang W, et al. (2019). Preparation, in vitro release and antibacterial activity evaluation of rifampicin and moxifloxacin-loaded poly(D,L-lactide-co-glycolide) microspheres. Artif Cells Nanomed Biotechnol 47:790–8.

Quigley H, Broman AT. (2006). The number of people with glaucoma worldwide in 2010 and 2020. Br J Ophthalmol 90:262–7. https://doi.org/10.1136/bjo.2005.081224.

Ramirez AI, de Hoz R, Salobrar-Garcia E, et al. (2017). The role of microglia in retinal neurodegeneration: Alzheimer's disease, Parkinson, and glaucoma. Front Aging Neurosci 9:214.

Ritch R. (2000). Neuroprotection: is it already applicable to glaucoma therapy? Curr Opin Ophthalmol 11:78–84.

Roberts AL, Mavlyutov TA, Perlmutter TE, et al. (2020). Fibronectin extra domain A (FN-EDA) elevates intraocular pressure through Toll-like receptor 4 signaling. Sci Rep 10:9815. https://doi.org/10.1038/s41598-020-66756-6.

Rodrigo MJ, Garcia-Herranz D, Aragón-Navas A, et al. (2021). Long-term corticosteroid-induced chronic glaucoma model produced by intra-cameral injection of dexamethasone-loaded PLGA microspheres. Drug Deliv 28:2427–46.

Rodrigo MJ, Garcia-Herranz D, Subias M, et al. (2021). Chronic glaucoma using biodegradable microspheres to induce intraocular pressure elevation. six-month follow-up. Biomedicines 9:682.

Rodrigo MJ, Martinez-Rincon T, Subias M, et al. (2020). Effect of age and sex on neurodevelopment and neurodegeneration in the healthy eye: longitudinal functional and structural study in the long–evans rat. Exp Eye Res 200:108208.

Rodrigo MJ, Martinez-Rincon T, Subias M, et al. (2021). Influence of sex on neuroretinal degeneration: six-month follow-up in rats with chronic glaucoma. Invest Ophthalmol Vis Sci 62:9.

Román BS, Gómez S, Irache JM, Espuelas S. (2014). Co-encapsulated CpG oligodeoxynucleotides and ovalbumin in PLGA microparticles; an in vitro and in vivo study. J Pharm Pharm Sci 17:541–53.

Roubeix C, Godefroy D, Mias C, et al. (2015). Intraocular pressure reduction and neuroprotection conferred by bone marrow-derived mesenchymal stem cells in an animal model of glaucoma. Stem Cell Res Ther 6:177. https://doi.org/10.1186/S13287-015-0168-0.

Rozsíval P, Hampl R, Obenberger J, et al. (1981). Aqueous humour and plasma cortisol levels in glaucoma and cataract patients. Curr Eye Res 1:391–6.

Salinas-Navarro M, Mayor-Torroglosa S, Jiménez-López M, et al. (2009). A computerized analysis of the entire retinal ganglion cell population and its spatial distribution in adult rats. Vision Res 49:115–26.

Samsel PA, Kisiswa L, Erichsen JT, et al. (2011). A novel method for the induction of experimental glaucoma using magnetic microspheres. Invest Ophthalmol Vis Sci 52:1671–5.

Sapienza A, Raveu AL, Reboussin E, et al. (2016). Bilateral neuroinflammatory processes in visual pathways induced by unilateral ocular hypertension in the rat. J Neuroinflammation 13:44. https://doi.org/10.1186/s12974-016-0509-7.

Schindelin J, Arganda-Carreras I, Frise E, et al. (2012). Fiji: an open-source platform for biological-image analysis. Nat Methods 9:676–82.

Schlamp CL, Li Y, Dietz JA, et al. (2006). Progressive ganglion cell loss and optic nerve degeneration in DBA/2J mice is variable and asym-metric. BMC Neurosci 7:66.

Shareef SR, Garcia-Valenzuela E, Salierno A, et al. (1995). Chronic ocular hypertension following episcleral venous occlusion in rats. Exp Eye Res 61:379–82.

Sharma TP, McDowell CM, Liu Y, et al. (2014). Optic nerve crush induces spatial and temporal gene expression patterns in retina and optic nerve of BALB/cJ mice. Mol Neurodegener 9:14

Shepard AR, Cameron Millar J, Pang IH, et al. (2010). Adenoviral gene transfer of active human transforming growth factor-β2 elevates intraocular pressure and reduces outflow facility in rodent Eyes. Invest Ophthalmol Vis Sci 51:2067–76.

Shi X, Li C, Gao S, et al. (2014). Combination of doxorubicin-based chemotherapy and polyethylenimine/p53 gene therapy for the treatment of lung cancer using porous PLGA microparticles. Colloids Surfaces B Biointerfaces 122:498–504. https://doi.org/10.1016/j.col-surfb.2014.07.020.

Smedowski A, Pietrucha-Dutczak M, Kaarniranta K, Lewin-Kowalik J. (2014). A rat experimental model of glaucoma incorporating rapid-onset elevation of intraocular pressure. Sci Rep 4:5910. https://doi.org/10.1038/srep05910.

Sokol MB, Nikolskaya ED, Yabbarov NG, et al. (2019). Development of novel PLGA nanoparticles with co-encapsulation of docetaxel and abiraterone acetate for a highly efficient delivery into tumor cells. J Biomed Mater Res 107:1150–8.

Stankowska DL, Nam MH, Nahomi RB, et al. (2019). Systemically administered peptain-1 inhibits retinal ganglion cell death in animal models: implications for neuroprotection in glaucoma. Cell Death Discov 5:112.

Sun H, Wang Y, Pang IH, et al. (2011). Protective effect of a JNK inhibitor against retinal ganglion cell loss induced by acute moderate ocular hypertension. Mol Vis 17:864. /pmc/articles/PMC3081797/ (accessed May 26, 2022).

Tham YC, Li X, Wong TY, et al. (2014). Global prevalence of glaucoma and projections of glaucoma burden through 2040: a systematic review and meta-analysis. Ophthalmology 121:2081–90.

Thanos C, Emerich D. (2005). Delivery of neurotrophic factors and therapeutic proteins for retinal diseases. Expert Opin Biol Ther 5:1443–52.

Ueda J, Sawaguchi S, Hanyu T, et al. (1998). Experimental glaucoma model in the rat induced by laser trabecular photocoagulation after an intracameral injection of India. Ink Jpn J Ophthalmol 42:337–44.

Urcola JH, Hernández M, Vecino E. (2006). Three experimental glaucoma models in rats: comparison of the effects of intraocular pressure elevation on retinal ganglion cell size and death. Exp Eye Res 83:429–37.

WoldeMussie WLAE; Ruiz G; Wijono M, Neuroprotection of retinal ganglion cells by brimonidine in rats with laser-induced chronic ocular hypertension. Invest Ophthalmol Vis Sci 42 (2001) 2849–2855. https://iovs.arvojournals.org/article.aspx?articleid=2123016.

Weinreb RN, Levin LA. (1999). Is neuroprotection a viable therapy for glaucoma? Arch Ophthalmol 117:1540–4.

Wilsey L, Gowrisankaran S, Cull G, et al. (2017). Comparing three different modes of electroretinography in experimental glaucoma: diagnostic performance and correlation to structure. Doc Ophthalmol 134:111–28.

Zeng W, Wang W, Wu S, et al. (2020). Mitochondria and autophagy dysfunction in glucocorticoid-induced ocular hypertension/glaucoma mice model. Curr Eye Res 45:190–8.

Zhao M, Rodríguez-Villagra E, Kowalczuk L, et al. (2017). Tolerance of high and low amounts of PLGA microspheres loaded with mineralo-corticoid receptor antagonist in retinal target site. J Control Release 266:187–97.

Zollinger AJ, Smith ML. (2017). Fibronectin, the extracellular glue. Matrix Biol 60–61:27–37.

CAPÍTULO II – CHAPTER II. Neuroprotective multi-approach strategy based on PLGA microspheres for the treatment of retinal neurodegenerative diseases.

Neuroprotective multi-approach strategy based on PLGA microspheres for the treatment of retinal neurodegenerative diseases.

Alba Aragón-Navas[1,2], MJ Rodrigo[3,5,6], David García-Herranz [1,2], Manuel Subías [5,6], Inés Munuera [5,6], Julián García-Feijoo [3,7], Luis Pablo[3,5,6], Elena Garcia-Martin[3,5,6], Rocio Herrero-Vanrell[1,2,3,4], Irene Bravo-Osuna[1,2,3,4].

[1]Innovation, Therapy and Pharmaceutical Development in Ophthalmology (InnOftal) Research Group, UCM 920415, Department of Pharmaceutics and Food Technology, Faculty of Pharmacy, Complutense University of Madrid, Madrid, Spain

[2] Health Research Institute, San Carlos Clinical Hospital (IdISSC), Madrid, Spain

[3] National Ocular Pathology Network (OFTARED), Carlos III Health Institute, Madrid, Spain

[4] University Institute for Industrial Pharmacy (IUFI), School of Pharmacy, Complutense University of Madrid, Madrid, Spain

[5] Department of Ophthalmology, Miguel Servet University Hospital, Zaragoza, Spain

[6] Miguel Servet Ophthalmology Research Group (GIMSO), Aragon Health Research Institute (IIS Aragon), University of Zaragoza, Spain

[7] Department of Ophthalmology, San Carlos Clinical Hospital, Health Research Institute of the San Carlos Clinical Hospital (IdISSC), Madrid, Spain.

ABSTRACT

This work aimed to co-encapsulate and co-deliver three different neuroprotective drugs in a microparticulate system for the treatment of neurodegenerative diseases. For that purpose, first it was optimised a co-loaded microspheres containing dexamethasone (anti-inflammatory) and ursodeoxycholic acid (UDCA) (antiapopototic) by the solid-in-oil-in-water emulsion solvent extraction-evaporation technique. Different strategies were studied such as the incorporation of a water-soluble co-solvent (ethanol) and different amounts of dexamethasone, resulting critical for drug encapsulation and the initial release. The optimised formulation resulted using 80:20 ratios of dicloromethane:ethanol and 60 mg of dexamethasone. The final formulation also included GDNF (glial cell line derived neurotrophic factor) and showed good encapsulation efficiencies for the three components (all above 50%) with suitable properties for long-term application, delivering low molecular weight compounds for 3 months and the protein for 6 months. Other physicochemical studies were carried out like morphology by SEM and TEM, DSC, XRD and gas chromatography. The evaluation of the kinetic release by the Gallagher-Corrigan analysis with Gorrasi correction demonstrated that the encapsulation of a second compound inside the microspheres mainly modifies the first stage of the release, which is the one produced by the dissolution of the active compounds. Degradation studies confirmed this hypothesis.

1. Introduction

Glaucoma is a multifactorial neurodegenerative disorder and one of the leading causes of irreversible vision loss, included in the top three causes of blindness in 2015 [1]. The prevalence increases over the years, and it is estimated a rise of 74% from 2013 until 2040 [2]. Glaucoma is characterised by the death of retinal ganglion cells (RGC) and the loss of their axons in the optic nerve. Recently, the role of microglia and astroglial cells (Müller cells and astrocytes) in neuroinflammation processes in glaucoma has been demonstrated [3,4]. Currently, the elevation of intraocular pressure (IOP) is one of the most important risk factors and the only one modifiable [5]. Therefore, the majority of the pharmacological treatments focus on lowering IOP by different mechanisms: prostaglandin analogues, beta-blockers, alpha agonists, carbonic anhydrase inhibitors, and cholinergic agents [6].

However, despite reducing IOP, visual loss continues progressing in some patients and in many others, glaucomatous retinal and optic nerve degeneration is observed in absence of IOP elevation. Therefore, new strategies such as neuroprotection have emerged. In the case of glaucoma, this therapeutic approach aims to prevent or improve the survival of RGCs and optic nerve fibres. Consequently, neuroprotection targets RGC protection, being a way to reduce RGCs loss in all cases (IOP-dependent and independent patients) [7–10]. There are different processes responsible for RGC apoptosis: oxidative stress, hyperglycemia, inflammation, glutamate excitotoxicity, ischemia, mitochondrial dysfunction, aggregation of misfolded proteins, neurotrophic deprivation, glial activation, and axonal transport dysregulation [9,11,12]. It is likely that not only one of these events but several of them converge to induce RGC loss. This fact suggests that combined therapy could be required to achieve effectiveness for the neuroprotective treatment of glaucoma [13]. In this sense, our research group has previously developed a multi-delivery microsystem loaded with three neuroprotective substances with anti-inflammatory and neuroprotective activities (dexamethasone, coenzyme Q10 and melatonin). This formulation showed beneficial results in RGCs survival in an experimental glaucoma model [14].

It exists, theoretically, four main routes to administrate drugs into the posterior segment of the eye: topical, systemic, intraocular (intracameral, intravitreal, subretinal), and periocular (subconjunctival, sub-Tenon, yuxtascleral, etc.) [15]. Although the most desirable route is the topical administration [16], the drug bioavailability in the posterior segment is generally reduced by multiple factors such as the short ocular contact time or the lacrimal drainage system, among others [17]. The blood-ocular barriers limit the systemic and periocular routes, requiring large amounts of drugs and, consequently, significant general side effects are linked to the systemic route. In addition, for periocular administration, the main obstacle is the drug penetration through the sclera that limits the drug access into the eye [15]. In fact, although periocular or topical administration of drugs in the eye is being evaluated with promising results to treat retinal diseases in some cases, currently the intravitreal administration of active substances in suitable vehicles (bolus injection) remains the most used in the clinic. Multiple injections are needed to maintain therapeutic concentrations. However, intraocular injections can cause inconvenience to patients such as adverse effects like cataracts, retinal detachment, haemorrhages, and increase the risk of side effects just as the number of administrations increases [15]. Furthermore, bolus administration can produce an initial toxic concentration of drugs in the retinal proximity to injection site causing additional damage [18].

Nevertheless, intraocular drug delivery systems (IODDS) may avoid these concerns. They can release drugs for a long time with a single administration instead of multiple injections. Biodegradable or not biodegradable polymers can compose IODDS, being the main advantage of the biodegradable ones that they can be degraded and eventually disappear after releasing the drug without the need of surgery [19]. On the other hand, they can sustain the release of drugs for weeks or months and avoid initial high drug concentrations in the site of action, reducing the potential retinal toxicity.

Biodegradable microsystems are emerging as an interesting tool to treat chronic posterior segment diseases in the last years. Among their benefits, microparticles can deliver drugs during long term and can encapsulate different drugs in the same device [20]. Furthermore, as the amount of microparticles administrated into the vitreous can be easily modified, they are considered promising candidates for personalized therapy

[21]. Moreover, microparticles can be easily administrated by suspending and injecting them through different needle gauges (between 25 and 32G) [22]. One of the most popular biodegradable polymers used in clinical devices is the poly (lactic-co-glycolic) acid (PLGA), whose use has been approved for ocular administration by the US Food and Drug Administration (FDA) and European Medicines Agency (EMA).

The present study optimizes a multi-loaded MSs formulation including three different substances with anti-inflammatory and neuroprotective effects (dexamethasone, UDCA, and GDNF). The corticosteroid dexamethasone (DX) has been used to treat ocular inflammation and it is marketed in an intraocular implant, Ozurdex®, for the treatment macular oedema [23,24]. Ursodeoxycholic acid (UDCA) is a component of bile acid with anti-oxidant, anti-apoptotic, and anti-inflammatory properties, which has also shown neuroprotective effects in retinal disorders [25,26]. Finally, the cell line-derived neurotrophic factor (GDNF) has been previously tested proving its neuroprotection effect in retinal diseases [27,28]. In this work, different technological strategies have been evaluated to obtain this tri-delivery system. In addition, as part of the characterization of the systems, an exhaustive study has been carried out on the kinetic mechanisms involved in the release of the active agents, and on the influence, that co-microencapsulation and subsequent simultaneous delivery of substances with a different nature can have on these mechanisms. These studies can help to understand multi-charged systems more deeply and to elaborate them with greater precision.

2. Materials and methods

2.1. Materials

PLGA (50:50) polymer (Resormer®503) was acquired from Evonik Nutrition & Care GmbH (Darmstadt, Germany). Ursodeoxycholic acid (UDCA) (purity >99%) was obtained from Alfa Aesar (Haverhill, Massachusetts, USA) and Dexamethasone (DX) (purity >98%), DL-alpha-tocopherol acetate, polyethylene glycol (PEG 1500), glycolide and stannous 2-ethylhexanoate were provided by Sigma-Aldrich (St. Louis Mo., USA). Polyvinyl alcohol 72000 g/mol (PVA) were purchased from Panreac Química (Castellar del Vallès, Spain). DL-Lactide was obtained from Corbion® (Gorichem, The Netherlands). Recombinant human Glial cell-line-derived neurotrophic factor (GDNF), fibronectin (FN) and enzyme-

linked immunosorbent assays (ELISA) for GDNF and FN quantification were purchased from R&D Systems (Minneapolis, MN, USA).

All organic solvents were HPLC-grade and used as received.

2.2. Microsphere elaboration

The tri-loaded microspheres were prepared following the Solid/Oil/Water (S/O/W) emulsion solvent extraction-evaporation technique.

In an initial step, DX-UDCA MSs were elaborated. 400 mg of PLGA and different amounts of UDCA (ranged 20-60 mg) were dissolved in 0.9 mL methylene chloride or 1.2 mL of a mixture of methylene chloride:ethanol (different proportions were studied: 75:25/80:20/85:15). 60 or 80 mg of DX were incorporated into the polymeric dissolution and dispersed by ultrasonication (Ultrasons; J.P. Selecta, Barcelona, Spain) in an ice-water bath for 5 minutes. 40 µL of alpha-tocopherol acetate were added to the O-phase and then, the mixture was sonicated (Sonicator XL; Heat Systems, Inc., Farmingdale, NY, USA) in an ice-water bath for 1 minute and emulsified adding 5 mL of PVA MilliQ® water solution (2% w/v) through a homogenizer (Polytron®RECO, Kinematica, GmbHT PT3000, Lucerna, Switzerland) for 1 minute at 5000 or 8500 rpms.

The obtained emulsion was incorporated into 100 mL of PVA MilliQ® water solution (0.1% w/v) and it was stirred for 3 hours to harden the MSs.

Once MSs maturated, they were washed and sieved. Finally, MSs were freeze-dried (Freezing: -60°C /15 min, drying: -60 °C/12h/0.1 mBar) and stored at -30°C in dry conditions. (Figure 1). Once the formulation was optimized, MSs loaded with only one component (UDCA or DX) were also elaborated at the selected conditions for comparison purpose.

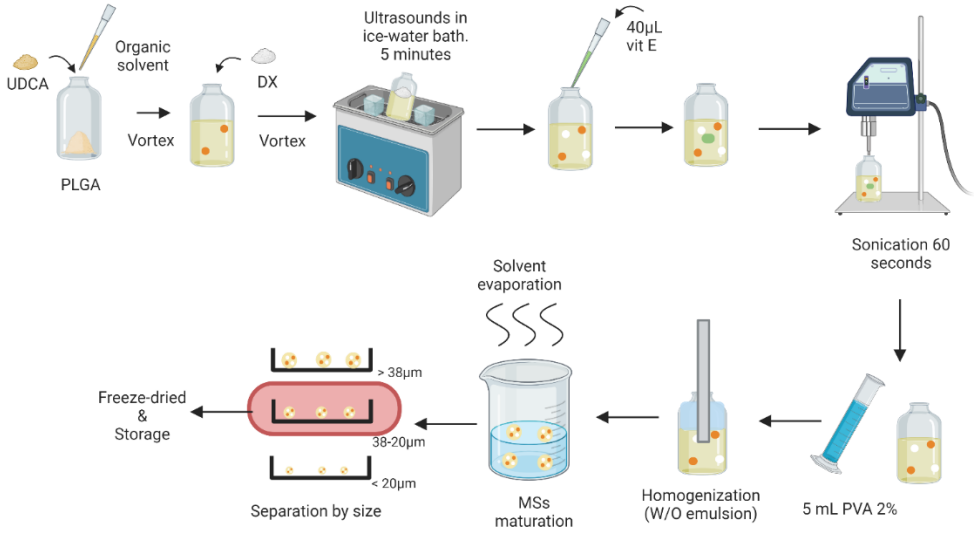

Figure 1. DX-UDCA MSs elaboration.

The different conditions studied for the optimisation of the formulation are summarizing in Table 1.

Table 1. Conditions studied for the formulation optimisation (A-H).

Formulation	Composition (UDCA/DX) (mg/mg)	rpms	Volume of Organic Solvent
A	20/80	5000	0.9 mL MC
B	40/80	5000	0.9 mL MC
C	40/80	8500	1.2 mL MC:EtOH (75:25)
D	60/80	8500	1.2 mL MC:EtOH (75:25)
E	40/80	8500	1.2 mL MC:EtOH (80:20)
F	40/60	8500	1.2 mL MC:EtOH (80:20)
G	40/80	8500	1.2 mL MC:EtOH (85:15)
H	40/60	8500	1.2 mL MC:EtOH (85:15)

In a second step of the optimization process, the third component, the protein, was included in the inner phase of the emulsion. Briefly, 20 µg of GDNF (final formulation) were added to the 40 µL of alpha-tocopherol acetate by using an ultrasonic probe for 30s. Then, the procedure was carried out as same as already mentioned before.

Moreover, MSs loaded with only one component (UDCA or DX) were also elaborated (Table 2).

Table 2. Summarized conditions of the selected formulation (F), only UDCA (F-UDCA) and only DX (F-DX) loaded MSs and the incorporation of the GDNF in the optimised formulation (F+GDNF).

Formulation	Composition (UDCA/DX/protein) (mg/mg/µg)	rpms	Volume of Organic Solvent
F	40/60/-	8500	1.2 mL MC:EtOH (80:20)
F-UDCA	40/-/-	8500	1.2 mL MC:EtOH (80:20)
F-DX	-/60/-	8500	1.2 mL MC:EtOH (80:20)
F+GDNF	40/60/20	8500	1.2 mL MC:EtOH (80:20)

2.3. UDCA quantification by LC/MS

The chromatographic system was made of a High-Performance Liquid Chromatography (Waters 1525 binary HPLC pump and Waters 2707 autosampler) coupled to a mass detector (Waters 3100 single quadrupole mass spectrometer). The quantification was performed by employing a Nova-Pak C18 column (4 µm, ID 2.1 mm×150 mm) connected previously to a guard column (4 µm, 3.9 mm ×20 mm), both were maintained at 45 °C. The mobile phase was composed of acetonitrile/ammonium acetate in water 15 mM (2:1 v/v), adjusted to pH 5.0 with formic acid and the flow rate was 0.15 mL/min.

Electrospray ion source (ESI) operated in a negative ionization mode. The parameters were set as follows: 3 kV for spray voltage, 80 °C for the capillary temperature and 3 V extractor voltage. Desolvation (925 L/h flow rate, 180 °C desolvation temperature) was performed employing nitrogen gas (>99.999 %).

2.4. DX quantification by LC/MS

The chromatographic system was the same as for UDCA quantification by LC/MS. The mobile phase was 15 mM ammonium acetate in water and acetonitrile (1:1 v/v) and the rate employed was 0.30 mL/min. The ESI source was adjusted to positive ion mode. The

instrument settings 3 kV electrospray voltage, nebulization (150 L/h flow rate, 120 °C source temperature, 3 V extractor voltage) and desolvation (500 L/h flow rate, 350 °C desolvation temperature) were performed employing nitrogen gas (> 99.999 %).

2.5. Microsphere characterization

2.5.1. Mean particle size and particle size distribution.

The mean particle size and particle size distribution of each formulation were measured by dual light scattering in a Microtrac®S3500 Series Particle Size Analyser (Montgomeryville, PA, USA) by suspending MSs in MilliQ® water. The particle size results are expressed as the mean ± standard deviation (SD) (n=3).

2.5.2. Morphological evaluation by scanning electron microscopy (SEM) and transmission electron microscopy (TEM)

The external morphology of MSs was observed by scanning electron microscopy (Jeol, JSM-6335F, Tokyo, Japan). Prior to observation, freeze-dried MSs were applied a gold sputter-coating.

The internal morphology was studied by transmission electron microscopy (TEM, Jeol JEM 1010, Tokyo, Japan). Previously, 50-70 µm of thickness cross-sectional cuts were made out by Reichert Ultracut S Ultramicrotome (Leica Microsystems Inc, Wetzlar, Germany) in samples deposited in a synthetic resin medium (Spurr Low Viscosity Embedding Kit).

Both external and internal morphology was considered as a key point to the optimisation since the formulations that contained external crystals were discarded to posterior characterisations.

2.5.3. Components distribution

To evaluate the MSs matrix and protein distribution through MSs, the formulation was elaborated according to the conditions for F+GDNF but with the following modifications: 3 µL of a Nile Red solution were added in the organic phase (4mg/mL) and the fluorescein isothiocyanate-conjugated bovine serum albumin (BSA-FITC) was employed as a model protein instead of GDNF. These MSs were observed by confocal fluorescence microscopy (Leica TCS SP8, Wetzlar, Germany)

2.5.4. Encapsulation efficiency

For UDCA and DX quantification, 1 mg of MSs was dissolved in 2.5 mL of methylene chloride. UDCA and DX were extracted with 6 mL of ethanol or methanol, respectively, which also promotes polymer precipitation. Then, it was vortex mixed and centrifuged (5000 rpms, 5 minutes, 20 °C). The supernatant was filtered and analysed in LC/MS as described before. Each batch was quantified in duplicate.

In the case of formulation F+GDNF, DX and UDCA were extracted as mentioned previously. To isolate GDNF, a liquid/liquid extraction was made as follows: 5 mg of MSs were dissolved in 0.7 mL of methylene chloride. Then, 0.7 mL of reagent diluent provided in the ELISA kit (1% BSA in PBS, pH= 7.4) was added and it was vortex mixed. After that, the samples were centrifuged at 12000 rpm, for 15 minutes at 4 °C and the aqueous phase was removed. According to previous studies [34], this procedure was carried out in a 4-total time, removing and replacing the aqueous phase to extract all the encapsulated protein. GDNF concentration was determined by ELISA.

2.5.5. *In vitro* release studies

Triplicate samples of 5 mg DX-UDCA-MSs and DX-UDCA-GDNF-MSs were suspended in 2 mL of phosphate-buffered saline (PBS, pH 7.4, isotonized with NaCl) with sodium azide (0.02%(w/v)). The samples were kept at 37 °C under constant agitation in a water shaker bath (WNB Memmert Shaking Bath, Memmert, Schwabach, Germany). At pre-set times (24h, 7 days and once a week until the end of the study), the MSs were centrifuged (5000 rpm, 5 min, 20 °C). The supernatants were recovered, filtered (0.22 µm) and replaced with 2 mL of fresh PBS/azide. The UDCA and DX concentrations of the before-mentioned filtered supernatants were analysed by LC/MS as described previously. This procedure was also carried out exactly for the burst release, removing the samples at 24 hours.

Moreover, triplicate samples of 5 mg DX-UDCA-GDNF-MSs were suspended in 2 mL of the aforementioned medium with the addition of BSA (1%(w/v)) according to previous studies [29]. The samples were kept at the same conditions and at the same pre-set times, the supernatants were extracted. GDNF concentrations were analysed by ELISA.

The similarity test (f_2) was calculated to compare the different drug release profiles (Equation 1). This equation is a logarithmic transformation of the sum-squared error of differences between the reference (R_t) and the test (T_t) formulations over all time points:

$$F_2 = 50 * \log \left\{ \frac{1}{\sqrt{1 + \frac{\sum_{t=t}^{t=n}(R_t - T_t)^2}{n}}} * 100 \right\}$$

Equation 1. Similarity test (f_2) to compare the dissolution profiles.

Where n is the number of experimental points, t the time points and R_t and T_t are the mean percentage of the dissolved drugs in the reference and test formulations, respectively. Time points with 85 % or more of the dissolved drug was not considered. When an f_2 value is in the range 50-100 indicates that the two release profiles are similar [30].

Moreover, with the aim of analysing the possible mechanism involved in the drug release kinetics, the release experimental data were fitted in different kinetic models (zero and first order, Korsmeyer-Peppas, Hixson-Crowell, Higuchi, Baker-Londsdale, Weibull and Gallagher-Corrigan).

The *zero-order* kinetic model describes a pharmaceutical form whose area remains unchangeable through time with a constant and slow drug release where no equilibrium conditions are achieved. It is represented by the following equation:

$$Q = Q_0 + K_0 t$$

Equation 2. Zero-order kinetic equation.

Where Q is the amount of released or dissolved drug, Q_0 is the initial amount of drug in the dosage form, K_0 is the zero-order constant, and t is the time [31].

The *first order kinetic model* corresponds to the general case in which the drug-liquid interface variation is directly proportional to the variation of the mass of remaining solid drug in the system, and therefore the release rate is proportional to that mass of remaining drug. It is described by this equation:

$$\ln\left(\frac{Q_t}{Q_0}\right) = -Kt$$

Equation 3. First order kinetic equation.

Where, Q_t is the amount of drug released in a determined time, Q_0 is the initial amount of drug in the solution and K is the first-order rate constant being its units time^{-1} [31].

The *Hixson-Crowell model* considers that the release rate is proportional to the mass of drug remaining to dissolve in the system raised to 2/3. This idea derives from considering the geometry of the solid particle to be dissolved and assumes that it is always spherical. Finally, the equation is expressed as follows:

$$M_0^{1/3} - M_i^{1/3} = Kt$$

Equation 4. Hixson-Crowell kinetic equation.

Where M_0 is the initial amount of drug, M_i is the remaining drug in the pharmaceutical dosage at a determined time, K is the constant and t the time [32].

The *Higuchi model* is based on Fick 1st law. In this model, it is estimated that once the drug is dissolved, it must diffuse to leave the polymeric matrix formed by excipients. It is this diffusion, and not the dissolution of the drug, that controls its release.

Despite the simplicity of its equation, this model considers six hypotheses that need to be followed: (i) the initial drug concentration in the matrix is much higher than its solubility, (ii) the diffusion of the drug only occurs in one dimension, (iii) the particle size is much smaller than the thickness of the system, (iv) it is insignificant the swelling or dissolution behaviour of the system, (v) drugs diffuses in a constant manner, and (vi) perfect sink conditions in the release media.

$$Q = K\sqrt{t}$$

Equation 5. Higuchi kinetic equation.

Where Q is the amount of drug release in an elapsed time (t) and K is the Higuchi release constant [33].

This Higuchi model has been the origin of many other release kinetic models that were appearing to explain the increasingly complex modified release systems, such as the *Korsmeyer-Peppas model* and the *Baker-Lonsdale model*.

In the case of Korsmeyer-Peppas model, not only Fickian diffusion through the polymeric matrix but also other phenomena such as matrix relaxation or erosion are considered.

$$\frac{M_t}{M_0} = Kt^n$$

Equation 6. Korsmeyer-Peppas kinetic equation.

Where M_t/M_0 represents the ratio of drug release at a determined time, K is the rate constant, t is the time and n is the release exponent. Only the first 60% drug release data points can be fitted into this equation. The exponent "n" indicates the drug mechanism of transport across the polymer [32]. These values change from thin films, cylinders, or spheres systems. In the case of spherical systems, if the n value is 0.43 the release suffers a Fickian diffusion – the drug is released through a diffusion due to a chemical potential gradient. If it is 0.85 is Case-II transport due to changes in the polymer such as relaxation and erosion. When an n value is between 0.43 and 0.85 is described as a non-Fickian release (anomalous), combining both phenomena [33].

The above-mentioned equation does not consider the burst effect, or the burst effect is zero. When it is not the case, this equation becomes [31]:

$$\frac{M_t}{M_0} = Kt^n + b$$

Equation 7. Korsmeyer-Peppas kinetic equation considering burst release.

The *Baker-Lonsdale model* explains the drug release from spherical matrixes, linearizing the data from microcapsules and microspheres. It follows the equation:

$$f_t = \frac{3}{2}\left[1 - \left(1 - \frac{M_t}{M_\infty}\right)^{\frac{2}{3}}\right] - \frac{M_t}{M_\infty} = Kt$$

Equation 8. Baker-Lonsdale kinetic equation.

Where M_t/M_∞ is the fraction of drug released at a time (t) [31,32].

The *Weibull model* is an empirical equation used generally to linearize data, however, it has been adapted to the dissolution-release processes. The equation lacks kinetic fundaments and for this reason, it possesses deficiencies, and its use is controversial [36]. It is expressed as:

$$F = F_{max}\left(1 - e^{-kt^{\beta}}\right)$$

Equation 9. Weibull equation.

Where F is the amount of drug dissolved in a determined time (t), F_{max} is the total amount to be released, and k and β are constants. Although several criticisms, some attempts have been made in order to validate its use in release studies. Therefore, the β constant has been related to a different mechanism based on its values. In this way, if this constant has values lower than 0.75, it exists a Fickian diffusion. For values between 0.75 and 1.0, there is a combination of mechanisms between diffusion with another release mechanism. When β =1, it is compatible with the first-order model. Finally, when the value is above 1 (sigmoid curve), it is indicative of a complex mechanism of release [34].

Finally, the experimental data were fitted too in the *Gallagher-Corrigan model* with some modifications. Gallagher and Corrigan developed a mathematical model that describes sigmoidal shape profiles, that usually occur in drug delivery systems where polymer undergoes degradation. The profile is described by the following equation that comprises the initial burst release because of the non-bounded drug to the matrix – the first addend –, followed by a slow-release due to matrix erosion, the second addend:

$$F_{TOT} = F_B(1 - e^{-k_B t}) + (1 - F_B)\left(\frac{e^{kt-kT_{max}}}{1 + e^{kt-kT_{max}}}\right)$$

Equation 10. Gallagher-Corrigan kinetic equation.

Where F_{TOT} is the total fraction of drug release at a time (t), F_B is the fraction of drug available for direct surface release (what they call “burst release”), K_B is the release rate constant, and K and T_{max} are the rate constant and the time to maximum drug release rate [35].

However, Gorrasi et al [36] modified this equation by adding a constant parameter (b) that considers the initial burst release. This factor shifts the model predictions up to

fit the experimental release data. In the case that burst release does not exist, the b value is zero, becoming the original release equation (Gallagher-Corrigan equation). This equation is described as follows:

$$Y(t) = b + Y_1(1 - e^{-k_1 t}) + Y_2\left(\frac{e^{-k_2(t_2 - t)}}{1 + e^{-k_2(t_2 - t)}}\right)$$

Equation 11. Gorrasi adjustment to Gallagher-Corrigan kinetic equation.

In this case, Y(t) is the drug fraction released in a t time, Y_1 and Y_2 are the relative amount of drug release in the first and second mechanisms, respectively; K_1 and K_2 are the kinetic constants of the first and second mechanisms, respectively; t_2 is characteristic time of the second step mechanism and b is the burst parameter. This equation possesses 7 unknown parameters that were determined by adjusting the equation to the experimental data releases, using MATLAB® (MathWorks, USA).

In order to choose the model which fits best, the coefficient of determination is used (R^2). However, when the models have different number of parameters, it is more meaningful use the adjusted coefficient of determination ($R^2_{adjusted}$):

$$R^2_{adjusted} = 1 - \frac{(n - 1)}{(n - p)}(1 - R^2)$$

Equation 12. $R^2_{adjusted}$ equation.

Where:

n is the number of dissolution data points, p is the number of parameters in the models and R^2 is the coefficient of determination [31].

2.5.6. Microspheres degradation studies

5 mg of the final formulations (Blank-MSs, F, F-DX, F-UDCA, F+GDNF but substituting GDNF with BSA) were placed in a water bath with similar conditions as *in vitro* studies, in order to assess its degradation. Media was replaced every week by centrifuging 5,000 rpms, 5 minutes and 20 °C, and at pre-set times (each 2 weeks) some samples were removed, washed thrice with MilliQ® water and freeze-dried. Then, samples were observed in SEM with the same conditions as before and molecular weight was assessed by GPC. GPC was composed by an Agilent 1260 Infinity II LC system coupled to a light scattering detector (Polymer Laboratories, Church Stretton, UK). The columns used were

2 x Plgel Mixed-D (300 x 7.5 mm x 5 µm) (Polymer Laboratories, Church Stretton, UK) at 25 °C with a rate of 0.8 mL/min of THF. The injection volume was 20 µL. Samples were dissolved in 1 mL of THF and filtered through 0.45 µm.

2.5.7. Differential scanning calorimetry (DSC)

Thermal analysis of raw material (PLGA, DX and UDCA), empty and drug-loaded MSs prepared with the different mixtures of dissolvents were made by a Mettler differential scanning calorimeter (DSC820, Mettler Toledo, Greifensee, Switzerland) connected to a TAC7/DX instrument controller. Between 5-10 mg samples were employed and an empty aluminium pan (Mettler Toledo, Greifensee, Switzerland) was used as a referenced standard. The samples were heated at a 10 °C/min rate in a heating-cooling-heating cycle where the temperature ranges were as follows 25-100 °C/100-25 °C/25-280 °C.

2.5.8. Gas chromatography (GC)

The remaining methylene chloride present in the loaded MSs prepared with the different dissolvent mixtures was measured by a Headspace method in Gas Chromatography Mass Spectrometry (GCMS). Microspheres samples (approximately 100 mg) were suspended in 10 mL of water. The samples were extracted by shaking at 250 rpms and 90 °C for 30 minutes. Then, 2 mL of the headspace were injected into the GC column. CP-SELEC 624 CD (30 m x 0.25 mm x 1.4 um) was used as column and helium at 1 mL/min flow rate was employed as a carrier. The GC temperature were equilibrated to 33 °C for 6 minutes. Then, a gradient from 33 °C to 250 °C at 20 °C/min was used and the temperature was maintained for 3 minutes. In order to quantify the amount, a line with 5 different points was made.

2.5.9. X-Ray diffractometry analysis

MSs and compound's crystalline structure were assessed by a X-ray diffractometer (Philips X'Pert, USA). The angular range employed was from 5.0° to 50.0° (2θ) with a step size of 0.033° and a scan rate of 100.0 seconds/step.

2.5.10. Statistical analysis

All data were analysed by one-way analysis of variance (one-way ANOVA) using GraphPad Prism 8 (GraphPad Software Inc, San Diego, CA, USA). Results were presented as means ± standard deviation (SD) and $P < 0.05$ was considered significant.

3. Results

3.1. Optimization of the formulation

3.1.1. Morphological studies, particle size distribution and drug distribution.

Figure 2 shows the internal and external morphologies of the different formulations. SEM images confirmed the spherical shapes and homogeneity in size. All formulations showed surficial pores and a slightly rough surface.

In the case of A and B, prepared with methylene chloride, the presence of small pores covering the MSs surface was previously related with the addition of vitamin E in the formulation and were not related with an inner porous structure [29,37], as shown in TEM pictures of formulations A and B. On the contrary, when microspheres were performed using the water-soluble organic solvent in the inner phase of the emulsion (EtOH), these surficial porous resulted clearly more numerous and bigger according to SEM pictures and were also observed through the polymeric matrix in the cross-sectional images from TEM.

Some of the preparations (C, D, G and H) presented some free drug on their surfaces (white arrows in Figure 2). This phenomenon was considered as a key point to be avoided in the optimization procedure. TEM analysis revealed the presence of drug accumulations encapsulated into the microspheres for all formulations, however, the use of ethanol in the inner phase seemed to induce a different distribution of the drug in the polymeric matrix, so, for formulations C-H, the drug was mainly located in the core of the particles in contrast to the more generalized distribution of drug that can be observed for formulations A and B, elaborated both using only methylene chloride as organic solvent of the inner phase.

The particle size distribution revealed that all formulations had a unimodal distribution in the selected range (20-38 µm).

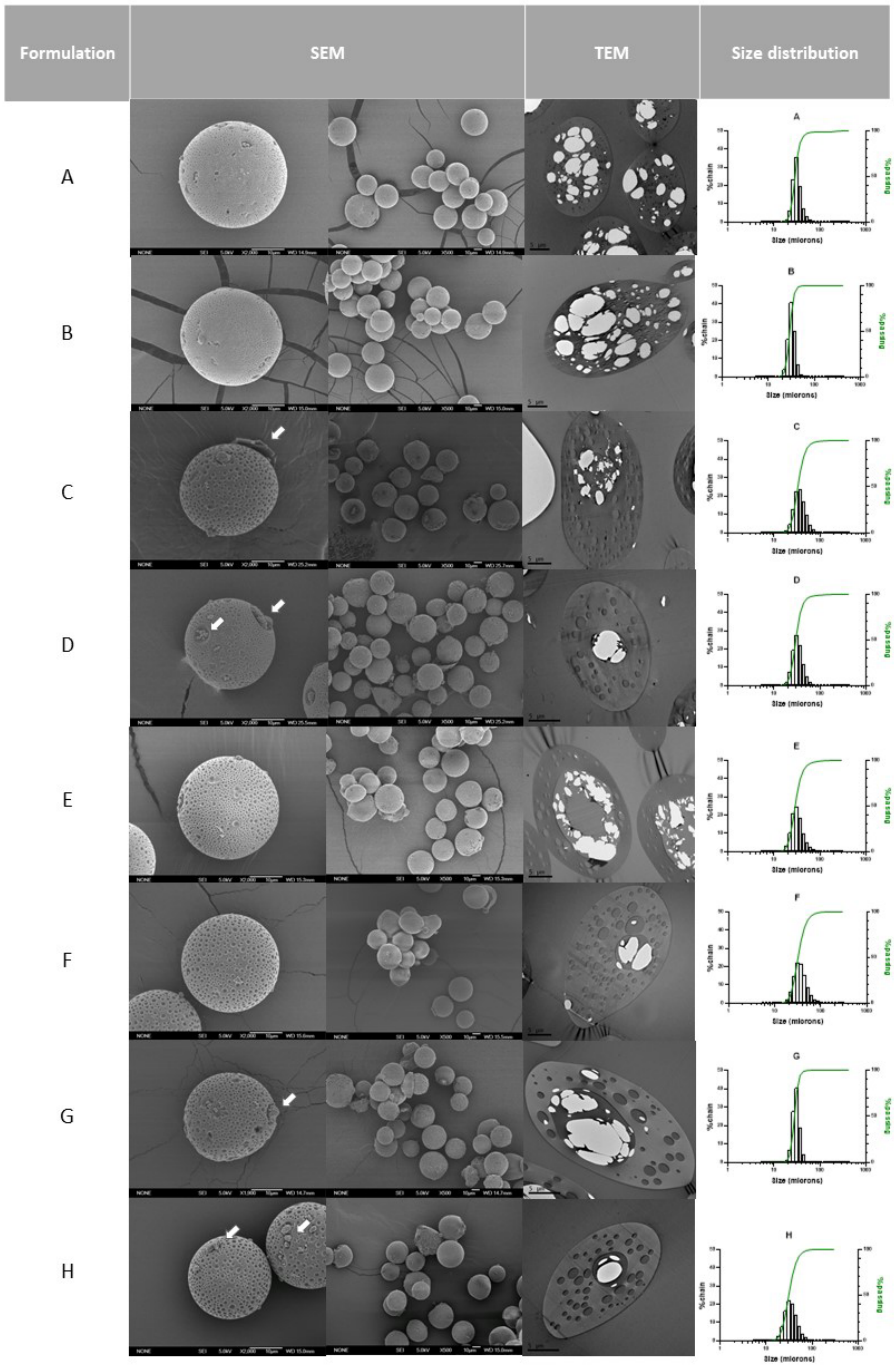

Figure 2. Scanning and transmission electron microscopies pictures and particle size distribution of the different MSs (A-H). Individual scanning pictures were made at x2000, group pictures at x500. White arrows mark the presence of crystals.

3.1.2. Mean particle size

All the formulations had a mean particle size between 27.90 and 33.30 µm (Table 3). No significant differences among formulations were found regarding to the solvents composition of the organic phase or the drugs content.

Table 3. Mean particle size of the different developed formulations (A-H).

Formulation	Mean particle size (μm ± sd)
A	28.65 ± 0.70
B	29.11 ± 0.76
C	33.30 ± 2.03
D	29.84 ± 0.48
E	28.82 ± 1.02
F	32.27 ± 1.74
G	27.90 ± 0.76
H	30.02 ± 1.02

3.1.3. DSC studies

DSC is a valuable technique to explore the change in the physical status of drugs once microencapsulated. DSC curves of pure substances (PLGA, UDCA and DX), different PLGA microspheres: PLGA, PLGA/vitamin E and DX-UDCA-loaded PLGA/vitamin E microspheres prepared with different organic solvent proportions (75:25, 80:20 and 85:15) and physical mixtures containing the same drug-polymer fraction than microspheres are provided in Figure 3.

When the raw substances were tested (Figure 3[A]), the curve of PLGA showed a slight endothermic peak corresponding to its glass transition (50 °C), whereas the DX and UDCA curves show sharp greater endothermic peaks corresponding to the melting points of their crystals (203 °C and 268 °C, respectively) as they are described in the literature [38,39]. These peaks were also observed in the physical mixture (Figure 3[B]).

Whereas in the case of formulations prepared with 80:20 MC:EtOH proportion, the melting endothermic peaks of drugs disappeared, suggesting a better drug dispersion into the polymeric matrix. In the case of formulations prepared with 75:25 and 85:15 MC:EtOH proportions, the profile decreased but it did not completely disappear (Figure 3[D] and [E]), which might be attributed to the presence of drug on the surface, as was expected in accordance with the images from scanning electron microscopy.

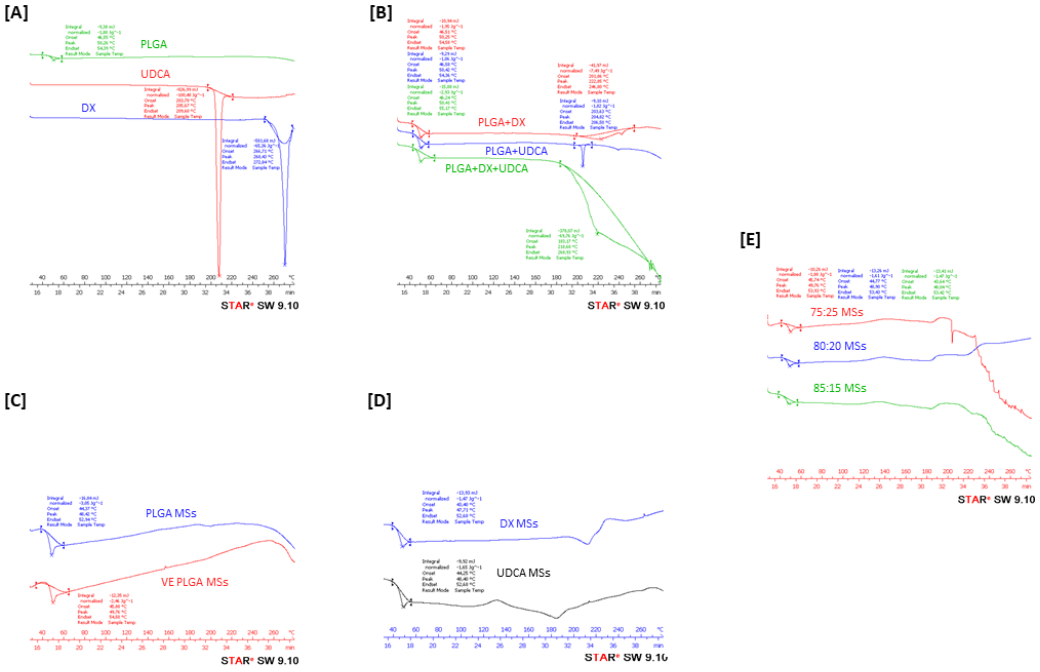

Figure 3. DSC curves of [A] PLGA (green), UDCA (red) and DX (blue), [B] physical mixtures of PLGA+DX (red), PLGA+UDCA (blue) and PLGA+DX+UDCA (green), [C] PLGA MSs (blue) and PLGA + vitamin E MSs (red), [D] DX MSs (blue) and UDCA MSs (black) and [E] with different proportions of solvents 75:25 (red), 80:20 corresponding to F (blue) and 85:15 corresponding to H (green).

3.1.4. X-Ray diffractometry analysis

The analysis by X-ray diffraction showed the presence of many diffraction bands in both drug's powder samples reflecting their crystalline state. On the contrary, for the PLGA, no high intensity peaks were observed, corresponding to an amorphous state.

The characteristics peaks of DX in the physical mixtures and MSs samples, suggesting that its incorporations in the MSs is in the crystalline state. However, no UDCA characteristics peaks were observed, neither in the physical mixture nor in the MSs samples, probably because the PLGA signal could hide these peaks. No differences in drugs spectra was observed in formulations prepared with different solvents proportions used in the organic phase of the emulsion with this X-ray diffraction analysis.

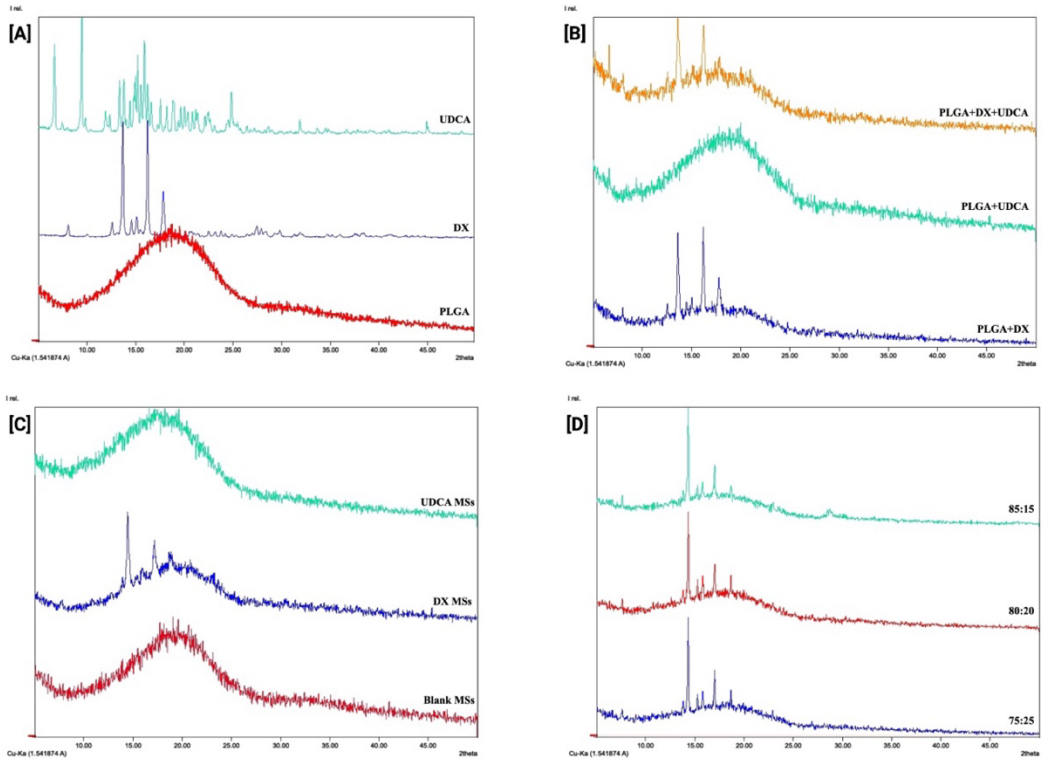

Figure 4. X-Ray diffractograms of [A] the different compounds (PLGA – red, DX – blue and UDCA – green), [B] physical mixtures of the compounds (PLGA+DX – blue, PLGA+UDCA – green and PLGA+DX+UDCA – orange), [C] non-loaded (red) and single loaded MSs (with DX – blue, with UDCA – green) and [D] co-loaded MSs elaborated with different solvent mixtures (MC:EtOH) (75:25 – blue, 80:20 – red and 85:15 – green).

3.1.5. Gas chromatography

Headspace method in GCMS is a useful technique to allow to know the content of organic solvent that remains after MSs manufacturing. Methylene chloride is a solvent of class 2, which means that its use must be limited. Both FDA and EMA limit its use to 600 ppm [28,29]. However, ethanol is a 3-class solvent, meaning low toxic potential and its limits are wider. Thus, in this work, we only determined the residual content of methylene chloride in 100:0, 85:15, 80:20 and 75:25 MSs, finding out in all of them a concentration of MC lower than 6 ppm/mg MSs (Table 4).

Table 4. Methylene chloride concentrations (ppm/mg MSs) of MSs elaborated with different dissolvent concentrations (100:0, 85:15, 80:20, 85:15 MC:EtOH).

MC:EtOH proportions	MC concentration (ppm/mg MSs)
100:0	3.61
85:15	3.89
80:20	4.56
75:25	5.34

3.1.6. Encapsulation efficiencies (EE)

Table 5 shows the values of entrapment efficiency of UDCA in the different formulations. To assess these data, the percentage of encapsulation has been statistically compared for those formulations that were made with the same initial amount of UDCA (40 mg). Thus, a statistically higher encapsulation has been observed for formulations C, E, F, and H, prepared including ethanol in different proportions in the internal phase of the emulsion, compared to formulation B ($p<0.01$ for C, E and H and $p<0.001$ for F), which was made exclusively using methylene chloride as organic solvent. No differences have been observed between the formulations prepared with different proportions of ethanol, so it seems that neither this parameter, nor the co-encapsulation of different amounts of dexamethasone has any influence on the encapsulation of UDCA.

Table 5. UDCA entrapment efficiencies of the different formulations (A-H). A and B were elaborated only with methylene chloride in the inner phase of the emulsion while C-H were elaborated with different mixtures of methylene chloride and ethanol.

Formulation	µg UDCA/mg MSs	Entrapment efficiency UDCA (%)
A	18.91 ± 2.95	45.08 ± 6.98
B	36.01 ± 0.87	45.73 ± 1.08
C	49.65 ± 2.78	63.08 ± 3.53
D	71.03 ± 4.11	63.00 ± 3.65
E	45.00 ± 3.09	61.38 ± 4.19
F	49.52 ± 7.53	65.15 ± 9.91
G	42.20 ± 1.46	57.57 ± 1.99
H	47.62 ± 2.03	62.50 ± 3.00

Table 6. DX entrapment efficiencies of the different formulations (A-H). A and B were elaborated only with methylene chloride. C-H were elaborated with different mixtures of methylene chloride and ethanol.

Formulation	µg DX/mg MSs	Entrapment efficiency DX (%)
A	123.64 ± 3.17	77.35 ± 2.09
B	117.25 ± 2.94	76.21 ± 1.94
C	140.68 ± 18.31	91.62 ± 11.93
D	148.93 ± 11.83	100.38 ± 8.54
E	131.45 ± 8.93	91.89 ± 6.28
F	95.79 ± 6.10	86.12 ± 5.49
G	133.95 ± 13.47	93.86 ± 9.57
H	92.15 ± 2.60	82.85 ± 2.34

Table 6 summarizes the entrapment efficiency of DX in the different formulations. To treat these data, the formulations that were prepared with the same initial amount of dexamethasone have also been compared. In the case of those formulations initially prepared with 80 milligrams of dexamethasone, statistical differences were observed between formulations B and D ($p<0.01$) and between formulations B and G ($p<0.05$). However, it should not be forgotten that both formulations D and G presented drug crystals on its surface, according to SEM pictures and DSC thermograms, which could explain this increase in the quantified encapsulation percentage, which, therefore, does not have to represent the amount of drug that is included inside the microspheres.

On the other hand, the formulations prepared with 60 milligrams of dexamethasone (F and H), both elaborated including ethanol in the internal phase of the emulsion but in a different proportion, do not show significant differences in terms of the percentage of dexamethasone encapsulation, indicating that this parameter should not influence in the drug loading, despite of the fact that the drug is more soluble in EtOH:MC mixtures than in MC alone.

The objective of this first set of experiments was to establish the better conditions to include all the drugs inside the microspheres. For that reason, the formulations which presented crystals on their surface according to SEM pictures and supported by DSC studies (C, D, G and H) were discarded for further studies, regardless of the drugs encapsulation values obtained. Furthermore, A and B were also discarded for presenting the lowest values of %EE for both drugs, UDCA and DX.

3.1.7. *In vitro* release studies

A preliminary *in vitro* release studies was performed with the formulations selected for further studies according to previous results (E and F). The release profile study of both drugs (UDCA and DX) was extended for 4 weeks, however, since the burst release (understood as the amount of drug released in the first 24h before becoming a stable released) is, together with the %EE, another crucial factor to consider in order to optimize a drug delivery system, special attention was paid to this parameter (Table 7).

Table 7. 24 h UDCA and DX burst release of selected formulations (E, F and H)

Formulation	µg UDCA/mg MSs	UDCA released (%)	µg DX/mg MSs	DX released (%)
E	17.64 ± 1.05	39.34 ± 3.28	26.60 ± 8.05	20.04 ± 4.87
F	8.78 ± 2.69	21.00 ± 4.48	18.13 ± 5.35	18.91 ± 5.50

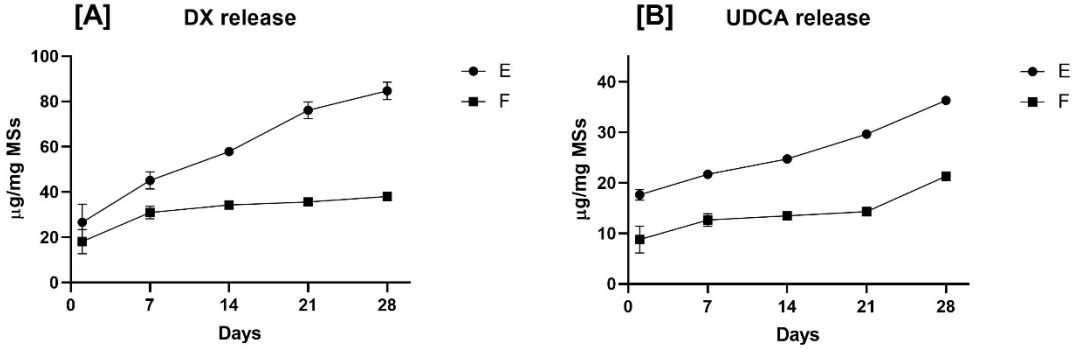

Figure 5. Cumulative *in vitro* release profiles (µg/mg MSs) of the formulations E and F and for 28 days of DX (A) and UDCA (B). Formulation E was made with 80 mg DX and 80:20 MC:EtOH, F with 60 mg DX and 80:20 MC:EtOH.

No statistical differences (p=0.1639) were observed in the initial release (24h) of dexamethasone from formulation E and F, even when different amounts of the anti-inflammatory drug were employed during microencapsulation. After that, as it can be observed in Figure 4A, a more rapid release of dexamethasone was observed for formulation E (2.15 µg DX/mg MSs/day) than for formulation F (0.74 µg DX/mg MSs/day). As for both formulations the UDCA loading was statistically similar and they were prepared with the same MC:EtOH proportion, the differences found in dexamethasone release might be related with the higher loading of the drug observed for formulation E, in comparison with formulation F, according to table 6 (131.45 ± 8.93 µg DX/mg MSs vs 95.79 ± 6.10 µg DX/mg MSs).

On the contrary, in the case of the more hydrophilic compound UDCA, statistical differences in the initial burst release were found ($p<0.05$), although in both cases 40 mg were used for microencapsulation and the UDCA loading resulted similar. This fact could be due to the better distribution of UDCA into the PLGA matrix core in presence of less initial amount of the corticosteroid. Interestingly, after this initial release, both

formulations showed similar UDCA release rate values (0.69 µg UDCA/mg MSs/day for E and 0.46 µg UDCA/mg MSs/day for F).

The similarity test (f_2) was evaluated for both drugs, finding out DX and UDCA releases from both formulations were not similar (25.80 and 45.56 values, respectively), however in the case of UDCA release these differences were observed only in the initial release.

According to the data obtained until this point, and keeping in mind that the goal of this optimization process is to obtain a microparticulate delivery system able to co-release the active compounds for several months, formulation F, able to promote a slower release of both UDCA an DX was the one selected as platform for further protein microencapsulation.

3.2. Protein inclusion in the optimised formulation

3.2.1. Morphological studies, mean particle size and particle size distribution.

As can be seen in Figure 5, all the formulations presented homogeny in spherical shapes with the presence of surficial pores and a slightly rough surface, in accordance with the previous results. The pores can be observed through the polymeric matrix thanks to the TEM images. These pictures also confirmed the presence of drug accumulations into all the MSs, not only in the multi-loaded formulations but also in the MSs loaded with only one active compound (F-DX and F-UDCA).

Table 8. Mean particle size of the selected formulation (F), the formulations with only DX or UDCA included (F-DX and F-UDCA) and the final formulation with GDNF included (F+GDNF).

Formulation	Mean particle size (µm ± sd)
F	32.27 ± 1.74
F-DX	29.49 ± 0.39
F-UDCA	32.29 ± 0.51
F+GDNF	31.76 ± 0.83

All formulations had a unimodal distribution of the particle size in the selected range (20-38 µm) (Figure 5) with similar mean particle size in all cases (between 29.49 and 32.29 µm) (Table 8).

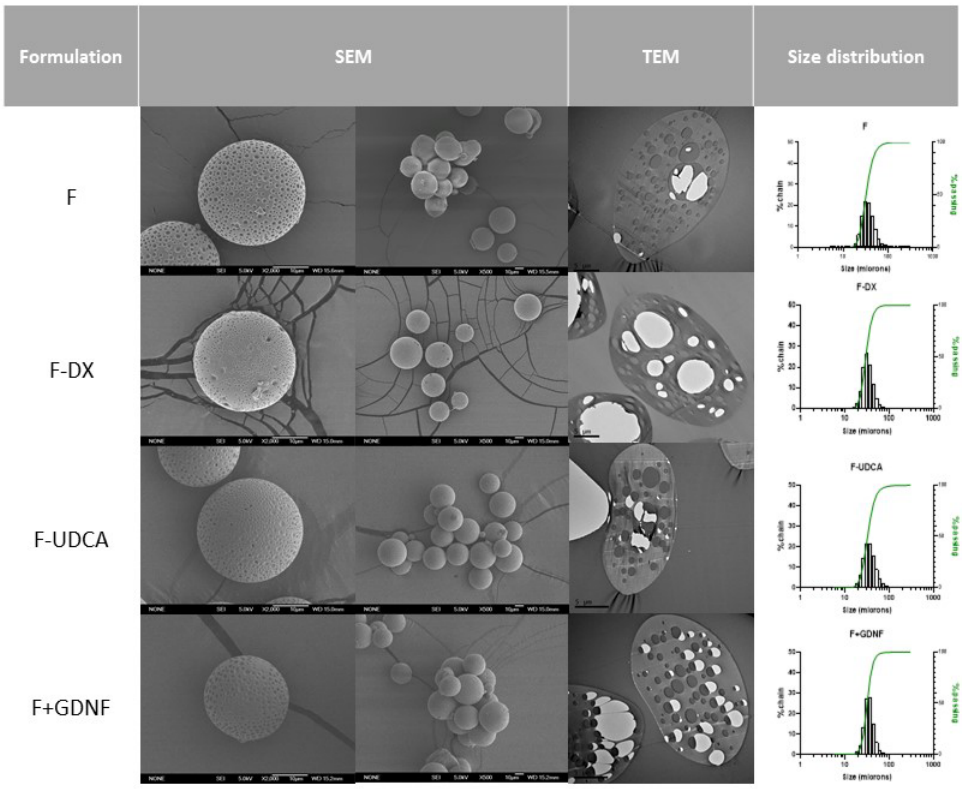

Figure 6. Scanning and transmission electron microscopies pictures and particle size distribution of the selected (F), the only loaded DX (F-DX), the only loaded UDCA (F-UDCA) and the selected with protein included (F+GDNF) MSs. Individual scanning pictures were made at x2000, group pictures at x500.

3.2.2. Matrix structure and protein distribution

To study the distribution of the protein, batches with the same composition of formulations F and F+GDNF were elaborated including red nile in the polymeric matrix and replacing GDNF by BSA-FITC in formulation F+GDNF. They were observed by confocal microscopy (Figure 6). It is well known that red nile possesses a high affinity for the PLGA, so the absence of red could be due to the presence of pores, but also to active compounds accumulations in solid-state. On the other hand, BSA-FITC is distributed heterogeneously through the microsphere, being a higher fluorescence located near the surface.

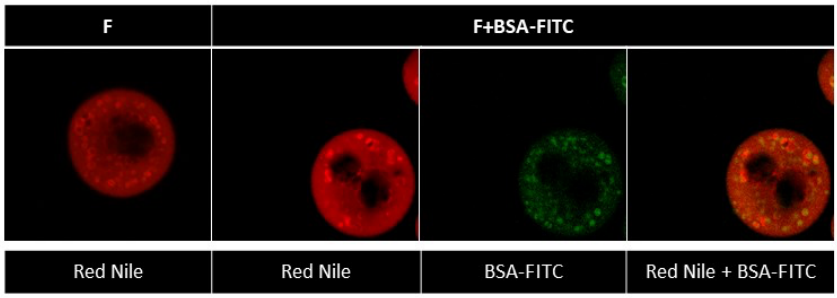

Figure 7. Confocal microscopy images of red nile labelled PLGA microsphere and BSA-FITC distribution. From left to right: microspheres of formulation F (without protein), microspheres of formulation F with the addition of BSA-FITC (red nile channel, BSA-FITC channel and the combination of red nile and BSA-FITC channels).

3.2.3. Encapsulation efficiencies

Table 9 compiles the encapsulation efficiencies of the different substances in the initially optimized, mono-loaded and protein-loaded MSs. No significant differences were found between mono-loaded and double or tri-loaded MSs in terms of drug loading. It is worthy to mention that the entrapment efficiency of each one of the three substances in the tri-loaded formulation (F+GDNF) was above 50% of the theorical amount.

Table 9. Entrapment efficiencies of the different active compounds (DX, UDCA, GDNF) in the mono-loaded, optimized and final formulations (F-DX, F-UDCA, F and F+GDNF, respectively)

Formulation	Entrapment efficiency UDCA (%)	Entrapment efficiency DX (%)	Entrapment efficiency GDNF (%)	Entrapment efficiency UDCA (µg/mg MSs)	Entrapment efficiency DX (µg/mg MSs)	Entrapment efficiency GDNF (ng/mg MSs)
F	65.15 ± 9.91	86.12 ± 5.49	-	49.52 ± 7.53	95.79 ± 6.10	-
F-DX	-	79.36 ± 1.37	-	-	103.74 ± 1.83	-
F-UDCA	59.79 ± 5.38	-	-	55.55 ± 4.98	-	-
F+GDNF	64.27 ± 1.34	84.36 ± 1.80	51.60 ± 1.10	52.65 ± 1.12	101.04 ± 2.17	19.83 ± 0.42

3.2.4. *In vitro* release studies

A prolonged *in vitro* study was carried out with the mono-loaded (F-DX and F-UDCA), the double (formulation F) and the tri-loaded MSs (formulation F+GDNF). According to Figure 7 a multiphasic profiles for both substances (DX and UDCA), characteristics of PLGA microspheres, where slow and fast release rates were alternating were observed until the end of the release (90 days) (Figure 8).

As expected after confocal microscopy observations, the GDNF delivery study (Figure 9) showed an important initial release (24h burst effect), due to the presence of the

protein near the MSs surface (5125.81 ± 1745.71 pg GDNF/mg MSs). After that, also a multiphase release rate profile was observed during the 180 days of the study.

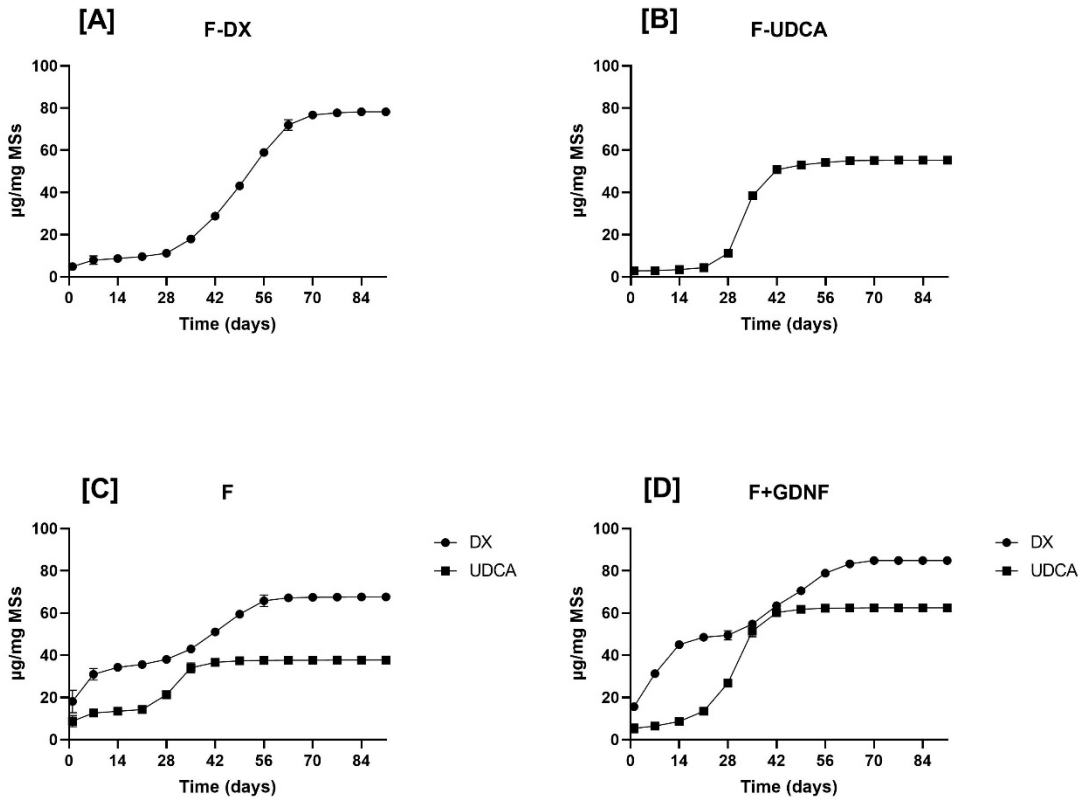

Figure 8. Cumulative *in vitro* release (µg/mg MSs) of DX from DX-loaded MSs (A), of UDCA from UDCA-loaded MSs (B), of DX and UDCA from DX-UDCA-loaded MSs (C) and of DX and UDCA from DX-UDCA-GDNF-loaded MSs (D).

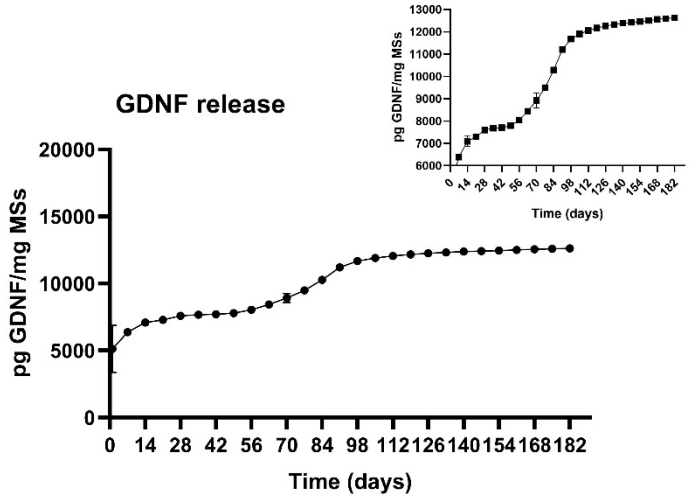

Figure 9. Release profile of GDNF from F+GDNF MSs. A more detailed zoom has been inserted of release from day 7 until the end.

As described in the materials and methods section, different equations were applied to the experimental release data in order to fit them in a kinetic model in an attempt to explain the influence of the co-loading and co-release on the release mechanism. Supplementary tables 1, 2, and 3 summarized the statistical data for a more accurate analysis.

For zero- and first-order, Korsmeyer-Peppas, Higuchi, Baker-Lonsdale and Weibull models it was not possible to fit the experimental date in only one time-step. It was necessary to divide the release profile in different steps (2 or 3) and even in that case none of them showed an accurate adjustment for these models (R^2 < 0.97) (see complementary data). On the contrary, the Gallagher-Corrigan models (with or without Gorrasi modification) showed the best adjustment for all the release profiles (DX, UDCA and GDNF) with $R^2_{adjusted}$ above 0.989 for the whole profile. This model describes the sigmoidal shape of the release profile by two stages: (stage 1) a "burst effect" step, that in this model does not only consider the 24h initial release but a more complex and prolonged process in which the "non-bonded" drug is released, and (stage 2) a "matrix erosion" step, in which the remaining drug in the system is released as the polymer degrades and therefore the matrix is eroded. In addition, when the data is treated using the Gorrasi adjustment, very similar results are observed between the "calculated B" values and the "experimental B" values, the latter obtained as the fraction of drug released in the first 24 hours in release studies. Table 10 shows the different parameters values in the final model.

Table 10. Values of the release model parameters in the different *In vitro* experiments.

Samples	Experimental B	Stage 1			Stage 2		
		B	Y_1 (-)	K_1 (day^{-1})	Y_2	K_2 (day^{-1})	T_2 (day)
UDCA release							
F-UDCA	0.0458	0.04079	0.2	0.008718	0.855	0.376	32.8
F	0.2100	0.1442	0.1264	0.3027	0.4866	0.3498	30.03
F+GDNF	0.1018	0.08815	0.1568	0.04692	0.9481	0.2997	30.37
DX release							
F-DX	0.0468	0.02982	0.04683	0.409	0.6986	0.1337	49.15
F	0.1891	0.1436	0.2225	0.2284	0.3442	0.1661	42.25
F+GDNF	0.1543	0.1066	0.3954	0.1157	0.3442	0.1537	46.41
GDNF release							
F+GDNF	0.2993	0.2648	0.1524	0.1185	0.2688	0.08849	81.07

According to this model, there is no difference in the fraction of UDCA released controlled by dissolution processes (stage 1), adding B and Y_1, regardless of the presence of dexamethasone, although it seems that the co-microencapsulation of this hydrophobic drug induces a greater presence of UDCA in the vicinity of the surface of the microspheres, and therefore a greater release in the first 24 h (B). The fraction of UDCA that is released controlled by dissolution processes but more slowly, that is Y_1, also does so at a lower rate when there is neither dexamethasone nor GDNF in the formulation, according to the K_1 values. Once the second stage of release is reached, controlled by mechanisms related to the degradation of the polymer according to this model, there seems to be no influence of co-microencapsulation, with similar higher release rate in all three cases.

On the other hand, when dexamethasone release profiles are studied using this kinetic model, the fraction of drug released in stage 1, governed by the dexamethasone dissolution rate according to the model, is clearly increased by the co-microencapsulation of UDCA, considering both the 24-hour release (B) and the global process ($B+Y_1$). Furthermore, according to the K_1 values, the presence of UDCA not only increases the fraction of dexamethasone released governed by dissolution processes, but also increases its release rate. As observed for UDCA release data, in the second stage of release, governed by polymer degradation mechanisms according to Gallagher and Corrigan [35], the influence of co-microencapsulation is less marked.

Finally, regarding the kinetic data for GDNF, an important release is described at 24h (B), which is consistent with the arrangement of the protein in the vicinity of the surface of the microspheres observed in confocal studies, followed by a slow release of the remaining protein, both in the stage governed by dissolution processes and in the stage controlled by polymer degradation processes.

3.2.5. Degradation

In order to complete the release study, degradation studies were carried out. As can be seen in Figure 9, all batches at time 0 presented a “golf-like” surface due to the presence of vitamin E [40] and it became smoother at week 2. It seems to be very crucial, for the release of DX and UDCA, the period between 4 and 6 weeks, when microspheres lost their spherical structure, having a spheroid morphology, and starting to appear

more cavities. According to release profiles, during this period, the release of DX and UDCA increased (that corresponded to the T_2 value), being sooner and more acute in the case of the UDCA. In this phase, the degradation stage in the kinetic model started. Moreover, it seems that the formulation exclusively made with dexamethasone presented shallower cavities after 4 weeks than the rest of the formulations in which there is UDCA, which would be in accordance with the hypothesis proposed after the kinetic treatment that the co-microencapsulation with UDCA enhances the release of dexamethasone in stage 1.

At week 8, all batches showed big pores, corresponding with the fast release of the protein. However, for the other compounds, the release had finished. Finally, at week 10, the microspheres structure collapsed.

Concerning molecular weight evaluated by GPC, a fast decrease was observed in the first 4 weeks in line with others authors results. From week 4, it was achieved a critical molecular weight approximately at 10000 g/mol [41, 42].

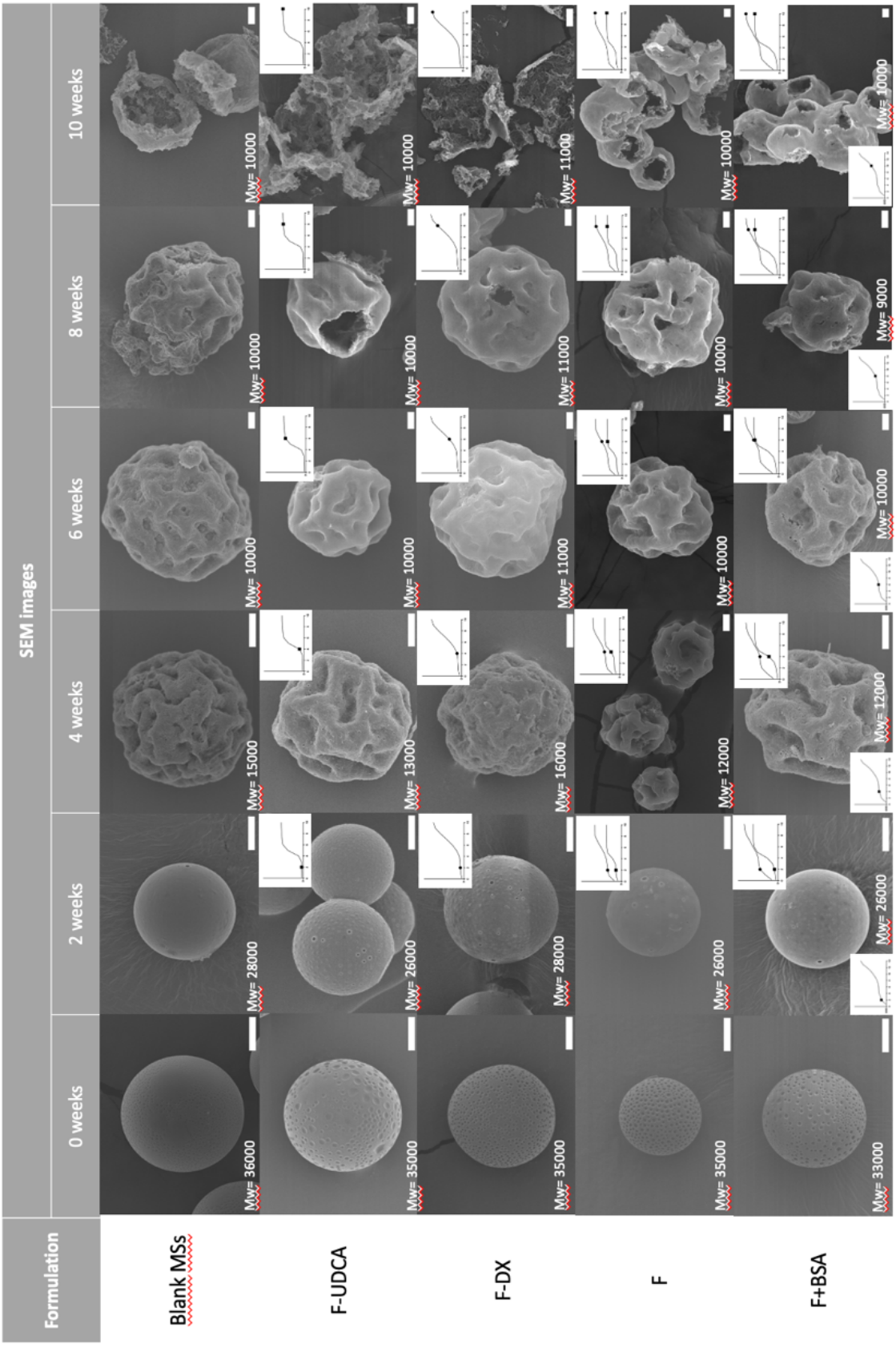

Figure 10. SEM images from different degradation dates (0, 2, 4, 6, 8 and 10 weeks) of different formulations (Blank MSs, F-UDCA, F-DX, F and F+BSA) with the PLGA molecular weight. Scale bars: 10 µm.

4. Discussion

The co-encapsulation of active compounds of different natures in the same microsystem is a major technological challenge. It is necessary to fine-tune the microencapsulation process to optimize not only the load of each of the compounds but also their subsequent controlled release. In this work, the starting point was the use of dichloromethane, widely employed in the preparation of PLGA microspheres as the only organic solvent for the internal phase of the emulsion in the solvent extraction/evaporation method [43]. However, it was also preferred to test the inclusion of ethanol as a co-solvent for the drugs to enhance their solubilization in the internal phase [44] and, at the same time, to promote a faster precipitation of the polymer that would also improve their entrapment [45]. Indeed, this modification managed to increase the percentage of encapsulation of both UDCA and DX. However, the physicochemical characterization of the different batches by electron microscopy and DSC revealed the presence drug crystals, probably DX according to RXD studies, on the surface of the microspheres that where prepared using combination of MC:EtOH of 75:25 and 85:15 as solvents in the inner phase of the emulsion. This phenomenon is widely reported in the scientific literature and can be explained by the rapid diffusion of the drug to the surface of the PLGA microsphere when ethanol is included as a co-solvent in the MC solution up to a percentage [46]. The fact that these surface crystals were observed when 25% or 15% of ethanol was included in the organic phase but not when 20% of the co-solvent was used, might suggest that not only the ratio MC:EtOH but also, the co-microencapsulation of several active compounds in the same system might play an important role. For the system proposed, the formulations employing a ratio 80:20 (MC:EtOH) seemed to be the balanced proportion between fast and slow solidification and drugs solubility [49,50], not presenting crystals on their surfaces.

The “golf-like” MS surface observed in all formulations was previously explained by the presence of the oily nature of Vitamin E, that might induce a slow and homogeneous diffusion of the remaining solvent from the droplet in the latest steps of the maturation process [40,47]. However, for formulations prepared including EtOH as co-solvent, bigger and more numerous porous were observed on the MSs surface, probably due to its rapid extraction and subsequent polymer matrix hardening of external layers of the

droplet in contact with the aqueous media. This rapid hardening might also explain the appearance of pores thorough the polymeric matrix [48] and the distribution of drugs mainly in the core of the microspheres, observed in TEM pictures, and suggested from preliminary *in vitro* release studies.

Once the DX and UDCA co-microencapsulation procedure was optimized, the following step was the inclusion of the active protein in its solid state dispersed in vit E. For comparison reasons also formulations loaded only with dexamethasone and only with UDCA were prepared. Confocal studies demonstrated that the protein was mainly located in the vicinity of the particles, which was already observed in previous studies and attributed to its displacement promoted by the solvent extraction [28,49]. Concerning the drugs encapsulation efficiencies, the final formulation achieved encapsulations over 50% of the initially incorporated amount for each component. Moreover, when the protein was combined, the encapsulation efficiencies of the other components did not change. To our awareness, this is the first tri-delivery formulation incorporating two low molecular weight compounds and a protein. It is worthy to mention that all MSs formulations evaluated showed residual solvent contents far below the allowed limits.

The release of DX and UDCA followed the typical behaviour of PLGA microspheres with different fast and slow releases, independently of the incorporation of one or more drugs. The formulation selected was able to release in a sustained manner DX until day 70, UDCA until day 70 and GDNF until day the end of the study, which makes the proposed microspheres very suitable as intraocular drug delivery systems for neuroprotective purpose.

It can be found in scientific literature a wide number of equations and models useful to describe the release behaviour from drug delivery systems. Some models explain the drug release by simple matrix diffusion mechanisms such as Higuchi's model [31]. Others describe the release profile only by polymer degradation [50]. Based on this, other models have been developed to explain all the release profiles due to the evolution of the system through time, combining these mechanisms together with the burst effect [35]. Depending on the system under study, it is not always easy to find kinetic models capable of describing the different processes involved in the drug release from

controlled release systems over long periods of time, since the mechanisms involved can change throughout the process. This kinetic evaluation is even more complicated when there is more than one active ingredient in the formulation. In fact, there is hardly any scientific literature in which this topic is addressed. In our study, for zero- and first-order, Korsmeyer-Peppas, Higuchi, Baker-Lonsdale and Weibull models it was possible to fit the experimental only after dividing the release profile in 2 or 3 different steps. This could be easily explained by the fact that the release mechanism from sustained drug delivery systems can change during the release process. On the contrary, the Gallagher-Corrigan models (with or without Gorrasi correction) showed the best adjustment for the whole profiles (DX, UDCA and GDNF) with $R^2_{adjusted}$ above 0.989. According to this model, in all cases two stages in the release profile can be detected, the first one governed by the drug dissolution and the second one by the polymer degradation. According to the data obtained in this work, it seems that the presence of both actives in the formulation mainly influenced the first stage. It can hypothesize that the presence of dexamethasone does not influence the proportion of UDCA released governed by dissolution (stage 1) although it does influence the distribution of UDCA in the microsphere, increasing the release at 24h. On the other hand, the presence of UDCA did increase the proportion of dexamethasone released by processes governed by dissolution and, also, the drug release rate, probably due to its amphiphilic nature or to the formation of bigger cavities in PLGA matrix.

5. Conclusions

The present work optimizes the encapsulation of three different active substances, a biotechnological compound, and two low molecular weight drugs with different solubilities (hydrophilic and hydrophobic). The inclusion of a water-soluble co-solvent (ethanol) in the microspheres' manufacturing, allowed an increase in the encapsulation efficiency of the bile acid and a more controlled delivery of it. The three drugs achieved good encapsulation efficiencies in the final formulation (all of them above the 50%) and presented suitable properties for its application for ocular pathologies, delivering each drug in a sustained manner for at least 3 months. According to the mathematical model used in this work, it seems that the presence of dexamethasone does influence the

distribution of UDCA in the microsphere, increasing its initial release. In addition, the presence of UDCA did increase the dexamethasone release rate in the first stage of the release profile.

This co-loaded formulation could be an interesting therapy for ophthalmic degenerative pathologies such as glaucoma.

Acknowledgements

This work was supported by Grant MAT2017-83858-C2-1 and MAT2017-83858-C2-2 funded by MCIN/AEI/ 10.13039/501100011033 and by "ERDF A way of making Europe" and Grant PID2020-113281RB-C21 and PID2020-113281RB-C22 funded by MCIN/AEI/ 10.13039/501100011033. Research Group UCM 920415 (InnOftal) and ISCIII-FEDER "Una manera de hacer Europa" RETICS (OFTARED) (RD16/0008/0009, RD16/0008/0004 and RD16/0008/0029). A.A.N thanks for the grant PRE2018-083951 funded by MCIN/AEI/10.13039/501100011033 and by "ESF Investing in your future". DGH acknowledges to UCM-Santander fellowship (CT17/17-CT17-18).

They also would like to thank the technical SEM and TEM assistance of the Centro de Microscopía Electrónica Luis Bru (CAI) in special to the Dr. Ángel Mazario Fernández, Dra Miriam González García and Dra María Luisa García Gil. GC studies were carried out in the C.A.I. Espectrometría de Masas, Facultad de Ciencias Químicas, UCM and X-Ray diffractometry analysis in CAI Técnicas Químicas, Unidad de Difracción de Rayos X, Facultad de Farmacia, UCM. Moreover, authors would like to thank to Jorge Rubio Retama for his technical advice with DSC, to Manuel Guzmán-Navarro for his help with GPC studies and the Unidad de Bioanálisis y Control de Calidad from CQAB for carrying out GPC analysis.

Supplementary Material

Supplementary Table 1. Fitting values of constants (K) and statistical parameters (R^2, $R^2_{adjusted}$ and SSE) in the different kinetics models from UDCA release.

Models **Steps (from day X to day X)**	**UDCA release**											
	F-UDCA				**F**				**F+GDNF**			
	K	**R^2**	**$R^2_{adjusted}$**	**SSE**	**K**	**R^2**	**$R^2_{adjusted}$**	**SSE**	**K**	**R^2**	**$R^2_{adjusted}$**	**SSE**
Zero-order												
1-21	2.591	0.905	0.858	0.138	0.256	0.820	0.730	3.237	0.396	0.923	0.884	2.945
21-42	2.378	0.952	0.927	70.530	1.138	0.949	0.924	17.050	2.357	**0.970**	0.955	42.320
42-70	0.123	0.825	0.782	2.748	0.033	0.748	0.664	0.177	0.073	0.728	0.638	0.967
First order												
1-21	-0.022	0.928	0.892	0.008	-0.032[a]	0.837[a]	0.674[a]	0.017[a]				
21-42	-0.123	0.952	0.927	0.188	-0.041[b]	0.939[b]	0.919[b]	0.053[b]	-0.065	**0.971**	0.965	0.168
42-70	-0.003	0.881	0.842	0.001	-0.0003	0.960	0.940	1.2e-06	-0.0004	0.766	0.649	1.47e-05
Korsmeyer-Peppas												
1-14	0.061	0.642	0.284	0.008	0.162[c]	**0.987**[c]	0.980[c]	0.002[c]	0.160	0.848	0.696	0.017
14-28	1.616	0.824	0.649	0.135					1.599	0.950	0.901	0.032
Hixson-Crowell												
1-21	-0.002	0.904	0.856	8.03e-05	-0.008	0.828	0.742	0.003	-0.011	0.914	0.872	0.002
21-49	-0.068	0.928	0.916	0.726	-0.038	0.904	0.872	0.075	-0.227	0.923	0.898	2.102
49-70					-0.00089	0.907	0.860	1.995e-05	-0.002	0.793	0.690	0.0003
Higuchi												
7-21	0.013	0.947	0.894	1.796e-05	0.031[c]	0.935[c]	0.903[c]	0.0005[c]	0.067	0.919	0.838	0.00074
21-42	0.471	0.940	0.911	0.028	0.255	0.957	0.936	0.006	0.496	**0.972**	0.959	0.014
42-70	0.042	0.914	0.885	0.0004	0.010	0.778	0.703	6.343e-05	0.021	0.760	0.680	0.0003
Baker-Lonsdale												
1-21	3.102e-05	0.878	0.816	3.017e-08	0.0005	0.867	0.801	8.102e-06	0.0005	0.849	0.773	1.029e-05
21-49	0.014	0.935	0.914	0.007	0.005	0.915	0.886	0.001	0.028[d]	0.836[d]	0.671[d]	0.015[d]
49-70	0.005	0.950	0.924	0.0003	0.0002	0.907	0.861	7.313e-07				
Weibull												
7-21	0.358	0.937	0.873	0.005	0.184[c]	**0.988**[c]	0.982[c]	0.002[c]	0.708	0.924	0.848	0.025
21-42	0.191	**0.977**	0.966	0.006	2.113	0.968	0.952	0.040	4.912	0.939	0.878	0.205
42-70	1.51	**0.989**	0.985	0.004	0.109	0.809	0.745	0.0005				
Gallagher-Corrigan	K1= 0.025 K2= 0.396	**0.9985**	0.9976	0.0032	K1 = 1.117 K2= 0.339	**0.9996**	0.9994	0.000026	K1 = 1.256 K2= 0.265	**0.9994**	0.9990	0.0017
Gallagher-Corrigan + Gorrasi correction	K1= 0.009 K2= 0.376	**0.9998**	0.9994	0.0007	K1= 0.303 K2= 0.350	**0.9998**	0.9996	0.00014	K1= 0.047 K2= 0.300	**0.9998**	0.9997	4.76e-04

[a]From day 1 to 14.[b] From day 14 to 42. [c] From day 1 to 21.[d] Until day 35. K in Korsmeyer-Peppas model refers to n. $R^2 \geq 0.97$ in bold.

Supplementary Table 2. Fitting values of constants (K) and statistical parameters (R^2, $R^2_{adjusted}$ and SSE) in the different kinetics models from DX release.

Models **Steps (from day X to day X)**	**DX release**											
	F-DX				**F**				**F+GDNF**			
	K	**R^2**	**$R^2_{adjusted}$**	**SSE**	**K**	**R^2**	**$R^2_{adjusted}$**	**SSE**	**K**	**R^2**	**$R^2_{adjusted}$**	**SSE**
Zero-order												
1-28	0.212	0.920	0.893	1.806	0.646	0.780	0.707	54.450	2.256	**0.993**	0.986	3.080
									0.316	0.893	0.787	1.170
28-70	1.707	**0.985**	0.982	60.84	0.773	0.929	0.915	62.680	0.912	**0.974**	0.970	30.120
First order												
1-28	-0.027	0.848	0.797	0.062	-0.009[a]	0.965[a]	0.948[a]	0.0008[a]	-0.056[b]	0.857[b]	0.786[b]	0.115[b]
28-56	-0.060	**0.994**	0.992	0.011	-0.020	**0.993**	0.991	0.001	-0.015[c]	**0.972**[c]	0.965[c]	0.006[c]
56-70	-0.019	0.919	0.838	0.003	-0.002	0.848	0.696	5.36e-05	-0.005	0.925	0.851	0.0002
Korsmeyer-Peppas												
1-28	0.238	**0.984**	0.979	0.007	0.222	**0.977**	0.969	0.008	0.358	**0.986**	0.983	0.015
28-42	2.426	**0.998**	0.998	0.003	0.716	**0.973**	0.947	0.001				
42-63												
Hixson-Crowell												
1-28	-0.003	0.923	0.897	0.0004	-0.002	0.945	0.939	0.001	-0.003	0.951	0.946	0.003
28-70	-0.039	**0.976**	0.971	0.053								
Higuchi												
1-28	0.013	**0.973**	0.964	5.745e+05	0.047	0.916	0.887	0.002	0.083	0.951	0.934	0.004
28-70	0.225	**0.978**	0.974	0.008	0.112	0.951	0.941	0.005	0.124	**0.984**	0.981	0.002
Baker-Lonsdale												
1-28	5.667E-05	0.961	0.947	6.117E-08	0.0009	0.865	0.820	5.407e-05	0.002	0.906	0.875	0.0002
28-70	0.004	0.919	0.902	0.002	0.003	0.946	0.935	0.0006	0.004	**0.982**	0.978	0.0005
Weibull												
1-21	0.233	**0.991**	0.987	0.003	0.270	**0.980**	0.970	0.008	0.457	**0.990**	0.986	0.011
21-70	2.432	0.964	0.958	0.270	0.938	0.952	0.944	0.054	0.971	0.935	0.924	0.079
Gallagher-Corrigan	K1= 0.006 K2= 0.184	**0.9936**	0.9899	0.0056	K1=0.747 K2= 0.159	**0.9966**	0.9953	0.0012	K1=0.163 K2= 0.164	**0.986**	0.977	0.008
Gallagher-Corrigan + Gorrasi correction	K1= 0.409 K2= 0.134	**0.9994**	0.9990	4.999e-04	K1= 0.228 K2=0.166	**0.9996**	0.9992	1.491e-04	K1 = 0.116 K2= 0.154	**0.997**	0.996	0.001

[a]From day 7 to 28. [b]From day 1 to 21. [c]From day 21 to 56. K in Korsmeyer-Peppas model refers to n.
$R^2 \geq 0.97$ in bold.

Supplementary Table 3. Fitting values of constants (K) and statistical parameters (R^2, $R^2_{adjusted}$ and SSE) in the different kinetics models from GDNF release.

Models **Steps (from day X to day X)**	**GDNF release** **F+GDNF** **K**	**R^2**	**$R^2_{adjusted}$**	**SSE**
Zero-order				
1-28	85.110	0.863	0.818	5.308e+05
28-49	8.789	0.963	0.944	733.100
49-98	83.520	**0.973**	0.969	3.991e+05
First-order				
1-28	-0.013	0.829	0.772	0.017
28-49	-0.001	0.963	0.944	1.235e-05
49-90	-0.009	**0.978**	0.974	0.002
Korsmeyer-Peppas				
1-28	0.118	**0.997**	0.996	2.920e-04
28-49	0.043	0.957	0.936	1.429e-05
49-84	0.508	0.954	0.943	0.003
Hixson-Crowell				
1-28	-0.055	0.875	0.834	0.200
28-49	-0.006	0.963	0.944	0.00036
49-90	-0.063	0.946	0.935	0.315
Higuchi				
1-28	0.032	0.968	0.957	3.802e-04
28-49	0.006	0.961	0.941	2.335e-06
49-90	0.073	0.942	0.931	0.002
Baker-Lonsdale				
1-28	0.0007	0.905	0.874	2.651e-05
28-49	9.738e-05	0.963	0.944	9.063e-08
49-90	1.545e-05	**0.993**	0.991	1.650e-05
Weibull				
1-28	0.147	**0.997**	0.995	5.469e-04
28-49	0.057	0.957	0.935	2.56e-05
49-90	0.848	0.931	0.917	0.016
Gallagher-Corrigan	K1= 1.269 K2=0.070	**0.993**	0.992	0.003
Gallagher-Corrigan + Gorrasi correction	K1= 0.119 K2= 0.089	**0.9988**	0.9985	5.431e-04

K in Korsmeyer-Peppas model refers to n. $R^2 \geq 0.97$ in bold.

6. References

[1] S.R. Flaxman, R.R.A. Bourne, S. Resnikoff, P. Ackland, T. Braithwaite, M. v. Cicinelli, A. Das, J.B. Jonas, J. Keeffe, J. Kempen, J. Leasher, H. Limburg, K. Naidoo, K. Pesudovs, A. Silvester, G.A. Stevens, N. Tahhan, T. Wong, H. Taylor, A. Arditi, Y. Barkana, B. Bozkurt, A. Bron, D. Budenz, F. Cai, R. Casson, U. Chakravarthy, J. Choi, N. Congdon, R. Dana, R. Dandona, L. Dandona, I. Dekaris, M. del Monte, J. Deva, L. Dreer, L. Ellwein, M. Frazier, K. Frick, D. Friedman, J. Furtado, H. Gao, G. Gazzard, R. George, S. Gichuhi, V. Gonzalez, B. Hammond, M.E. Hartnett, M. He, J. Hejtmancik, F. Hirai, J. Huang, A. Ingram, J. Javitt, C. Joslin, M. Khairallah, R. Khanna, J. Kim, G. Lambrou, V.C. Lansingh, P. Lanzetta, J. Lim, K. Mansouri, A. Mathew, A. Morse, B. Munoz, D. Musch, V. Nangia, M. Palaiou, M.B. Parodi, F.Y. Pena, T. Peto, H. Quigley, M. Raju, P. Ramulu, D. Reza, A. Robin, L. Rossetti, J. Saaddine, M. Sandar, J. Serle, T. Shen, R. Shetty, P. Sieving, J.C. Silva, R.S. Sitorus, D. Stambolian, J. Tejedor, J. Tielsch, M. Tsilimbaris, J. van Meurs, R. Varma, G. Virgili, Y.X. Wang, N.L. Wang, S. West, P. Wiedemann, R. Wormald, Y. Zheng, Global causes of blindness and distance vision impairment 1990–2020: a systematic review and meta-analysis, Lancet Glob Health. (2017). https://doi.org/10.1016/S2214-109X(17)30393-5.

[2] Y.C. Tham, X. Li, T.Y. Wong, H.A. Quigley, T. Aung, C.Y. Cheng, Global prevalence of glaucoma and projections of glaucoma burden through 2040: A systematic review and meta-analysis, Ophthalmology. (2014). https://doi.org/10.1016/j.ophtha.2014.05.013.

[3] M. Almasieh, L.A. Levin, Neuroprotection in Glaucoma: Animal Models and Clinical Trials, Annu Rev Vis Sci. (2017). https://doi.org/10.1146/annurev-vision-102016-061422.

[4] X. Wei, K.S. Cho, E.F. Thee, M.J. Jager, D.F. Chen, Neuroinflammation and microglia in glaucoma: time for a paradigm shift, J Neurosci Res. (2019). https://doi.org/10.1002/jnr.24256.

[5] A. v. Mantravadi, N. Vadhar, Glaucoma, Primary Care - Clinics in Office Practice. (2015). https://doi.org/10.1016/j.pop.2015.05.008.

[6] A.C. Gauthier, J. Liu, Neurodegeneration and neuroprotection in glaucoma, Yale Journal of Biology and Medicine. (2016).

[7] S. Naik, A. Pandey, S.A. Lewis, B.S.S. Rao, S. Mutalik, Neuroprotection: A versatile approach to combat glaucoma, Eur J Pharmacol. (2020). https://doi.org/10.1016/j.ejphar.2020.173208.

[8] Y. Liu, I.H. Pang, Challenges in the development of glaucoma neuroprotection therapy, Cell Tissue Res. 353 (2013). https://doi.org/10.1007/s00441-013-1584-z.

[9] M. Almasieh, A.M. Wilson, B. Morquette, J.L. Cueva Vargas, A. Di Polo, The molecular basis of retinal ganglion cell death in glaucoma, Prog Retin Eye Res. (2012). https://doi.org/10.1016/j.preteyeres.2011.11.002.

[10] A. Arranz-Romera, S. Esteban-Pérez, D. Garcia-Herranz, A. Aragón-Navas, I. Bravo-Osuna, R. Herrero-Vanrell, Combination therapy and co-delivery strategies to optimize treatment of posterior segment neurodegenerative diseases, Drug Discov Today. 24 (2019). https://doi.org/10.1016/j.drudis.2019.03.022.

[11] J. Qu, D. Wang, C.L. Grosskreutz, Mechanisms of retinal ganglion cell injury and defense in glaucoma, Exp Eye Res. (2010). https://doi.org/10.1016/j.exer.2010.04.002.

[12] R. Russo, G.P. Varano, A. Adornetto, C. Nucci, M.T. Corasaniti, G. Bagetta, L.A. Morrone, Retinal ganglion cell death in glaucoma: Exploring the role of neuroinflammation, Eur J Pharmacol. (2016). https://doi.org/10.1016/j.ejphar.2016.03.064.

[13] M. Almasieh, A.M. Wilson, B. Morquette, J.L. Cueva Vargas, A. Di Polo, The molecular basis of retinal ganglion cell death in glaucoma, Prog Retin Eye Res. (2012). https://doi.org/10.1016/j.preteyeres.2011.11.002.

[14] A. Arranz-Romera, B.M. Davis, I. Bravo-Osuna, S. Esteban-Pérez, I.T. Molina-Martínez, E. Shamsher, N. Ravindran, L. Guo, M.F. Cordeiro, R. Herrero-Vanrell, Simultaneous co-delivery of neuroprotective drugs from multi-loaded PLGA microspheres for the treatment of glaucoma, Journal of Controlled Release. (2019). https://doi.org/10.1016/j.jconrel.2019.01.012.

[15] R. Herrero-Vanrell, M.F. Refojo, Biodegradable microspheres for vitreoretinal drug delivery, Adv Drug Deliv Rev. (2001). https://doi.org/10.1016/S0169-409X(01)00200-9.

[16] D.A. Lee, E.J. Higginbotham, Glaucoma and its treatment: A review, American Journal of Health-System Pharmacy. (2005). https://doi.org/10.1093/ajhp/62.7.691.

[17] G.A. Peyman, G.J. Ganiban, Delivery systems for intraocular routes, Adv Drug Deliv Rev. (1995). https://doi.org/10.1016/0169-409X(95)00018-3.

[18] V. Delplace, A. Ortin-Martinez, E.L.S. Tsai, A.N. Amin, V. Wallace, M.S. Shoichet, Controlled release strategy designed for intravitreal protein delivery to the retina, Journal of Controlled Release. 293 (2019) 10–20. https://doi.org/10.1016/J.JCONREL.2018.11.012.

[19] R. Herrero-Vanrell, J.A. Cardillo, Ocular pharmacokinetic, drug bioavailability, and intraocular drug delivery systems, in: Retinal Pharmacotherapy, 2010. https://doi.org/10.1016/b978-1-4377-0603-1.00014-4.

[20] I. Bravo-Osuna, V. Andrés-Guerrero, P. Pastoriza Abal, I.T. Molina-Martínez, R. Herrero-Vanrell, Pharmaceutical microscale and nanoscale approaches for efficient treatment of ocular diseases, Drug Deliv Transl Res. (2016). https://doi.org/10.1007/s13346-016-0336-5.

[21] R. Herrero-Vanrell, I. Bravo-Osuna, V. Andrés-Guerrero, M. Vicario-de-la-Torre, I.T. Molina-Martínez, The potential of using biodegradable microspheres in retinal diseases and other intraocular pathologies, Prog Retin Eye Res. (2014). https://doi.org/10.1016/j.preteyeres.2014.04.002.

[22] R. de HOZ, B. ROJAS, A. RAMíREZ, J. SALAZAR, B. GALLEGO, A. TRIVIñO, V. ANDRéS-GUERRERO, R. HERRERO-VANRELL, G. MIHOV, A. DIAS, M. ZONG, J. RAMíREZ, Assessment of polyesteramide of PEA Microparticles for in vivo intraocular injections, Acta Ophthalmol. (2013). https://doi.org/10.1111/j.1755-3768.2013.f005.x.

[23] N. v. Saraiya, D.A. Goldstein, Dexamethasone for ocular inflammation, Expert Opin Pharmacother. 12 (2011). https://doi.org/10.1517/14656566.2011.571209.

[24] J. Ruiz-Medrano, R. Rodríguez-Leor, E. Almazán, F. Lugo, E. Casado-Lopez, L. Arias, J.M. Ruiz-Moreno, Results of dexamethasone intravitreal implant (Ozurdex) in diabetic macular edema patients: Early versus late switch, Eur J Ophthalmol. (2020). https://doi.org/10.1177/1120672120929960.

[25] A. Daruich, E. Picard, J.H. Boatright, F. Behar-Cohen, Review: The bile acids urso- and tauroursodeoxycholic acid as neuroprotective therapies in retinal disease, Mol Vis. 25 (2019).

[26] A. Daruich, T. Jaworski, H. Henry, M. Zola, J. Youale, L. Parenti, M.C. Naud, K. Delaunay, M. Bertrand, M. Berdugo, L. Kowalczuk, J. Boatright, E. Picard, F. Behar-Cohen, Oral Ursodeoxycholic Acid Crosses the Blood Retinal Barrier in Patients with Retinal Detachment and Protects Against Retinal Degeneration in an Ex Vivo Model, Neurotherapeutics. (2021). https://doi.org/10.1007/s13311-021-01009-6.

[27] C. García-Caballero, B. Lieppman, A. Arranz-Romera, I.T. Molina-Martínez, I. Bravo-Osuna, M. Young, P. Baranov, R. Herrero-Vanrell, Photoreceptor preservation induced by intravitreal controlled delivery of gdnf and gdnf/melatonin in rhodopsin knockout mice, Mol Vis. (2018).

[28] P. Checa-Casalengua, C. Jiang, I. Bravo-Osuna, B.A. Tucker, I.T. Molina-Martínez, M.J. Young, R. Herrero-Vanrell, Retinal ganglion cells survival in a glaucoma model by GDNF/Vit e PLGA microspheres prepared according to a novel microencapsulation procedure, Journal of Controlled Release. (2011). https://doi.org/10.1016/j.jconrel.2011.06.023.

[29] P. Checa-Casalengua, C. Jiang, I. Bravo-Osuna, B.A. Tucker, I.T. Molina-Martínez, M.J. Young, R. Herrero-Vanrell, Retinal ganglion cells survival in a glaucoma model by GDNF/Vit E PLGA microspheres prepared according to a novel microencapsulation procedure, Journal of Controlled Release. 156 (2011) 92–100. https://doi.org/10.1016/J.JCONREL.2011.06.023.

[30] EMA, Guideline on the investigation of bioequivalence, 2010.

[31] P. Costa, J.M. Sousa Lobo, Modeling and comparison of dissolution profiles, Eur J Pharm Sci. 13 (2001) 123–133. https://doi.org/10.1016/S0928-0987(01)00095-1.

[32] M. Padmaa Paarakh, P. Ani Jose, C.M. Setty, G.V.P. Christoper, RELEASE KINETICS-CONCEPTS AND APPLICATIONS, 12| International Journal of Pharmacy Research & Technology |. (n.d.).

[33] J. Siepmann, N.A. Peppas, Modeling of drug release from delivery systems based on hydroxypropyl methylcellulose (HPMC), Adv Drug Deliv Rev. 64 (2012) 163–174. https://doi.org/10.1016/J.ADDR.2012.09.028.

[34] V. Papadopoulou, K. Kosmidis, M. Vlachou, P. Macheras, On the use of the Weibull function for the discernment of drug release mechanisms, Int J Pharm. 309 (2006) 44–50. https://doi.org/10.1016/J.IJPHARM.2005.10.044.

[35] K.M. Gallagher, O.I. Corrigan, Mechanistic aspects of the release of levamisole hydrochloride from biodegradable polymers, J Control Release. 69 (2000) 261–272. https://doi.org/10.1016/S0168-3659(00)00305-9.

[36] G. Gorrasi, G. Attanasio, L. Izzo, A. Sorrentino, Controlled release mechanisms of sodium benzoate from a biodegradable polymer and halloysite nanotube composite, Polym Int. 66 (2017) 690–698. https://doi.org/10.1002/PI.5309.

[37] P. Checa-Casalengua, C. Jiang, I. Bravo-Osuna, B.A. Tucker, I.T. Molina-Martínez, M.J. Young, R. Herrero-Vanrell, Preservation of biological activity of glial cell line-derived neurotrophic factor (GDNF) after

microencapsulation and sterilization by gamma irradiation, Int J Pharm. 436 (2012) 545–554. https://doi.org/10.1016/J.IJPHARM.2012.07.019.

[38] E. Yonemochi, Y. Ueno, T. Ohmae, T. Oguchi, S.I. Nakajima, K. Yamamoto, Evaluation of amorphous ursodeoxycholic acid by thermal methods, Pharm Res. 14 (1997) 798–803. https://doi.org/10.1023/A:1012114825513.

[39] N.M. Vacanti, H. Cheng, P.S. Hill, J.D.T. Guerreiro, T.T. Dang, M. Ma, S. Watson, N.S. Hwang, R. Langer, D.G. Anderson, Localized Delivery of Dexamethasone from Electrospun Fibers Reduces the Foreign Body Response, Biomacromolecules. 13 (2012) 3031. https://doi.org/10.1021/BM300520U.

[40] P. Checa-Casalengua, C. Jiang, I. Bravo-Osuna, B.A. Tucker, I.T. Molina-Martínez, M.J. Young, R. Herrero-Vanrell, Retinal ganglion cells survival in a glaucoma model by GDNF/Vit E PLGA microspheres prepared according to a novel microencapsulation procedure, Journal of Controlled Release. 156 (2011) 92–100. https://doi.org/10.1016/J.JCONREL.2011.06.023.

[41] P. Checa-Casalengua, C. Jiang, I. Bravo-Osuna, B.A. Tucker, I.T. Molina-Martínez, M.J. Young, R. Herrero-Vanrell, Preservation of biological activity of glial cell line-derived neurotrophic factor (GDNF) after microencapsulation and sterilization by gamma irradiation, Int J Pharm. 436 (2012) 545–554. https://doi.org/10.1016/J.IJPHARM.2012.07.019.

[42] D. Barbosa-Alfaro, V. Andrés-Guerrero, I. Fernandez-Bueno, M.T. García-Gutiérrez, E. Gil-Alegre, I.T. Molina-Martínez, J.C. Pastor-Jimeno, R. Herrero-Vanrell, I. Bravo-Osuna, Dexamethasone PLGA Microspheres for Sub-Tenon Administration: Influence of Sterilization and Tolerance Studies, Pharmaceutics. 13 (2021) 1–21. https://doi.org/10.3390/PHARMACEUTICS13020228.

[43] S. Suri, G. Ruan, J. Winter, C.E. Schmidt, Microparticles and Nanoparticles, in: Biomaterials Science: An Introduction to Materials in Medicine, Third Edition, Academic Press, 2013: pp. 360–388. https://doi.org/10.1016/B978-0-08-087780-8.00034-6.

[44] F. Ramazani, W. Chen, C.F. Van Nostrum, G. Storm, F. Kiessling, T. Lammers, W.E. Hennink, R.J. Kok, Strategies for encapsulation of small hydrophilic and amphiphilic drugs in PLGA microspheres: State-of-the-art and challenges, Int J Pharm. 499 (2016) 358–367. https://doi.org/10.1016/J.IJPHARM.2016.01.020.

[45] Y. Yeo, K. Park, Control of encapsulation efficiency and initial burst in polymeric microparticle systems, Arch Pharm Res. 27 (2004) 1–12. https://doi.org/10.1007/BF02980037.

[46] A. Rawat, D.J. Burgess, Effect of ethanol as a processing co-solvent on the PLGA microsphere characteristics, Int J Pharm. 394 (2010). https://doi.org/10.1016/j.ijpharm.2010.05.013.

[47] P. Checa-Casalengua, C. Jiang, I. Bravo-Osuna, B.A. Tucker, I.T. Molina-Martínez, M.J. Young, R. Herrero-Vanrell, Preservation of biological activity of glial cell line-derived neurotrophic factor (GDNF) after microencapsulation and sterilization by gamma irradiation, Int J Pharm. 436 (2012) 545–554. https://doi.org/10.1016/J.IJPHARM.2012.07.019.

[48] Y. Yeo, K. Park, Control of encapsulation efficiency and initial burst in polymeric microparticle systems, Arch Pharm Res. 27 (2004). https://doi.org/10.1007/BF02980037.

[49] C. García-Caballero, E. Prieto-Calvo, P. Checa-Casalengua, E. García-Martín, V. Polo-Llorens, J. García-Feijoo, I.T. Molina-Martínez, I. Bravo-Osuna, R. Herrero-Vanrell, Six month delivery of GDNF from PLGA/vitamin E biodegradable microspheres after intravitreal injection in rabbits, European Journal of Pharmaceutical Sciences. 103 (2017). https://doi.org/10.1016/j.ejps.2017.02.037.

[50] I. Katzhendler, A. Hoffman, A. Goldberger, M. Friedman, Modeling of Drug Release from Erodible Tablets, J Pharm Sci. 86 (1997) 110–115. https://doi.org/10.1021/JS9600538.

CAPÍTULO III – CHAPTER III. Biodegradable smart hydrogels: drug delivery platforms for the treatment of ophthalmic chronic diseases affecting the back of the eye.

Biodegradable smart hydrogels: drug delivery platforms for the treatment of ophthalmic chronic diseases affecting the back of the eye.

Alba Aragón-Navas[1,2], José Javier López-Cano[1,2], Melissa Johnson[3], Sigen A[3], Marta Vicario-de-la-Torre[1,2], Vanessa Andrés-Guerrero[1,2], Hongyun Tai[4], Wenxin Wang[3], Irene Bravo-Osuna[1,2,5,6], Rocío Herrero-Vanrell[1,2,5,6]

[1]Innovation, Therapy, and Pharmaceutical Development in Ophthalmology (InnOftal) Research Group, UCM 920415, Department of Pharmaceutics and Food Technology, Faculty of Pharmacy, Complutense University of Madrid, Madrid, Spain

[2] Health Research Institute, San Carlos Clinical Hospital (IdISSC), Madrid, Spain

[3]Charles Institute of Dermatology, School of Medicine, University College Dublin, Dublin 4, Ireland.

[4] Blafar Ltd., Belfield Innovation Park, University College Dublin, Belfield, D04 V1W8 Dublin 4, Ireland.

[5] National Ocular Pathology Network (OFTARED), Carlos III Health Institute, Madrid, Spain

[6] University Institute for Industrial Pharmacy (IUFI), School of Pharmacy, Complutense University of Madrid, Madrid, Spain

ABSTRACT

This work aimed to develop smart hydrogels based on functionalised hyaluronic acid (HA) and PLGA-PEG-PLGA (PLGA=poly-(DL-lactic-co-glycolic acid); PEG=polyethylene glycol) as platforms for intraocular drug delivery. In this study, the drug selected to load hydrogels was the anti-inflammatory agent dexamethasone-phosphate (0.2% w/v). Initially, different ratios of HA-aldehyde (HA-CHO) and thiolated-HA (HA-SH) were assayed, selecting as optimal concentrations 2 and 3% (w/v), respectively. Optimised HA hydrogels formulations presented fast degradation (8 days) and drug release (91.46±3.80% in 24h) resulting suitable for short-term intravitreal treatments. Different technological strategies were also performed to accelerate water solubility of PLGA-PEG-PLGA polymer such as substituting PEG1500, in the synthesis, by a higher molecular weight (PEG3000) or adding cryopreserving substances in the buffer dissolution. PEG1500 was chosen to continue optimisation and final PLGA-PEG-PLGA hydrogels (PPP1500) were dissolved in trehalose or mannitol carbonate buffer. They presented a more sustained release (71.77±1.59% and 73.41±0.83% in 24 hours, respectively) and a slower degradation (>14 days). *In vitro* cytotoxicity studies in retinal-pigmented epithelial cell line (RPE-1) demonstrated good tolerance (viability values >90%). PLGA-PEG-PLGA hydrogels are proposed as suitable candidate for long-term intravitreal treatments. Preliminary studies of wound healing performed for PLGA-PEG-PLGA hydrogels suggested a faster rate of proliferation at 8h than control.

1. Introduction

A growth in ophthalmic chronic diseases has been reported in developed countries in the last decades, mainly due to the increase in life expectancy and change in lifestyle towards unfavourable habits. These diseases cause deterioration and visual impairment. Among them, glaucoma, and age-related macular degeneration (AMD) are the post prevalent in aged [1]. The pathophysiology of both diseases is complex. They have in common cellular senescence, oxidative stress, and inflammatory pathways [2].

Oxidative stress and inflammation have in common the generation of reactive oxygen species (ROS). ROS can be produced by two pathways; one involves mitochondrial dysfunction, and the other route is related to the inflammatory response by nicotinamide adenine dinucleotide phosphate oxidase (NADPH oxidases) [2]. Apart from oxidative stress, lipid peroxidation can also cause the activation of local para-inflammation, understood as "a tissue adaptive response to noxious stress or malfunction and has characteristics that are considered as intermediate between basal and inflammatory states" [3]. Although a physiological response resulted essential to maintain homeostasis and restore tissue functionality, uncontrolled dysregulation can produce damage in the retina and the start and progression of the disease. In fact, an excess of para-inflammation seems to cause the production of cytokines/chemokines as a response to inflammation with a neuroretinal damage [3,4].

Treatments for ocular chronic diseases affecting the posterior segment require repeated intraocular administrations to maintain effective concentrations in the retinal tissues. However, intraocular injections are poorly tolerated, and the side effects increase with the number of interventions [5]. In order to solve this issue, drug delivery systems (DDS) have been emerging with the main objective of spreading their application since they can control drug release for long periods with a significant decrease of interventions [6].

Hydrogels are gaining attention in the last decades. They are defined as highly hydrated mesh networks formed from natural, synthetic or semi-synthetic polymers that are physically or covalently crosslinked. In recent years, smart biomaterials have been developed and assessed to achieve personalized precision medicine such as the

case of smart hydrogels, or stimuli-responsive hydrogels. They have the advantage of easy preparation process and can prolong the drug release [7]. Furthermore, the use of small external triggers (i.e., changes in the pH, temperature, electricity, magnetics, light, or biomolecules) can generate changes in the physical properties of these smart hydrogels, tuning their properties.

Hydrogels are remarkable for local drug delivery because of their biocompatibility, drug protection, and, as mentioned, physicochemical tailor-made properties [8]. Moreover, in the treatment of chronic retinal diseases, they are a promising system since they are capable of sustaining drug release and thus, extending their local presence, avoiding repeated administration [9]. They can be made of natural polymers like chitosan, alginate, fibrin, gelatin, hyaluronic acid, or synthetic like poly(ethylene glycol) (PEG) or poly(vinyl alcohol). There are also semi-synthetic hydrogels constituted of gelatin functionalised by synthetic groups like, for example, methacryloyl groups [8].

In this work, we developed two different smart injectable hydrogels for the treatment of ophthalmic diseases. One is composed of a natural polymer (hyaluronic acid) and the other one is a synthetic hydrogel constituted by poly(lactic-co-glycolic acid) (PLGA) and PEG monomer units to form the PLGA-PEG-PLGA (PPP) triblock.

Hyaluronic acid (HA), also called hyaluronan, is a glycosaminoglycan composed of a repetition of disaccharide units of α-1,4-D-glucuronic acid, and β-1,3-N-acetyl-D-glucosamine. It is a naturally ubiquitous polymer present in all vertebrates and presents crucial roles in the composition and structure of extracellular matrix, development, organization or remodelling of tissue, and modulation of inflammation, among others [10,11]. However, the use of uncrosslinked HA is limited since its rapid degradation, *in vivo* clearance, or poor mechanical properties. To solve this, HA can be chemically modified, by esterification of the carboxylic acid groups and by other modifications of the alcohol groups (by divinyl sulfone or diglycidyl ethers) [12]. In literature, crosslinked hydrogels with injectable properties obtained by the interaction of thiol (SH) and aldehyde (CHO) groups have been described [13]. In this work we have explored the development of crosslinking hydrogels by combination of HA-SH and HA-CHO.

In the case of synthetic PPP hydrogels, PEG is a biodegradable polymer with nontoxic nature and absence of antigenic and immunogenic effects widely used in pharmacological applications. PEG could be copolymerized with PLGA but also, with other aliphatic polyesters such as polylactic acid (PLA) or poly(ε-caprolactone), among others. Biodegradability and biocompatibility are key properties in order to develop hydrogels. For this reason, PPP hydrogels are widely studied, since PLGA also possesses these properties [14]. PPP hydrogels are thermosensitive, and the gelation process involves micelles aggregation. Once formed, the micelles are composed of a hydrophobic core (PLGA) surrounded by PEG tails. At room temperature, the micelles are separated increasing their size suffering aggregation with temperature rise [14,15].

In the present study, both hydrogels have been developed and characterized to finally assess the suitability for sustained release of an anti-inflammatory drug. The final aim of these hydrogels is to be a drug delivery platform for chronic ophthalmic diseases affecting the back of the eye. Their *in vitro* tolerance has been evaluated in retinal cells. Finally, a preliminary *in vitro* wound healing study has been performed with the final formulation.

2. Materials and methods

2.1. Materials

Polyethylene glycol (PEG1500 and PEG3000), stannous 2-ethylhexanoate, glycolide, hyaluronidase from sheep testes (≥300 units/mg) and dexamethasone phosphate were obtained from Sigma-Aldrich (Leinster, Ireland). DL-Lactide was purchased from Corbion® (Gorinchem, The Netherlands).

HA-SH (220kDa raw material HA) was kindly donated by Blafar Ltd (Dublin, Ireland). Hyaluronic acid (1000 kDa, food grade) was obtained from Stanford chemical Ltd. Sodium (meta) periodate ($NaIO_4$, 99.5%) was purchased from Sigma-Aldrich.

2.2. Synthesis of HA-CHO and characterization.

HA-CHO was obtained by the method described by Cai Y et al. [16]. Briefly, HA (1000 kDa) was oxidized by sodium periodate ($NaIO_4$). This molecule produces the breakup of the glucuronic acid ring by oxidizing -OH terminal groups and transforming them into

aldehyde groups. The oxidation reaction was carried out in dark conditions at room temperature for 24 hours. The pure product was obtained after dialysis and freeze-drying, and the oxidation degree was assessed by TNBS (2,4,6-Trinitrobenzene Sulfonic Acid) assay. The oxidation degree of the resulting HA-CHO was 21.5%.

2.3. Synthesis of PPP triblock copolymer and characterization.

PPP polymers were synthesized according to the ring-opening polymerization (ROP) method described previously by Lopez-Cano JJ et al. [15].

Briefly, 0.01 mol of PEG 1500 (PPP 1500) or PEG 3000 (PPP 3000) were dried at 100°C in a two-necked flask overnight under vacuum. After drying, 0.015 mol of GA and 0.231 mol of LA (GA:LA 1:15) were added under the protection of nitrogen. Then, the mixture was further heating (130°C) and stirred until the monomers were melted (0.5-1h). Stannous 2-ethylhexanoate was added (0.2% w/w of monomers) and the reaction was kept at 150°C for 8 hours under a nitrogen atmosphere. Unreacted monomers were removed by vacuum (1 hour). Then, the crude polymer was purified by complete dissolution in ice-cold water, then, precipitation was carried out at 80 °C and the supernatant was removed. After that, the crude polymer was redissolved in ice-cold water. This cycle of dissolution-precipitation-decantation of the crude polymer was repeated three times. Finally, the crude polymer was freeze-dried and stored at -30 °C.

In order to characterize PPP triblock polymers, the structure was evaluated by 1H-NMR. The crude polymer was dissolved in deuterated chloroform ($CDCl_3$) and measured at 25°C in a Bruker AV 500MHz.

The molecular weight of PLGA-PEG-PLGA triblock was measured by gel permeation chromatography (GPC) composed of a binary pump (Waters 1525) coupled to a guard column PLgel 5µm 50x7.5, a PLgel 5um MIXED-D 300 x 7.5 mm column and a diffractive index detector (Waters 2414 detector). The analysis was made at a rate of 1.0 mL/min using tetrahydrofuran as eluent, the column temperature was set at 30°C.

2.4. Fabrication of HA-SH/HA-CHO hydrogels.

Both, HA-SH with a 20% substitution degree and HA-CHO of 21.5% oxidation degree were dissolved in PBS (pH= 7.4, isotonised with NaCl). The crosslinked hydrogel was

formed by mixing both solutions in a ratio of 1:1 at room temperature. Different concentrations of each compound were assessed in order to select the most suitable.

2.5. Fabrication of PLGA-PEG-PLGA hydrogels.

PLGA-PEG-PLGA polymer was dissolved in bicarbonate-carbonate buffer composed of $NaHCO_3$ (0.095M) and Na_2CO_3 (0.005M) with a final buffer pH of 8.8-9 and isotonised with one of the following compounds: trehalose (3.25%), mannitol (1.25%), urea (1%), proline (0.92%), taurine (1%), propylene glycol (0.61%) or glycerol (0.74%).

For freeze-dried hydrogels, after complete dissolution, they were freeze-dried and redissolved in water MilliQ®.

2.6. PH of hydrogels.

The pH of the hydrogels was measured with a pH meter (model GLP 22, Crison, Barcelona, Spain).

2.7. Rheological properties analysis.

2.7.1. HA-based hydrogels.

Rheological properties were carried out by an HR-2 Rheometer (TA instruments, New Castle, DE, USA) equipped with 8- and 20-mm steel parallel-plate geometries at room temperature (25°C). For the time sweep assessment, a 20 mm plate and a 1000 µm gap were used and 400 µL of hydrogel was formed at the time of measurements. Frequency (1 Hz) and strain (1%) were constant.

To evaluate the evolution of loss and storage modulus, an 8 mm plate was used. At time points pre-established, the gel was placed in the instrument and left equilibrated for a few minutes. The test was measured with constant frequency (1 Hz) and strain (1%). The gap used was 2000 µm.

For oscillation strain steps, a constant frequency was used (1 Hz) for 2 cycles with preformed gel. Each cycle started at a low strain (1 %) for 1 minute, followed by a high strain (1000 %) for another minute.

2.7.2. PPP hydrogels.

The rheology (G' module vs temperature) was assessed for PPP hydrogels by using a Discovery HR-hybrid rheometer (TA instruments, New Castle, DE, USA) with a parallel

plate system with an 8 mm diameter. The shear rates increased from 0 to 1000 s^{-1} in 20 steps. The temperature ramp range was from 25 °C to 50 °C with a heating rate of 0.6 °C/min at 10 rad/s.

2.8. Size of micelles.

The mean size and size distribution of micelles from PPP hydrogels were measured by dynamic light scattering (DLS) using a Zetatrac® Particle Size Analyzer (Montgomeryville, PA, USA). Samples were diluted in MilliQ® water and measured by triplicate.

2.9. *In vitro* hydrogel degradation.

The degradation properties of hydrogels formulations were tested by immersion of hydrogels in PBS or PBS containing 110 UI/mL of hyaluronidase. Hyaluronidase was selected since is the enzyme which cleaves the HA, and it is presented in the vitreous humour with that average activity [17]. Hydrogels (200 µL) (n=3) were placed in an Eppendorf tube. Then, 1 mL of PBS or PBS containing hyaluronidase was added. The tubes were placed in a shaker at 37 °C and 100 rpms. At pre-set times, the PBS was removed, the remaining PBS was wiped off softly with a tissue and the tubes were weighed. The percentage of degradation – called here as percentage of polymer weight since the final result referrers to the remaining polymer weight – was calculated by division of the weight of the hydrogel at a t time (W_t) to the initial weight of the hydrogel at 0 (W_0). The test was carried out in triplicate.

$$Polymer\ weight\ (\%) = \frac{Wt}{W0}\, x\ 100$$

Equation 1. Percentage of hydrogel degradation.

2.10. Swelling studies.

The swelling ratio was evaluated under the same conditions used in the *in vitro* degradation. Briefly, the initial hydrogel weight (W_i) was determined immediately after hydrogel formation inside the Eppendorf tube. Then, PBS was added and at pre-set times the medium was removed. The surface medium was wiped off softly, hydrogels were weighted (W_f) and PBS has added again and placed in the same conditions as before. The swelling index was determined from the ratio between W_f and W_i.

$$Swelling\ ratio = \frac{Wf}{Wi}$$

Equation 1. Swelling ratio.

2.11. Hydrogels drug loading

2.11.1. HA-based hydrogels.

Once each functionalised HA was dissolved in PBS, 0.4% of DXP was added and dissolved in HA-CHO to become a final concentration of 0.2% DXP when it was mixed 1:1 with HA-SH to eventually form the hydrogel.

2.11.2. PPP hydrogels.

Prior to starting *in vitro* release studies, 0.2% DXP was dissolved in 100 µL of the PPP hydrogels.

2.12. *In vitro* release studies.

In order to evaluate the suitability of HA-based and PPP hydrogels for long-term release, *in vitro* studies were carried out for both types of hydrogels (n=3). At pre-set times (24h and once per week until 28 days) supernatants were removed and the DXP concentration was quantified by HPLC-UV. The equipment was composed of a Waters Alliance 2695 separation module coupled to a Waters photodiode array 2996 (Waters corp, Barcelona, Spain). Dexamethasone phosphate was quantified as described by Lopez-Cano JJ et al. [15] where the mobile phase was 0.05 M potassium dihydrogen phosphate in water (pH=4, adjusted with formic acid) and acetonitrile (ratio 70:30) with a flow rate of 1 mL/min. The column used was Ascentis C18 HPLC Column (5 µm particle size, 25 cm × 4.6 mm). Dexamethasone wavelength was 240.5 nm and the software used for data acquisition and processing was Empower 3 (Waters, Barcelona, Spain).

2.12.1. HA-based hydrogels.

100 µL of final loaded hydrogel formulation (ratio 1:1 HA-SH and HA-CHO) were placed in a tube. 1.5 mL of PBS with sodium azide (0.02% w/v) was added and tubes were placed in a water bath at 37°C and 100 rpm (JULABO GmbH, Seelbach, Germany). As described before, at pre-set times, the supernatant was removed and replaced with fresh PBS media, and DXP content was measured.

2.12.2. PPP hydrogels

PPP DXP loaded hydrogels using trehalose and mannitol buffer to dissolve the polymer were employed for *in vitro* release studies. 100 µL of the hydrogel formulation (trehalose or mannitol buffer) was placed in a tube and 1.5 mL of PBS with sodium azide (0.02% w/v) was added. Tubes were placed in a water bath at 37°C and 100 rpms (JULABO GmbH, Seelbach, Germany). As mentioned before, the supernatant was collected, DXP content was quantified, and the medium was replaced with pre-warm (37°C) PBS media.

2.13. Injectability of final PPP hydrogels formulations.

Injectability of PPP hydrogels formulations was tested using a 1 mL plastic syringe couple to three different needles (21G – 0.514 mm I.D, 25G – 0.26 mm I.D, and 30G – 0.159 mm I.D). As PPP hydrogels become gel with increase of temperature, injectability tests were also assessed at two different temperatures: 20 °C – sol state – and 37°C – gel state. At each temperature, hydrogels formulations were left 20 minutes to reach system equilibration before injectability assay.

2.14. *In vitro* studies in cell cultures of final PPP hydrogel formulations

2.14.1. Cell cultures.

Retinal-pigmented epithelial cell line hTERT (RPE-1) cells kindly donated by the UCD (University College of Dublin) Conway Institute were employed for *in vitro* studies. Cells were cultured at 37 °C and 5% CO_2 in Dulbecco's Modified Eagle Medium/Nutrient Mixture F-12 (DMEM/F-12), supplemented with of FBS (10%), L-Glutamine (1%), sodium bicarbonate at 7.5% (3.5%) and penicillin-streptomycin (1%). Cell passage was made twice-thrice per week.

2.14.2. Cell viability.

In vitro cell viability was assessed by Trypan blue. 12 wells-plates were used to seed the cells at a density of 70,000 cells/well, overnight. Hydrogels formulations were added and incubated for 24 hours. Then, cells were washed and detached with trypsin. Trypsin was neutralised with culture medium, and the cell suspension was placed in a tube. Cells suspension was mixed with Trypan blue in a ratio 1:1, with a total volume of 40 µL. Viable cell number was determined by counting the not stained cells in an automated cell

counter (Invitrogen, ThermoFisher Scientific, Waltham, Massachusetts, USA). As controls, NaCl (0.9% w/v) was employed for the positive control of viability and DMSO (5% w/v) as negative control. Three replicates of each formulation in three different days were carried out.

2.14.3. Wound healing assay (preliminary studies).

Cell migration and proliferation of the final formulation (DXP loaded PPP hydrogel) were evaluated by wound healing assay. In 12 wells-plate the cells were cultured at a density of 120,000 cells/well until confluence. A linear wound was created with a 20 µL pipette-tip and the detached cells were eliminated by washing with DPBS. 1 mL of medium and 10 µL of each final formulation were added and incubated 24 hours. Photographs of 3 areas in each time point (8 hours and 24 hours) were taken from each well. Photographs were taken by an inverted microscope equipped with a digital camera (ProgRes5, Jenoptik, Jena, Germany). Each image was analysed with Fiji software (ImageJ). Non-treated cells were used as control. Three replicates of each formulation in three different days were carried out.

3. Results

3.1. Optimisation of HA-based hydrogels

The functionalised-HA-based hydrogels were formed by mixing both, HA-CHO and HA-SH solutions, in a ratio of 1:1. Different concentrations were evaluated considering their pH and the increase in viscosity in the first 30 minutes as key parameters for the selected ocular application. After preliminary studies with different HA-CHO/HA-SH ratios, the mixture prepared with 2% (w/v) of HA-CHO and 3% (w/v) of HA-SH was selected (pH between 6.4 and 6.7) since it was able to constitute a viscous solution-soft gel in a few minutes (Table 1).

Table 1. Different concentrations of HA-CHO and HA-SH were tested.

HA-CHO % (w/v)	HA-SH % (w/v)	Aspect in 30 mins	pH
1.5	4	Gel	6.4
1.75	4	Gel	6.4
1.75	3	Gel	6.4
2	3	Gel	6.4-6.7
2	2	Liquid	6.4-6.7

Rheological tests were carried out to monitor the crosslinking process. As Figure 1 shows, the gelation process was fast (storage modulus -G'- is above loss modulus -G''-) and it seemed to have the maximum storage modulus at 60 minutes. The addition of DXP into the hydrogel did not seem to modify the gelation process. However, when the hydrogel was monitored through time (Figure 2), the storage modulus continued increasing, having its maximum at 48 hours (a limitation of the experiment, since if it was carried out for more time, evaporation could affect the result).

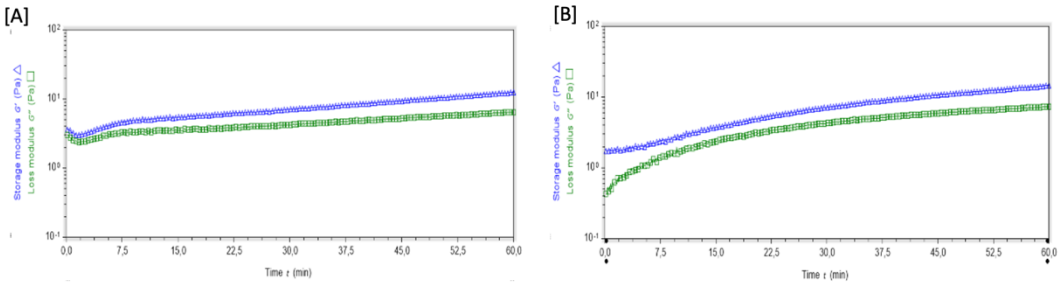

Figure 2. Time sweeps analysis to monitor the gel formation in the first hour ([A]- blank hydrogel, [B] – hydrogel + 0.20 % dexamethasone phosphate).

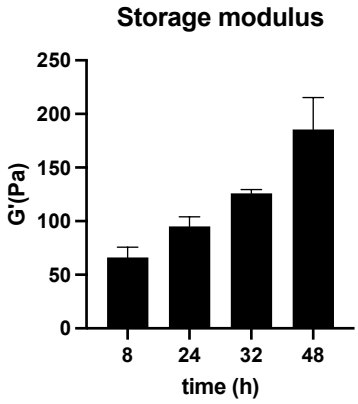

Figure 2. Storage modulus through the time of hydrogel made with HA-SH (2% w/v) and HA-CHO (3% w/v).

Then, the self-healing capacity was assessed employing a 2-cycle of oscillation strain steps method. The experiment started with a low strain (1%) for 1 minute followed by a high strain (1000 %) for an additional minute. As can be seen in Figure 3, G' started around 100 Pa, decreasing to approximately 10 Pa when the high strain was applied. These values were constant in the two cycles.

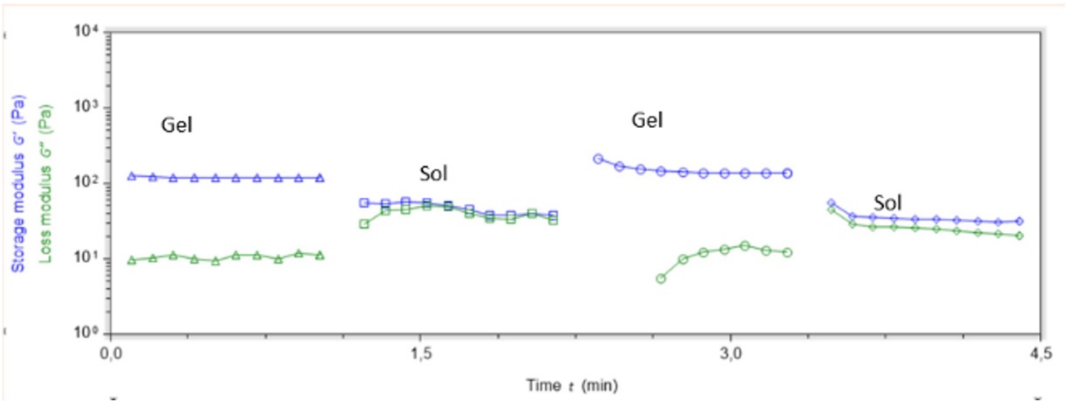

Figure 3. Shear-thinning capacity. Oscillatory strain steps analysis in the rheometer.

3.2. Optimisation of PPP hydrogels.

PPP1500 polymer takes around 3 days for being completely dissolved. In order to improve its solubility, different technological strategies were carried out. First of all, the initial PEG used in the PPP synthesis (PEG1500) was changed by a higher molecular weight PEG (PEG3000). Then, two triblock polymers were synthesized (PPP1500 and PPP3000) with a theoretical molecular weight target of 5,000 g/mol. They were characterized in terms of molecular weight, NMR, and gel formation at 37°C.

Macroscopically, both crude polymers showed a main difference between them. PPP1500 presented a yellowish viscous appearance whereas PPP3000 resulted in a white and solid consistency, as it can be seen in Figure 4.

Figure 4. Crude PPP1500 (left) and PPP3000 (right) polymers after their synthesis and freeze-dried.

^{1}H-NMR confirmed PLGA-PEG-PLGA structures for both polymers, PPP1500 and PPP3000. Briefly, as it is described in the literature, each shift can be identified with chemical structures of the polymer: lactic acid showed peaks at 5.20 ppm (a) which corresponded to CH groups signals, and at 1.55 ppm (e) which was CH_3 groups; glycolic acid CH_2 groups were indicated by peak presence at 4.75 ppm (b) and finally, PEG presented two peaks, at 4.30 ppm (c) and at 3.65 ppm (d) for CH_2 groups. The

experimental ratio was calculated as described by Jeong et al. and it is shown in Table 2 [18].

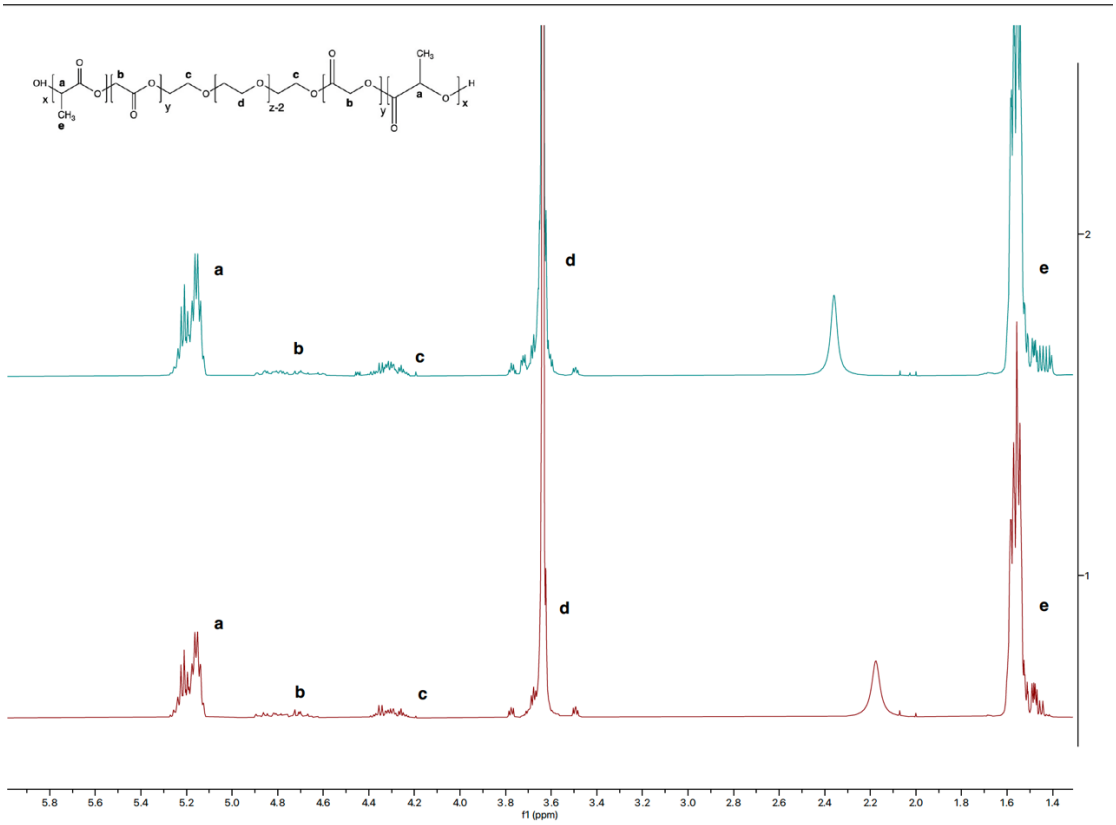

Figure 5. Nuclear Magnetic Resonance (NMR) spectrum of PPP3000 (1) and PPP1500 (2).

GPC results showed unimodal peaks with a polydispersity index values of 1.23 for PPP1500 and 1.21 for PPP3000. The average molecular weight number (Mn), weight average molecular weight (Mw), and molecular weight of the highest peak (Mp) were shown in Table 2.

Table 2. GPC and ^{1}H-NMR characterization of PPP triblock polymers synthesized with two different molecular weights of PEG. Mn is the number average molecular weight (calculated by GPC (1) and by ^{1}H-NMR (2)), Mw weight average molecular weight, Mp molecular weight of the highest peak, and PDI (polydispersity) analysed as Mw/Mn by GPC.

Polymer	Mn^{1} (g/mol)	Mw (g/mol)	Mp (g/mol)	PDI	Mn^{2} (g/mol)	Ratio (PEG:GA:LA)		Ratio (GA:LA)	
						Theoretical	NRM Experimental	Theoretical	NRM Experimental
PPP1500	5199.1	6401.30	6620.43	1.23	5036.42	1:1.54:23.10	1:1.56:23.28	1:15	1:14.96
PPP3000	5602.33	6794.06	7871.69	1.21	7001.62		1:1.88:26.25		1:14

Furthermore, both triblock polymers were dissolved in the buffer and their dissolution time and gelation were evaluated. For PPP3000 copolymer, dissolution occurred faster than PPP1500 (overnight vs. 3 days), however, the gelation temperature

decreased from the range of 32-35°C observed in PPP1500 to temperatures between 2 and 8°C for PPP3000. According with the results obtained, PPP3000 was discarded for further studies.

The second technological approach to enhance the triblock polymer rate dissolution in water was to include different compounds (Table 3) in the buffer media to enhance, not only the dissolution process, but also the freeze-drying and re-dissolution procedures. The concentration of each substance was based on the osmolarity values of each hydrogel composition loaded with DXP.

Table 3. Dissolution time, pH and gelation (yes or not) in PPP1500 dissolved in the different compounds included in the buffer. Original means that no freeze-drying procedure was performed. Dissolution time after freeze-drying was also assessed (Freeze-dried).

	Original			*Freeze-dried*
Compound (%)	**Dissolution time**	**pH**	**Gelation at 37ºC**	**Dissolution time**
Trehalose (3.25%)	2.5-3D	7-7.3	Yes	overnight
Urea (1%)	1D-2D	7-7.5	Yes	overnight
Proline (0.92%)	~1D	7.1	Yes	8-10h
Mannitol (1.25%)	2D-2.5D	7.2-7.3	Yes	overnight
Taurine (1%)	~1D	7.1	Yes	8-10h
Propylene glycol (0.61%)	~1D	7.8	Yes	4h
Glycerol (0.74%)	overnight	7.2	Yes	4h

Urea, proline, mannitol, taurine, propylene glycol, and glycerol at the concentrations shown in table 3 were tested. All of them were able to reduce the dissolution time of the PPP1500 forming hydrogels. However, as can be seen in Figures 6A and 6B, the inclusion of the different compounds affected the rheological properties of the formed hydrogels. When mannitol was included, hydrogels presented a similar profile in storage and loss modulus. The gelling point differed with the different components. Gel point is defined as the temperature in which G’ = G’’ and therefore, tan δ = 1 – since tan δ = G''/ G' (indicated in orange in Figure 6B) [19]. This parameter resulted in increasing order: 30.28 ± 0.21 °C (mannitol) and 30.56 ± 0.56 °C (trehalose) < 31.16 ± 0.51 °C (proline) <

31.56 ± 1.29 °C (taurine) < 32.25 ± 0.51 °C (glycerol) < 33.34 ± 3.53 °C (propylene glycol) <36.83 ± 0.14 °C (urea).

As hydrogels prepared with trehalose and mannitol presented similar storage and loss modulus profiles, they were evaluated after freeze-drying and redissolution, showing a decreased in both parameters, G' and G'', and a slightly increase in the gel point temperature (33.69 ± 0.27 °C and 34.81 ± 0.66 °C, respectively).

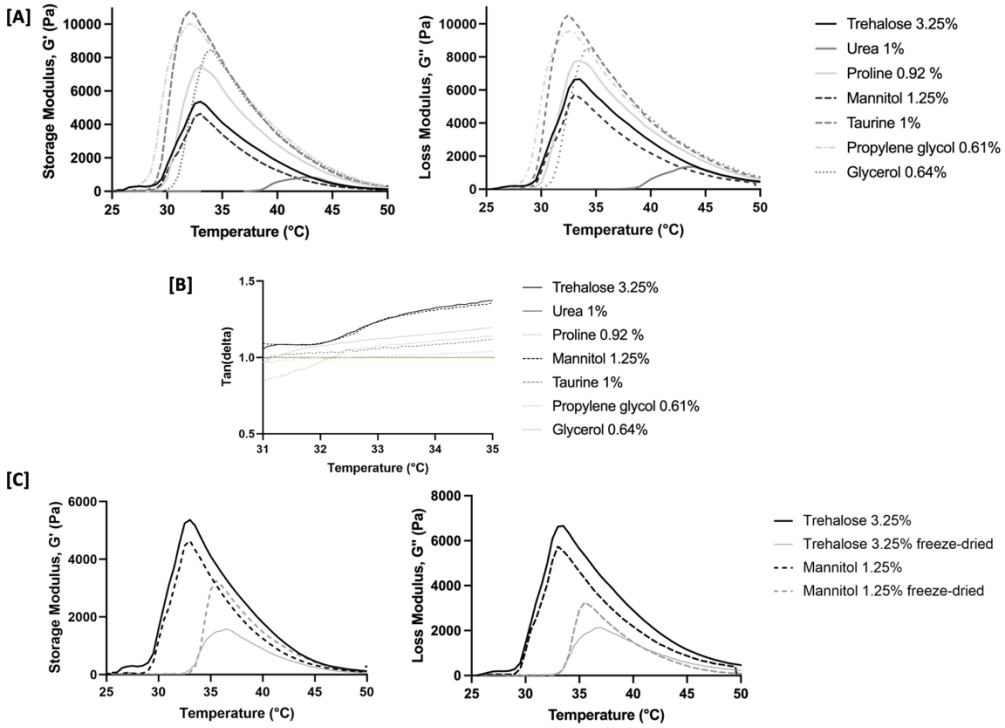

Figure 6. Rheological analysis of PPP hydrogels: storage and loss modulus [A], tan δ [B], and storage and loss modulus of freeze-dried and redissolved hydrogels [C].

When hydrogels were placed in a water bath to test gel duration under the same conditions as *in vitro* release studies, hydrogels prepared with glycerol suffered degradation in 10 days (Figure 7A), followed by those prepared with proline, taurine, and propylene glycol, that degraded in 30 days (Figure 7B). The hydrogels including trehalose and mannitol lasted more than 30 days (Figures 7C and 7D).

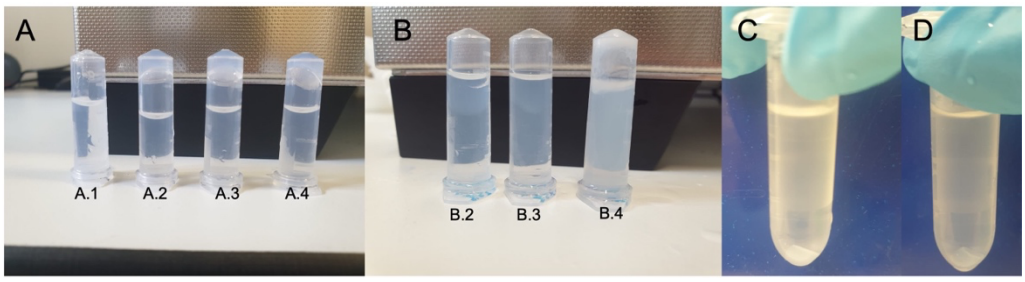

Figure 7. PPP1500 hydrogels degradation with different buffers. A.1. glycerol (10 days), A.2 and B.2 proline (10 and 30 days), A.3 and B.3 taurine (10 and 30 days), A.4 and B.4 propylene glycol (10 and 30 days), C trehalose and D mannitol (both 30 days).

No significant differences were observed in micelle sizes among the different hydrogels, with mean values between 17 and 31 nm in all cases.

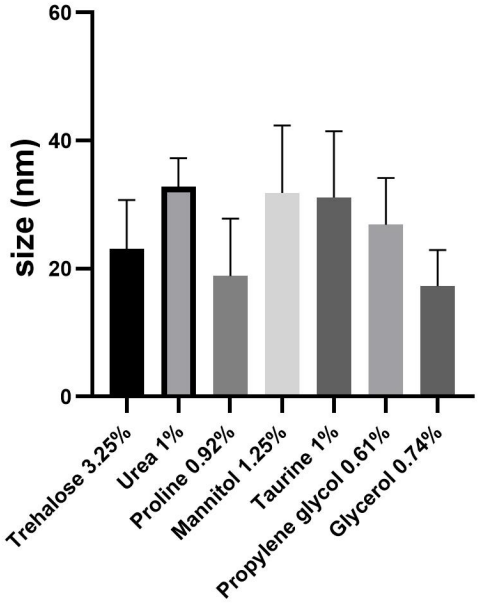

Figure 8. Micelles sizes of the PPP1500 hydrogels with different vehicles.

3.3. Optimised HA-based and PPP hydrogel formulations.

After selecting the optimised HA-based (mixture prepared with 2% (w/v) of HA-CHO and 3% (w/v) of HA-SH) and PPP1500 hydrogel formulations (PPP1500+Mannitol and PPP1500+Trehalose), *in vitro* degradation, swelling, and *in vitro* drug release were carried out.

Swelling index results are shown in Figure 9. HA-based hydrogel formulation showed a lower swelling index during the study with the highest value at 24 hours (1.18 ± 0.05). On the other hand, both types of PPP1500 hydrogels formulations presented similar behaviour between them at least in the first 72 hours. At 24 hours, they had a swelling

index between 1.7 and 1.9 achieving the highest rate at 96 hours (for PPP1500+Mannitol with an index of 2.66 ± 0.17) and at 120 hours (for PPP1500+Trehalose with an index of 2.54 ± 0.21). From 120 hours, a slight decrease in swelling behaviour was observed.

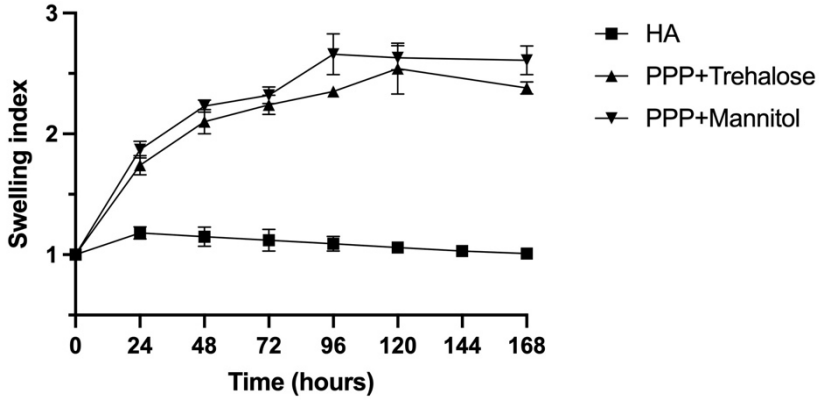

Figure 9. Swelling index of HA-based hydrogel (squares), PPP1500+Trehalose hydrogel (triangle), and PPP1500+Mannitol hydrogel (reverse triangle).

Regarding degradation studies (Figure 10), for HA hydrogels formulations, hyaluronidase was added into the solution media in order to replicate the posterior segment of the eye conditions. HA based formulations suffered a higher degradation than PPP1500 ones, showing a complete degradation in 8 days whereas, as expected, at the same time, PPP1500 formulations continued suffering swelling (percentage of weight above 100%). However, this behaviour changed at 7 days, when the percentage of weight started to decrease, being less than 100% at 14 days.

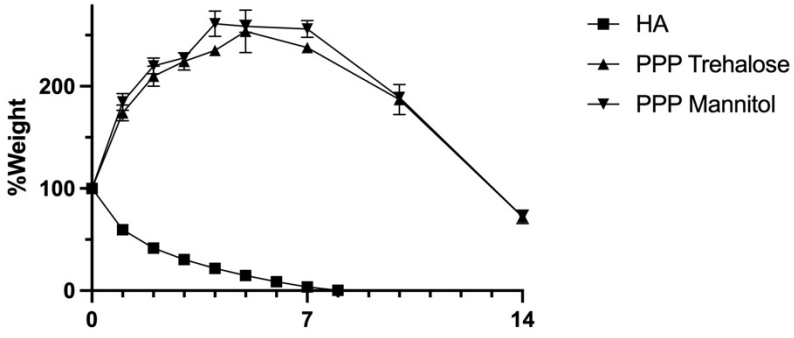

Figure 10. Degradation of HA (squares) and PPP (triangles) hydrogels expressed as a percentage of weight from time 0 versus time.

The three optimised hydrogel formulations suffered a fast initial DXP release being higher for HA (91.46±3.80%) than for PPP1500 ones (71.77±1.59% PPP1500+Trehalose and 73.41±0.83% PPP1500+Mannitol), ($p<0.0001$ and $p=0.0001$, respectively). All hydrogel formulations released DXP for 21 days. After the initial burst, DXP releases until

the end of the study in a slow and sustained manner, with a release rate of 0.10±0.01% DXP/day for HA, 0.25±0.04% DXP/day for PPP1500+Trehalose and 0.35±0.02% DXP/day for PPP1500+Mannitol in the period comprised between 7 and 21 days.

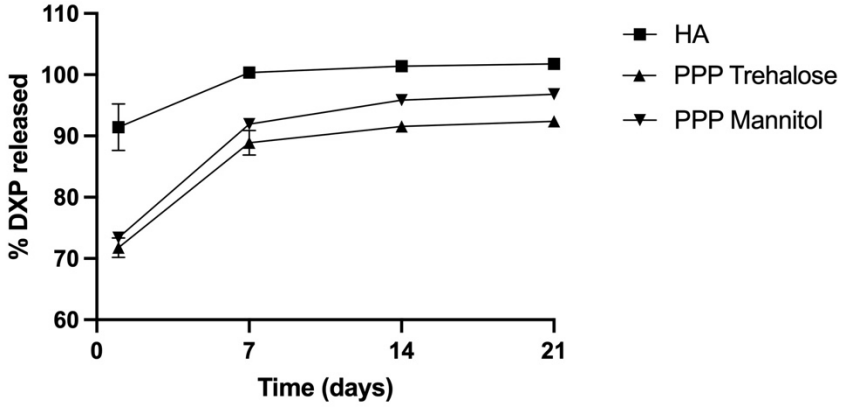

Figure 11. *In vitro* DXP release from HA (squares) and PPP1500 (triangles) hydrogels.

Regarding these results where PPP1500 hydrogels formulations showed better properties for long term treatment, they were deeply characterized in terms of injectability behaviour, *in vitro* tolerance and effect on cell proliferation and migration.

3.4. Injectability of final PPP hydrogel formulations.

Regarding hydrogel injectability, it was carried out at two different temperatures (room temperature – sol state – and at 37°C – gel state –) and with three different needles. Only hydrogels at 37°C with 30G needle presented difficulties to be injected. Hydrogels in the rest of temperatures and needles tested were well injected.

Table 4. Injectability of PPP1500 hydrogels. Codes: V – injectable, X – not injectable.

		PPP+Trehalose	PPP+Mannitol
20°C	21G	V	V
	25G	V	V
	30G	V	V
37°C	21G	V	V
	25G	V	V
	30G	X	X

3.5. Tolerance *in vitro* studies of final PPP hydrogel formulations.

Cell viability of the different PPP1500 loaded and non-loaded hydrogels formulations was tested. As Figure 12 shows, formulations presented viability above 90% in the study

conditions and no significant differences were found between them nor the positive control (0.9% NaCl).

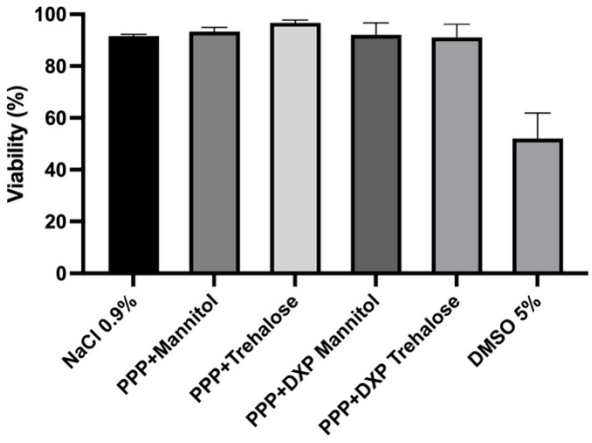

Figure 12. Cell viability (%) in Retinal-pigmented epithelial cell line hTERT (RPE-1) of the different PPP1500 formulations. As a positive control of viability NaCl (0.9% w/v) was employed and as negative control DMSO (5% w/v).

3.6. Cell proliferation and migration studies of final PPP hydrogel formulations.

Preliminary studies of cell proliferation and migration of the selected formulations (PPP1500 DXP-loaded hydrogels) were carried out by wound healing assay (Figure 13). The wound area at 8 hours resulted significant smaller in treated cells than in the control ($p<0.05$ for PPP1500+DXP+Mannitol and $p<0.01$ for PPP1500+DXP+Trehalose). At this time points, the scratches edges also showed less defined due to cell growth. At 24 hours, all scratches were recovered. No significant differences were found among the treatments in the time points studied.

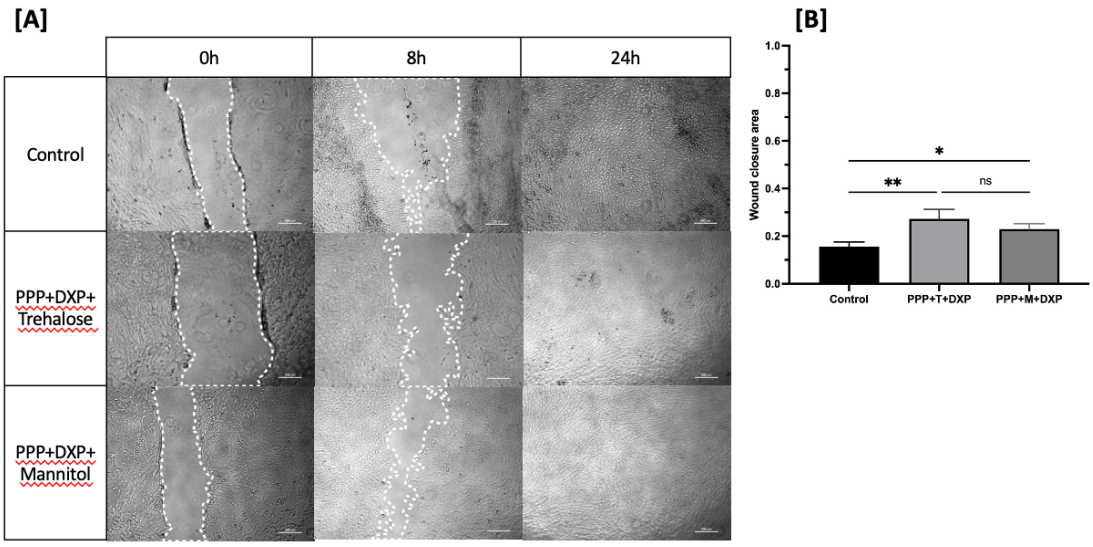

Figure 13. [A] Wound closure area in RPE-1 cells at 0, 8 and 24 h. Scale bars: 200 µm [B] At 8h, control showed a less closure area than treated cells (* means $p<0.05$ for PPP1500+DXP+Mannitol and ** means $p<0.01$ for PPP1500+DXP+Trehalose also compared to control).

4. Discussion

Hydrogels are an appealing drug delivery system due to their tuneable physical properties, controllable degradability, and their capacity to protect some drugs from degradation. Over the last few years, hydrogels have been gained attention to be used as constituents of drug delivery systems and their development has highly increased [20,21].

In this work, we have developed two different hydrogels (natural and synthetic) and we assessed their properties as a potential platform for intraocular drug delivery systems for the treatment of chronic ophthalmic pathologies affecting the back of the eye.

4.1. HA-based hydrogels.

HA is a natural polysaccharide present in the human body, possessing biocompatibility and biodegradable properties that make this polymer appealing for biomedical applications. Indeed, the interest of developing HA hydrogels has augmented in the last 10 years. However, some properties of native HA should be improved such as stability, half-life, or its capacity to form hydrogels. All these aspects can be improved by chemical modification of HA [22].

In the present work, the functionalised-HA-based hydrogels were formed by mixing both, HA-CHO and HA-SH solutions, in a ratio of 1:1. Different concentrations of both components were evaluated considering the pH and the increase in viscosity observed in the first 30 minutes as key parameters for our application. From the different concentrations tested, the chosen ones were 2% (w/v) of HA-CHO and 3% (w/v) of HA-SH, resulting in a final hydrogel pH between 6.4 and 6.7 (ocular tolerable range is between 5.5 and 7.8, although recent studies suggested to extend the lower value to 4.5 [23–25]) and forming a viscous solution-soft gel in a few minutes.

Rheological experiments were carried out to monitor the crosslinking process. As shown in Figure 1, the gelation process occurs fast (storage modulus (G') with a value above loss modulus (G'')), characteristic of a gel-like behaviour [22]. A gradual increase of G' through time, was observed when it was monitored across the time. In fact, the storage and loss modulus continued increasing, having its maximum at 48 hours (this end time point was selected in order to avoid evaporation). These results suggested that the instant gelation could be due to the crosslinking between the aldehyde groups of HA-CHO and thiol groups of HA-SH, as it is described in the literature [26]. The behaviour of these hydrogels observed with the time could be explained by the oxidation of the free thiol groups to form disulphide bonds (R-S-S-R) since this link takes longer to occur [27].

Self-healing capacity, defined as the ability to recover the original shape, structure, and functionality, as well as physical and chemical hydrogel properties after damage, was assessed employing a 2-cycle of oscillation strain steps method. This is an interesting property for injectable hydrogels since they can undergo a liquid state when they are injected and then, they can behave as a gel-state, restoring immediately when the shear force is removed [28]. This fact results critical in the clinical practice as the injection is easily performed when the hydrogel is in its liquid state. As can be seen in Figure 3, G' starting around 100 Pa, when the high strain was applied the viscosity decreased to approximately 10 Pa, being this value was close to G'', which suggested the breakdown of the hydrogel networks. When the hydrogel suffered low strains (1%), the G' increased its value, showing, therefore, its self-healing property, as it was described in the literature [29].

4.2. PPP hydrogels

PLGA and PEG are frequently used in biomaterial applications and approved by FDA and EMA [30–32]. PLGA is degraded in the body to CO_2 and H_2O by Krebs' Cycle and PEG is reported to be degraded by hydrolysis [33,34].

Thermosensitive hydrogels have been gaining attention lately as an innovative strategy for injectable drug delivery systems [35]. The present work aimed to increase the rate of dissolution of this kind of triblock copolymers to endow with optimal properties for intraocular injection. To this, we have developed different technological strategies. First, PEG1500 was changed for a higher molecular one polymer (PEG3000) in the PPP synthesis but keeping the same molecular weight of PPP. As shown in the results, low polydispersity and unimodal distribution was observed after GPC analysis for both PPP polymers and ^{1}H-NMR confirmed the characteristic peaks of PEG, LA, and GA for both compositions as they were described in the literature [18]. Though crude polymer consistency changed, and the dissolution was faster, the temperature range in which it formed gel decreased until 2-8°C, making impossible its use for human body temperature.

Another technological strategy was the use of freeze-drying as a method to accelerate the water solubility of PPP1500 triblock. Freeze-drying is a good strategy to increase the water solubility and the dissolution rate of substances [36]. Nevertheless, it can imply physical stress that could result in a modification of their properties [37]. Initial freezing of samples is a critical step in lyophilization procedure and cryopreserving substances are usually employed to maintain the integrity of the samples. In this case, we have substituted trehalose by other cryopreserving substances, and we have compared them before freeze-drying to assess if its inclusion could affect hydrogel properties, especially the rheological ones [15]. Glycerol was the compound that most reduced dissolution times. This effect could be due to its polar nature as it is widely employed to enhance the dissolution of inorganic salts, enzymes, or poorly miscible in water organic compounds [38,39]. Opposite to other organic solvents such as DMSO or DMF, glycerol has no toxicity, and it is biodegradable. Due to its properties, the potential use of glycerol as a green solvent for organic reactions is being studied [38]. On the other hand, sugars such as trehalose and mannitol are widely known as cryoprotectants. Both

are used as bulking agents but whereas the trehalose state is glassy after freeze-drying, mannitol is crystalline [40]. Mannitol has been studied to increase the solubility of poorly soluble molecules such as clotrimazole [41]. Propylene glycol is a cryoprotective agent and one of the most common cosolvents used to increase the solubility of low water-soluble compounds [42,43]. The production of proline has been found in plants as a response against environmental stresses such as freezing temperatures and has been tested as a cryoprotectant *in vitro*, showing similar results than the traditional ones [44]. Urea is hydrotropic, and it has been explored to increase the solubility of poorly water-soluble drugs such as diclofenac [45]. Finally, taurine has been assessed for its protective properties in freeze-dried samples and has been studied for its capacity to convert liposoluble substances into a water-soluble state [46,47]

We have shown that the addition of the different compounds could affect the gelation behaviour of our systems, especially the gel point from 30.56 °C when trehalose is used, to 39.79 °C when urea is included in the formulation. López-Cano et al. observed that the addition of TPGS (D-α-Tocopherol polyethylene glycol 1000 succinate) in dexamethasone-loaded PLGA-PEG-PLGA hydrogels interacted with the micelles changing their rheological behaviour as well as dexamethasone release [15]. Qiao et al. assessed peptide-polymer interactions in PLGA-PEG-PLGA polymer too, indicating that not only drug release can be modified but also hydrogel properties – as degradation or swelling – changed with the addition of the peptide [48]. In the same direction, Chan et al. found that the addition of higher amount of rhodamine B (2 and 4 mg/mL) avoided gel formation in PLGA-PEG-PLGA hydrogels, affecting the system balance [49]. Danafar et al. studied the interactions between atorvastatin and the copolymer PLA-PEG-PLA by FTIR and DSC, showing a clear chemical interaction and affecting the drug release. However, lisinopril did not show any evidence for interaction between it and the copolymer. They explained that behaviour because of the hydrophobic-hydrophilic balance of the drug since it is associated with the amphiphilic micelles by different affinities [50]. In this work, we also have found rheological changes. We hypothesized that gel point is related to dissolution time and gel duration since the hydrogels with higher gel points degraded before and the polymer dissolution was faster, thus,

producing their faster degradation and changing micelle aggregation, mechanism implicated in the gelation process.

The balance between dissolution rate and gel structure maintenance results of highly important in the formulations intended for drug delivery purposes. With this idea in mind, we would like to mention that glycerol, for example, was the compound with faster dissolution time, but also, with less gel duration submerged in aqueous media (only 10 days). That was followed by taurine, proline, and propylene glycol. It is also remarkable the change in storage and loss modulus units for PPP1500 formulations including urea. Considering all the parameters, it seems that the inclusion of mannitol in the PPP1500 hydrogels lead to the most similar behaviour compared to the initial PPP1500 hydrogels incorporating trehalose. The long-lasting hydrogels formulations were the ones including trehalose and mannitol, which at 28 days, the gel structure remains. As a long-term delivery system, PPP with trehalose and with mannitol were chosen.

4.3. HA-based versus PPP hydrogels.

The water retention capacity of hydrogels depends on the hydrogel structure as well as the molecular weight. That could explain the differences found between HA and PPP1500 hydrogels. As we could not measure the molecular weight of HA hydrogel, we cannot establish any relationship between molecular weight. However, the different natures of the polymers employed to fabricate the hydrogels should play an important role too, since the hydrogel formation is different for both. For example, in HA hydrogels the gelation mechanism is the spontaneous interaction between aldehyde groups with thiol groups (crosslinking), whereas PPP1500 polymers become a gel due to micelles aggregation as a response to the heat [51,52].

Regarding degradation, there are also differences between them. It is known that in the human vitreous humour, the presence of hyaluronidase at a 110 UI cleaves hyaluronic acid [17]. For this reason, we decided to simulate these conditions in the phosphate buffer saline with the addition of hyaluronidase at the same value of the activity. We have shown that in one week the HA hydrogel will be completely degraded with a higher initial degradation occurring at 24 hours (around 40%). However, PPP1500 polymers have been reported to be degraded by hydrolysis. For this reason, this kind of

hydrogel was evaluated only in the phosphate buffer saline and showed that at day 14 it remains around 70 % of its weight, meaning that approximately only the 30% was degraded.

HA hydrogel did not swell as much as PPP1500 hydrogels, which may have a strong influence in its release behaviour. HA showed a sudden release of dexamethasone in the first 24h, delivering almost the total of the loaded drug (91.46 ± 3.80 %), whereas PPP1500 hydrogels formulations at the same time point still retained 25-30 % of DXP. Both types of PPP1500 hydrogels formulations showed a high initial release rate (until 7 days) and then, they sustained the release until 21 days. These results, along with degradation studies, demonstrated that the use of PPP1500 hydrogels will be more suitable for long-term therapy, necessary for intraocular drug delivery systems, than HA hydrogels. However, HA hydrogels may be appropriate in short-term treatments.

As the hydrogels developed in the present work are intended for long-term therapies, Injectability and *in vitro* viability studies in retinal-pigmented epithelial cell line hTERT (RPE-1) were only evaluated for PPP1500 hydrogels formulations. Furthermore, wound healing studies were performed for the final formulations (PPP1500 loaded with dexamethasone). Trypan blue dye exclusion assay is commonly used to assess viability. It is based on the principle that membranes in healthy cells are not permeable to the dye [53]. Tetrazolium salt (3-(4,5-dimethylthiazol-2-yl)-2,5-diphenyltetrazolium bromide (MTT) assay is also employed to test *in vitro* tolerance, however, in this work, PPP1500 hydrogels interfere with the dye, underestimating the viability results. In this study, dexamethasone loaded and not loaded hydrogels indicated a viability value higher than 90%.

In pathological conditions as the case of wet age-related macular degeneration, retinal pigment epithelium dysfunction may trigger cell layer disruption and choroidal neovascularization [54]. In those conditions RPE proliferation occurs in response to that damage [55]. In patients with subretinal neovascularization, it has been described that the induction of RPE proliferation may prevent the leakage [56]. For this reason, active agents that promote RPE proliferation and the restoration of the cellular layer results of great interest. Dexamethasone has been reported to have a growth factor-like proliferative effect on RPE cells [56]. Taking into account the beneficial effects of

dexamethasone, preliminary studies of RPE cells proliferation and migration from hydrogels loaded with this active agent were assessed by wound healing studies. The results revealed that DXP loaded PPP1500 hydrogels presented a faster wound recuperation at 8 hours than non-treated (control) cells. Further studies are necessary to confirm this potential restorative effect.

5. Conclusions

We have developed two different types of biodegradable hydrogels for drug delivery. One was synthetized from the natural polymer hyaluronic acid, created by the crosslinking of functionalized hyaluronic acid with different chemical groups (aldehyde and thiol groups). These hydrogels showed fast degradation and drug release, resulting suitable for short-term intravitreal treatments.

On the other hand, PLGA-PEG-PLGA (PPP) hydrogels were developed as a synthetic thermos-responsive hydrogel. The inclusion of cryoprotectant such as trehalose and mannitol reduced the PPP1500 dissolution time. The PPP1500 hydrogels formulations developed in this work led to slow degradation and long-term drug release, as well as good viability so they can be an interesting candidate for the treatment of eye posterior segment chronic diseases.

Acknowledgements

This work was supported by Grant MAT2017-83858-C2-1 funded by MCIN/AEI/ 10.13039/501100011033 and by “ERDF A way of making Europe” and Grant PID2020-113281RB-C21 funded by MCIN/AEI/ 10.13039/501100011033. Research Group UCM 920415 (InnOftal) and ISCIII-FEDER “Una manera de hacer Europa” RETICS (OFTARED) (RD16/0008/0009). MSCA-RISE-3DNEONET/734907. A.A.N thanks for the grant PRE2018-083951 funded by MCIN/AEI/10.13039/501100011033 and by “ESF Investing in your future”.

6. References

[1] P.K.M. Purola, J.E. Nättinen, M.U.I. Ojamo, S.V.P. Koskinen, H.A. Rissanen, P.R.J. Sainio, H.M.T. Uusitalo, Prevalence and 11-year incidence of common eye diseases and their relation to health-related quality of life, mental health, and visual impairment, Quality of Life Research. 30 (2021) 2311–2327. https://doi.org/10.1007/S11136-021-02817-1/FIGURES/7.

[2] A. Dammak, F. Huete-Toral, C. Carpena-Torres, A. Martin, C. Pastrana, G. Carracedo, From Oxidative Stress to Inflammation in the Posterior Ocular Diseases: Diagnosis and Treatment, Pharmaceutics. 13 (2021). https://doi.org/10.3390/PHARMACEUTICS13091376.

[3] C. Baudouin, M. Kolko, S. Melik-Parsadaniantz, E.M. Messmer, Inflammation in Glaucoma: From the back to the front of the eye, and beyond, Prog Retin Eye Res. 83 (2021). https://doi.org/10.1016/J.PRETEYERES.2020.100916.

[4] M.J. Rodrigo, M. Subías, A. Montolío, S. Méndez-Martínez, T. Martínez-Rincón, L. Arias, D. García-Herranz, I. Bravo-Osuna, J. Garcia-Feijoo, L. Pablo, J. Cegoñino, R. Herrero-Vanrell, A. Carretero, J. Ruberte, E. Garcia-Martin, A.P. Del Palomar, Analysis of Parainflammation in Chronic Glaucoma Using Vitreous-OCT Imaging, Biomedicines 2021, Vol. 9, Page 1792. 9 (2021) 1792. https://doi.org/10.3390/BIOMEDICINES9121792.

[5] K.G. Falavarjani, Q.D. Nguyen, Adverse events and complications associated with intravitreal injection of anti-VEGF agents: a review of literature, Eye. 27 (2013) 787. https://doi.org/10.1038/EYE.2013.107.

[6] K.K. Jain, An Overview of Drug Delivery Systems, in: Methods in Molecular Biology, 2020: pp. 1–54. https://doi.org/10.1007/978-1-4939-9798-5_1.

[7] A. Bordbar-Khiabani, M. Gasik, Smart Hydrogels for Advanced Drug Delivery Systems, International Journal of Molecular Sciences 2022, Vol. 23, Page 3665. 23 (2022) 3665. https://doi.org/10.3390/IJMS23073665.

[8] M. Vigata, C. Meinert, D.W. Hutmacher, N. Bock, Hydrogels as Drug Delivery Systems: A Review of Current Characterization and Evaluation Techniques, Pharmaceutics. 12 (2020) 1–45. https://doi.org/10.3390/PHARMACEUTICS12121188.

[9] B.C. Ilochonwu, A. Urtti, W.E. Hennink, T. Vermonden, Intravitreal hydrogels for sustained release of therapeutic proteins, Journal of Controlled Release. 326 (2020) 419–441. https://doi.org/10.1016/J.JCONREL.2020.07.031.

[10] S. Bian, M. He, J. Sui, H. Cai, Y. Sun, J. Liang, Y. Fan, X. Zhang, The self-crosslinking smart hyaluronic acid hydrogels as injectable three-dimensional scaffolds for cells culture, Colloids Surf B Biointerfaces. 140 (2016) 392–402. https://doi.org/10.1016/J.COLSURFB.2016.01.008.

[11] G. Abatangelo, V. Vindigni, G. Avruscio, L. Pandis, P. Brun, Hyaluronic Acid: Redefining Its Role, Cells. 9 (2020) 1–19. https://doi.org/10.3390/CELLS9071743.

[12] T. Segura, B.C. Anderson, P.H. Chung, R.E. Webber, K.R. Shull, L.D. Shea, Crosslinked hyaluronic acid hydrogels: a strategy to functionalize and pattern, Biomaterials. 26 (2005) 359–371. https://doi.org/10.1016/J.BIOMATERIALS.2004.02.067.

[13] R. Yang, X. Liu, Y. Ren, W. Xue, S. Liu, P. Wang, M. Zhao, H. Xu, B. Chi, Injectable adaptive self-healing hyaluronic acid/poly (γ-glutamic acid) hydrogel for cutaneous wound healing, Acta Biomater. 127 (2021) 102–115. https://doi.org/10.1016/J.ACTBIO.2021.03.057.

[14] P. Wang, W. Chu, X. Zhuo, Y. Zhang, J. Gou, T. Ren, H. He, T. Yin, X. Tang, Modified PLGA–PEG–PLGA thermosensitive hydrogels with suitable thermosensitivity and properties for use in a drug delivery system, J Mater Chem B. 5 (2017) 1551–1565. https://doi.org/10.1039/C6TB02158A.

[15] J.J. López-Cano, A. Sigen, V. Andrés-Guerrero, H. Tai, I. Bravo-Osuna, I.T. Molina-Martínez, W. Wang, R. Herrero-Vanrell, Thermo-Responsive PLGA-PEG-PLGA Hydrogels as Novel Injectable Platforms for Neuroprotective Combined Therapies in the Treatment of Retinal Degenerative Diseases, Pharmaceutics 2021, Vol. 13, Page 234. 13 (2021) 234. https://doi.org/10.3390/PHARMACEUTICS13020234.

[16] Y. Cai, M. Johnson, A. Sigen, Q. Xu, H. Tai, W. Wang, A Hybrid Injectable and Self-Healable Hydrogel System as 3D Cell Culture Scaffold, Macromol Biosci. 21 (2021). https://doi.org/10.1002/MABI.202100079.

[17] D.M. Schwartz, S. Shuster, M.D. Jumper, A. Chang, R. Stern, Human vitreous hyaluronidase: isolation and characterization, Curr Eye Res. 15 (1996) 1156–1162. https://doi.org/10.3109/02713689608995150.

[18] B. Jeong, Y.H. Bae, S.W. Kim, Drug release from biodegradable injectable thermosensitive hydrogel of PEG-PLGA-PEG triblock copolymers, J Control Release. 63 (2000) 155–163. https://doi.org/10.1016/S0168-3659(99)00194-7.

[19] H. Murata, Chapter 17. Rheology - Theory and Application to Biomaterials, in: Polymerization, IntechOpen, 2012: pp. 403–426. https://doi.org/10.5772/48393.
[20] J. Li, D.J. Mooney, Designing hydrogels for controlled drug delivery, Nature Reviews Materials 2016 1:12. 1 (2016) 1–17. https://doi.org/10.1038/natrevmats.2016.71.
[21] B.X. Wang, W. Xu, Z. Yang, Y. Wu, F. Pi, An Overview on Recent Progress of the Hydrogels: From Material Resources, Properties, to Functional Applications, Macromol Rapid Commun. 43 (2022) 2100785. https://doi.org/10.1002/MARC.202100785.
[22] L.A. Pérez, R. Hernández, J.M. Alonso, R. Pérez-González, V. Sáez-Martínez, Hyaluronic Acid Hydrogels Crosslinked in Physiological Conditions: Synthesis and Biomedical Applications, Biomedicines 2021, Vol. 9, Page 1113. 9 (2021) 1113. https://doi.org/10.3390/BIOMEDICINES9091113.
[23] J.C. Freiberg, A. Hedengran, S. Heegaard, G. Petrovski, J. Jacobsen, B. Cvenkel, M. Kolko, An Evaluation of the Physicochemical Properties of Preservative-Free 0.005% (w/v) Latanoprost Ophthalmic Solutions, and the Impact on In Vitro Human Conjunctival Goblet Cell Survival, Journal of Clinical Medicine 2022, Vol. 11, Page 3137. 11 (2022) 3137. https://doi.org/10.3390/JCM11113137.
[24] N.G. Tassew, S.T. Laing, J. Aaronson, I. de Jong, C. Schuetz, F. Lorget, Tolerability Assessment of Formulation pH in New Zealand White Rabbits Following Intravitreal Administration, Toxicol Pathol. 49 (2021) 605–609. https://doi.org/10.1177/0192623320969667.
[25] B. Sobolewska, P. Heiduschka, K.U. Bartz-Schmidt, F. Ziemssen, pH of anti-VEGF agents in the human vitreous: low impact of very different formulations, Int J Retina Vitreous. 3 (2017) 22. https://doi.org/10.1186/S40942-017-0075-X.
[26] Y. Hua, Y. Gan, Y. Zhang, B. Ouyang, B. Tu, C. Zhang, X. Zhong, C. Bao, Y. Yang, Q. Lin, Q. Zhou, L. Zhu, Adaptable to Mechanically Stable Hydrogels Based on the Dynamic Covalent Cross-Linking of Thiol-Aldehyde Addition, ACS Macro Lett. 8 (2019) 310–314. https://doi.org/10.1021/ACSMACROLETT.9B00020.
[27] R.J. Ouellette, J.D. Rawn, Alcohols: Reactions and Synthesis, in: Organic Chemistry, 2018. https://doi.org/10.1016/b978-0-12-812838-1.50016-5.
[28] V.K. Anupama Devi, R. Shyam, A. Palaniappan, A.K. Jaiswal, T.H. Oh, A.J. Nathanael, Self-Healing Hydrogels: Preparation, Mechanism and Advancement in Biomedical Applications, Polymers (Basel). 13 (2021). https://doi.org/10.3390/POLYM13213782.
[29] S. Li, M. Pei, T. Wan, H. Yang, S. Gu, Y. Tao, X. Liu, Y. Zhou, W. Xu, P. Xiao, Self-healing hyaluronic acid hydrogels based on dynamic Schiff base linkages as biomaterials, Carbohydr Polym. 250 (2020). https://doi.org/10.1016/J.CARBPOL.2020.116922.
[30] E. Padín-González, P. Lancaster, M. Bottini, P. Gasco, L. Tran, B. Fadeel, T. Wilkins, M.P. Monopoli, Understanding the Role and Impact of Poly (Ethylene Glycol) (PEG) on Nanoparticle Formulation: Implications for COVID-19 Vaccines, Front Bioeng Biotechnol. 10 (2022). https://doi.org/10.3389/FBIOE.2022.882363.
[31] S.N.S. Alconcel, A.S. Baas, H.D. Maynard, FDA-approved poly(ethylene glycol)-protein conjugate drugs, Polym Chem. 2 (2011) 1442–1448. https://doi.org/10.1039/C1PY00034A.
[32] R.A. Jain, The manufacturing techniques of various drug loaded biodegradable poly(lactide-co-glycolide) (PLGA) devices, Biomaterials. 21 (2000) 2475–2490. https://doi.org/10.1016/S0142-9612(00)00115-0.
[33] A.T.C.R. Silva, B.C.O. Cardoso, M.E.S.R. e Silva, R.F.S. Freitas, R.G. Sousa, A.T.C.R. Silva, B.C.O. Cardoso, M.E.S.R. e Silva, R.F.S. Freitas, R.G. Sousa, Synthesis, Characterization, and Study of PLGA Copolymer in Vitro Degradation, J Biomater Nanobiotechnol. 6 (2015) 8–19. https://doi.org/10.4236/JBNB.2015.61002.
[34] B.J. Tarasevich, A. Gutowska, X.S. Li, B.M. Jeong, The effect of polymer composition on the gelation behavior of PLGA-g-PEG biodegradable thermoreversible gels, J Biomed Mater Res A. 89 (2009) 248–254. https://doi.org/10.1002/jbm.a.32025.
[35] Y. Xiao, Y. Gu, L. Qin, L. Chen, X. Chen, W. Cui, F. Li, N. Xiang, X. He, Injectable thermosensitive hydrogel-based drug delivery system for local cancer therapy, Colloids Surf B Biointerfaces. 200 (2021) 111581. https://doi.org/10.1016/J.COLSURFB.2021.111581.
[36] M. Dixit, P.K. Kulkarni, Lyophilization monophase solution technique for improvement of the solubility and dissolution of piroxicam, Res Pharm Sci. 7 (2012) 13. /pmc/articles/PMC3500553/ (accessed January 3, 2023).
[37] K.I. Izutsu, Applications of Freezing and Freeze-Drying in Pharmaceutical Formulations, Adv Exp Med Biol. 1081 (2018) 371–383. https://doi.org/10.1007/978-981-13-1244-1_20.
[38] A. Wolfson, C. Dlugy, Y. Shotland, Glycerol as a green solvent for high product yields and selectivities, Environ Chem Lett. 5 (2007) 67–71. https://doi.org/10.1007/S10311-006-0080-Z/TABLES/2.

[39] J. Vovers, K.H. Smith, G.W. Stevens, Bio-Based Molecular Solvents, in: The Application of Green Solvents in Separation Processes, Elsevier, 2017: pp. 91–110. https://doi.org/10.1016/B978-0-12-805297-6.00004-8.

[40] K.N. Kumar, S. Mallik, K. Sarkar, Role of freeze-drying in the presence of mannitol on the echogenicity of echogenic liposomes, J Acoust Soc Am. 142 (2017) 3670. https://doi.org/10.1121/1.5017607.

[41] A. Madgulkar, M. Bandivadekar, T. Shid, S. Rao, Sugars as solid dispersion carrier to improve solubility and dissolution of the BCS class II drug: clotrimazole, Drug Dev Ind Pharm. 42 (2016) 28–38. https://doi.org/10.3109/03639045.2015.1024683.

[42] D. Whaley, K. Damyar, R.P. Witek, A. Mendoza, M. Alexander, J.R.T. Lakey, Cryopreservation: An Overview of Principles and Cell-Specific Considerations, Cell Transplant. 30 (2021). https://doi.org/10.1177/0963689721999617.

[43] S. Vahdati, A. Shayanfar, J. Hanaee, F. Martínez, W.E. Acree, A. Jouyban, Solubility of carvedilol in ethanol + propylene glycol mixtures at various temperatures, Ind Eng Chem Res. 52 (2013) 16630–16636. https://doi.org/10.1021/IE403054Z/SUPPL_FILE/IE403054Z_SI_001.PDF.

[44] T.A. Pemberton, B.R. Still, E.M. Christensen, H. Singh, D. Srivastava, J.J. Tanner, Proline: Mother Natures cryoprotectant applied to protein crystallography, Acta Crystallogr D Biol Crystallogr. 68 (2012) 1010–1018. https://doi.org/10.1107/S0907444912019580/DW5018SUP1.PDF.

[45] Y. Inoue, D. Niiyama, I. Murata, I. Kanamoto, Usefulness of Urea as a Means of Improving the Solubility of Poorly Water-Soluble Ascorbyl Palmitate, Int J Med Chem. 2017 (2017) 1–9. https://doi.org/10.1155/2017/4391078.

[46] M. Bottrel, D. Acha, I. Ortiz, M. Hidalgo, J. Gósalvez, J. Camisão, J. Dorado, Cryoprotective effect of glutamine, taurine, and proline on post-thaw semen quality and DNA integrity of donkey spermatozoa, Anim Reprod Sci. 189 (2018) 128–135. https://doi.org/10.1016/J.ANIREPROSCI.2017.12.021.

[47] A.M. Petrosian, J.E. Haroutounian, Taurine as a universal carrier of lipid soluble vitamins: A hypothesis, Amino Acids. 19 (2000) 409–421. https://doi.org/10.1007/S007260070020.

[48] M. Qiao, D. Chen, T. Hao, X. Zhao, H. Hu, X. Ma, Effect of bee venom peptide–copolymer interactions on thermosensitive hydrogel delivery systems, Int J Pharm. 345 (2007) 116–124. https://doi.org/10.1016/J.IJPHARM.2007.05.056.

[49] P.S. Chan, J.W. Xian, Q. Li, C.W. Chan, S.S.Y. Leung, K.K.W. To, Biodegradable Thermosensitive PLGA-PEG-PLGA Polymer for Non-irritating and Sustained Ophthalmic Drug Delivery, AAPS Journal. 21 (2019) 1–13. https://doi.org/10.1208/S12248-019-0326-X/FIGURES/8.

[50] H. Danafar, K. Rostamizadeh, M. Hamidi, Polylactide/poly(ethylene glycol)/polylactide triblock copolymer micelles as carrier for delivery of hydrophilic and hydrophobic drugs: a comparison study, J Pharm Investig. 48 (2018) 381–391. https://doi.org/10.1007/S40005-017-0334-8/TABLES/7.

[51] Haryanto, S. Kim, J.H. Kim, J.O. Kim, S. Ku, H. Cho, D.H. Han, P. Huh, Fabrication of poly(ethylene oxide) hydrogels for wound dressing application using E-beam, Macromol Res. 22 (2014) 131–138. https://doi.org/10.1007/S13233-014-2023-Z.

[52] L. Yu, Z. Zhang, J. Ding, Influence of LA and GA sequence in the PLGA block on the properties of thermogelling PLGA-PEG-PLGA block copolymers, Biomacromolecules. 12 (2011) 1290–1297. https://doi.org/10.1021/BM101572J.

[53] M.J. Stoddart, Cell viability assays: introduction, Methods Mol Biol. 740 (2011) 1–6. https://doi.org/10.1007/978-1-61779-108-6_1.

[54] S. Binder, B. V. Stanzel, I. Krebs, C. Glittenberg, Transplantation of the RPE in AMD, Prog Retin Eye Res. 26 (2007). https://doi.org/10.1016/j.preteyeres.2007.02.002.

[55] H. Al-Hussaini, J.H. Kam, A. Vugler, M. Semo, G. Jeffery, Mature retinal pigment epithelium cells are retained in the cell cycle and proliferate in vivo, Mol Vis. 14 (2008) 1784. /pmc/articles/PMC2562424/ (accessed March 14, 2023).

[56] S. He, H.M. Wang, J. Ye, T.E. Ogden, S.J. Ryan, D.R. Hinton, Dexamethasone induced proliferation of cultured retinal pigment epithelial cells, Curr Eye Res. 13 (1994). https://doi.org/10.3109/02713689408995786.

CAPÍTULO IV – CHAPTER IV. Hybrid therapeutic platform of multi-loaded PLGA microspheres for the treatment of glaucoma.

Hybrid therapeutic platform of multi-loaded PLGA microspheres for the treatment of glaucoma.

Alba Aragón-Navas[1,2], Maria J Rodrigo[3,5,6], Javier López-Cano[1,2], Manuel Subías[5,6], Inés Munuera[5,6], Julián García-Feijoo[3,7], Luis E Pablo[3,5,6], Irene Bravo-Osuna[1,2,3,4], Elena Garcia-Martin[3,5,6], Rocio Herrero-Vanrell[1,2,3,4].

[1]Innovation, Therapy and Pharmaceutical Development in Ophthalmology (InnOftal) Research Group, UCM 920415, Department of Pharmaceutics and Food Technology, Faculty of Pharmacy, Complutense University of Madrid, Madrid, Spain

[2] Health Research Institute, San Carlos Clinical Hospital (IdISSC), Madrid, Spain

[3] National Ocular Pathology Network (OFTARED), Carlos III Health Institute, Madrid, Spain

[4] University Institute for Industrial Pharmacy (IUFI), School of Pharmacy, Complutense University of Madrid, Madrid, Spain

[5] Department of Ophthalmology, Miguel Servet University Hospital, Zaragoza, Spain

[6] Miguel Servet Ophthalmology Research Group (GIMSO), Aragon Health Research Institute (IIS Aragon), University of Zaragoza, Spain

[7]Department of Ophthalmology, San Carlos Clinical Hospital, Health Research Institute of the San Carlos Clinical Hospital (IdISSC), Madrid, Spain.

ABSTRACT

This work proposed a hybrid neuroprotective formulation where tri-loaded PLGA (poly-(DL-lactic-co-glycolic acid) microspheres were dispersed in PLGA-PEG-PLGA (PEG=polyethylene glycol) thermosensitive hydrogels for intraocular delivery of neuroprotective agents. PLGA microspheres were elaborated by the solvent extraction-evaporation method and were loaded with low molecular weight drugs (dexamethasone and ursodeoxycholic acid) and the biotechnological agent GDNF (glial cell line-derived neurotrophic factor). PLGA-PEG-PLGA were synthethized by ring-opening method and the hydrogel was loaded with dexamethasone-phosphate. Both drug delivery systems were characterized separately. The hybrid formulation was prepared by the dispersion of the tri-loaded microspheres in PLGA-PEG-PLGA hydrogel 25%(w/v). Physicochemical characterization of the hybrid platform and *in vitro* release of the different neuroprotective agents was evaluated. The inclusion of microspheres in the hydrogels did not show differences in the physicochemical hybrid system characterization in swelling index or injectability. Tube inverting test showed a decrease of 1°C. Hydrogel modified the initial burst release of the encapsulated drugs in the microspheres, reducing the burst release for each component. Moreover, *in vitro* release data was fitted to a sigmoidal equation model (Gallagher-Corrigan). The hybrid formulation resulted well tolerated in retinal cells (>90%). The presence of the hydrogel promoted the aggregation of the microspheres. In conclusion, the novel platform developed in this work can be considered as a promising strategy for glaucoma treatment.

1. Introduction

In developed countries, neurodegenerative diseases in the retina are the main causes of vision loss and blindness in the world. These diseases are characterized by the progressive neuronal loss [1]. In the case of glaucoma, this progressive neurodegeneration occurs in the retinal ganglion cells (RCG) and their axons in the optic nerve and extended to the retina [2]. Currently, glaucoma treatments are focusing on lowering intraocular pressure (IOP), since it is the only risk factor that can been successfully modified. However, there are some patients whose glaucoma courses without an increase in IOP, the so-called normal tension glaucoma (NTG). Moreover, in other cases, retinal glaucomatous degeneration continues progressing despite a well-controlled IOP. These facts suggest a complex aetiology where not only IOP is involved but also other factors [3]. For these reasons, neuroprotective agents are considered as a promising therapy to stimulate neurons survival or inhibit their death [4].

Intraocular drug delivery systems (IODDS) have emerged as interesting neuroprotective platforms since administrations can be spaced to reduce the damage associated with intraocular injections themselves and achieve relatively constant concentrations of the loaded drug(s) for long periods. Among the IODDS, the most explored are liposomes, niosomes, hydrogels, dendrimers, in situ gels, micro- and nanoparticles, microneedles, and ocular implants [5].

One crucial characteristic of IODDS is the material that is composed of, that affects its release kinetics, degradation rate, and biocompatibility. The use of biodegradable polymers avoids device removal, and their use has been increasing through the years. Among the biodegradable polymers currently available for clinical use, poly(caprolactone) (PCL) and poly(lactic-co-glycolic acid) (PLGA) are the most used and both can be tuneable to modulate release kinetics [6].

Biodegradable microparticles result appealing for several reasons. For example, they can encapsulate different drugs in the same device and subsequently co-deliver them in a sustained manner for long periods [7]. Due to the multifactorial aetiology of glaucoma, and other retinal neurodegenerative diseases, this strategy might allow acting simultaneously on different targets. Furthermore, due to the reduced particle size, they

can be easily administrated by suspending and injecting them through different needle gauges (between 25 and 32G) [8]. In addition, therapy can be easily personalized by modifying the concentration of the microparticles suspension administrated [9].

The intraocular administration of hydrogels loaded with active substances is another technological strategy that can be very beneficial for the treatment of degenerative pathologies of the retina. Especially the use of in situ hydrogels, such as thermosensitive ones since they can be easily injected in their "sol" state and once inside the body they change to a "gel" state due to the effect of temperature. This is the case of the hydrogels created from the PLGA-PEG-PLGA copolymers. These hydrogels are capable of controlling the release of the active substances they contain, although to a lesser extent than solid systems (microsystems or implants), and are very attractive due to their excellent biocompatibility, biodegradability, and lack of an organic solvent for their synthesis [10].

Taking into consideration the above-mentioned, the combination of microspheres suspended in PLGA-PEG-PLGA hydrogels could be an interesting platform for intravitreal administration. Since its instantaneous gelation, microspheres will have limited their migration from the site of administration as well as the hydrogel may offer protection against enzymatic and cellular degradation [11,12]. Furthermore, the combination of microspheres with hydrogels for intraocular administration could exert some type of control over the initial release of the active agents encapsulated in the microspheres.[11].

The present work aims to study the incorporation of PLGA microspheres loaded with 3 neuroprotective agents, the anti-inflammatory corticosteroid dexamethasone, the neurotrophic factor GDNF (cell line-derived neurotrophic factor) and the antiapoptotic agent UDCA (ursodeoxycholic acid) [13,14] in thermosensitive hydrogels formed with the PLGA-PEG-PLGA polymer, which in turn can be also loaded with an anti-inflammatory compound (dexamethasone-phosphate).

2. Materials and Methods

2.1. Materials

Dexamethasone (DX) (purity >98%), dexamethasone 21-phosphate disodium salt (DXP) (purity >98%), DL-alpha-tocopherol acetate, polyethylene glycol (PEG 1500), glycolide and stannous 2-ethylhexanoate were supplied by Sigma-Aldrich (St. Louis Mo., USA). Polyvinyl alcohol 72,000 g/mol (PVA) was acquired from Panreac. DL-Lactide was bought from Corbion® (Gorichem, The Netherlands). Recombinant human Glial cell-line-derived neurotrophic factor (GDNF) and enzyme-linked immunosorbent assay (ELISA) for GDNF quantification were purchased from R&D Systems (Minneapolis, MN, USA). PLGA (50:50) polymer (Resormer®503) was obtained from Evonik Nutrition & Care GmbH (Darmstadt, Germany). Ursodeoxycholic acid (UDCA) (purity >99%) was acquired from Alfa Aesar (Haverhill, Massachusetts, USA)

All organic solvents were HPLC-grade and used as received.

2.2. Microspheres elaboration.

Tri-loaded microspheres were elaborated by the solid-in-oil-in-water method (S/O/W) as explained in chapter II. Briefly, a 33.33% PLGA solution (w/v) incorporating 40 mg of UDCA was prepared by dissolving PLGA in 1.2 mL of a mixture of 80:20 methylene chloride:ethanol. Then, 60 mg DX were incorporated and dispersed by ultrasonication (Ultrasons; J.P. Selecta, Barcelona, Spain) at a low temperature for 5 minutes. In parallel, 20 µg GDNF were suspended in 40 µL alpha-tocopherol acetate by gentle sonication at low temperature for 30 seconds (Sonicator XL, Head System, Inc., Farmingdale, NY, USA) and after, it was incorporated into the organic phase and sonicated (Sonicator XL; Heat Systems, Inc., Farmingdale, NY, USA) at low temperature. Then, the organic phase was emulsified at 8,500 rpms for 1 minute with 5 mL of PVA (2% w/v) in a homogeniser (Polytron® PT 10-35, Kinematica GmbH, Luzcerna, Switzerland). The resulting emulsion was poured into 100 mL of PVA (0.1% w/v) and stirred for 3 hours in order to harden the MSs.

The obtained MSs were washed and 38-20 µm fraction was collected by sieving. MSs were freeze-died (Freezing: -60°C/15 min, drying: -60°C/12h/0.1 mBar) and stored at -30°C in dry condition.

2.3. Microspheres characterization.

2.3.1. Particle size and particle size distribution.

Particle size distribution and mean particle size were measured by a Microtrac®S3500 Series Particle Size Analyser (Montgomeryville, PA, USA) where MSs samples were previously suspended in MilliQ® water. Each sample was measured 3 times and mean particle size is expressed as mean ± standard deviation (SD)

2.3.2. Morphological evaluation

External and internal morphology evaluation were assessed. For external morphology, freeze-dried MSs were applied with a gold-sputter coating and were observed by scanning electron microscopy (Jeol, JSM-6335F, Tokyo, Japan). For the internal morphology, MSs were embedded in a synthetic resin medium (Spurr Low Viscosity Embedding Kit) and cut cross-sectionally by Reichert Ultracut S Ultramicrotome (Leica Microsystems Inc, Wetzlar, Germany) in cuts of 50-70 µm of thickness. Then, the internal structure was visualized by transmission electron microscopy (TEM, Jeol JEM 1010, Tokyo, Japan)

2.3.3. Encapsulation efficiency

For UDCA and DX quantification, 2.5 mL of methylene chloride was added to 1 mg of MSs. Then, 6 mL of ethanol was subsequently added in order to precipitate the polymer and to extract both drugs. It was vortex mixed and centrifuged (5,000 rpms, 5 minutes, 20°C). The supernatant was filtered and analysed in LC/MS as will be described after. Each batch was quantified in duplicate.

For GDNF, the method employed was liquid-liquid extraction as described elsewhere [15], where 0.7 mL of methylene chloride was added to 5 mg of MSs. Then, 0.7 mL of reagent diluent composed of 1% BSA in PBS (pH= 7.4), provided in the ELISA kit, was added. Samples were centrifuged (12,000 rpms, 15 minutes, 4°C) and the aqueous phase was collected. This procedure was repeated a total of 4 times, by collecting and adding the reagent diluent and each batch was quantified in duplicate. GDNF concentration was evaluated by ELISA as described after.

2.4. Synthesis of PLGA-PEG-PLGA.

The co-polymer PLGA-PEG-PLGA was synthesized according to the Ring Opening Method (ROP) previously described by our group [27]. The ratios PEG:GA:LA used were 1:1.54:23.1. Briefly, 0.01 mol of PEG 1500 were dried in a two-neck flask under vacuum (100°C) and stirring overnight. 0.015 mol of GA and 0.231 mol of LA were added under the protection of nitrogen. It was stirred and heated for 0.5-1h at 130 °C and in a reduced atmosphere. Then, stannous 2-ethylhexanoate was added (0.2% w/w of monomers) and the reaction was carried out for 8h at 150 °C under a nitrogen atmosphere. The unreacted monomers were removed under 1h of vacuum. The crude polymer was dissolved in ice-cold water (5-8 °C) and after its completed dissolution, it was precipitated by heating it until 80 °C. The supernatant was decanted, and the copolymer was dissolved in ice-cold water. This process of dissolving-heating-precipitation-decantation was repeated a total of three times. Then, the copolymer was freeze-dried and stored at -30 °C.

2.5. PLGA-PEG-PLGA characterization.

The molecular weight of PLGA-PEG-PLGA triblock was measured by gel permeation chromatography (GPC) composed of a binary pump (Waters 1525) coupled to a guard column Plgel 5µm 50x7.5, a Plgel 5um MIXED-D 300 x 7.5 mm column and a diffractive index detector (Waters 2414 detector). The analysis was made at a rate of 1.0 mL/min using tetrahydrofuran as eluent, the column temperature was set at 30 °C.

The chemical structure was determined by ^{1}H-NMR (Nuclear magnetic resonance) by a Bruker AV 500MHz. The polymer was dissolved in deuterated chloroform ($CDCl_3$) and measured at 25 °C.

2.6. Hydrogel preparation

To prepare the hydrogel, the copolymer PLGA-PEG-PLGA (25% w/v) was dissolved in a bicarbonate buffer ($NaHCO_3$ 0.095M, Na_2CO_3 0.005M, pH = 8.81) isotonized with sodium trehalose (3.25%) or mannitol (1.25%). The micelles were confirmed by transmission electron cryo-microscopy (cryo-EM; 200 kV FEI TALOS Arctica). The hydrogel was applied to the quant foil Lacey Carbon film Cu/Rh lacey carbon grids by one side. Then, they were blotted, plunged into liquid ethane in a FEI Vitrobot Mark IV,

and analysed with an X field emission gun operating at 200 kV. The conditions used were under low dose and a nominal magnification of 45000 and 73000 (2.2 Å/pixel and 1.4 Å/pixel sampling rate respectively). Pictures were acquired by EPU Software (ThermoFisher Scientific®) and processed with ImageJ (Fiji) analysis software 2.1.0/1.53c (National Institute of Mental Health, Bethesda, Md USA).

For the dexamethasone loaded-hydrogels, 0.2% dexamethasone 21-disodium phosphate was added once the hydrogel was fully dissolved in the buffer.

2.7. Hydrogel characterization

2.7.1. Rheological behaviour

Rheological behaviour was assessed using a Discovery HR-1 hybrid rheometer (New Castle, DE, USA). A parallel 8-mm diameter plate was used. Analysis was carried out by a temperature ramp starting at 25 °C and finishing at 50 °C with a ramp rate of 0.6 °C/min at 10 rad/s. Results were plotted as G' modulus vs temperature.

2.7.2. Micelles size

Micelles particle size was analyzed by dynamic light scattering (DLS) (Zetatrac® Particle Size Analyzer, Montgomeryville, PA, USA) by diluting the sample in MilliQ® water (n=3).

2.7.3. pH

pH was measured immediately after dissolution with a pH meter (model GLP 22, Crison, Barcelona, Spain).

2.7.4. Tube inverting test

Tube inverting test was carried out in order to visually evaluate the hydrogel sol-to-gel transition temperature. 1 mL of samples were deposited in a 2 mL glass vial and placed in a cooled incubator (Velp Scientifica FOC120I, Velp Scientifica, Usmate Velate, Italy) with a temperature range from 30 to 50 °C. Each temperature increase consisted of 1 ± 0.2 °C and samples were kept under that temperature for 15 minutes to ensure that all systems achieved the temperature. Then, tube inversion was performed to inspect the sol-to-gel transition. After 30s of inversion, sol was defined as "flow liquid sol" and gel as "no flow solid gel" as previously described elsewhere [16].

2.7.5. Density

2 mL of sample were placed in a volumetric flask and weighted (RADWAG MYA 11.3Y microbalance, Radwag, Radom, Poland). Density was calculated by the subtraction of the empty flask from the filled flask. Each measure was performed in triplicate and results were expressed as mean ± standard deviation.

2.7.6. Swelling and degradation

100 µL of hydrogels and 1.5 mL of PBS were placed in 2 mL tubes and placed in a water bath at 37 °C, 100 rpms (Julabo GmbH, Seelbach, Germany) in triplicate. Twice per week, hydrogels were centrifuged (5,000 rpms, 5 mins, 20 °C) (Hettich EBA 12R, Andreas Hettich GmbH & Co. KG, Tuttlingen, Germany) and the supernatant was removed. For swelling studies, hydrogels were weighted (W_f), and the index of swelling was estimated as follows, being Wi the weight of initial hydrogel:

$$Swelling\ index\ = \frac{W_f}{W_i}$$

Equation 1. Swelling index equation.

Then, the media was replaced, and the tubes were placed back in the water bath.

For weight loss studies, after supernatant removal, media was replaced, and at pre-set times (each week until week 10), three samples were collected in order to freeze-dry and to weigh the dry polymer ($W_{freeze\text{-}dried\text{-}f}$). Control samples (not incubated) were freeze-dried and weighted too ($W_{freeze\text{-}dried\text{-}i}$). Before freeze-drying, samples were washed with MilliQ® water in order to remove residual salts from the media. The percentage of polymer weight loss was determined as follows:

$$\%\ Weight\ loss\ = \frac{W_{freeze-dried-i}\ -\ W_{freeze-dried-f}}{W_{freeze-dried-i}}\ x\ 100$$

Equation 2. Percentage of weight loss.

2.7.7. CMC

The critical micelle concentration (CMC) was assessed for both bicarbonate buffer vehicles (trehalose 3.25% and mannitol 1.25%). Measures were carried out with a tensiometer (K-11, Krüss, Hamburg, Germany) by the Wilhelmy plate method. Prior to measures, equipment was calibrated with MilliQ® water (73.5 ± 0.3 mN/m), and, each

vehicle, without hydrogel, was measured too (71.3 ± 0.5 mN/m for trehalose buffer and 70.8 ± 0.3 mN/m for mannitol). A curve of 15 different concentrations of each hydrogel ranging from 5 mg/mL to 0.0156 mg/mL was carried out. Each concentration was equilibrated for 5 minutes and measured 3 times.

2.8. Preparation of the MSs/hydrogel hybrid system

For MSs/hydrogel hybrid system preparation, 5 mg of MSs were incorporated into 100 µL of the hydrogel.

2.8.1. Physico-chemical properties characterisation

Physico-chemical characterisation were made in terms of tube inverting test, swelling, and injectability as have been described before.

2.8.2. *In vitro* release studies

In vitro release studies were carried out in triplicate as follows: the MSs/hydrogel hybrid system was placed in a 2 mL tube, vortex mixed to have a suspension, and left at 37°C for 10 minutes to assure the gel state. Then, 1.5 mL of PBS/Azide (0.02%) or PBS/BSA (1%) /Azide (0.02%) were added. Once per week, the tubes were centrifuged (5,000 rpm, 5 minutes, 20 °C) and the release media were removed and replaced by fresh media. Drugs quantifications were carried out as follows:

DX and UDCA were quantified by LC/MS composed of a 1525 binary HPLC pump, a 2707 autosampler, and a 3100-mass detector (Waters Corp, Barcelona, Spain). The column was a Nova-Pak C18 column (4 µm, ID 2.1 mmx150 mm) at 45°C. As a mobile phase, ammonium acetate in water (5 mM) was adjusted to pH 5 (UDCA) and 4 (DX) with formic acid. For UDCA, the conditions were: mobile phase composed of acetonitrile/ammonium acetate (2:1 v/v) with a flow rate of 0.15 mL/min, electrospray ion source (ESI) in negative ionization mode, 3kV of spray voltage, 3V extractor voltage, 80°C for capillary temperature, 180 °C desolvation temperature and 925 L/h desolvation flow rate. For DX, the mobile phase was composed of 1:1 v/v of ammonium acetate:acetonitrile, flow rate 0.30 mL/min, ESI positive ion mode, 3 kV electrospray voltage, 3 V extractor voltage, 120 °C source temperature, 350 °C desolvation temperature and 500 L/h for desolvation flow rate. Prior to LC/MS analyses, samples were freeze-dried and resuspended in ethanol.

GDNF quantification was made using the ELISA technique and following the manufacturer's kit instructions and diluting samples when necessary.

DXP was quantified by HPLC as described previously by Lopez-Cano et al [10]. The equipment was composed of a Water Alliance 2605 separation module coupled to a Waters photodiode array 2996 (Waters corp, Barcelona, Spain). The column was a C18 HPLC Column (5 µm particle size, 25 cm × 4.6 mm). The mobile phase was composed of 70% of 0.05 M potassium dihydrogen phosphate in water at pH 4 (adjusted with formic acid) and 30% of acetonitrile at a flow rate of 1 mL/min. Dexamethasone wavelength was 240.5 nm and Empower 3 (Waters, Barcelona, Spain) was the software employed for data acquisition and processing.

In order to compare the dissolution profiles, the similarity factor (f_2) was chosen (Equation 3).

$$f_2 = 50 \cdot log\left[\frac{1}{\sqrt{1 + \frac{\sum_{t=t}^{t=n}(R_t - T_t)^2}{n}}} \cdot 100\right]$$

Equation 3. Similarity factor equation (f_2)

Where:

N= number of experimental points in the *in vitro* dissolution experiment,
Tt and Rt are the mean percentages of dissolved drugs from test and reference formulations, respectively.
T is each time point.

Moreover, no more than one sampling time point after 85% dissolution was considered. If the f_2 value is between 50 and 100, it can be considered that the difference between the two release profiles is lower than 10% [17].

Experimental *in vitro* release data were fitted into the Gallagher-Corrigan model with Gorrasi adjustment. Gallagher-Corrigan kinetic model describes sigmoidal shape releases. The mathematical following equation can be divided into two parts, the first and second addends correspond to the first release stage, where "non-bounded" drug to the matrix is delivered, and the last addend corresponds to matrix erosion. Gorrasi et

al added the first addend to the original equation – b –, considering the initial burst release. This parameter is zero when burst release does not exist [18,19].

$$Y(t) = b + Y_1(1 - e^{-k_1 t}) + Y_2\left(\frac{e^{-k_2(t_2 - t)}}{1 + e^{-k_2(t_2 - t)}}\right)$$

Equation 4. Gallagher-Corrigan equation with Gorrasi adjustment.

Where:

Y(t) is the drug fraction release in a t time, b is the burst release parameter added by Gorrasi et al, Y_1 and Y_2 are the relative amount of drug release and K_1 and K_2 are the kinetic constants in the first and second stages, respectively; t_2 is a characteristic time of the second step mechanism, when time to maximum drug release rate.

2.8.3. Hybrid system injectability

Hybrid hydrogel/MSs system injectability was tested using a 1 mL plastic syringe couple to three different needles. The needles used were 21G, 25G, and 30G which differed in their internal diameter (0.514, 0.26, and 0.159 mm I.D, respectively). Moreover, injectability tests were carried out at two different temperatures (20 and 37 °C). Before injection, the hybrid system was left 20 minutes at the tested temperature to allow system equilibration in the sol or gel state.

2.9. Cell culture studies

2.9.1. Cell cultures

Retinal-pigmented epithelial cell line hTERT (RPE-1) cells kindly donated by the UCD (University College of Dublin) Conway Institute were employed for cytotoxicity studies. Cells were cultured at 37 °C with 5% CO_2 in Dulbecco's Modified Eagle Medium/Nutrient Mixture F-12 (DMEM/F-12) supplemented with 10% of FBS, 1% of L-Glutamine, 3.5% of sodium bicarbonate at 7.5% and 1% penicillin-streptomycin. Each 48-72h, cellules were passed.

2.9.2. Tolerance studies

For cell tolerability assays, unfortunately it was not possible to use the tetrazolium salt (3-(4,5-dimethylthiazol-2-yl)-2,5-diphenyltetrazolium bromide (MTT) assay, widely employed for these types of studies, since hydrogels interfere in the signals,

underestimating the viability results [20]. *In vitro* cell viability was then assessed by Trypan blue. To this, cells were cultured in a 12 wells-plate with a density of 70,000 cells/well, overnight. Different formulations were added and incubated for 24 hours. For this, a suspension of MSs (5% w/v) were prepared with the corresponding vehicle (NaCl or PLGA-PEG-PLGA hydrogels) and a final concentration of 0.5 mg of MSs/mL were added to the wells. After incubation, cells were washed and detached with trypsin. Trypsin was neutralised with culture medium, and the cell suspension was placed in a tube. 20 µL of cells suspension were mixed with another 20 µL of Trypan blue (1:1). The cell number was determined by counting the viable cells (not stained cells) in an automated cell counter (Invitrogen, ThermoFisher Scientific, Waltham, Massachusetts, USA). NaCl (0.9% w/v) was employed for the positive control of viability and DMSO (5% w/v) as negative control. Three replicates of each formulation in three different days were carried out.

2.9.3. Preliminary studies of microspheres aggregation

In order to study microspheres aggregation, a suspension of MSs (5% w/v) in NaCl (0.9%) or in PLGA-PEG-PLGA hydrogels were prepared by vortex-mixing. Then, 10 µL of the corresponding suspension was added to the wells with media previously heated at 37°C.

3. Results

3.1. Microspheres characterization.

3.1.1. Particle size and particle size distribution, morphological evaluation, and encapsulation efficiency.

MSs visualized at SEM presented a spherical shape with surficial pores and a slightly rough surface. Moreover, MSs presented homogeneity in size which was an average of 30.39 ± 2.09 µm measured by DLS. The particle size distribution of MSs showed a unimodal distribution under the desired range (20-38 µm) (Figure 1).

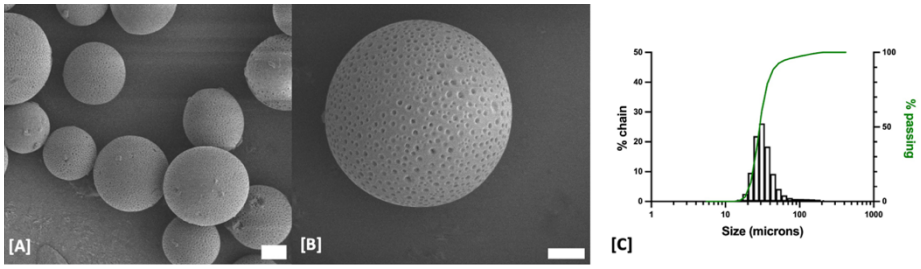

Figure 1. [A] and [B] Scanning Electron Microscopy pictures of DX+UDCA+GDNF loaded MSs. Scale bars: 10 µm [C] Particle size distribution of DX+UDCA+GDNF loaded MSs.

The encapsulation efficiency of each one of the drugs was assessed, presenting the following values: 81.21 ± 2.94 % for DX (97.25 ± 3.52 µg DX/mg MSs), 56.32 ± 3.23 % for UDCA (46.09 ± 2.65 µg UDCA/mg MSs) and 49.25 ± 4.95 % for GDNF (18.93 ± 1.90 ng GDNF/mg MSs)

3.2. Synthesis of PLGA-PEG-PLGA.

3.2.1. PLGA-PEG-PLGA characterization.

The molecular weight of PLGA-PEG-PLGA was determined by GPC as it is shown in Table 1. Moreover, in order to determine the molecular structure, ^{1}H-NMR analysis was carried out as can be seen in Figure 2, showing the characteristic peaks of each component (GA in 4.75 ppm – CH_2 groups – LA in 5.20 and 1.55 ppm – for CH and CH_3 groups respectively, – and PEG in 4.30 and 3.65 – for CH_2 groups) [21].

Table 1. Characterization of PLGA-PEG-PLGA triblock by GPC and ^{1}H-NMR.

Mn[1] (g/mol)	Mw (g/mol)	Mp (g/mol)	PDI[2]	Mn[3] (g/mol)	Ratio (PEG:GA:LA)		Ratio (GA:LA)	
					Theoretical	NRM Experimental	Theoretical	NRM Experimental
4582	5996	5551	1.3	4609.03	1:1.54:23.10	1:1.52:20.34	1:15	1:13.39

[1]Number molecular weight (Mn) calculated by GPC. [2]Polydispersity (Mw/Mn) calculated by GPC. [3]Mn calculated by ^{1}H-NMR.

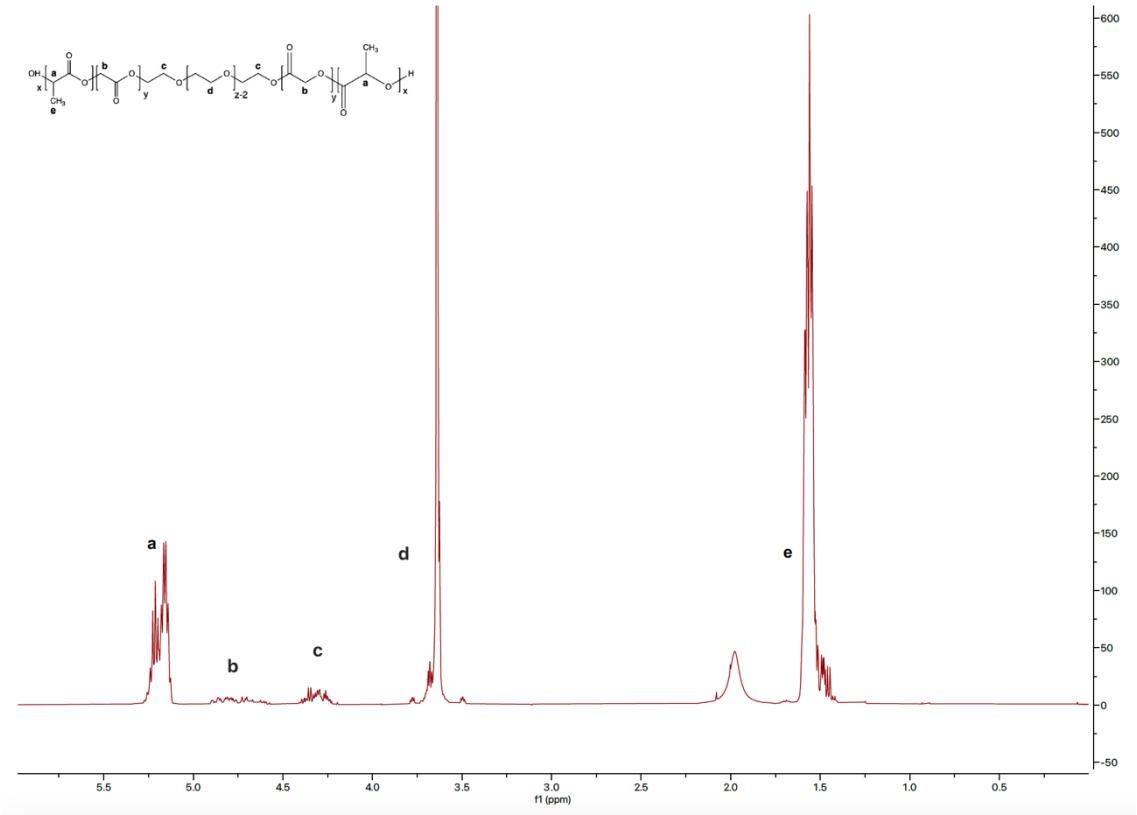

Figure 2. ^{1}H-NMR spectrum of PLGA-PEG-PLGA polymer.

3.3. PLGA-PEG-PLGA hydrogel and hybrid system characterization

3.3.1. Rheological behaviour

The rheological behaviour of the polymer dissolved in bicarbonate buffer with trehalose (3.25% w/v) and mannitol (1.25% w/v) and loaded with DXP (0.2% w/v) was studied. Both showed similar profiles with a sol state at room temperature and a sol-gel transition starting at 30°C. Either trehalose or mannitol experimented a maximum sol-gel transition point around 32-33°C. From this threshold the values began to decrease.

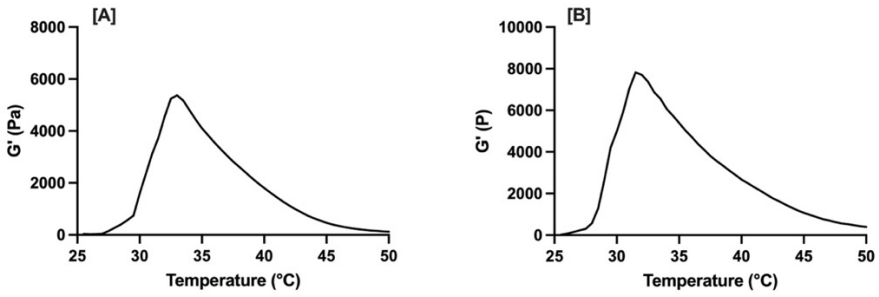

Figure 3. Rheological behaviour (Storage values) of DXP-loaded-PLGA-PEG-PLGA polymers dissolved in bicarbonate buffer with [A] – 3.25% trehalose – and [B] – 1.25% mannitol.

3.3.2. Sizes, micelles visualization, and pH

Both PLGA-PEG-PLGA loaded with DXP presented a unimodal micelles size distribution (Figure 4) with an average of 23.11 ± 7.63 nm for PPP+Trehalose and 26.25 ± 10.02 nm for PPP+Mannitol. Both PPP hydrogels presented a neutral pH inside the range of 7-7.3.

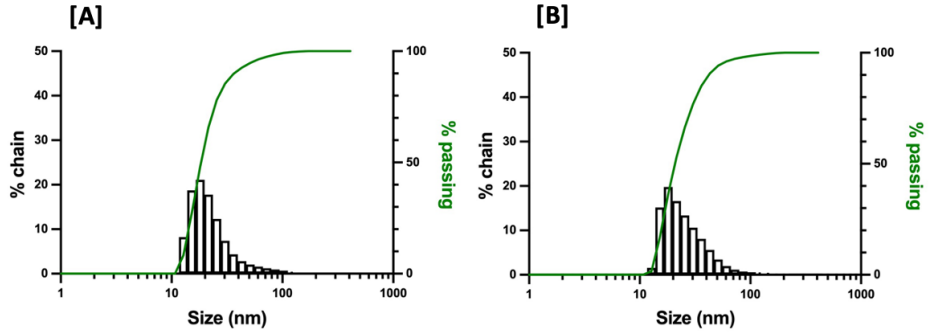

Figure 4. Micelles size distribution. [A] PPP+Trehalose loaded with 0.2% DXP and [B] PPP+Mannitol loaded with 0.2% DXP.

Cryo-EM images confirmed the existence of micelles as well as their homogeneity in size. Micelle sizes were measured being around 20 nm, similar as the sizes obtained with DLS technique. Also, the aggregation of micelles was observed (Figure 5). The chains were also measured with a size range from 50 nm for the smallest to 100-150 nm for the biggest.

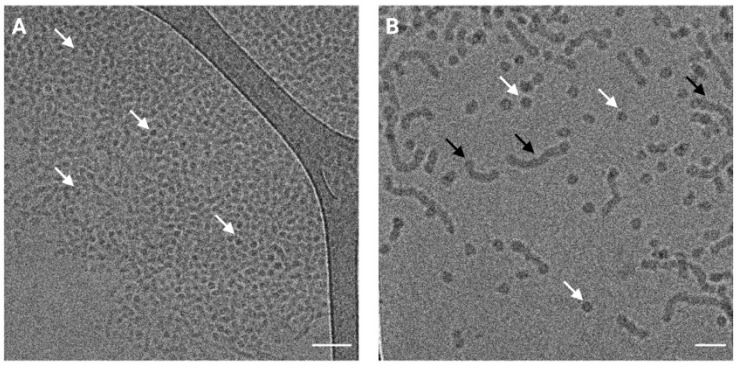

Figure 5. Cryo-EM images of hydrogels where micelles (white arrows) and micelles aggregation (black arrows) are markets. Scale bars: 100 nm (A) and 50 nm (B).

3.3.3. Tube inverting test.

Tube inverting tests were carried out in hydrogels and hybrid systems (Figure 6). It was found that gel temperature resulted 1°C cooler for the hydrogels which included microspheres – the hybrid system – (32°C) than hydrogels alone (33°C). Trehalose and

mannitol did not affect the gel behaviour. When the temperature achieved 47°C, the gel structure was lost due to micelle precipitation.

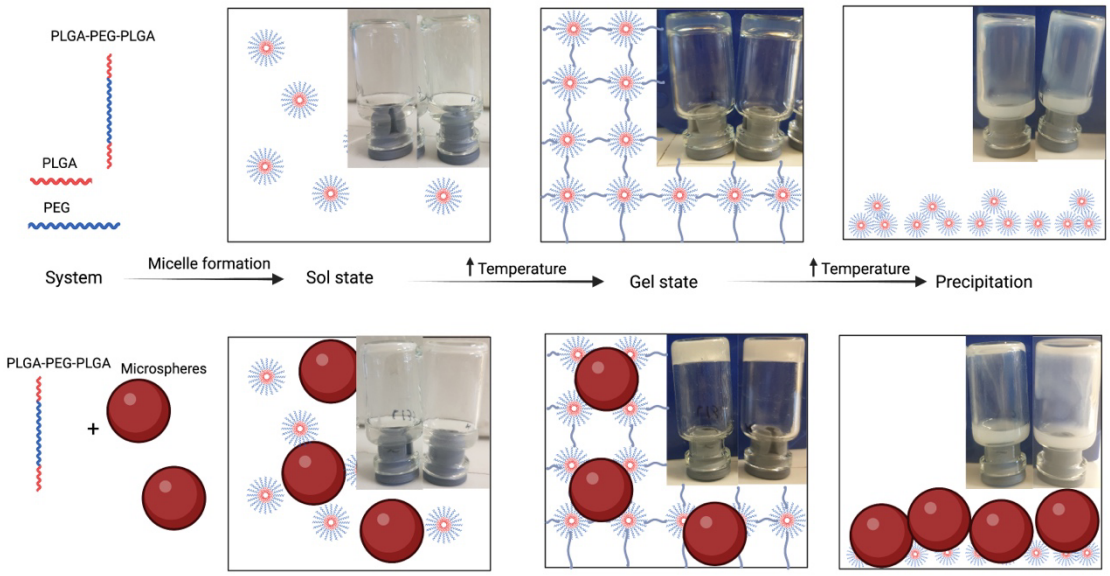

Figure 6. Schematic presentation (not scaled) of PLGA-PEG-PLGA sol-gel transition in response to temperature. Inside the squares, photographs of the hybrid systems were inserted (the left vial corresponded to trehalose hydrogels and the right one to mannitol hydrogels). Image-based on [22,23]. Image created with BioRender.com.

3.3.4. Density

PPP density was assessed, showing a value of 1.06 ± 0.00 g/mL for PPP+Trehalose and 1.06 ± 0.01 g/mL for PPP+Mannitol, not presenting any difference between them.

3.3.5. Swelling

The swelling index was assessed for the non-loaded hydrogel, non-loaded hydrogel with blank microspheres (blank hybrid system) and loaded hydrogel with loaded microspheres (loaded hybrid system), in order to study if the inclusion of microspheres and the inclusion of the different compounds could affect the swelling properties. However, as can be seen in the figures above, no differences were found among systems and buffers. All of them achieved the maximum swelling index around day 5-7 and then, the values started to decrease.

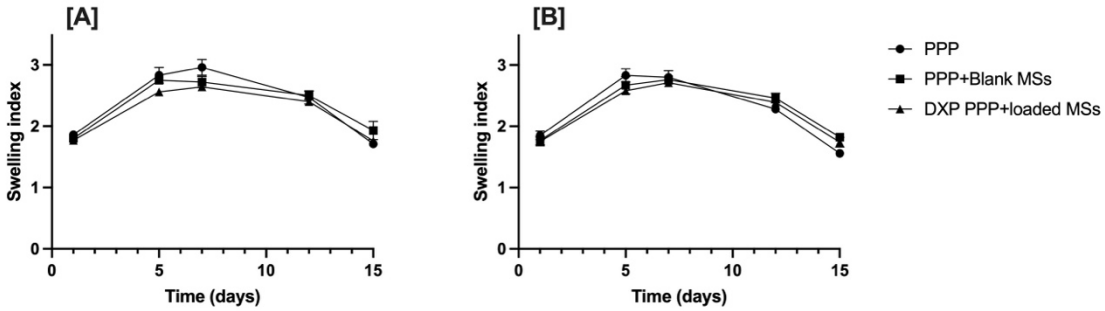

Figure 7. Swelling index of PLGA-PEG-PLGA hydrogels of trehalose buffer [A] and mannitol buffer [B]. In both images, circles represented hydrogel, squares hydrogels including blank microspheres (blank hybrid system), and triangles hydrogels loaded with DXP and tri-loaded microspheres (loaded hybrid system).

3.3.6. Degradation

Figure 8 presented the degradation in weight of polymers dissolved in the different buffers. As it can be seen, from weeks 0 to 4, the degradation occurred faster, achieving almost 50% in trehalose buffer and around 60% in mannitol buffer, presenting a more abrupt degradation in this last one. However, from week 4 until week 7, the degradation in both occurred in a slower fashion (around 12-15% for both).

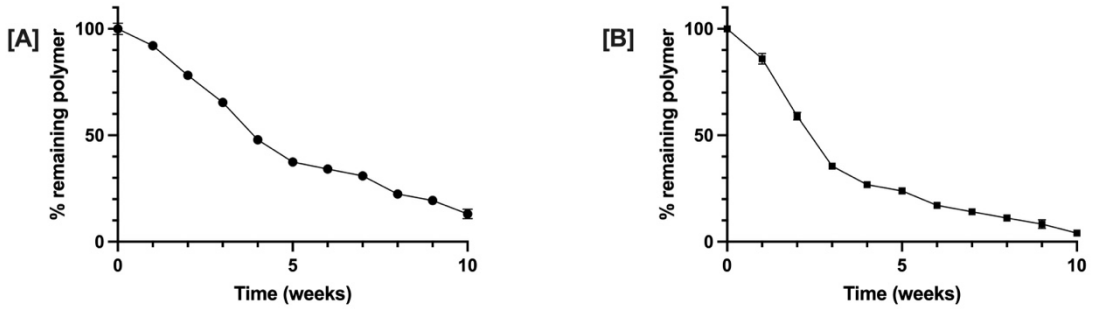

Figure 8. Degradation in weight of PLGA-PEG-PLGA polymers. [A] showed the percentage of remaining polymer dissolved in trehalose buffer, and [B] presented the percentage of remaining polymer dissolved in mannitol buffer.

3.3.7. MSs/hydrogel hybrid systems injectability

Injectability of the hybrid systems was carried out at two temperatures (room temperature – sol state – and at 37°C – gel state –) and with three different needles. Both were injectable except at 37°C with 30G needle, where difficulties to pass through the needle were found.

Table 2. Injectability of PLGA-PEG-PLGA hydrogels including MSs (hybrid system). Codes: V – injectable, X – not injectable.

		PPP+Trehalose+MSs	PPP+Mannitol+MSs
20°C	21G	V	V
	25G	V	V
	30G	V	V
37°C	21G	V	V
	25G	V	V
	30G	X	X

3.3.8. Critical Micelle Concentration (CMC)

CMC values were calculated at 25°C as described by Lopez-Cano JJ [10], where the CMC value is the crossing point between the two lines created by the experimental data of surface tension/concentration curves. CMC allows us to know the PLGA-PEG-PLGA hydrogel concentration needed to create stable micelles. These micelles with the increase in temperature will aggregate to form the thermo-responsive hydrogel. In this case, for both hydrogels, the results were similar 0.13 mg/mL for trehalose hydrogel and 0.15 mg/mL for mannitol. These results are in concordance with other works where the values range was between 0.1 and 0.3 mg/mL [10,24].

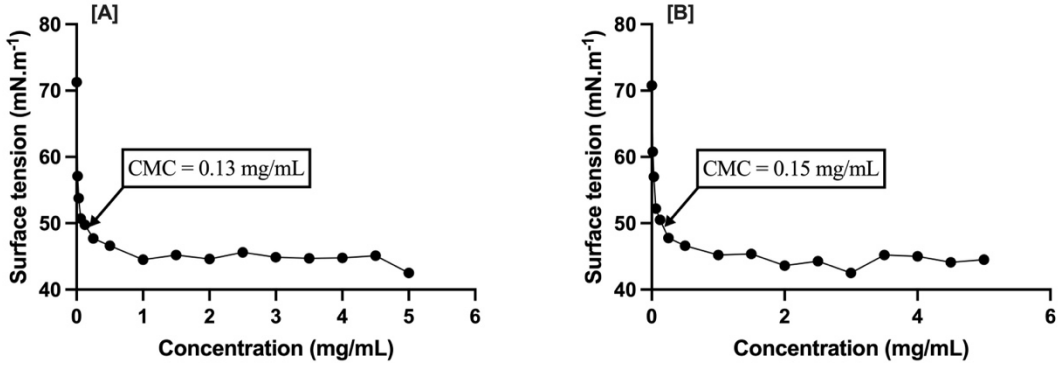

Figure 9. Surface tension showing critical micelle concentration (CMC) of trehalose hydrogel [A] and mannitol hydrogel [B].

3.3.9. *In vitro* release

Figure 11 shows the release profiles of DX and UDCA from the microcarriers and the hybrid system. It is remarkable the lower burst release achieved for hybrid formulations

for both drugs in comparison to the ones obtained for MSs alone ($p<0.0001$ for DX and UDCA) (Figure 10). These values in percentage for DX were 22.15 ± 2.99% for MSs, 6.77 ± 1.84 % PPP+MSs, 6.22 ± 0.84 % for PPP+DXP+MSs and 6.78 ± 1.81 % for PPP+DXP+MSs in mannitol buffer. In the case of UDCA, 13.38 ± 0.03 % for MSs, 6.40 ± 0.47 % for PPP+MSs, 6.60 ± 0.05 % for PPP+DXP+MSs and 7.23 ± 0.04 % for PPP+DXP+MSs in mannitol buffer. Finally, for GDNF, these values presented a more dramatic difference: 38.14 ± 4.74 % for MSs, 0.24 ± 0.08 % for PPP+MSs, 0.22 ± 0.11 % for PPP+DXP+MSs and 0.19 ± 0.11 % for PPP+DXP+MSs in mannitol buffer.

Comparing the release profiles (Table 3), when f_2 (similarity test) was calculated, PPP+MSs in trehalose buffer resulted different compared to MSs alone ($f_2<50$) for DX. For the rest of the formulations no differences were found ($f_2>50$). The hydrogel controlled burst release but through time, the delivery presented equal results with microspheres alone.

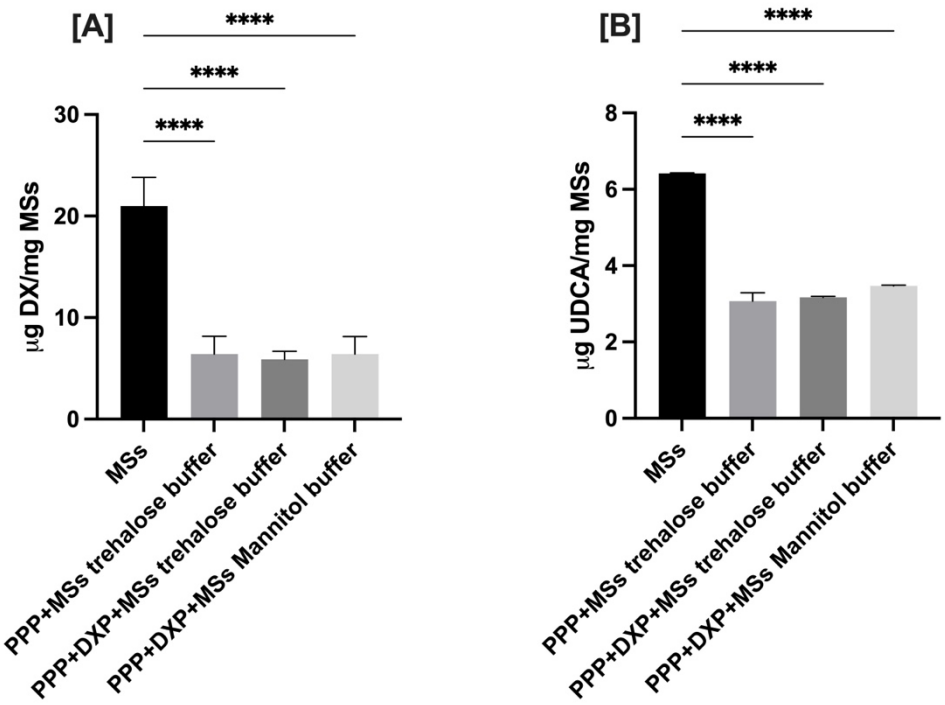

Figure 10. Initial burst release (24h) comparisons for DX release [A] and UDCA [B] from MSs and MSs/hydrogel hybrid formulations.

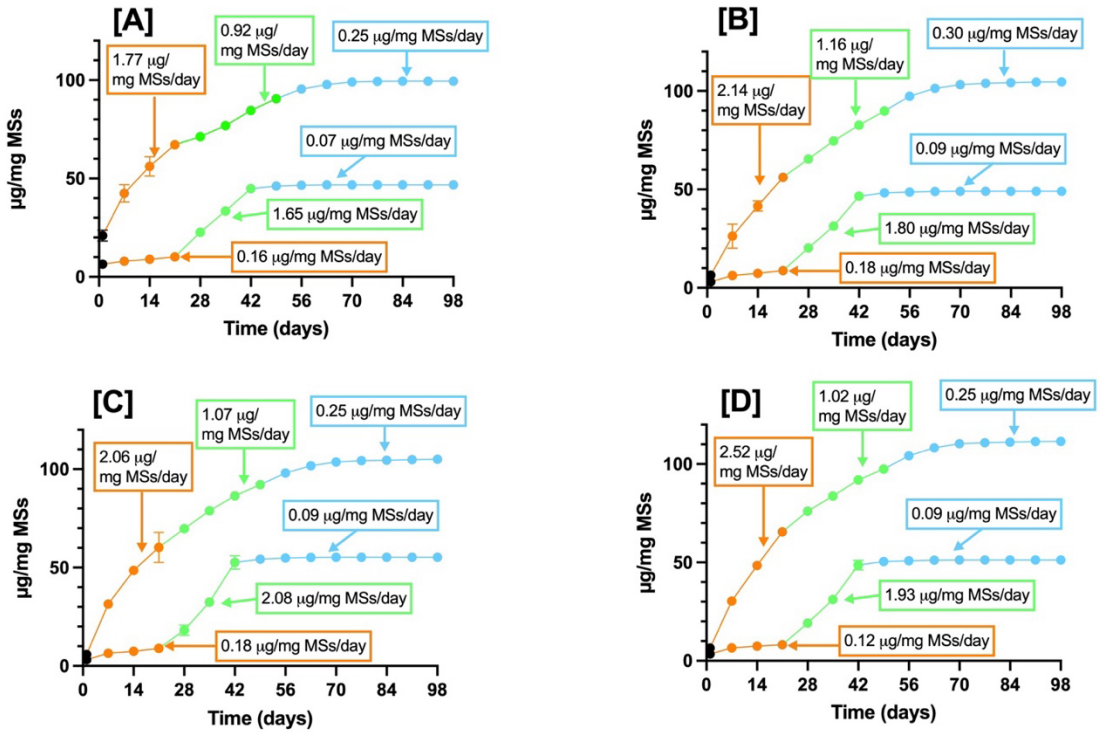

Figure 11. Dexamethasone and UDCA release profiles from MSs [A], from MSs included in PPP trehalose hydrogel [B], from MSs included in PPP trehalose hydrogel loaded with 0.2 % DXP [C], and from MSs included in PPP mannitol hydrogel loaded with 0.2% DXP [D]. DX profiles are represented by circles and UDCA by squares. Release rate values of DX and UDCA are detailed (burst release has not been considered).

For DX, as mentioned before, burst release presented significant differences ($p<0.0001$) (Figure 10A). For MSs, it seems to be a little slow down delivery phase between 21-28 days that it was not noticeable for hydrogels release. Taking into account delivery rates detailed in Figure 11, MSs/hydrogels hybrid systems experienced a higher release from day 7 to day 21, followed by a slow fashion delivery that was not as different compared to MSs and the last slower step of the release was similar for all the formulations.

For UDCA delivery, all formulations followed a well-noticeable triphasic behaviour. After the initial release in the first 24h (Figure 10B), UDCA was delivered in a slow manner followed by a fast step between day 28 and 42, to finally being delivered gradually until the end of the release. It is worth mentioning that the effect of the presence of hydrogel in the UDCA release from the hybrid formulations is only manifested in the rapid release steps, that is the initial burst and the release during the 28-42 days regardless of the hydrogel used. (Figure 11).

Table 3. f_2 values calculated for the different formulations for DX, UDCA, GDNF, and DXP. In bold, the f_2 values < 50, meaning that no similarities in the release were found.

Formulations	**f_2**			
	DX	**UDCA**	**GDNF**	**DXP**
MSs vs PPP+MSs	**45.01**	68.36	**9.68**	-
MSs vs PPP+DXP+MSs	51.61	66.88	**9.58**	-
MSs vs PPP+DXP+MSs Mannitol buffer	50.89	67.06	**10.43**	-
PPP+MSs vs PPP+DXP + MSs	65.03	82.03	94.55	-
PPP+MSs vs PPP+DXP+MSs Mannitol buffer	54.58	90.49	79.35	-
PPP+DXP+MSs vs PPP+DXP+MSs Mannitol buffer	68.38	86.69	77.24	60.42

On the contrary, the combination of MSs with hydrogels was much more evident for GDNF release in comparison to the protein release from the microspheres not included in hydrogels. As Figure 12 shows, GDNF release from MSs alone presented a high burst release (7218.18 ± 898.5 pg GDNF/mg MSs at 24 hours) that was controlled with the hydrogel in the different hydrogel/MSs hybrid formulations (45.45 ± 8.98 pg GDNF/mg MSs for PPP+MSs, 41.85 ± 20.93 pg GDNF/mg MSs for PPP+DXP+MSs and 35.45 ± 20.30 pg GDNF/mg MSs for PPP+DXP+MSs in mannitol buffer) ($p<0.0001$). None of the hydrogel formulations equalled the amount of GDNF delivered to the amount delivered from MSs through the time of the release study. GDNF release from all hydrogel/MSs hybrid formulations showed similar profile, suggesting that the incorporation of DXP or the changes in the buffer did not affect GDNF delivery ($f_2>50$). Moreover, while MSs showed 4 different release rates divided as follows: 14-42, 42-70, 70-126, and 126-168 days, in the hybrid systems the two first steps were compiled in a single one (from day 1 to 70). After day 70 no differences in release rate were observed in presence or in absence of any of the tested hydrogel in the formulations.

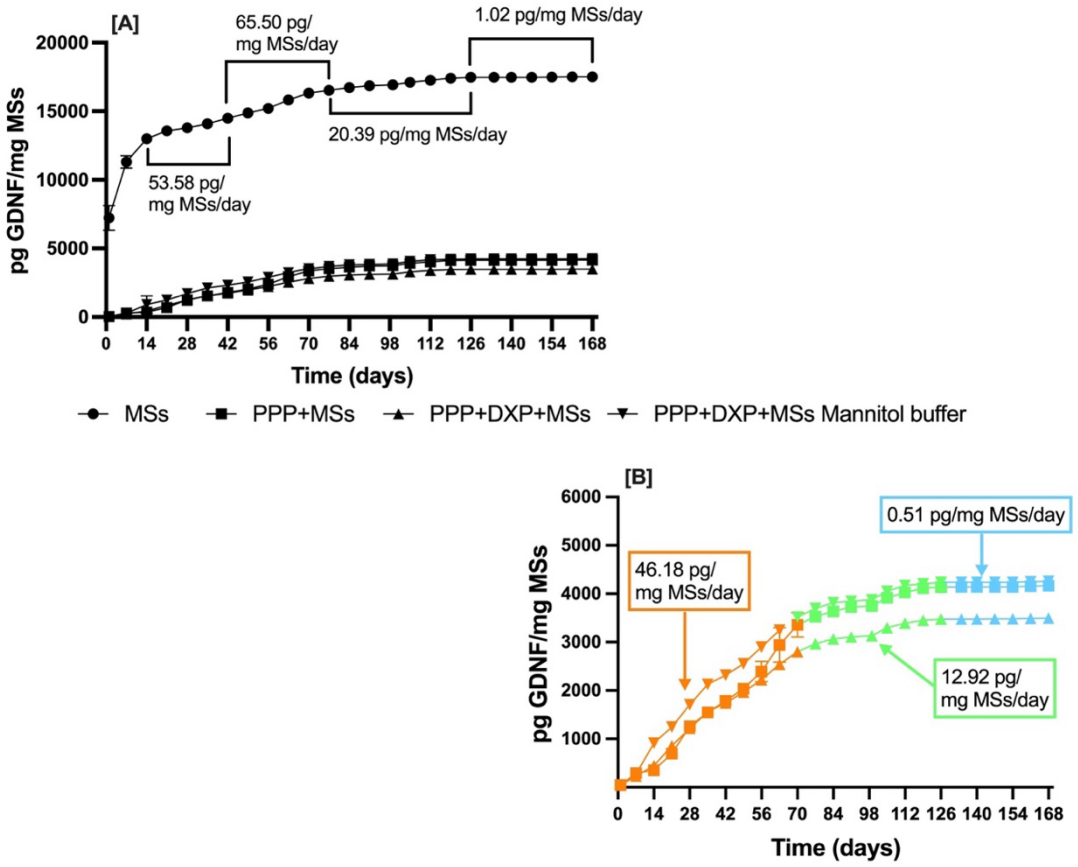

Figure 12. GDNF release profiles from MSs (circles), MSs included in: PPP blank hydrogel dissolved in trehalose (squares), in DXP-loaded PPP hydrogel dissolved in trehalose (triangle), and in DXP-loaded PPP hydrogel dissolved in mannitol buffer (reverse triangle). A more detailed picture of hydrogel formulations was added above [B]. GDNF release rates have been added in the different figures (for GDNF release from MSs, delivery in the first 7 days has not been considered).

Concerning the DXP delivery, the change in the buffer did not affect it according to f_2 values (Table 3). For both cases, hydrogels presented a fast initial release of DXP until day 7 (5.31 µg DXP/day for trehalose buffer and 4.04 µg DXP/day for mannitol buffer), followed by a sustained release until day 21 (0.61 µg DXP/day for trehalose buffer and 0.47 µg DXP/day for mannitol buffer), when they finished its delivery (Figure 13). Moreover, the DXP release profile from hydrogel free from microspheres presented the same profiles as the ones incorporating them.

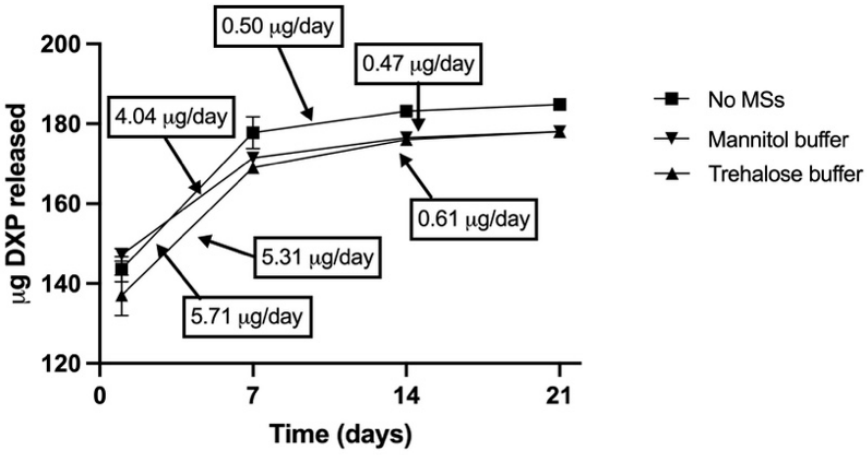

Figure 13. DXP release profiles and release rates from the different loaded hydrogels incorporating or not incorporating MSs. Triangles are for hydrogel dissolved in trehalose incorporating MSs, inverted triangles for the hydrogel dissolved in mannitol incorporating MSs and squares for hydrogel dissolved in trehalose without incorporating MSs.

DX, UDCA and GDNF releases were fitted in the Gallagher-Corrigan kinetic model with Gorrasi adjustments. This model describes the drug release by two different stages. The first stage is related with the "non-bounded" drug release, whereas the second stage considers the delivery as a result of the "matrix erosion", being the drug delivered while the polymer is degraded, and the matrix eroded. Table 4 summarizes the different kinetic parameters as well as $R^2_{adjusted}$. This last one was above 0.990 in all the cases.

According to the data obtained from the model used, it can be seen that the combination of microspheres with hydrogels mainly involves a modification of the release of the different active compounds during the burst release (b parameter). However, for DX and UDCA, the Y_1 parameter – which is the relative amount of drug release in the first mechanism – is higher in the hybrid formulations than microspheres not included in hydrogels, indicating that although the burst is controlled, the release in this step is higher up to be equaled as the one of naked MSs in the first phase, in line with the above-mentioned results. The control of this first step was more marked in the GDNF release, where B parameter is almost inexistent for hydrogel/MSs hybrid systems, suggesting that Gorrasi adjustment (that includes parameter B in Gallagher-Corrigan equation) is indeed no necessary since the burst release is no significant. However, in this case, the delivery is still slower in the hybrid systems.

Table 4. Value of the different parameters after being fitted in Gallagher-Corrigan kinetic model.

Samples	B	Y_1(-)	K_1 (day^{-1})	Y_2(-)	K_2 (day^{-1})	T_2 (day)	$R^2_{adjusted}$
UDCA release							
MSs	0.106	0.055	0.669	0.818	0.222	31.42	0.996
PPP+MSs	0.028	0.102	0.432	0.899	0.211	32.41	0.993
PPP+DXP+MSs	0.059	0.123	0.119	0.975	0.264	34.21	0.994
PPP+M+DXP+MSs	0.043	0.100	0.341	0.933	0.230	33.32	0.992
DX release							
MSs	0.173	0.633	0.080	0.246	0.151	44.22	0.999
PPP+MSs	0.024	0.860	0.049	0.235	0.133	44.15	0.999
PPP+DXP+MSs	0.040	0.828	0.059	0.244	0.121	43.91	0.999
PPP+M+DXP+MSs	0.026	0.955	0.052	0.210	0.110	43.67	0.999
GDNF release							
MSs	0.303	0.385	0.187	0.237	0.054	54.89	0.999
PPP+MSs	1.97e-6	0.107	0.020	0.114	0.082	53.53	0.995
PPP+DXP+MSs	2.40e-14	0.129	0.017	0.070	0.071	50.95	0.996
PPP+M+DXP+MSs	4.84e-8	0.174	0.023	0.057	0.085	53.99	0.996

3.3.10. Tolerance studies.

Cell viability of the hybrid systems and MSs suspended in NaCl were tested. As Figure 14 shows, all the formulations presented viability above 90% and no significant differences were found among formulations nor formulations vs positive control (0.9% NaCl).

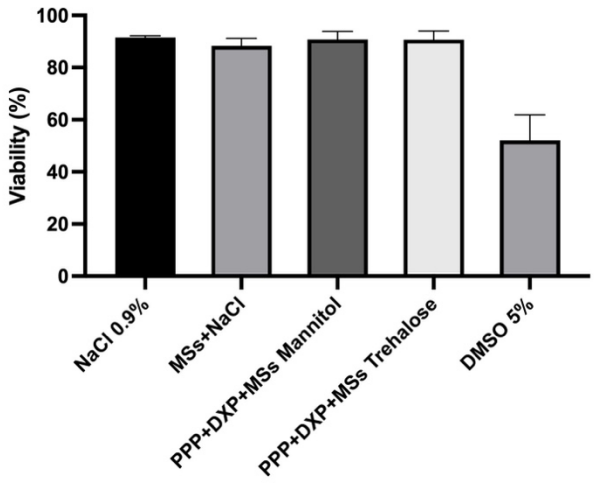

Figure 14. Cell viability (%) of the different formulations. As a positive control of viability NaCl (0.9 % w/v) was employed and as negative control DMSO (5% w/v).

3.3.11. Preliminary studies of microspheres aggregation

As can be seen in Figure 15, the wells containing the hybrid systems showed the aggregation of microspheres upon injected, in contrast to the well containing microspheres suspended in NaCl where it could not be seen any aggregation. In addition, microspheres suspended in hydrogels presented less adhesion in the vials than when NaCl was used as vehicle (Figure 16).

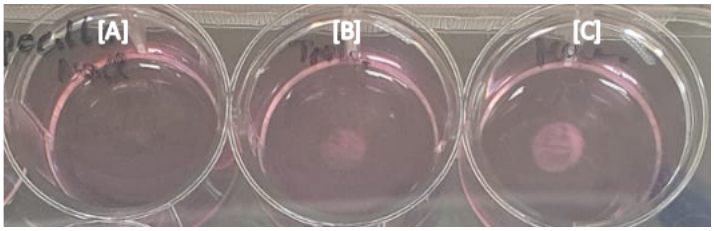

Figure 15. Preliminary studies of microspheres aggregation. [A] Microspheres suspended in NaCl. [B] and [C] Microspheres suspended in PPP hydrogels dissolved in trehalose and in mannitol, respectively.

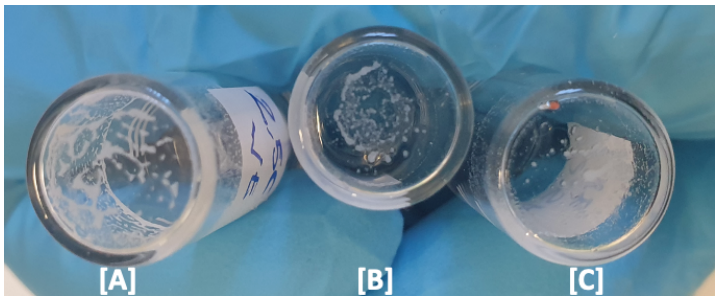

Figure 16. Microspheres adhesion in the vials after injection. [A] was microspheres suspended in NaCl (0.9 % w/v), [B] and [C] were microspheres suspended in PPP hydrogels dissolved in trehalose and mannitol.

4. Discussion

PLGA microparticles are useful platforms for drug delivery where different parameters can be changed to control the release of the encapsulated drugs (such as polymer type and composition, particle size, porosity, etc). The multi-loaded microspheres used in this work have been optimized in previous studies in order to achieve a suitable loading of each one of the compounds and their subsequent simultaneous controlled release. To our knowledge, when this tri-delivery platform was developed, it was the first tri-delivery that was composed of two low molecular weight substances and a protein. It is interesting to remark that at least 50% of the initial amounts of each one of the components have been successfully encapsulated. Although PLGA microspheres can control the release of the loaded active compounds for long periods, it exits a principal drawback: the initial burst release of many drugs – a significant amount of drugs is released in the short period of time that follows the injection. This phenomenon can be undesirable not only because it could shorten the overall duration of the drug's therapeutic effect, but also because it may cause toxicity effects if its extent is excessive [25]. To solve this challenge, in this work we have developed a hybrid system in which a thermo-responsive PLGA-PEG-PLGA hydrogel has been used as vehicle. Also, the aggregation of the microcarriers after their administration results in a clinical advantage. As previously described, several days after injection, microspheres tend to aggregate behaving like an implant [26]. The inclusion of the microspheres in a hydrogel could facilitate their aggregation at the site of injection, and at the same time, improve their administration. Usually, microspheres are suspended in phosphate buffer or saline salt solution, therefore, special care has to be taken in order to prepare a homogenous suspension and usually an amount of them left adhered to the syringes after injection. The use of other vehicles more viscous have been pointed out as a strategy to avoid it [26,27]. Other authors have already explored this idea by combining different drug delivery systems in hydrogels to form a hybrid system to try to reduce the aforementioned burst release [12,28,29]. In this work we have decided to load also the hydrogel with an anti-inflammatory agent, since inflammation is the most frequent clinical sign described after intravitreal injection of PLGA MSs [26]. Moreover, corticoids could be beneficial for neuroprotection treatment since they can

modulate microglial activity because of its anti-inflammatory and immunosuppressive activities, they can modulate the neurotoxicity substances production by the microglia and the rate of phagocytosis of apoptotic neurons [30].

Rheological properties on the MSs/hydrogel hybrid systems showed a sol behaviour between 20-27°C making it ideal to be injected, and a maximum gel point between 31-34 °C. However, injectability assays showed that although at 37°C hydrogels were in a gel state, they could be injected through 21 and 25G needles. Tube inverting test also showed the sol behaviour until 32°C for hydrogels including microspheres and 33°C for hydrogels alone. The gelation process in this kind of platform is due to micelle aggregation. When the temperature rises, the PEG chains dehydrate, causing micelles shrinkage and enhancing PLGA-PEG interactions. With higher temperatures, micelles eventually precipitate, and the system is separated into two phases (water and polymer) [23,31]. The inclusion of microspheres could likely participate in the micelle network and produce this earlier behaviour. However, it did not affect the precipitation temperature. Swelling studies demonstrated that the inclusion of microspheres in the hydrogels did neither affect their water uptake.

Both assayed hydrogels (using trehalose or mannitol) showed an abrupt initial degradation that was more marked in the mannitol hydrogel. That could be explained by the mannitol nature to dissolve water-insoluble substances. In fact, other authors had already reported the ability of mannitol to improve the solubility and dissolution of poorly water-soluble molecules [32], being in this case, PLGA-PEG-PLGA hydrogels. This behaviour coincides in the first 3-4 weeks when the hydrogel is capable to release DXP, so it is plausible that after that time no trehalose nor mannitol remains, although further studies are required. However, it did not show any difference in the release of actives from hydrogels prepared with trehalose or with mannitol.

In vitro release data were successfully fitted in Gallagher-Corrigan kinetic model. This model describes sigmoidal release shapes as occurred in PLGA microspheres. *In vitro* release studies showed significant differences in burst release in hydrogels/MSs hybrid systems than MSs alone that was confirmed also by the kinetic model. It can be hypothesised that when the MSs are included in a hydrogel, the initial drugs release is retained in some extent in the hydrogel net, conferring, maybe, a role of protection.

These results are in accordance with previous studies where microspheres were included in PLGA-PEG-PLGA hydrogels [33,34]. After this initial step, hydrogel could retain the drugs inside its structure for a while but after that, spread them to the aqueous media while hydrogel degradation and swelling occur (Figure 15). That could be seen in DXP (included in the hydrogel and not encapsulated in the microspheres) release profiles. In these studies, after an initial fast release rate, the hydrogel could deliver DXP slowly from day 7 to day 21.

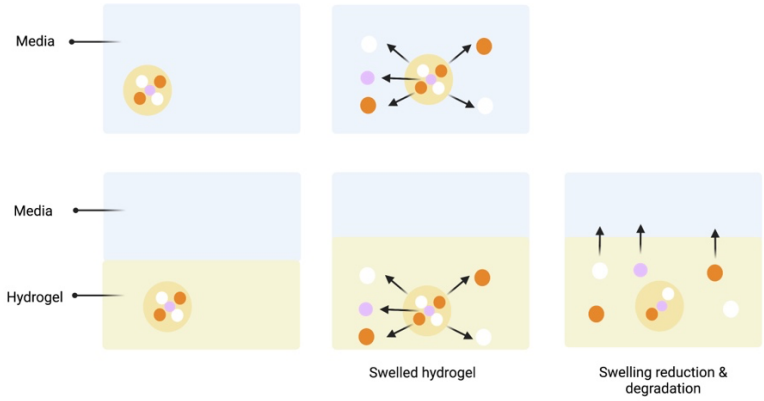

Figure 17. Microspheres and hybrid systems release hypothesis.

All the hybrid formulations tested, and the microspheres suspended in NaCl 0.9% presented optimal retinal cell tolerance results, not showing differences among them but with the negative control ($p<0.0001$).

5. Conclusions

In the present work, it has been developed a hybrid system composed of a combination of a biodegradable microspheres loaded with three neuroprotective compounds with a biodegradable thermo-responsive hydrogel loaded with an anti-inflammatory agent. The combination of microspheres and hydrogels seemed not to change the hydrogel properties and helped to control the *in vitro* burst-released characteristic of microspheres. This formulation demonstrated well retinal cell tolerance as well as good injectability properties. This hybrid system could entail a new strategy for sustained neuroprotective treatment for ophthalmic neurodegenerative diseases.

Acknowledgments

This work was supported by Grant MAT2017-83858-C2-1 funded by MCIN/AEI/ 10.13039/501100011033 and by "ERDF A way of making Europe" and Grant PID2020-113281RB-C21 funded by MCIN/AEI/ 10.13039/501100011033. Research Group UCM 920415 (InnOftal) and ISCIII-FEDER "Una manera de hacer Europa" RETICS (OFTARED) (RD16/0008/0009). A.A.N thanks for the grant PRE2018-083951 funded by MCIN/AEI/10.13039/501100011033 and by "ESF Investing in your future".

They also would like to thank the technical SEM and TEM assistance of the Centro de Microscopía Electrónica Luis Bru (CAI) and the access to the cryoEM CNB-CSIC facility in the context of the CRIOMECORR project (ESFRI-2019-01-CSIC-16), and in particular the help of Rocío Arranz, Noelia Zamarreño y M. Teresa Bueno-Carrasco.

6. References

[1] Madeira MH, Boia R, Santos PF, et al. Contribution of Microglia-Mediated Neuroinflammation to Retinal Degenerative Diseases. Mediators Inflamm [Internet]. 2015 [cited 2022 Sep 23];2015. Available from: /pmc/articles/PMC4385698/.

[2] He S, Stankowska DL, Ellis DZ, et al. Targets of Neuroprotection in Glaucoma. Journal of Ocular Pharmacology and Therapeutics. 2018;34:85.

[3] Jutley G, Luk SM, Dehabadi MH, et al. Management of glaucoma as a neurodegenerative disease. http://dx.doi.org/102217/nmt-2017-0004. 2017;7:157–172.

[4] Khatib TZ, Martin KR. Neuroprotection in Glaucoma: Towards Clinical Trials and Precision Medicine. https://doi.org/101080/0271368320191663385. 2019;45:327–338.

[5] Yadav KS, Rajpurohit R, Sharma S. Glaucoma: Current treatment and impact of advanced drug delivery systems. Life Sci. 2019;221:362–376.

[6] Cao Y, Samy KE, Bernards DA, et al. Recent advances in intraocular sustained-release drug delivery devices. Drug Discov Today. 2019;24:1694–1700.

[7] Bravo-Osuna I, Andrés-Guerrero V, Pastoriza Abal P, et al. Pharmaceutical microscale and nanoscale approaches for efficient treatment of ocular diseases. Drug Deliv Transl Res. 2016.

[8] de HOZ R, ROJAS B, RAMíREZ A, et al. Assessment of polyesteramide of PEA Microparticles for in vivo intraocular injections. Acta Ophthalmol. 2013;

[9] Herrero-Vanrell R, Bravo-Osuna I, Andrés-Guerrero V, et al. The potential of using biodegradable microspheres in retinal diseases and other intraocular pathologies. Prog Retin Eye Res. 2014.

[10] López-Cano JJ, Sigen A, Andrés-Guerrero V, et al. Thermo-responsive PLGA-PEG-PLGA hydrogels as novel injectable platforms for neuroprotective combined therapies in the treatment of retinal degenerative diseases. Pharmaceutics. 2021;13.

[11] Duvvuri S, Janoria KG, Mitra AK. Development of a novel formulation containing poly(D,L-lactide-co-glycolide) microspheres dispersed in PLGA-PEG-PLGA gel for sustained delivery of ganciclovir. Journal of Controlled Release. 2005;108.

[12] Duvvuri S, Janoria KG, Pal D, et al. Controlled delivery of ganciclovir to the retina with drug-loaded poly(D,L-lactide-co-glycolide) (PLGA) microspheres dispersed in PLGA-PEG-PLGA gel: A novel intravitreal delivery system for the treatment of cytomegalovirus retinitis. Journal of Ocular Pharmacology and Therapeutics. 2007;23.

[13] Daruich A, Picard E, Boatright JH, et al. Review: The bile acids urso- and tauroursodeoxycholic acid as neuroprotective therapies in retinal disease. Mol Vis. 2019;25.

[14] Daruich A, Jaworski T, Henry H, et al. Oral Ursodeoxycholic Acid Crosses the Blood Retinal Barrier in Patients with Retinal Detachment and Protects Against Retinal Degeneration in an Ex Vivo Model. Neurotherapeutics. 2021;

[15] Checa-Casalengua P, Jiang C, Bravo-Osuna I, et al. Retinal ganglion cells survival in a glaucoma model by GDNF/Vit e PLGA microspheres prepared according to a novel microencapsulation procedure. Journal of Controlled Release. 2011;

[16] Pontremoli C, Boffito M, Fiorilli S, et al. Hybrid injectable platforms for the in situ delivery of therapeutic ions from mesoporous glasses. Chemical Engineering Journal. 2018;340:103–113.

[17] Costa P, Sousa Lobo JM. Modeling and comparison of dissolution profiles. European Journal of Pharmaceutical Sciences. 2001;13:123–133.

[18] Gallagher KM, Corrigan OI. Mechanistic aspects of the release of levamisole hydrochloride from biodegradable polymers. J Control Release. 2000;69:261–272.

[19] Gorrasi G, Attanasio G, Izzo L, et al. Controlled release mechanisms of sodium benzoate from a biodegradable polymer and halloysite nanotube composite. Polym Int. 2017;66:690–698.

[20] Chung DM, Kim JH, Kim JK. Evaluation of MTT and Trypan Blue assays for radiation-induced cell viability test in HepG2 cells. Iranian Journal of Radiation Research. 2015;13:331–335.

[21] Jeong B, Bae YH, Kim SW. Drug release from biodegradable injectable thermosensitive hydrogel of PEG-PLGA-PEG triblock copolymers. Journal of Controlled Release. 2000;63.

[22] Yu L, Zhang Z, Zhang H, et al. Mixing a sol and a precipitate of block copolymers with different block ratios leads to an injectable hydrogel. Biomacromolecules. 2009;10:1547–1553.

[23] El-Zaafarany GM, Soliman ME, Mansour S, et al. A Tailored Thermosensitive PLGA-PEG-PLGA/Emulsomes Composite for Enhanced Oxcarbazepine Brain Delivery via the Nasal Route. Pharmaceutics. 2018;10.

[24] Yu L, Zhang Z, Ding J. Influence of la and GA sequence in the PLGA block on the properties of thermogelling PLGA-PEG-PLGA block copolymers. Biomacromolecules. 2011;12:1290–1297.
[25] Yoo J, Won YY. Phenomenology of the Initial Burst Release of Drugs from PLGA Microparticles. ACS Biomater Sci Eng. 2020;6:6053–6062.
[26] Herrero-Vanrell R, Bravo-Osuna I, Andrés-Guerrero V, et al. The potential of using biodegradable microspheres in retinal diseases and other intraocular pathologies. Prog Retin Eye Res. 2014.
[27] Herrero-Vanrell R, Refojo MF. Biodegradable microspheres for vitreoretinal drug delivery. Adv Drug Deliv Rev. 2001.
[28] Rong X, Ji Y, Zhu X, et al. Neuroprotective effect of insulin-loaded chitosan nanoparticles/PLGA-PEG-PLGA hydrogel on diabetic retinopathy in rats. Int J Nanomedicine. 2018;14:45–55.
[29] Cao D, Zhang X, Akabar MD, et al. Liposomal doxorubicin loaded PLGA-PEG-PLGA based thermogel for sustained local drug delivery for the treatment of breast cancer. https://doi.org/101080/2169140120181548470. 2019;47:181–191.
[30] Arranz-Romera A, Davis BM, Bravo-Osuna I, et al. Simultaneous co-delivery of neuroprotective drugs from multi-loaded PLGA microspheres for the treatment of glaucoma. Journal of Controlled Release. 2019;
[31] Nguyen MK, Lee DS. Injectable Biodegradable Hydrogels. Macromol Biosci. 2010;10:563–579.
[32] Madgulkar A, Bandivadekar M, Shid T, et al. Sugars as solid dispersion carrier to improve solubility and dissolution of the BCS class II drug: clotrimazole. http://dx.doi.org/103109/0363904520151024683. 2015;42:28–38.
[33] Zhao J, Guo B, Ma PX. Injectable alginate microsphere/PLGA–PEG–PLGA composite hydrogels for sustained drug release. RSC Adv. 2014;4:17736–17742.
[34] Wang P, Zhuo X, Chu W, et al. Exenatide-loaded microsphere/thermosensitive hydrogel long-acting delivery system with high drug bioactivity. Int J Pharm. 2017;528:62–75.

DISCUSIÓN GENERAL

La presente tesis se basa en dos objetivos principales: el primero de ellos es la elaboración de microesferas biodegradables co-cargadas para el desarrollo de un modelo animal de glaucoma crónico y el segundo, el desarrollo de varias plataformas neuroprotectoras de liberación sostenida (microesferas, hidrogeles y la inclusión de microesferas en hidrogeles para formar un sistema híbrido) cargados con varios principios activos neuroprotectores para el tratamiento del glaucoma. En ambos casos, se ha procedido a la encapsulación, en dichos sistemas de liberación controlada, de varias sustancias activas, y además se ha mostrado una nueva aplicación de los mismos, ya que aparte de su aplicación convencional para tratar enfermedades, se han utilizado para el desarrollo de un modelo animal de daño.

El glaucoma se caracteriza por ser una enfermedad neurodegenerativa, crónica y multifactorial que finalmente conlleva a la pérdida irreversible de la visión. Tiene una alta prevalencia, siendo de alrededor del 3,5% en las personas cuya edad se sitúa entre los 40 y 80 años, pero se estima que el número de personas afectadas siga aumentando conforme lo hace el envejecimiento de la población. Aunque el glaucoma ha sido estudiado ampliamente, puesto que se trata de una enfermedad multifactorial, su patogénesis no ha sido complemente dilucidada (18). El principal factor de riesgo modificable es el aumento de la presión intraocular (PIO) y, por tanto, la mayoría de los tratamientos se centran en el descenso y control de la misma. Sin embargo, existen pacientes que cursan con valores considerados normales de la PIO pero que desarrollan glaucoma conocido como “glaucoma normotensivo”, y es, en estos casos, el tratamiento un reto desafiante (226). Por ello, resulta de gran interés terapéutico la neuroprotección.

El desarrollo de modelos animales crónicos de esta enfermedad, que simulen las condiciones humanas, resulta de gran utilidad para la comprensión más profunda de su fisiopatología y de los mecanismos involucrados. Así mismo, el desarrollo de estos modelos animales permitiría la evaluación adecuada de la eficacia tanto de nuevos principios activos neuroprotectores, como de nuevas formulaciones, especialmente de sistemas de liberación modificada (227).

Existen numerosos modelos animales de los que se ha hablado anteriormente en la introducción de esta tesis doctoral. Estos se pueden dividir en modelos dependientes o

no dependientes de la PIO. El mecanismo por el cual se produce el daño en la retina es diverso y puede ir desde el bloqueo de la evacuación del humor acuoso o el daño directo en el nervio óptico, pasando por modelos de edición genética (164).

Es importante destacar que para que un modelo animal sea ideal tiene que cumplir los siguientes requisitos: fácil de realizar, ser reproducible, con efectos secundarios mínimos, plausible biológicamente, predecible de principio a fin y, además, que imite las condiciones fisiopatológicas del ojo humano (165). A todo esto, hay que añadir que el desarrollo del modelo permita cumplir la regla de las 3Rs (228).

Por tanto, el **capítulo I** recogido en esta tesis doctoral, titulado "**Mimicking chronic glaucoma over 6 months with a single intracameral injection of dexamethasone/fibronectin-loaded PLGA microspheres**", presenta el desarrollo de un modelo murino de glaucoma crónico mediante la inducción de un daño físico combinado con un daño farmacológico. Este trabajo surge como continuación de anteriores trabajos que ha realizado nuestro grupo de investigación en colaboración con el Grupo de Investigación e Innovación Miguel Servet Oftalmología (GIMSO) en el Centro de Investigación Biomédica de Aragón (CIBA), bajo la supervisión de los Dres. María Jesús Rodrigo, Elena García Martín y Luis E. Pablo. En un primer trabajo se procedió a la comparación del efecto hipertensor que tiene la inyección en cámara anterior de microesferas blanco de PLGA de dos tamaños distintos (38-20 µm y 20-10 µm) con la inyección epiescleral de una solución hipertónica de cloruro sódico 1,8 M, teniendo este estudio, una duración total de 8 semanas (176). Los resultados de este primer trabajo condujeron a un segundo en el que se administraron también dichas microesferas blanco de PLGA, de ambas fracciones de tamaños, pero con una duración total de 6 meses, realizándose un total de 7 intervenciones (177). Se seleccionaron las microesferas de tamaño 20-10 µm como las más idóneas para conseguir el efecto deseado. Con el fin de conseguir un modelo animal con una neurodegeneración más lenta y con una disminución del número de intervenciones se desarrollaron microesferas de PLGA cargadas con dexametasona del tamaño previamente seleccionado (20-10 µm) con el objetivo de producir un daño físico y farmacológico (178). Gracias a esta estrategia se consiguió disminuir en número de intervenciones (2 inyecciones en lugar de 7). Siguiendo la línea de estos trabajos, el siguiente paso ha sido el desarrollo de

microesferas cargadas con dos agentes activos (dexametasona y fibronectina) con la reducción de las intervenciones, pasando a 1 intervención con estas microesferas co-cargadas. Este trabajo, como se ha mencionado anteriormente, es el que aparece recogido en esta tesis como capítulo I. El desarrollo de los distintos modelos animales han sido objeto de una patente internacional (ver Anexo I).

Este modelo se basa en el daño físico que produce la inyección de microesferas de PLGA en la cámara anterior junto con el daño farmacológico que provocan la dexametasona y la fibronectina liberadas a partir de las mismas, produciendo esta combinación un aumento progresivo de la PIO y una neurodegeneración progresiva con una reducción del número de intervenciones. Es bien sabido que el uso continuado de corticoides produce una reducción de la salida del humor acuoso debido a modificaciones en la malla trabecular (168,191,229). Por otro lado, en cuanto a la fibronectina, se ha estudiado que su sobreexpresión está relacionada con el envejecimiento ocular y con la progresión del glaucoma, ya que su deposición en la malla trabecular produciría la oclusión de ésta en el glaucoma humano (230–232). Para la inclusión de estos dos principios activos en las microesferas se procedió a su encapsulación por el método de extracción-evaporación del solvente a partir de una doble emulsión ($A_1/O/A_2$), en la que los principios activos fueron incorporados en la fase de la emulsión en la que eran más solubles. A pesar de que hay numerosos trabajos en los que se utiliza una doble emulsión para la elaboración de microesferas, las publicaciones donde se propone la encapsulación de dos principios activos incorporándose cada uno de ellos en una fase distinta, no son muy numerosas (233–237). La co-microencapsulación de dos agentes de naturaleza tan distinta, junto con la obtención de una liberación sostenida en el tiempo de ambos principios activos, supuso un reto desde el punto de vista tecnológico. La utilización del método de microencapsulación que supone la formación de una doble emulsión ($A_1/O/A_2$) permitió la obtención de microesferas porosas que permitieran una liberación de la proteína relativamente rápida, gracias a la presencia de poros, tanto en la superficie de la microesfera como en su interior, que se produce al incorporar la fase acuosa interna en su elaboración (238,239). Las microesferas resultantes de este desarrollo tuvieron una distribución unimodal con un tamaño medio de partícula dentro del rango deseado de

20-10 µm y una encapsulación de dexametasona del 71,94 ± 2,40 µg dexametasona/mg MSs, lo que supone un 79,13 ± 2,64 % de la cantidad inicial. Desafortunadamente, la labilidad de la fibronectina hizo imposible su cuantificación tras extracción líquido-líquido de la matriz polimérica. La microscopía electrónica, tanto de barrido como de transmisión, confirmó la presencia de poros en la superficie y en el interior de las microesferas, característicos, como se ha comentado, de los sistemas microparticulares preparados por la técnica de doble emulsión.

La liberación de ambos principios activos mostró un perfil multifásico, típico de las microesferas de PLGA (152), donde se observó una liberación inicial muy rápida seguido de una alternancia entre liberaciones más lentas y rápidas. En el caso de la fibronectina, esta presentó una liberación inicial durante los primeros 10 días de 35,90 ng/mg MSs, seguida de distintas fases cuyas velocidades de liberación fueron variando hasta finalizar el estudio (168 días). En cuanto a la liberación de dexametasona, se experimentaron también varias fases de liberación, comenzando con una liberación de 53,42 µg/mg MSs en los primeros 10 días. A continuación, se fueron alternando fases de liberaciones lentas y rápidas hasta el día 77, a partir del cual no se liberó más dexametasona.

La inducción del modelo animal se llevó a cabo con la realización de una única inyección de las microesferas anteriormente desarrolladas en la cámara anterior del ojo derecho de ratas Long-Evans de 4 semanas de edad con unos pesos de entre 50 y 100 gramos y tomando como ojo control el ojo contralateral. Se obtuvo un incremento de la PIO gradual siendo superior en los ojos a los que se les inyectó microesferas hasta la semana 6, a partir de la cual, los valores de ambos ojos fueron similares hasta el final del estudio en la semana 24. Al principio de la inducción del modelo, se apreció un ligero aumento de la PIO que coincide con el bloqueo físico producido por la deposición de las microesferas en el ángulo iridocorneal (confirmado por inmunohistoquímica) y con el daño farmacológico que produce la primera liberación, tanto de dexametasona como de fibronectina. A continuación, el incremento observado fue más lento y sostenido coincidiendo con las liberaciones más mantenidas de ambos agentes.

De forma paralela se evaluó también la respuesta a corticoesteroides. Esta respuesta varía entre los pacientes y los modelos animales. En humanos, los pacientes se dividen en tres grupos en función de su respuesta: no respondedores (un incremento de menos

de 6 mmHg), pacientes con una respuesta moderada que suponen un 30-40% de los casos (el incremento se sitúa entre 6-15 mmHg) y altos respondedores, el 4-6%, (cuyo incremento supera los 15 mmHg) (178,240). Sin embargo, en los animales la respuesta cambia según la especie. En el caso de las ratas, la respuesta a corticosteroides se sitúa en un 80% (241), valores similares a los que se observan en este trabajo, siendo la mayoría de los animales respondedores medios.

El examen neurorretiniano a las 24 semanas del estudio por ERG mostró una disminución de la funcionalidad de células bipolares y fotorreceptores en ambos ojos. En cuanto a las células ganglionares, los ojos inyectados mostraron un número menor de células funcionales. Respecto a la OCT, se observó un descenso de todas las capas retinianas sin diferencias significativas entre ambos ojos en la mayoría en los sectores estudiados. Estos hallazgos sugieren una neurodegeneración bilateral.

La afectación bilateral debida a la inducción unilateral de hipertensión ocular no es algo nuevo y ha sido observado en distintos modelos animales (177,178,242,243). Este hallazgo está siendo estudiado por distintos autores y se están dando al respecto diversas explicaciones. Una de ellas sería debida a que la activación de la glía en los ojos glaucomatosos liberaría compuestos que podrían activar la glía del ojo contralateral por vía retrógrada (196). Otra hipótesis sería la activación del sistema inmune. En este caso, en los ojos hipertensos, el deterioro de la barrera hematorretiniana podría desencadenar una respuesta inmune que produciría una activación temprana de la microglía del ojo contralateral (243). También en esa activación de la microglía del ojo contralateral, podrían estar involucrados los linfocitos T (244,245). Además, otra hipótesis sería la implicación de procesos inflamatorios que producirían la liberación de citoquinas proinflamatorias a la circulación, y por respuesta autoinmune sistémica propagarían el daño (246) o por la proyección de las fibras de las células ganglionares retinianas (242). Esta afectación del ojo contralateral se ha visto incluso en modelos en los que el incremento de la PIO se ha producido de forma lenta y gradual (177,178). De hecho, en un trabajo en el que se inyectaron nanopartículas cargadas con dexametasona por vía subconjuntival y periocular se observó también una elevación de la PIO en el ojo contralateral. En este trabajo, los autores atribuyeron el efecto a una posible comunicación linfática o venosa entre ambos ojos. (194) Otra hipótesis podría ser la

acumulación periocular en el tejido adiposo al liberarse de forma lenta la dexametasona o una comunicación vascular que produciría una distribución del principio activo en el ojo contralateral (178,247). Sin embargo, al igual que en nuestro trabajo, no se han cuantificado la cantidad de principios activos en el ojo contralateral. Independientemente de las distintas hipótesis, lo que no cabe duda es que el ojo contralateral se ve afectado y se necesitan más estudios para aclarar cuáles son los mecanismos y vías implicados en su afectación. Así, estos resultados e hipótesis demuestran que el ojo contralateral no debería usarse como control, ya que está igualmente implicado en los procesos neurodegenerativos.

Estos hallazgos enlazan con el segundo objetivo de esta tesis y hace que cada vez cobre más importancia la neuroprotección en el tratamiento del glaucoma. El segundo objetivo principal es el desarrollo de terapias neuroprotectoras con una liberación sostenida y controlada de sus principios activos. Para su consecución, se puede dividir a su vez en tres objetivos que corresponderían a los distintos **capítulos (II, III y IV).** El capítulo II corresponde con el desarrollo y optimización de un sistema microparticular cargado con tres principios activos neuroprotectores con características adecuadas para una liberación controlada y sostenida. A continuación, el capítulo III propone el desarrollo y optimización de distintos hidrogeles para la liberación sostenida y controlada de sustancias antiinflamatorias. Finalmente, en el capítulo IV, estos dos sistemas convergerían ya que, una vez seleccionados, se desarrolla un sistema terapéutico híbrido formado por un hidrogel y un sistema microparticular tri-cargado para la liberación de sustancias neuroprotectoras.

El glaucoma se caracteriza por una muerte progresiva de las células ganglionares retinianas (RGCs) cuyos axones forman el nervio óptico. Se han descrito varios mecanismos fisiopatológicos que estarían involucrados en esta muerte neuronal. Se ha hipotetizado que la viabilidad de estas células depende de un balance entre estímulos positivos (supervivencia) y negativos (muerte) y un fracaso en dicho balance hacia los estímulos negativos, daría como resultado la muerte de dichas células (248). El principal factor de riesgo modificable es la elevación de la PIO, que se ha venido mencionando anteriormente, y que se produce por varios mecanismos, como puede ser un daño mecánico en las células ganglionares y fibras nerviosas ópticas de la lámina cribosa o

daño isquémico por compresión de los vasos sanguíneos, entre otros (249). En la muerte de las RGCs también están relacionados otros desencadenantes como pueden ser: excitotoxicidad, descenso de factores de crecimiento neuronales, compresión axonal de la lámina cribosa, estrés oxidativo, despolarización de las mitocondrias, procesos inflamatorios… en los que puede estar implicada la elevación de la PIO, aunque no siempre (248,250).

Este estímulo dañino afectaría a un número reducido de células (daño primario) que al morir liberarían factores tóxicos (oxidantes, pro-apoptóticos, etc.) que serían los responsables de la llamada "segunda degeneración" o daño secundario, donde se produce la muerte de las neuronas adyacentes (251).

Actualmente, la principal estrategia terapéutica que se sigue para el tratamiento del glaucoma es la reducción de la PIO en aquellos casos en los que se encuentra elevada, pero existen casos en los que esta reducción no previene la neurodegeneración. Además, hay pacientes que padecen glaucoma y que cursan con valores normales de la PIO en los que se conoce como glaucoma normotensivo. Por estas razones, desde hace algunos años ha crecido el interés por las terapias neuroprotectoras. En el caso del glaucoma, el objetivo de la neuroprotección sería el "descenso o prevención de la muerte de las células ganglionares retinianas y sus axones, para que mantengan su función fisiológica" (252).

La patogénesis del glaucoma es multifactorial, abarcando diferentes y complejos mecanismos, por lo que su abordaje terapéutico neuroprotector requiere un enfoque multidiana. Por ello, el uso de terapias neuroprotectoras combinadas basadas en la potencial sinergia de principios activos con diferentes mecanismos de acción resulta interesante desde el punto de vista terapéutico (22). Sin embargo, hay que tener en cuenta que, el lugar de acción se encuentra en el segmento posterior y al tratarse de una enfermedad crónica requiere de múltiples inyecciones intravítreas para conseguir niveles terapéuticos mantenidos de los principios activos en el lugar de acción. Este hecho aparte de ser desagradable para el paciente y caro para el sistema sanitario, no está exento de efectos adversos, como pueden ser la aparición de cataratas, hemorragias retinianas o infecciones, entre otros. Una buena alternativa a las inyecciones frecuentes son los sistemas de liberación controlada intraoculares que

permiten la cesión sostenida durante largos periodos de tiempo de los principios activos encapsulados (118,253).

Teniendo todo esto en cuenta, en el **capítulo II, "Neuroprotective multi-approach strategy based on PLGA microspheres for the treatment of retinal neurodegenerative diseases"** se presenta el desarrollo y optimización de un sistema microparticular en el que se han encapsulado 3 principios activos distintos con actividades neuroprotectoras. Los principios activos encapsulados presentan propiedad antiinflamatoria (dexametasona – DX), antiapoptótica (ácido ursodesoxicólico – UDCA) y neurotrófica (factor neurotrófico derivado de la glía – GDNF). Todos ellos podrían ser de utilidad para evitar la muerte de las RGCs, ya que, como se ha mencionado anteriormente, entre los estímulos que favorecen su muerte se encuentran la inflamación, apoptosis o la privación de compuestos neurotróficos, entre otros (248,250).

La primera parte de este trabajo se centró en la optimización de la formulación cargada con DX y UDCA para, posteriormente, en un segundo paso, incluir la proteína. Esta formulación se elaboró a partir del método de extracción-evaporación del solvente a partir de una emulsión sólido/óleo/acuosa (S/O/A), en la que el compuesto de naturaleza proteica es encapsulado al estado sólido (90). La optimización de esta formulación se basó tanto en las eficacias de encapsulación como en la liberación controlada de sus componentes. Para su elaboración, se tomó como punto de partida el uso de diclorometano como disolvente orgánico de la emulsión. Sin embargo, dada la baja eficacia de encapsulación, especialmente del compuesto más hidrófilo (UDCA), se decidió la inclusión de distintas proporciones de etanol. La inclusión de etanol en la fase orgánica permitiría aumentar la encapsulación de los principios activos, ya que mejora la solubilización de estos, a la vez que produce una precipitación más rápida del polímero durante la maduración de las microesferas (254,255). Merece la pena mencionar que, además, el etanol es un disolvente orgánico de clase 3, y su empleo permitiría reducir el uso del disolvente de clase 2 (256). Es importante destacar que la inclusión de etanol no sólo mejoró la encapsulación del UDCA, sino que también la de la DX. El empleo de etanol en la elaboración de las microesferas ya se había estudiado anteriormente en nuestro grupo de investigación en un trabajo anterior en el que se encapsulaba otra sal biliar (el ácido tauroursodeoxicólico – TUDCA). En este trabajo se

vio que su encapsulación también se aumentaba al incorporar etanol en la fase orgánica, con resultados similares a los obtenidos en este trabajo, en cuanto a aumento de porcentaje de encapsulación de las sales biliares (>20-25%) (130).

Las proporciones de diclorometano:etanol estudiadas en este capítulo fueron 85:15, 80:20 y 75:25. Los estudios por DSC y las imágenes por SEM corroboraron la encapsulación y buena dispersión de ambos principios activos en las microesferas cuya proporción de disolventes era 80:20. El uso de disolventes con polímeros como el PLGA puede modificar su temperatura de transición vítrea (257). Sin embargo, el estudio de DSC no mostró ninguna modificación en este parámetro, con valores coincidentes con los descritos en la bibliografía (258), independientemente de la utilización de diclorometano o la mezcla diclorometano:etanol. Además, los estudios por difracción de rayos X confirmaron la incorporación de DX en las microesferas en estado cristalino en todas las proporciones estudiadas y el estado amorfo del PLGA. Para el UDCA, no se pudo determinar debido a que en las proporciones en las que se añade a las microesferas no se obtenía ninguna señal.

Cuando se microencapsula más de un compuesto en la misma matriz polimérica es posible que la presencia de un compuesto influya tanto en la encapsulación como en el perfil de liberación del otro. Para valorar si esto ocurre en los sistemas propuestos se evaluaron dos formulaciones (E y F) que presentaban la misma proporción de disolventes orgánicos y misma cantidad de UDCA (40 mg), pero distinta cantidad de DX (80 mg y 60 mg, respectivamente) en su elaboración. Ambas formulaciones no presentaron diferencias significativas en porcentaje de encapsulación de los dos principios activos, sin embargo, sí que se observó una liberación más rápida tanto para DX como para UDCA en la formulación que contenía más DX. Al tratarse de una formulación, cuya variación era la cantidad de DX, se puede establecer que las diferencias observadas se deben a la cantidad de principios activos incluidas dentro de las microesferas, demostrando que la microencapsulación de varios compuestos puede tener un papel importante en el control de su liberación.

Una vez optimizada la formulación, se procedió al segundo paso, la inclusión de la proteína en estado sólido dispersada en vitamina E. Su encapsulación no modificó las encapsulaciones de DX y UDCA, siendo según nuestro conocimiento, el primer sistema

cargado con tres principios activos distintos. Se obtuvieron unos valores de eficacias de encapsulación que superan el 50% de las cantidades iniciales para cada uno de los componentes. De acuerdo con los estudios realizados, la proteína se sitúo en las proximidades de la superficie de las microesferas, debido al desplazamiento de la proteína suspendida en la vitamina E que se produce al elaborar las microesferas mediante este método (90).

La liberación de los principios activos es uno de los parámetros más importantes en el desarrollo de sistemas de liberación controlada. En el caso de las microesferas de PLGA los perfiles de cesión suelen estar caracterizados por distintas fases de liberación. La proteína, al estar situada más cerca de la superficie de las microesferas, mostró una liberación inicial alta, del orden de 5 ng/mg MSs, en las primeras 24 horas. También se observaron diferencias entre las microesferas cargadas con un solo principio activo y la inclusión de dos o de tres en el mismo sistema. Así, la liberación inicial de DX y de UDCA es mucho menor con las formulaciones cargadas con un único agente que en la combinación. Este hecho confirma lo que se había mencionado anteriormente, cuando al aumentar la cantidad de uno de los principios activos, la liberación es mucho más rápida.

El estudio de liberación se completó con un estudio cinético en el que se emplearon distintos modelos para identificar qué mecanismo de liberación se produce. Sin embargo, el PLGA muestra un comportamiento multifásico, sugiriendo que más de un proceso está implicado en su liberación (152). Esto dificulta mucho más la búsqueda y el ajuste de un modelo matemático que explique correctamente lo que pasa en cada momento de la liberación. A este hecho se le une la liberación de más de un principio activo, lo que hace complicado encontrar bibliografía científica donde hayan quedado reflejados estos estudios anteriormente. Tras la evaluación de varios modelos cinéticos, como son las cinéticas de orden cero y uno, Korsmeyer-Peppas, Higuchi, Baker-Lonsdale o incluso Weibull, el modelo de Gallagher-Corrigan resultó ser el que mejor describía la liberación de las formulaciones desarrolladas. Este modelo describe liberaciones sigmoidales donde se produce una primera liberación que es la debida al principio activo “no unido” a la matriz polimérica y una segunda parte que se produciría por la erosión de esta matriz. Cuando se le añade el ajuste que propone Gorrasi a esta ecuación, que

tiene en cuenta el "*burst release*" o liberación rápida inicial, se obtiene un ajuste mucho más preciso y que coincide prácticamente con los resultados experimentales obtenidos (259,260).

Los estudios de degradación confirmaron las hipótesis establecidas gracias a la utilización del modelo matemático. Así, cuando el modelo proponía que la liberación estaba gobernada por procesos de erosión, es cuando las microesferas, observadas por SEM, se veían mucho más degradadas. La rápida disminución del peso molecular evaluada por GPC durante las primeras 4 semanas se corresponde con estudios de otros autores en los que se ven los mismos resultados, donde a partir de la semana 4 se llega a un peso molecular crítico de en torno a 10000 g/mol. En estos sistemas inicialmente las matrices no pierden su forma, aunque finalmente acaban por colapsar (128,238). Estas observaciones se han visto también en nuestro trabajo en la que las microesferas mantienen una conformación esferoide hasta las 4-6 semanas a partir de la cual matriz colapsa.

En el trabajo recogido en el **capítulo III, "Biodegradable Smart hydrogels: drug delivery platforms for the treatment of ophthalmic chronic diseases**", se desarrollan y evalúan dos tipos diferentes de hidrogeles para su aplicación en el tratamiento de enfermedades crónicas oculares. Parte de este capítulo se ha realizado en colaboración con el grupo del Dr. Wenxin Wang en Irlanda (UCD Charles Institute of Dermatology, Blafar Ltd).

Los hidrogeles como sistemas de liberación controlada son una plataforma bastante atractiva para su aplicación en terapia dirigida. La creciente atención hacia la medicina personalizada y de precisión ha incrementado la innovación en este tipo de formulaciones. Los biomateriales llamados "inteligentes" no son menos y, entre ellos, se encuentran los hidrogeles sensibles a estímulos ("*stimuli-responsive hydrogels*"), en los que un desencadenante externo como podría ser pH, temperatura o concentraciones de biomoléculas, entre otros, producen cambios en sus propiedades físicas y macroscópicas (132).

Los hidrogeles elaborados en este trabajo corresponden a dos tipos diferentes. En primer lugar, su naturaleza, ya que uno de ellos está compuesto de ácido hialurónico, un polímero natural, mientras que el otro tipo de hidrogel está formado por la unión de

PLGA y polietilenglicol (PEG), ambos polímeros sintéticos. Además, los mecanismos de gelificación también son distintos. El hidrogel formado por ácido hialurónico ha sido funcionalizado con distintos grupos químicos (grupos tiol – SH – y grupos aldehído – CHO) para que las moléculas pudieran interaccionar entre ellas, en una reacción de "*crosslinking*" o reticulación, siempre y cuando, ambos grupos estén presentes. En cambio, el formado por la unión de PLGA y PEG (PLGA-PEG-PLGA) se trata de un hidrogel termorrespuesta, es decir, a temperatura ambiente el hidrogel se encuentra en un estado de sol o líquido, convirtiéndose en gel cuando alcanza las temperaturas corporales. El mecanismo de gelificación de este tipo de hidrogeles es debido a la agregación micelar que se produce a estas temperaturas (261,262). Lo interesante de ambos hidrogeles es su biocompatibilidad y su biodegradación, e incluso los polímeros sintéticos que forman el PLGA-PEG-PLGA han sido aprobados por la FDA (263,264).

En la optimización del hidrogel de ácido hialurónico se emplearon distintas concentraciones de los dos compuestos hasta conseguir que se formara un gel con un pH cercano a la neutralidad. La reticulación de este gel se ha visto que evoluciona con el tiempo y que tiene propiedades de "autocuración" ("*self-healing capacity*"), al aplicar una fuerza, el gel se comporta como un líquido, volviendo a su estado de gel cuando la fuerza es retirada. Esta capacidad es muy interesante para su uso como inyectable, aplicación que se busca en este trabajo (137).

En el caso de los hidrogeles formados por PLGA-PEG-PLGA se acudió a la búsqueda de un aumento de su solubilidad en agua ya que su principal inconveniente es el tiempo tan prolongado (a veces días) necesario para su disolución. Con el fin de disminuir el tiempo de solubilización se decidió acudir al empleo de un PEG con un peso molecular mayor. Ambos polímeros fueron caracterizados por GPC y resonancia magnética nuclear para comprobar su estructura química y sus pesos moleculares. Aunque se mejoró su solubilidad, la temperatura de gelificación se vio afectada, siendo imposible su uso a la temperatura corporal humana. En todas las formulaciones los polímeros se disuelven en un tampón carbonato para conseguir un pH óptimo y se acude al empleo de azúcares o polioles para conseguir condiciones isotónicas. En un primer momento se empleó la trehalosa como agente isotonizante, siendo el tiempo necesario para la disolución de tres días. Con el fin de disminuir el tiempo de disolución se acudió al empleo de la

liofilización (57). Con esta idea en mente, se procedió a la sustitución de la trehalosa por otras sustancias que pudieran facilitar la disolución y con propiedades crioprotectoras. Todos los compuestos probados disminuyeron los tiempos de disolución desde los 3 días que tarda la trehalosa hasta una noche conseguido con la sustitución de la trehalosa por glicerol. El comportamiento reológico y duración de los geles fueron evaluados, encontrando que el único compuesto que tenía un comportamiento similar al de referencia (trehalosa) era el manitol. Sin embargo, cuando los hidrogeles se liofilizaron se produjo una modificación en sus propiedades reológicas, debido, probablemente, al estrés físico que conlleva la liofilización (58).

Para la comparación de los geles de ácido hialurónico y de PLGA-PEG-PLGA se realizaron estudios de degradación, hinchamiento y liberación *in vitro* de una sustancia antiinflamatoria. Para ello, ambos geles se cargaron con un 0,2% de dexametasona fosfato. En cuanto a la degradación, se llevó a cabo una simulación de las condiciones enzimáticas presentes en el segmento posterior del ojo con la adición de hialuronidasa para poder determinar correctamente la degradación de los hidrogeles de ácido hialurónico. Estos presentaron una degradación completa al cabo de una semana, en contraste a los hidrogeles de PLGA-PEG-PLGA, cuya degradación es principalmente por hidrólisis, y presentaron una degradación del 30% aproximadamente a los 7 días. Además, los estudios de liberación *in vitro* mostraron una liberación más rápida del compuesto antiinflamatorio en los hidrogeles de ácido hialurónico. Teniendo todo esto en cuenta, los hidrogeles de ácido hialurónico se propusieron utilizar como tratamiento inyectable en enfermedades oftálmicas de corta duración, mientras que los de PLGA-PEG-PLGA pueden considerarse para tratamientos más prolongados. Por ello se procedió a la evaluación *in vitro* de la tolerancia de los hidrogeles de PLGA-PEG-PLGA en células epiteliales de retina. Estos estudios mostraron unos valores óptimos de viabilidad tanto para los hidrogeles cargados con dexametasona como para los hidrogeles sin cargar. También se realizaron estudios de cicatrización o "*Wound healing*" (265), ya que en algunas enfermedades neurodegenerativas de la retina se produce un daño las células del epitelio pigmentario de la retina y un tratamiento que actúe a nivel de la proliferación o la regeneración de ellas podría ser interesante (266). En este caso,

las formulaciones desarrolladas en este trabajo mostraron una recuperación más rápida a las 8 horas en comparación con el control.

Finalmente, en el **capítulo IV** que recoge esta tesis, **"Hybrid therapeutic platform of multi-loaded PLGA microspheres for the treatment of glaucoma"** se desarrolla un sistema híbrido formado por las microesferas optimizadas del capítulo II y los hidrogeles desarrollados en el capítulo III.

Aunque, como ya se ha puesto de manifiesto en otros capítulos, los sistemas microparticulares son plataformas muy convenientes para liberar concentraciones sostenidas de agentes activos a lo largo del tiempo, en algunos casos presentan una liberación inicial rápida de parte de su contenido que durante el proceso de microencapsulación queda retenido cerca de la superficie de las microesferas o incluidas en poros de fácil acceso. Esto produce lo que se conoce como "*burst release*" o liberación rápida inicial, típicamente cuantificada durante las primeras 24h del ensayo de cesión. Aunque en esta tesis doctoral se han utilizado estrategias tecnológicas durante el proceso de microencapsulación para reducir con éxito este efecto, en el capítulo IV se ha procedido a evaluar otra estrategia interesante, una vez elaboradas las microesferas. Así, se ha procedido a la combinación de las microesferas optimizadas del capítulo II (cargadas con dexametasona, UDCA y GDNF) con los hidrogeles termosensibles preparados y caracterizados en el capítulo III de PLGA-PEG-PLGA para, entre otras cosas, intentar reducir aún más esta liberación inicial. Esta combinación también permite favorecer la agregación de las microesferas el lugar de administración cuando son inyectadas, además de tener un potencial papel de protección frente a la degradación, ya sea enzimática o celular cuando es inyectado *in vivo* (148). Como beneficio adicional, la suspensión de las microesferas en el hidrogel podría evitar la pérdida de estas por adhesión a la jeringa en el momento de la inyección (118).

Así, se procedió a hacer una la caracterización fisicoquímica del sistema híbrido MSs/hidrogel para comprobar si las características del hidrogel se veían modificadas por la presencia de las microesferas. Aunque sistemas similares formados también por la combinación de microesferas de PLGA e hidrogeles de PLGA-PEG-PLGA ya han sido estudiados con anterioridad por otros autores, esos estudios se limitaban exclusivamente a evaluar la modificación de la cesión de las microesferas (147,148,267).

En cuanto a la prueba del "frasco invertido" se puede ver que las formulaciones que contienen las microesferas presentaron una temperatura de gelificación que resulta 1 grado inferior al de los hidrogeles que no los contenían, pudiendo deberse a que las microesferas en suspensión interaccionarían de alguna forma con las micelas, produciendo una agregación más temprana en temperatura. En cuanto a las pruebas de inyectabilidad, todos los sistemas fueron capaces de inyectarse a 20°C mostrando su idoneidad como una formulación inyectable. Cabe mencionar que a 37°C también era capaz de inyectarse salvo con agujas de menor diámetro (30G). Sin embargo, esto no supondría ningún inconveniente en su aplicación ya que no está previsto que este sistema se inyecte a 37°C, sino que la gelificación se produzca a esta temperatura. Tampoco se vio que las microesferas afectaran a la capacidad de hinchamiento o absorción de agua de los hidrogeles, mostrando resultados similares tanto si se comparaba con la inclusión de microesferas como con la adición de manitol en el tampón. En estos estudios se vio que se alcanzaba un máximo a los 5-7 días, comenzando, a continuación, a disminuir dicho parámetro.

Los estudios de liberación *in vitro* de los distintos principios activos sí que mostraron diferencias entre la liberación de las microesferas y la liberación de las microesferas suspendidas en el hidrogel. Las liberaciones iniciales (el "*burst effect*" antes mencionado) de todos los principios activos encapsulados en las microesferas se vieron disminuidas cuando estas estaban incorporadas en el hidrogel, produciéndose una media de disminución de los principios activos, en cantidad, de entre el 46%-52% para el UDCA y de entre el 72%-82% para la DX. Esta reducción fue más acusada para la liberación del GDNF pasando de una liberación de aproximadamente 7 ng/mg MSs a una liberación de en torno a 35-45 pg/mg MSs para las que sí que estaban incluidas en el gel (siendo una reducción en torno a 150-200 veces su valor). Está modificación en la liberación inicial ha sido también descrita por otros autores que incluían microesferas en los hidrogeles termorrespuesta (147–149,267).

Sin embargo, los estudios con el factor de similitud f_2 mostraron que la liberación del UDCA y de la DX, a pesar de presentar diferencias en la liberación en 24 horas, eran similares a lo largo del estudio. En cambio, el factor de similitud fue diferente en las liberaciones de GDNF corroborando la gran diferencia observada en la liberación de las

24 horas. Además, hay que destacar que en este compuesto se observó 3 fases de diferentes velocidades en la cesión, en contraposición a las 4 fases que se observaban en la liberación de las microesferas sin hidrogel.

La liberación de la dexametasona fosfato, incorporada en el hidrogel, no presentó diferencias en los diferentes tampones ni con la inclusión de las microesferas, mostrando una liberación rápida en los primeros 7 días y una fase más lenta y sostenida hasta los 21 días.

Los estudios de viabilidad celular *in vitro* mostraron una buena tolerancia de todas las formulaciones, ya fueran las microesferas en suspensión en una solución de cloruro sódico (0,9% p/v) o suspendidas en los hidrogeles, no encontrándose diferencias entre los tratamientos. Además, al incorporar las formulaciones en las células, se pudo comprobar la agregación de las microesferas gracias a la presencia de los hidrogeles, evitando la dispersión de estas en la zona de inyección. Este hecho supone una mejora importante en cuanto a la administración del preparado ya que se garantiza la agregación inicial de las partículas comportándose, así, como un implante.

CONCLUSIONES – CONCLUSIONS

CONCLUSIONES

1. Es posible la co-microencapsulación y posterior co-liberación sostenida de dexametasona y fibronectina a partir de las microesferas de PLGA elaboradas en esta Tesis Doctoral mediante la técnica de emulsión-evaporación del disolvente tras la formación de una doble emulsión acuo-óleo-acuosa

2. La inyección intracameral de microesferas biodegradables de PLGA co-cargadas con dexametasona y fibronectina es una herramienta eficaz para desarrollar un modelo animal de elevación crónica de la PIO en ratas, de seis meses de duración, que se acompaña además de una degeneración progresiva de las estructuras retinianas con una sola administración de los sistemas.

3. El modelo animal crónico de glaucoma inducido por microesferas co-cargadas resulta de utilidad para el estudio de esta patología a largo plazo, así como para la evaluación de las propiedades neuroprotectoras de los principios activos, y de la eficacia de los sistemas intraoculares de liberación controlada.

4. El sistema microparticular cargado con tres principios activos de distinta naturaleza (un antiinflamatorio – dexametasona –, un antiapoptótico – UDCA – y un factor neurotrófico – GDNF) presenta una buena eficacia de encapsulación y una liberación de forma controlada durante aproximadamente tres meses para los compuestos de bajo peso molecular (dexametasona y UDCA) y seis meses en el caso de la proteína. De acuerdo con el modelo matemático empleado, la incorporación de dexametasona o UDCA en el mismo sistema microparticular incrementó la liberación inicial del otro componente en la primera fase de la liberación, debido a la influencia en la distribución de los principios activos dentro de la matriz polimérica.

5. El sistema microparticular cargado con tres agentes neuroprotectores de distinta naturaleza (dexametasona/UDCA/GDNF) desarrollado en esta Tesis Doctoral, puede ser considerado como una estrategia muy interesante para el tratamiento de patologías neurodegenerativas crónicas de la retina mediante inyecciones intravítreas espaciadas en el tiempo varios meses.

6. Los hidrogeles biodegradables desarrollados en esta Tesis Doctoral a base de ácido hialurónico funcionalizado mostraron propiedades adecuadas para ser considerados sistemas de administración intraocular de sustancias activas para el tratamiento de enfermedades oculares agudas.

7. Los hidrogeles biodegradables optimizados en esta Tesis Doctoral a base de PLGA-PEG-PLGA mostraron buenas propiedades para su administración intraocular en enfermedades oculares crónicas.

8. La inclusión de sustancias crioprotectoras en la disolución de los hidrogeles termorrespuesta de PLGA-PEG-PLGA ha mostrado afectar a la estructura del gel y sus propiedades de gelificación.

9. Los sistemas híbridos formados por la combinación de hidrogeles termorrespuesta y microesferas multicargadas han permitido el control de la liberación rápida inicial de los agentes activos y la agregación de las microesferas en el momento de la inyección, además de presentar buenas propiedades de inyectabilidad. La inclusión de las microesferas no afectó de forma relevante las propiedades fisicoquímicas de los hidrogeles.

CONCLUSIONS

1. Co-microencapsulation and subsequent sustained co-release of dexamethasone and fibronectin from the PLGA microspheres elaborated in this PhD Thesis is possible using the solvent emulsion-evaporation technique after the formation of a water-in-oil-in-water double emulsion.

2. Intracameral injection of biodegradable PLGA microspheres co-loaded with dexamethasone and fibronectin is an effective tool to develop an animal model of chronic IOP elevation in rats, lasting six months, which is also accompanied by progressive degeneration of retinal structures with a single administration of the microparticule system.

3. The chronic animal model of glaucoma induced by co-loaded microspheres is useful for the long-term study of this pathology, as well as for the evaluation of the neuroprotective properties of the active ingredients and the efficacy of the intraocular drug delivery systems.

4. The microparticular system loaded with three active ingredients of different nature (an anti-inflammatory - dexamethasone -, an anti-apoptotic - UDCA - and a neurotrophic factor - GDNF) presents a good encapsulation efficiency and a controlled release for approximately three months for the low molecular weight compounds (dexamethasone and UDCA) and six months in the case of the protein. According to the mathematical model used, the incorporation of dexamethasone or UDCA in the same microparticulate system increased the initial release of the other component in the first release phase, due to the influence on the distribution of the active ingredients within the polymeric matrix.

5. The microparticular system loaded with three neuroprotective agents of different nature (dexamethasone/UDCA/GDNF) developed in this Doctoral Thesis can be considered as a very interesting strategy for the treatment of chronic neurodegenerative pathologies of the retina by intravitreal injections spaced in time several months.

6. The biodegradable hydrogels developed in this Doctoral Thesis based on functionalised hyaluronic acid showed suitable properties to be considered as intraocular administration systems of active substances for the treatment of acute eye diseases.

7. The biodegradable hydrogels optimised in this Doctoral Thesis based on PLGA-PEG-PLGA showed good properties for intraocular delivery in chronic eye diseases.

8. The inclusion of cryoprotective substances in the dissolution of PLGA-PEG-PLGA thermo-responsive hydrogels has been shown to affect gel structure and gelation properties.

9. Hybrid systems composed of the combination of thermo-responsive hydrogels and multi-loaded microspheres have allowed the control of the initial rapid release of the active agents and the aggregation of the microspheres upon of injection, as well as good injectability properties. The inclusion of the microspheres did not significantly affect the physicochemical properties of the hydrogels.

BIBLIOGRAFÍA

1. A K Khurana. Comprehensive ophthalmology 6th ed. Jaypee Brothers Medical Publishers (P) Ltd; 2015. 623.

2. Van De Pol C. CHAPTER 6: BASIC ANATOMY AND PHYSIOLOGY OF THE HUMAN VISUAL SYSTEM. In: Helmet-Mounted Displays: Sensation, Perception and Cognition Issues. U.S. Army Aeromedical Research Laboratory; 2000. p. 237–47.

3. Eghrari AO, Riazuddin SA, Gottsch JD. Overview of the Cornea: Structure, Function, and Development. Prog Mol Biol Transl Sci. 2015 Jan 1;134:7–23.

4. Tortora GJ, Derrickson B. Principles of Anatomy and Physiology. 12th ed. John Wiley & Sons, Inc; 2009. 604–620 p.

5. Behar-Cohen F, Gelizé E, Jonet L, Lassiaz P. Anatomy of the retina. Med Sci (Paris). 2020;36(6–7).

6. Reichenbach A, Bringmann A. Glia of the human retina. Glia. 2020 Apr 1;68(4):768–96.

7. Vecino E, Rodriguez FD, Ruzafa N, Pereiro X, Sharma SC. Glia-neuron interactions in the mammalian retina. Prog Retin Eye Res. 2016 Mar 1;51:1–40.

8. Colonna M, Butovsky O. Microglia Function in the Central Nervous System During Health and Neurodegeneration. Annu Rev Immunol. 2017 Apr 26;35:441–68.

9. Carreon T, van der Merwe E, Fellman RL, Johnstone M, Bhattacharya SK. Aqueous outflow - A continuum from trabecular meshwork to episcleral veins. Prog Retin Eye Res. 2017 Mar 1;57:108–33.

10. Le Goff MM, Bishop PN. Adult vitreous structure and postnatal changes. Eye 2008 22:10. 2008 Feb 29;22(10):1214–22.

11. Guidoboni G, Sacco R, Szopos M, Sala L, Verticchio Vercellin AC, Siesky B, et al. Neurodegenerative Disorders of the Eye and of the Brain: A Perspective on Their Fluid-Dynamical Connections and the Potential of Mechanism-Driven Modeling. Front Neurosci. 2020 Nov 12;14:1173.

12. Marchesi N, Fahmideh F, Boschi F, Pascale A, Barbieri A. Ocular Neurodegenerative Diseases: Interconnection between Retina and Cortical Areas. Cells. 2021 Sep 1;10(9).

13. Bourne RRA, Steinmetz JD, Saylan M, Mersha AM, Weldemariam AH, Wondmeneh TG, et al. Causes of blindness and vision impairment in 2020 and trends over 30 years, and prevalence of avoidable blindness in relation to VISION 2020: the Right to Sight: an analysis for the Global Burden of Disease Study. Lancet Glob Health. 2021 Feb 1;9(2):e144–60.

14. Jonas JB, Aung T, Bourne RR, Bron AM, Ritch R, Panda-Jonas S. Glaucoma. Lancet. 2017 Nov 11;390(10108):2183–93.

15. Khaw PT, Elkington AR. ABC of Eyes: Glaucoma—1: Diagnosis. BMJ : British Medical Journal. 2004 Jan 1;328(7431):97.

16. Abe RY, Gracitelli CPB, Diniz-Filho A, Tatham AJ, Medeiros FA. Lamina Cribrosa in Glaucoma: Diagnosis and Monitoring. Curr Ophthalmol Rep. 2015 Jun 6;3(2):74.

17. Killer HE, Pircher A. Normal tension glaucoma: review of current understanding and mechanisms of the pathogenesis. Eye (Lond). 2018 May 1;32(5):924–30.

18. Kang JM, Tanna AP. Glaucoma. Medical Clinics of North America. 2021 May 1;105(3):493–510.

19. Leske MC. Ocular perfusion pressure and glaucoma: clinical trial and epidemiologic findings. Curr Opin Ophthalmol. 2009 Mar;20(2):73.

20. Ch'ng TW, Chua CY, Ummi KMA, Azhany Y, Gong VHM, Rasool AHG, et al. Ocular Perfusion Pressure and Severity of Glaucoma: Is There a Link? J Curr Glaucoma Pract. 2021 Oct 1;15(2):78.

21. Baudouin C, Kolko M, Melik-Parsadaniantz S, Messmer EM. Inflammation in Glaucoma: From the back to the front of the eye, and beyond. Prog Retin Eye Res. 2021 Jul 1;83:100916.

22. Arranz-Romera A, Esteban-Pérez S, Garcia-Herranz D, Aragón-Navas A, Bravo-Osuna I, Herrero-Vanrell R. Combination therapy and co-delivery strategies to optimize treatment of posterior segment neurodegenerative diseases. Vol. 24, Drug Discovery Today. 2019.

23. Ammar MJ, Hsu J, Chiang A, Ho AC, Regillo CD. Age-related macular degeneration therapy: A review. Curr Opin Ophthalmol. 2020 May 1;31(3):215–21.

24. Flores R, Carneiro A, Vieira M, Tenreiro S, Seabra MC. Age-Related Macular Degeneration: Pathophysiology, Management, and Future Perspectives. Ophthalmologica. 2021 Dec 1;244(6):495–511.

25. García-Layana A, Cabrera-López F, García-Arumí J, Arias-Barquet L, Ruiz-Moreno JM. Early and intermediate age-related macular degeneration: update and clinical review. Clin Interv Aging. 2017 Oct 3;12:1579–87.

26. Wang W, Lo ACY. Diabetic Retinopathy: Pathophysiology and Treatments. Int J Mol Sci. 2018 Jun 20;19(6).

27. Pierce EA. Retinitis pigmentosa and related disorders. In: Levin LA, Albert DM, editors. Ocular Disease: Mechanisms and Management Expert Consult. W.B. Saunders; 2010. p. 579–89.

28. Hartong DT, Berson EL, Dryja TP. Retinitis pigmentosa. The Lancet. 2006 Nov 18;368(9549):1795–809.

29. Hage R, Vignal-Clermont C. Leber Hereditary Optic Neuropathy: Review of Treatment and Management. Front Neurol. 2021 May 26;12.

30. Sundaramurthy S, SelvaKumar A, Ching J, Dharani V, Sarangapani S, Yu-Wai-Man P. Leber hereditary optic neuropathy-new insights and old challenges. Graefes Arch Clin Exp Ophthalmol. 2021 Sep 1;259(9):2461–72.

31. Gote V, Sikder S, Sicotte J, Pal D. Ocular Drug Delivery: Present Innovations and Future Challenges. J Pharmacol Exp Ther. 2019;370(3):602–24.

32. Leclercq B, Mejlachowicz D, Behar-Cohen F. Ocular Barriers and Their Influence on Gene Therapy Products Delivery. Pharmaceutics 2022, Vol 14, Page 998. 2022 May 6;14(5):998.

33. Urtti A. Challenges and obstacles of ocular pharmacokinetics and drug delivery. Adv Drug Deliv Rev. 2006 Nov 15;58(11):1131–5.

34. Gunda S, Hariharan S, Mandava N, Mitra AK. Barriers in Ocular Drug Delivery. In: Tombran-Tink J, Barnstable CJ, editors. Ocular Transporters In Ophthalmic Diseases And Drug Delivery. Humana Press; 2008. p. 399–413.

35. Andrés-Guerrero V, Herrero-Vanrell R. Absorción de fármacos por vía tópica: Papel de la conjuntiva. Arch Soc Esp Oftalmol. 2008;83(12):683–5.

36. Awwad S, Mohamed Ahmed AHA, Sharma G, Heng JS, Khaw PT, Brocchini S, et al. Principles of pharmacology in the eye. Br J Pharmacol. 2017 Dec 1;174(23):4205–23.

37. Cunha-Vaz J, Bernardes R, Lobo C. Blood-Retinal Barrier. https://doi.org/105301/EJO20106049. 2010 Nov 11;21(SUPPL.6):3–9.

38. Gaudana R, Ananthula HK, Parenky A, Mitra AK. Ocular Drug Delivery. AAPS J. 2010 Sep;12(3):348.

39. Kompella UB, Hartman RR, Patil MA. Extraocular, periocular, and intraocular routes for sustained drug delivery for glaucoma. Prog Retin Eye Res. 2021 May 1;82.

40. Peng Y, Tang L, Zhou Y. Subretinal Injection: A Review on the Novel Route of Therapeutic Delivery for Vitreoretinal Diseases. Ophthalmic Res. 2017 Oct 1;58(4):217–26.

41. Waite D, Wang Y, Jones D, Stitt A, Raj Singh TR. Posterior drug delivery via periocular route: challenges and opportunities. Ther Deliv. 2017 Jul 1;8(8):685–99.

42. Shalaby WS, Shankar V, Razeghinejad R, Katz LJ. Current and new pharmacotherapeutic approaches for glaucoma. https://doi.org/101080/1465656620201795130. 2020 Nov 1;21(16):2027–40.

43. Oh DJ, Chen JL, Vajaranant TS, Dikopf MS. Brimonidine tartrate for the treatment of glaucoma. Expert Opin Pharmacother. 2019 Jan 2;20(1):115–22.

44. Bhatti A, Singh G. Efficacy of three different formulations of brimonidine for control of intraocular pressure in primary open-angle glaucoma: A 6-week randomized trial. Oman J Ophthalmol. 2018 May 1;11(2):140.

45. Costagliola C, Dell'Omo R, Romano MR, Rinaldi M, Zeppa L, Parmeggiani F. Pharmacotherapy of intraocular pressure: part I. Parasympathomimetic, sympathomimetic and sympatholytics. Expert Opin Pharmacother. 2009;10(16):2663–77.

46. Costagliola C, Dell'Omo R, Romano MR, Rinaldi M, Zeppa L, Parmeggiani F. Pharmacotherapy of intraocular pressure - part II. Carbonic anhydrase inhibitors, prostaglandin analogues and prostamides. Expert Opin Pharmacother. 2009 Dec;10(17):2859–70.

47. Tanna AP, Johnson M. Rho Kinase Inhibitors as a Novel Treatment for Glaucoma and Ocular Hypertension. Ophthalmology. 2018 Nov 1;125(11):1741–56.

48. Moura-Coelho N, Tavares Ferreira J, Bruxelas CP, Dutra-Medeiros M, Cunha JP, Pinto Proença R. Rho kinase inhibitors-a review on the physiology and clinical use in Ophthalmology. Graefes Arch Clin Exp Ophthalmol. 2019 Jun 4;257(6):1101–17.

49. Hoy SM. Latanoprostene Bunod Ophthalmic Solution 0.024%: A Review in Open-Angle Glaucoma and Ocular Hypertension. Drugs. 2018 May 1;78(7):773–80.

50. Belamkar A, Harris A, Zukerman R, Siesky B, Oddone F, Verticchio Vercellin A, et al. Sustained release glaucoma therapies: Novel modalities for overcoming key treatment barriers associated with topical medications. Ann Med. 2022;54(1):343.

51. Lim LS, Mitchell P, Seddon JM, Holz FG, Wong TY. Age-related macular degeneration. Lancet. 2012;379(9827):1728–38.

52. Cho YK, Park DH, Jeon IC. Medication Trends for Age-Related Macular Degeneration. Int J Mol Sci. 2021 Nov 1;22(21).

53. Pardue MT, Allen RS. Neuroprotective strategies for retinal disease. Vol. 65, Progress in Retinal and Eye Research. 2018.

54. He S, Stankowska DL, Ellis DZ, Krishnamoorthy RR, Yorio T. Targets of Neuroprotection in Glaucoma. J Ocul Pharmacol Ther [Internet]. 2018 Jan 1 [cited 2023 Feb 24];34(1–2):85–106. Available from: https://pubmed.ncbi.nlm.nih.gov/28820649/

55. Park YH, Mueller BH, McGrady NR, Ma HY, Yorio T. AMPA receptor desensitization is the determinant of AMPA receptor mediated excitotoxicity in purified retinal ganglion cells. Exp Eye Res. 2015 Mar 1;132:136–50.

56. Weinreb RN, Liebmann JM, Cioffi GA, Goldberg I, Brandt JD, Johnson CA, et al. Oral Memantine for the Treatment of Glaucoma: Design and Results of 2 Randomized, Placebo-Controlled, Phase 3 Studies. Ophthalmology. 2018 Dec 1;125(12):1874–85.

57. Park YH, Broyles H v., He S, McGrady NR, Li L, Yorio T. Involvement of AMPA Receptor and Its Flip and Flop Isoforms in Retinal Ganglion Cell Death Following Oxygen/Glucose Deprivation. Invest Ophthalmol Vis Sci. 2016 Feb 1;57(2):508–26.

58. Sivakumar V, Foulds WS, Luu CD, Ling EA, Kaur C. Hypoxia-induced retinal ganglion cell damage through activation of AMPA receptors and the neuroprotective effects of DNQX. Exp Eye Res. 2013 Apr;109:83–97.

59. Mysona BA, Zhao J, De Greef O, Beisel A, Patel PA, Berman L, et al. Sigma-1 receptor agonist, (+)-pentazocine, is neuroprotective in a Brown Norway rat microbead model of glaucoma. Exp Eye Res. 2023 Jan 1;226.

60. Li L, He S, Liu Y, Yorio T, Ellis DZ. Sigma-1R Protects Retinal Ganglion Cells in Optic Nerve Crush Model for Glaucoma. Invest Ophthalmol Vis Sci. 2021 Aug 1;62(10).

61. Chaphalkar RM, Stankowska DL, He S, Kodati B, Phillips N, Prah J, et al. Endothelin-1 Mediated Decrease in Mitochondrial Gene Expression and Bioenergetics Contribute to Neurodegeneration of Retinal Ganglion Cells. Sci Rep. 2020 Dec 1;10(1).

62. Shoshani YZ, Harris A, Shoja MM, Rusia D, Siesky B, Arieli Y, et al. Endothelin and its suspected role in the pathogenesis and possible treatment of glaucoma. Curr Eye Res. 2012 Jan;37(1):1–11.

63. Tezel G. TNF-alpha signaling in glaucomatous neurodegeneration. Prog Brain Res. 2008;173:409–21.

64. Roh M, Zhang Y, Murakami Y, Thanos A, Lee SC, Vavvas DG, et al. Etanercept, a widely used inhibitor of tumor necrosis factor-α (TNF-α), prevents retinal ganglion cell loss in a rat model of glaucoma. PLoS One. 2012 Jul 3;7(7).

65. Nucci C, Russo R, Martucci A, Giannini C, Garaci F, Floris R, et al. New strategies for neuroprotection in glaucoma, a disease that affects the central nervous system. Eur J Pharmacol. 2016 Sep 15;787:119–26.

66. Hui F, Tang J, Williams PA, McGuinness MB, Hadoux X, Casson RJ, et al. Improvement in inner retinal function in glaucoma with nicotinamide (vitamin B3) supplementation: A crossover randomized clinical trial. Clin Exp Ophthalmol. 2020 Sep 1;48(7):903–14.

67. Han FF, Fu XX. Vitamin intake and glaucoma risk: A systematic review and meta-analysis. J Fr Ophtalmol. 2022 May 1;45(5):519–28.

68. Patel S, Mathan JJ, Vaghefi E, Braakhuis AJ. The effect of flavonoids on visual function in patients with glaucoma or ocular hypertension: a systematic review and meta-analysis. Graefes Arch Clin Exp Ophthalmol. 2015 Nov 1;253(11):1841–50.

69. Nucci C, Tartaglione R, Cerulli A, Mancino R, Spanò A, Cavaliere F, et al. Retinal Damage Caused by High Intraocular Pressure–Induced Transient Ischemia is Prevented by Coenzyme Q10 in Rat. Int Rev Neurobiol. 2007 Jan 1;82:397–406.

70. Parisi V, Centofanti M, Gandolfi S, Marangoni D, Rossetti L, Tanga L, et al. Effects of coenzyme Q10 in conjunction with vitamin e on retinal-evoked and cortical-evoked responses in patients with open-angle glaucoma. J Glaucoma. 2014;23(6):391–404.

71. Yuki K, Ozawa Y, Yoshida T, Kurihara T, Hirasawa M, Ozeki N, et al. Retinal ganglion cell loss in superoxide dismutase 1 deficiency. Invest Ophthalmol Vis Sci. 2011 Jun;52(7):4143–50.

72. Yuki K, Yoshida T, Miyake S, Tsubota K, Ozawa Y. Neuroprotective role of superoxide dismutase 1 in retinal ganglion cells and inner nuclear layer cells against N-methyl-d-aspartate-induced cytotoxicity. Exp Eye Res. 2013 Oct;115:230–8.

73. Nafissi N, Foldvari M. Neuroprotective therapies in glaucoma: I. Neurotrophic factor delivery. Wiley Interdiscip Rev Nanomed Nanobiotechnol. 2016 Mar 1;8(2):240–54.

74. Almasieh M, Wilson AM, Morquette B, Cueva Vargas JL, Di Polo A. The molecular basis of retinal ganglion cell death in glaucoma. Progress in Retinal and Eye Research. 2012.

75. Beltran WA, Wen R, Acland GM, Aguirre GD. Intravitreal injection of ciliary neurotrophic factor (CNTF) causes peripheral remodeling and does not prevent photoreceptor loss in canine RPGR mutant retina. Exp Eye Res. 2007 Apr;84(4):753–71.

76. Cayouette M, Behn D, Sendtner M, Lachapelle P, Gravel C. Intraocular Gene Transfer of Ciliary Neurotrophic Factor Prevents Death and Increases Responsiveness of Rod Photoreceptors in theretinal degeneration slow mouse. Journal of Neuroscience. 1998 Nov 15;18(22):9282–93.

77. Tao W, Wen R, Goddard MB, Sherman SD, O'Rourke PJ, Stabila PF, et al. Encapsulated cell-based delivery of CNTF reduces photoreceptor degeneration in animal models of retinitis pigmentosa. Invest Ophthalmol Vis Sci. 2002 Oct;43(10):3292–8.

78. Fudalej E, Justyniarska M, Kasarełło K, Dziedziak J, Szaflik JP, Cudnoch-Jędrzejewska A. Neuroprotective Factors of the Retina and Their Role in Promoting Survival of Retinal Ganglion Cells: A Review. Ophthalmic Res. 2021 Jun 1;64(3):345–55.

79. Arranz-Romera A, Hernandez M, Checa-Casalengua P, Garcia-Layana A, Molina-Martinez IT, Recalde S, et al. A Safe GDNF and GDNF/BDNF Controlled Delivery System Improves Migration in Human Retinal Pigment Epithelial Cells and Survival in Retinal Ganglion Cells: Potential Usefulness in Degenerative Retinal Pathologies. Pharmaceuticals (Basel). 2021 Jan 1;14(1):1–24.

80. Frank L, Ventimiglia R, Anderson K, Lindsay RM, Rudge JS. BDNF Down-regulates Neurotrophin Responsiveness, TrkB Protein and TrkB mRNA Levels in Cultured Rat Hippocampal Neurons. European Journal of Neuroscience. 1996 Jun 1;8(6):1220–30.

81. Knusel B, Gao HG, Okazaki T, Yoshida T, Mori N, Hefti F, et al. Ligand-induced down-regulation of trk messenger RNA, protein and tyrosine phosphorylation in rat cortical neurons. Neuroscience. 1997 Mar 27;78(3):851–62.

82. Osborne A, Khatib TZ, Songra L, Barber AC, Hall K, Kong GYX, et al. Neuroprotection of retinal ganglion cells by a novel gene therapy construct that achieves sustained enhancement of brain-derived neurotrophic factor/tropomyosin-related kinase receptor-B signaling. Cell Death & Disease 2018 9:10. 2018 Sep 26;9(10):1–18.

83. SJ L, DS D, FD E, WM M, JB H, RM S. Pressure-Induced Alterations in PEDF and PEDF-R Expression: Implications for Neuroprotective Signaling in Glaucoma. J Clin Exp Ophthalmol. 2015;6(5).

84. Bürger S, Meng J, Zwanzig A, Beck M, Pankonin M, Wiedemann P, et al. Pigment Epithelium-Derived Factor (PEDF) Receptors Are Involved in Survival of Retinal Neurons. Int J Mol Sci. 2020 Jan 1;22(1):1–15.

85. Vigneswara V, Esmaeili M, Deer L, Berry M, Logan A, Ahmed Z. Eye drop delivery of pigment epithelium-derived factor-34 promotes retinal ganglion cell neuroprotection and axon regeneration. Molecular and Cellular Neuroscience. 2015 Sep 1;68:212–21.

86. Miyazaki M, Ikeda Y, Yonemitsu Y, Goto Y, Murakami Y, Yoshida N, et al. Pigment Epithelium-Derived Factor Gene Therapy Targeting Retinal Ganglion Cell Injuries: Neuroprotection against Loss of Function in Two Animal Models. https://home.liebertpub.com/hum. 2010 Dec 22;22(5):559–65.

87. Frasson M, Picaud S, Léveillard T, Simonutti M, Mohand-Said S, Dreyfus H, et al. Glial cell line-derived neurotrophic factor induces histologic and functional protection of rod photoreceptors in the rd/rd mouse. Invest Ophthalmol Vis Sci. 1999 Oct;40(11):2724–34.

88. Koeberle PD, Ball AK. Effects of GDNF on retinal ganglion cell survival following axotomy. Vision Res. 1998 May;38(10):1505–15.

89. Jiang C, Moore MJ, Zhang X, Klassen H, Langer R, Young M. Intravitreal injections of GDNF-loaded biodegradable microspheres are neuroprotective in a rat model of glaucoma. Mol Vis. 2007 Sep 24;13:1783–92.

90. Checa-Casalengua P, Jiang C, Bravo-Osuna I, Tucker BA, Molina-Martínez IT, Young MJ, et al. Retinal ganglion cells survival in a glaucoma model by GDNF/Vit e PLGA microspheres prepared according to a novel microencapsulation procedure. Journal of Controlled Release. 2011;

91. Ward MS, Khoobehi A, Lavik EB, Langer R, Young MJ. Neuroprotection of retinal ganglion cells in DBA/2J mice with GDNF-loaded biodegradable microspheres. J Pharm Sci. 2007;96(3):558–68.

92. Oveson BC, Iwase T, Hackett SF, Lee SY, Usui S, Sedlak TW, et al. Constituents of bile, bilirubin and TUDCA, protect against oxidative stress-induced retinal degeneration. J Neurochem. 2011 Jan;116(1):144–53.

93. Phillips MJ, Walker TA, Choi HY, Faulkner AE, Kim MK, Sidney SS, et al. Tauroursodeoxycholic acid preservation of photoreceptor structure and function in the rd10 mouse through postnatal day 30. Invest Ophthalmol Vis Sci. 2008 Apr;49(5):2148–55.

94. Drack A V., Dumitrescu A V., Bhattarai S, Gratie D, Stone EM, Mullins R, et al. TUDCA slows retinal degeneration in two different mouse models of retinitis pigmentosa and prevents obesity in Bardet-Biedl syndrome type 1 mice. Invest Ophthalmol Vis Sci. 2012 Jan;53(1):100–6.

95. Gaspar JM, Martins A, Cruz R, Rodrigues CMP, Ambrósio AF, Santiago AR. Tauroursodeoxycholic acid protects retinal neural cells from cell death induced by prolonged exposure to elevated glucose. Neuroscience. 2013 Dec 3;253:380–8.

96. Fu J, Aung MH, Prunty MC, Hanif AM, Hutson LM, Boatright JH, et al. Tauroursodeoxycholic Acid Protects Retinal and Visual Function in a Mouse Model of Type 1 Diabetes. Pharmaceutics. 2021 Aug 1;13(8).

97. Gómez-Vicente V, Lax P, Fernández-Sánchez L, Rondón N, Esquiva G, Germain F, et al. Neuroprotective Effect of Tauroursodeoxycholic Acid on N-Methyl-D-Aspartate-Induced Retinal Ganglion Cell Degeneration. PLoS One. 2015 Sep 17;10(9):e0137826.

98. Xia H, Nan Y, Huang X, Gao J, Pu M. Effects of Tauroursodeoxycholic Acid and Alpha-Lipoic-Acid on the Visual Response Properties of Cat Retinal Ganglion Cells: An In Vitro Study. Invest Ophthalmol Vis Sci. 2015 Oct;56(11):6638–45.

99. Daruich A, Jaworski T, Henry H, Zola M, Youale J, Parenti L, et al. Oral Ursodeoxycholic Acid Crosses the Blood Retinal Barrier in Patients with Retinal Detachment and Protects Against Retinal Degeneration in an Ex Vivo Model. Neurotherapeutics. 2021 Apr 1;18(2):1325–38.

100. Williams PA, Marsh-Armstrong N, Howell GR, Bosco A, Danias J, Simon J, et al. Neuroinflammation in glaucoma: A new opportunity. Exp Eye Res. 2017 Apr 1;157:20–7.

101. Madeira MH, Boia R, Santos PF, Ambrósio AF, Santiago AR. Contribution of Microglia-Mediated Neuroinflammation to Retinal Degenerative Diseases. Mediators Inflamm. 2015;2015.

102. Wei X, Cho KS, Thee EF, Jager MJ, Chen DF. Neuroinflammation and microglia in glaucoma: time for a paradigm shift. Journal of Neuroscience Research. 2019.

103. Turan-Vural E, Torun-Acar B, Acar S. Effect of Ketorolac Add-On Treatment on Intra-Ocular Pressure in Glaucoma Patients Receiving Prostaglandin Analogues. Ophthalmologica. 2012 Apr;227(4):205–9.

104. Nikkhah H, Niazpour Moez R, Entezari M, Ramezani A, Hassanpour K, Karimi S, et al. Topical ketorolac as an adjunctive treatment with intravitreal bevacizumab in the management of diabetic macular edema: A double-masked placebo-controlled randomized clinical trial. Graefes Arch Clin Exp Ophthalmol. 2021 Oct 1;259(10):2949–59.

105. Callanan D, Williams P. Topical nepafenac in the treatment of diabetic macular edema. Clinical Ophthalmology. 2008 Oct;689.

106. Saraiya N V., Goldstein DA. Dexamethasone for ocular inflammation. http://dx.doi.org/101517/146565662011571209. 2011 May;12(7):1127–31.

107. Boyer DS, Yoon YH, Belfort R, Bandello F, Maturi RK, Augustin AJ, et al. Three-year, randomized, sham-controlled trial of dexamethasone intravitreal implant in patients with diabetic macular edema. Ophthalmology. 2014 Oct 1;121(10):1904–14.

108. Sun WH, He F, Zhang NN, Zhao ZA, Chen HS. Time dependent neuroprotection of dexamethasone in experimental focal cerebral ischemia: The involvement of NF-κB pathways. Brain Res. 2018 Dec 15;1701:237–45.

109. Pereiro X, Ruzafa N, Acera A, Fonollosa A, David Rodriguez F, Vecino E. Dexamethasone protects retinal ganglion cells but not Müller glia against hyperglycemia in vitro. PLoS One. 2018 Nov 1;13(11).

110. WoldeMussie E, Ruiz G, Wijono M, Wheeler LA. Neuroprotection of retinal ganglion cells by brimonidine in rats with laser-induced chronic ocular hypertension. Invest Ophthalmol Vis Sci. 2001 Nov;42(12):2849–55.

111. Hernández M, Urcola JH, Vecino E. Retinal ganglion cell neuroprotection in a rat model of glaucoma following brimonidine, latanoprost or combined treatments. Exp Eye Res. 2008 May 1;86(5):798–806.

112. Mohan N, Chakrabarti A, Nazm N, Mehta R, Edward D. Newer advances in medical management of glaucoma. Indian J Ophthalmol. 2022 Jun 1;70(6):1920.

113. Tsai JC. Innovative IOP-Independent Neuroprotection and Neuroregeneration Strategies in the Pipeline for Glaucoma. J Ophthalmol. 2020;2020.

114. Zhang X, Tenerelli K, Wu S, Xia X, Yokota S, Sun C, et al. Cell transplantation of retinal ganglion cells derived from hESCs. Restor Neurol Neurosci. 2020 Jan 1;38(2):131–40.

115. Chew EY, Clemons TE, Jaffe GJ, Johnson CA, Farsiu S, Lad EM, et al. Effect of Ciliary Neurotrophic Factor on Retinal Neurodegeneration in Patients with Macular Telangiectasia Type 2: A Randomized Clinical Trial. Ophthalmology. 2019 Apr 1;126(4):540–9.

116. Rhee J, Shih KC. Use of Gene Therapy in Retinal Ganglion Cell Neuroprotection: Current Concepts and Future Directions. Biomolecules. 2021 Apr 1;11(4).

117. Maguire AM, Russell S, Wellman JA, Chung DC, Yu ZF, Tillman A, et al. Efficacy, Safety, and Durability of Voretigene Neparvovec-rzyl in RPE65 Mutation-Associated Inherited Retinal Dystrophy: Results of Phase 1 and 3 Trials. Ophthalmology. 2019 Sep 1;126(9):1273–85.

118. Herrero-Vanrell R, Refojo MF. Biodegradable microspheres for vitreoretinal drug delivery. Advanced Drug Delivery Reviews. 2001.

119. Nayak K, Misra M. A review on recent drug delivery systems for posterior segment of eye. Biomedicine & Pharmacotherapy. 2018 Nov 1;107:1564–82.

120. Kang-Mieler JJ, Rudeen KM, Liu W, Mieler WF. Advances in ocular drug delivery systems. Eye 2020 34:8. 2020 Feb 18;34(8):1371–9.

121. Bravo-Osuna I, Andrés-Guerrero V, Arranz-Romera A, Esteban-Pérez S, Molina-Martínez IT, Herrero-Vanrell R. Microspheres as intraocular therapeutic tools in chronic diseases of the optic nerve and retina. Vol. 126, Advanced Drug Delivery Reviews. 2018.

122. García-Estrada P, García-Bon MA, López-Naranjo EJ, Basaldúa-Pérez DN, Santos A, Navarro-Partida J. Polymeric Implants for the Treatment of Intraocular Eye Diseases: Trends in Biodegradable and Non-Biodegradable Materials. Pharmaceutics. 2021 May 1;13(5).

123. Jemni-Damer N, Guedan-Duran A, Fuentes-Andion M, Serrano-Bengoechea N, Alfageme-Lopez N, Armada-Maresca F, et al. Biotechnology and Biomaterial-Based Therapeutic Strategies for Age-Related Macular Degeneration. Part I: Biomaterials-Based Drug Delivery Devices. Front Bioeng Biotechnol. 2020 Nov 3;8:1257.

124. Vilos C, Velasquez LA. Therapeutic Strategies Based on Polymeric Microparticles. J Biomed Biotechnol [Internet]. 2012 [cited 2023 Feb 26];2012. Available from: /pmc/articles/PMC3363323/

125. Herrán E, Ruiz-Ortega JÁ, Aristieta A, Igartua M, Requejo C, Lafuente JV, et al. In vivo administration of VEGF- and GDNF-releasing biodegradable polymeric microspheres in a severe lesion model of Parkinson's disease. European Journal of Pharmaceutics and Biopharmaceutics. 2013;

126. Fernández-Sánchez L, Bravo-Osuna I, Lax P, Arranz-Romera A, Maneu V, Esteban-Párez S, et al. Controlled delivery of tauroursodeoxycholic acid from biodegradable microspheres slows retinal degeneration and vision loss in P23H rats. PLoS One. 2017 May 1;12(5).

127. Ye Z, Ji YL, Ma X, Wen JG, Wei W, Huang SM. Pharmacokinetics and distributions of bevacizumab by intravitreal injection of bevacizumab-PLGA microspheres in rabbits. Int J Ophthalmol. 2015 Aug 18;8(4):653–8.

128. Barbosa-Alfaro D, Andrés-Guerrero V, Fernandez-Bueno I, García-Gutiérrez MT, Gil-Alegre E, Molina-Martínez IT, et al. Dexamethasone PLGA Microspheres for Sub-Tenon Administration: Influence of Sterilization and Tolerance Studies. Pharmaceutics. 2021 Feb 1;13(2):1–21.

129. García-Caballero C, Lieppman B, Arranz-Romera A, Molina-Martínez IT, Bravo-Osuna I, Young M, et al. Photoreceptor preservation induced by intravitreal controlled delivery of gdnf and gdnf/melatonin in rhodopsin knockout mice. Mol Vis. 2018;

130. Arranz-Romera A, Esteban-Pérez S, Molina-Martínez IT, Bravo-Osuna I, Herrero-Vanrell R. Co-delivery of glial cell–derived neurotrophic factor (GDNF) and tauroursodeoxycholic acid (TUDCA) from PLGA microspheres: potential combination therapy for retinal diseases. Drug Deliv Transl Res. 2021;11(2).

131. Arranz-Romera A, Davis BM, Bravo-Osuna I, Esteban-Pérez S, Molina-Martínez IT, Shamsher E, et al. Simultaneous co-delivery of neuroprotective drugs from multi-loaded PLGA microspheres for the treatment of glaucoma. Journal of Controlled Release. 2019;

132. Bordbar-Khiabani A, Gasik M. Smart Hydrogels for Advanced Drug Delivery Systems. International Journal of Molecular Sciences 2022, Vol 23, Page 3665. 2022 Mar 27;23(7):3665.

133. Ilochonwu BC, Urtti A, Hennink WE, Vermonden T. Intravitreal hydrogels for sustained release of therapeutic proteins. Journal of Controlled Release. 2020 Oct 10;326:419–41.

134. Torres-Luna C, Fan X, Domszy R, Hu N, Wang NS, Yang A. Hydrogel-based ocular drug delivery systems for hydrophobic drugs. European Journal of Pharmaceutical Sciences. 2020 Nov 1;154:105503.

135. Zhang X, Wei D, Xu Y, Zhu Q. Hyaluronic acid in ocular drug delivery. Carbohydr Polym. 2021 Jul 15;264:118006.

136. Yang R, Liu X, Ren Y, Xue W, Liu S, Wang P, et al. Injectable adaptive self-healing hyaluronic acid/poly (γ-glutamic acid) hydrogel for cutaneous wound healing. Acta Biomater. 2021 Jun 1;127:102–15.

137. Anupama Devi VK, Shyam R, Palaniappan A, Jaiswal AK, Oh TH, Nathanael AJ. Self-Healing Hydrogels: Preparation, Mechanism and Advancement in Biomedical Applications. Polymers (Basel). 2021 Nov 1;13(21).

138. Cai Y, Johnson M, Sigen A, Xu Q, Tai H, Wang W. A Hybrid Injectable and Self-Healable Hydrogel System as 3D Cell Culture Scaffold. Macromol Biosci. 2021;21(9).

139. Yu Y, Lau LCM, Lo AC yin, Chau Y. Injectable Chemically Crosslinked Hydrogel for the Controlled Release of Bevacizumab in Vitreous: A 6-Month In Vivo Study. Transl Vis Sci Technol. 2015 Mar;4(2):5.

140. Xie B, Jin L, Luo Z, Yu J, Shi S, Zhang Z, et al. An injectable thermosensitive polymeric hydrogel for sustained release of Avastin® to treat posterior segment disease. Int J Pharm. 2015;490(1–2):375–83.

141. Wang R, Gao Y, Liu A, Zhai G. A review of nanocarrier-mediated drug delivery systems for posterior segment eye disease: challenges analysis and recent advances. J Drug Target. 2021;29(7):687–702.

142. Luo L, Yang J, Oh Y, Hartsock MJ, Xia S, Kim YC, et al. Controlled release of corticosteroid with biodegradable nanoparticles for treating experimental autoimmune uveitis. Journal of Controlled Release. 2019 Feb 28;296:68–80.

143. López-Cano JJ, González-Cela-Casamayor MA, Andrés-Guerrero V, Herrero-Vanrell R, Molina-Martínez IT. Liposomes as vehicles for topical ophthalmic drug delivery and ocular surface protection. Expert Opin Drug Deliv. 2021;18(7):819–47.

144. Iezzi R, Guru BR, Glybina I v., Mishra MK, Kennedy A, Kannan RM. Dendrimer-based targeted intravitreal therapy for sustained attenuation of neuroinflammation in retinal degeneration. Biomaterials. 2012 Jan 1;33(3):979–88.

145. Qamar Z, Qizilbash FF, Iqubal MK, Ali A, Narang JK, Ali J, et al. Nano-Based Drug Delivery System: Recent Strategies for the Treatment of Ocular Disease and Future Perspective. Recent Pat Drug Deliv Formul. 2019 Dec 30;13(4):246.

146. Esteban-Pérez S, Bravo-Osuna I, Andrés-Guerrero V, Molina-Martínez IT, Herrero-Vanrell R. Trojan Microparticles Potential for Ophthalmic Drug Delivery. Curr Med Chem. 2020 Sep 5;27(4):570–82.

147. Duvvuri S, Janoria KG, Pal D, Mitra AK. Controlled delivery of ganciclovir to the retina with drug-loaded poly(D,L-lactide-co-glycolide) (PLGA) microspheres dispersed in PLGA-PEG-PLGA gel: A novel intravitreal delivery system for the treatment of cytomegalovirus retinitis. Journal of Ocular Pharmacology and Therapeutics. 2007;23(3).

148. Duvvuri S, Janoria KG, Mitra AK. Development of a novel formulation containing poly(D,L-lactide-co- glycolide) microspheres dispersed in PLGA-PEG-PLGA gel for sustained delivery of ganciclovir. Journal of Controlled Release. 2005;108(2–3).

149. Zhao J, Guo B, Ma PX. Injectable alginate microsphere/PLGA–PEG–PLGA composite hydrogels for sustained drug release. RSC Adv [Internet]. 2014 Apr 10 [cited 2023 Feb

16];4(34):17736–42. Available from: https://pubs.rsc.org/en/content/articlehtml/2014/ra/c4ra00788c

150. Rong X, Ji Y, Zhu X, Yang J, Qian D, Mo X, et al. Neuroprotective effect of insulin-loaded chitosan nanoparticles/PLGA-PEG-PLGA hydrogel on diabetic retinopathy in rats. Int J Nanomedicine. 2019;14:45.

151. Cao D, Zhang X, Akabar MD, Luo Y, Wu H, Ke X, et al. Liposomal doxorubicin loaded PLGA-PEG-PLGA based thermogel for sustained local drug delivery for the treatment of breast cancer. Artif Cells Nanomed Biotechnol. 2019 Dec 4;47(1):181–91.

152. Yoo J, Won YY. Phenomenology of the Initial Burst Release of Drugs from PLGA Microparticles. ACS Biomater Sci Eng. 2020 Nov 9;6(11):6053–62.

153. Yu Z, Ma S, Wu M, Cui H, Wu R, Chen S, et al. Self-assembling hydrogel loaded with 5-FU PLGA microspheres as a novel vitreous substitute for proliferative vitreoretinopathy. J Biomed Mater Res A. 2020 Dec 1;108(12):2435–46.

154. Lee YS, Johnson PJ, Robbins PT, Bridson RH. Production of nanoparticles-in-microparticles by a double emulsion method: A comprehensive study. European Journal of Pharmaceutics and Biopharmaceutics. 2013 Feb 1;83(2):168–73.

155. Bhavsar MD, Tiwari SB, Amiji MM. Formulation optimization for the nanoparticles-in-microsphere hybrid oral delivery system using factorial design. J Control Release. 2006 Jan 10;110(2):422–30.

156. Bhavsar MD, Amiji MM. Development of Novel Biodegradable Polymeric Nanoparticles-in-Microsphere Formulation for Local Plasmid DNA Delivery in the Gastrointestinal Tract. AAPS PharmSciTech. 2008 Mar;9(1):288.

157. Gómez-Gaete C, Fattal E, Silva L, Besnard M, Tsapis N. Dexamethasone acetate encapsulation into Trojan particles. Journal of Controlled Release. 2008 May 22;128(1):41–9.

158. Sun W, Zhang N, Li X. Release mechanism studies on TFu nanoparticles-in-microparticles system. Colloids Surf B Biointerfaces. 2012 Jun 15;95:115–20.

159. Su Y, Zhang B, Sun R, Liu W, Zhu Q, Zhang X, et al. PLGA-based biodegradable microspheres in drug delivery: recent advances in research and application. https://doi.org/101080/1071754420211938756. 2021;28(1):1397–418.

160. Giri TK, Choudhary C, Ajazuddin, Alexander A, Badwaik H, Tripathi DK. Prospects of pharmaceuticals and biopharmaceuticals loaded microparticles prepared by double emulsion technique for controlled delivery. Saudi Pharmaceutical Journal : SPJ. 2013 Apr;21(2):125.

161. Iqbal M, Zafar N, Fessi H, Elaissari A. Double emulsion solvent evaporation techniques used for drug encapsulation. Int J Pharm. 2015 Dec 30;496(2):173–90.

162. Leach WT, Simpson DT, Val TN, Yu Z, Lim KT, Park EJ, et al. Encapsulation of protein nanoparticles into uniform-sized microspheres formed in a spinning oil film. AAPS PharmSciTech. 2005 Dec 6;6(4).

163. Kimura A, Noro T, Harada T. Role of animal models in glaucoma research. Neural Regen Res. 2020 Jul 1;15(7):1257.

164. Pang IH, Clark AF. Inducible rodent models of glaucoma. Vol. 75, Progress in Retinal and Eye Research. 2020.

165. Biswas S, Wan KH. Review of rodent hypertensive glaucoma models. Vol. 97, Acta Ophthalmologica. 2019.

166. Weber AJ, Zelenak D. Experimental glaucoma in the primate induced by latex microspheres. J Neurosci Methods. 2001;111(1):39–48.

167. Valderrama CM, Li R, Liu JHK. Direct effect of light on 24-h variation of aqueous humor protein concentration in Sprague–Dawley rats. Exp Eye Res. 2008 Nov 1;87(5):487–91.

168. Patel GC, Phan TN, Maddineni P, Kasetti RB, Millar JC, Clark AF, et al. Dexamethasone-Induced Ocular Hypertension in Mice: Effects of Myocilin and Route of Administration. American Journal of Pathology. 2017;187(4).

169. Cone FE, Gelman SE, Son JL, Pease ME, Quigley HA. Differential susceptibility to experimental glaucoma among 3 mouse strains using bead and viscoelastic injection. Exp Eye Res. 2010 Sep 1;91(3):415–24.

170. Sappington RM, Carlson BJ, Crish SD, Calkins DJ. The Microbead Occlusion Model: A Paradigm for Induced Ocular Hypertension in Rats and Mice. Invest Ophthalmol Vis Sci. 2010 Jan 1;51(1):207–16.

171. Chen H, Wei X, Cho KS, Chen G, Sappington R, Calkins DJ, et al. Optic Neuropathy Due to Microbead-Induced Elevated Intraocular Pressure in the Mouse. Invest Ophthalmol Vis Sci. 2011 Jan 1;52(1):36–44.

172. Urcola JH, Hernández M, Vecino E. Three experimental glaucoma models in rats: Comparison of the effects of intraocular pressure elevation on retinal ganglion cell size and death. Exp Eye Res. 2006;83(2).

173. Cone FE, Steinhart MR, Oglesby EN, Kalesnykas G, Pease ME, Quigley HA. The effects of anesthesia, mouse strain and age on intraocular pressure and an improved murine model of experimental glaucoma. Exp Eye Res. 2012 Jun;99(1):27–35.

174. Samsel PA, Kisiswa L, Erichsen JT, Cross SD, Morgan JE. A Novel Method for the Induction of Experimental Glaucoma Using Magnetic Microspheres. Invest Ophthalmol Vis Sci. 2011 Mar 1;52(3):1671–5.

175. Bunker S, Holeniewska J, Vijay S, Dahlmann-Noor A, Khaw P, Ng YS, et al. Experimental Glaucoma Induced by Ocular Injection of Magnetic Microspheres. JoVE (Journal of Visualized Experiments). 2015 Feb 2;(96):e52400.

176. Garcia-Herranz D, Rodrigo MJ, Subias M, Martinez-Rincon T, Mendez-Martinez S, Bravo-Osuna I, et al. Novel use of plga microspheres to create an animal model of glaucoma with progressive neuroretinal degeneration. Pharmaceutics. 2021;13(2).

177. Rodrigo MJ, Garcia-Herranz D, Subias M, Martinez-Rincón T, Mendez-Martínez S, Bravo-Osuna I, et al. Chronic Glaucoma Using Biodegradable Microspheres to Induce Intraocular Pressure Elevation. Six-Month Follow-Up. Biomedicines. 2021;9(6).

178. Rodrigo MJ, Garcia-Herranz D, Aragón-Navas A, Subias M, Martinez-Rincón T, Mendez-Martínez S, et al. Long-term corticosteroid-induced chronic glaucoma model produced by intracameral injection of dexamethasone-loaded PLGA microspheres. Drug Deliv. 2021;28(1):2427–46.

179. Rodrigo MJ, Bravo-Osuna I, Subias M, Montolío A, Cegoñino J, Martinez-Rincón T, et al. Tunable degrees of neurodegeneration in rats based on microsphere-induced models of chronic glaucoma. Sci Rep. 2022 Dec 1;12(1):20622.

180. Frankfort BJ, Kareem Khan A, Tse DY, Chung I, Pang JJ, Yang Z, et al. Elevated intraocular pressure causes inner retinal dysfunction before cell loss in a mouse model of experimental glaucoma. Invest Ophthalmol Vis Sci. 2013;

181. Benozzi J, Nahum LP, Campanelli JL, Rosenstein RE. Effect of hyaluronic acid on intraocular pressure in rats. Invest Ophthalmol Vis Sci. 2002;43(7):2196–200.

182. Morrison JC, Moore CG, Deppmeier LMH, Gold BG, Meshul CK, Johnson EC. A rat model of chronic pressure-induced optic nerve damage. Exp Eye Res. 1997;64(1).

183. Morrison JC. Elevated intraocular pressure and optic nerve injury models in the rat. J Glaucoma. 2005 Aug;14(4):315–7.

184. Morrison JC, Cepurna WO, Johnson EC. Modeling glaucoma in rats by sclerosing aqueous outflow pathways to elevate intraocular pressure. Exp Eye Res. 2015;141.

185. Morrison JC, Johnson EC, Cepurna WO. Hypertonic saline injection model of experimental glaucoma in rats. Methods in Molecular Biology. 2018;1695:11–21.

186. Ishikawa M, Yoshitomi T, Zorumski CF, Izumi Y. Experimentally Induced Mammalian Models of Glaucoma. Biomed Res Int. 2015;2015.

187. Sun H, Wang Y, Pang IH, Shen J, Tang X, Li Y, et al. Protective effect of a JNK inhibitor against retinal ganglion cell loss induced by acute moderate ocular hypertension. Mol Vis. 2011;17:864–75.

188. Crowston JG, Kong YXG, Trounce IA, Dang TM, Fahy ET, Bui B v., et al. An acute intraocular pressure challenge to assess retinal ganglion cell injury and recovery in the mouse. Exp Eye Res. 2014 Dec 12;141:3–8.

189. He Z, Bui B v., Vingrys AJ. Effect of Repeated IOP Challenge on Rat Retinal Function. Invest Ophthalmol Vis Sci. 2008 Jul 1;49(7):3026–34.

190. Clark AF. Basic sciences in clinical glaucoma: steroids, ocular hypertension, and glaucoma. J Glaucoma. 1995 Oct 1;4(5):354–69.

191. Clark AF, Wordinger RJ. The role of steroids in outflow resistance. Exp Eye Res. 2009 Apr 30;88(4):752–9.

192. Andrew Whitlock N, Mcknight B, Corcoran KN, Rodriguez LA, Rice DS. Increased intraocular pressure in mice treated with dexamethasone. Invest Ophthalmol Vis Sci. 2010 Dec;51(12):6496–503.

193. Zode GS, Sharma AB, Lin X, Searby CC, Bugge K, Kim GH, et al. Ocular-specific ER stress reduction rescues glaucoma in murine glucocorticoid-induced glaucoma. J Clin Invest. 2014 May 5;124(5):1956.

194. Li G, Lee C, Agrahari V, Wang K, Navarro I, Sherwood JM, et al. In vivo measurement of trabecular meshwork stiffness in a corticosteroid-induced ocular hypertensive mouse model. Proc Natl Acad Sci U S A. 2019 Jan 29;116(5):1714–22.

195. Wang K, Li G, Read AT, Navarro I, Mitra AK, Stamer WD, et al. The relationship between outflow resistance and trabecular meshwork stiffness in mice. Scientific Reports 2018 8:1. 2018 Apr 11;8(1):1–12.

196. Howell GR, Libby RT, Jakobs TC, Smith RS, Phalan FC, Barter JW, et al. Axons of retinal ganglion cells are insulted in the optic nerve early in DBA/2J glaucoma. J Cell Biol. 2007 Dec 31;179(7):1523–37.

197. Anderson DR, Hendrickson AE. Failure of increased intracranial pressure to affect rapid axonal transport at the optic nerve head. INVESTOPHTHALVISUAL SCI. 1977;16(5).

198. Quigley HA, Addicks EM. Chronic experimental glaucoma in primates. II. Effect of extended intraocular pressure elevation on optic nerve head and axonal transport. Invest Ophthalmol Vis Sci. 1980;19(2).

199. Quigley HA, Addicks EM, Green WR, Maumenee AE. Optic nerve damage in human glaucoma. II. The site of injury and susceptibility to damage. Arch Ophthalmol. 1981;99(4):635–49.

200. Isenmann S, Engel S, Gillardon F, Bähr M. Bax antisense oligonucleotides reduce axotomy-induced retinal ganglion cell death in vivo by reduction of Bax protein expression. Cell Death & Differentiation 1999 6:7. 1999 Jul 22;6(7):673–82.

201. Kilic E, Hermann DM, Isenmann S, Bähr M. Effects of pinealectomy and melatonin on the retrograde degeneration of retinal ganglion cells in a novel model of intraorbital optic nerve transection in mice. J Pineal Res. 2002;32(2):106–11.

202. Levkovitch-Verbin H, Quigley HA, Martin KRG, Zack DJ, Pease ME, Valenta DF. A Model to Study Differences between Primary and Secondary Degeneration of Retinal Ganglion Cells in Rats by Partial Optic Nerve Transection. Invest Ophthalmol Vis Sci. 2003 Aug 1;44(8):3388–93.

203. Choudhury S, Liu Y, Clark AF, Pang IH. Caspase-7: A critical mediator of optic nerve injury-induced retinal ganglion cell death. Mol Neurodegener. 2015 Aug 26;10(1):1–14.

204. Gellrich NC, Schimming R, Zerfowski M, Theodor Eysel U. Quantification of histological changes after calibrated crush of the intraorbital optic nerve in rats. Br J Ophthalmol. 2002;86(2):233–7.

205. Liu Y, McDowell CM, Zhang Z, Tebow HE, Wordinger RJ, Clark AF. Monitoring Retinal Morphologic and Functional Changes in Mice Following Optic Nerve Crush. Invest Ophthalmol Vis Sci. 2014 Jun 1;55(6):3766–74.

206. Klöcker N, Zerfowski M, Gellrich NC, Bähr M. Morphological and functional analysis of an incomplete CNS fiber tract lesion: Graded crush of the rat optic nerve. J Neurosci Methods. 2001 Sep 30;110(1–2):147–53.

207. Kaiser HJ, Flammer J, Burckhardt D. Silent Myocardial Ischemia in Glaucoma Patients. Ophthalmologica. 1993;207(1):6–8.

208. Harris A, Sergott RC, Spaeth GL, Katz JL, Shoemaker JA, Martin BJ. Color Doppler analysis of ocular vessel blood velocity in normal-tension glaucoma. Am J Ophthalmol. 1994;118(5):642–9.

209. Büchi ER, Suivaizdis I, Fu J. Pressure-induced retinal ischemia in rats: an experimental model for quantitative study. Ophthalmologica. 1991;203(3):138–47.

210. Joo CK, Choi JS, Ko HW, Park KY, Sohn S, Chun MH, et al. Necrosis and apoptosis after retinal ischemia: Involvement of NMDA- mediated excitotoxicity and p53. Invest Ophthalmol Vis Sci. 1999;40(3).

211. Adachi M, Takahashi K, Nishikawa M, Miki H, Uyama M. High intraocular pressure-induced ischemia and reperfusion injury in the optic nerve and retina in rats. Graefes Arch Clin Exp Ophthalmol. 1996 Jul;234(7):445–51.

212. Mosinger JL, Olney JW. Photothrombosis-induced ischemic neuronal degeneration in the rat retina. Exp Neurol. 1989;105(1):110–3.

213. Buchi ER, Lam TT, Suvaizdis I, Tso MOM. Injuries induced by diffuse photodynamic action in retina and choroid of albino rats. Morphologic study of an experimental model. Retina. 1994;14(4):370–8.

214. Uckermann O, Uhlmann S, Pannicke T, Franche M, Gamsalijew R, Makarov F, et al. Ischemia-reperfusion causes exudative detachment of the rabbit retina. Invest Ophthalmol Vis Sci. 2005;46(7):2592–600.

215. Lafuente MP, Villegas-Pérez MP, Sellés-Navarro I, Mayor-Torroglosa S, Miralles de Imperial J, Vidal-Sanz M. Retinal ganglion cell death after acute retinal ischemia is an ongoing process whose severity and duration depends on the duration of the insult. Neuroscience. 2002 Jan 18;109(1):157–68.

216. El-Remessy AB, Khalil IE, Matragoon S, Abou-Mohamed G, Tsai NJ, Roon P, et al. Neuroprotective effect of (-)Delta9-tetrahydrocannabinol and cannabidiol in N-methyl-D-aspartate-induced retinal neurotoxicity: involvement of peroxynitrite. Am J Pathol. 2003;163(5):1997–2008.

217. Siliprandi R, Canella R, Carmignoto G, Schiavo N, Zanellato A, Zanoni R, et al. N-methyl-D-aspartate-induced neurotoxicity in the adult rat retina. Vis Neurosci. 1992;8(6):567–73.

218. Balaiya S, Edwards J, Tillis T, Khetpal V, Chalam K V. Tumor necrosis factor-alpha (TNF-α) levels in aqueous humor of primary open angle glaucoma. Clin Ophthalmol. 2011;5(1):553–6.

219. Nakazawa T, Nakazawa C, Matsubara A, Noda K, Hisatomi T, She H, et al. Tumor necrosis factor-alpha mediates oligodendrocyte death and delayed retinal ganglion cell loss in a mouse model of glaucoma. J Neurosci. 2006 Dec 6;26(49):12633–41.

220. Kitaoka Y, Kitaoka Y, Kwong JMK, Ross-Cisneros FN, Wang J, Rong KT, et al. TNF-alpha-induced optic nerve degeneration and nuclear factor-kappaB p65. Invest Ophthalmol Vis Sci. 2006 Apr;47(4):1448–57.

221. W N, J H, M W. Endothelin-like immunoreactivity in aqueous humor of patients with primary open-angle glaucoma and cataract. Graefes Arch Clin Exp Ophthalmol. 1997;235(9):551–2.

222. Cioffi GA, Orgül S, Onda E, Bacon DR, Van Buskirk EM. An in vivo model of chronic optic nerve ischemia: the dose-dependent effects of endothelin-1 on the optic nerve microvasculature. Curr Eye Res. 1995;14(12):1147–53.

223. Chauhan BC, LeVatte TL, Jollimore CA, Yu PK, Reitsamer HA, Kelly MEM, et al. Model of endothelin-1-induced chronic optic neuropathy in rat. Invest Ophthalmol Vis Sci. 2004 Jan;45(1):144–52.

224. Krishnamoorthy RR, Rao VR, Dauphin R, Prasanna G, Johnson C, Yorio T. Role of the ETB receptor in retinal ganglion cell death in glaucoma. Can J Physiol Pharmacol. 2008 Jun;86(6):380–93.

225. Blanco R, Martínez-Navarrete G, Valiente-Soriano FJ, Avilés-Trigueros M, Pérez-Rico C, Serrano-Puebla A, et al. The S1P1 receptor-selective agonist CYM-5442 protects retinal ganglion cells in endothelin-1 induced retinal ganglion cell loss. Exp Eye Res. 2017 Nov 1;164:37–45.

226. L Leung DY, Tham CC, Kin Chung Jet King-Shing Ho L, Leung DY, Shu Fan Block L. Normal-tension glaucoma: Current concepts and approaches-A review. Clin Exp Ophthalmol. 2022 Mar 1;50(2):247–59.

227. Almasieh M, Levin LA. Neuroprotection in Glaucoma: Animal Models and Clinical Trials. Annual Review of Vision Science. 2017.

228. Vitale A, Ricceri L. The principle of the 3Rs between aspiration and reality. Front Physiol. 2022 Aug 12;13.

229. Zhang X, Ognibene CM, Clark AF, Yorio T. Dexamethasone inhibition of trabecular meshwork cell phagocytosis and its modulation by glucocorticoid receptor beta. Exp Eye Res [Internet]. 2007 Feb [cited 2023 Feb 10];84(2):275–84. Available from: https://pubmed.ncbi.nlm.nih.gov/17126833/

230. Faralli JA, Filla MS, Peters DM. Role of Fibronectin in Primary Open Angle Glaucoma. Cells 2019, Vol 8, Page 1518. 2019 Nov 26;8(12):1518.

231. Babizhayev MA, Brodskaya MW. Fibronectin detection in drainage outflow system of human eyes in ageing and progression of open-angle glaucoma. Mech Ageing Dev. 1989;47(2).

232. Kasetti RB, Maddineni P, Millar JC, Clark AF, Zode GS. Increased synthesis and deposition of extracellular matrix proteins leads to endoplasmic reticulum stress in the trabecular meshwork. Sci Rep. 2017;7(1).

233. Román BS, Gómez S, Irache JM, Espuelas S. Co-encapsulated CpG oligodeoxynucleotides and ovalbumin in PLGA microparticles; an in vitro and in vivo study. Journal of Pharmacy and Pharmaceutical Sciences. 2014;17(4).

234. Shi X, Li C, Gao S, Zhang L, Han H, Zhang J, et al. Combination of doxorubicin-based chemotherapy and polyethylenimine/p53 gene therapy for the treatment of lung cancer using porous PLGA microparticles. Colloids Surf B Biointerfaces. 2014;122.

235. Baek JS, Choo CC, Tan NS, Loo SCJ. Sustained-releasing hollow microparticles with dual-anticancer drugs elicit greater shrinkage of tumor spheroids. Oncotarget. 2017;8(46).

236. Qiao ZW, Yuan Z, Zhang W, Wei D, Hu N. Preparation, in vitro release and antibacterial activity evaluation of rifampicin and moxifloxacin-loaded poly(D,L-lactide-co-glycolide) microspheres. Artif Cells Nanomed Biotechnol. 2019;

237. Jiang B, Zhang G, Brey EM. Dual delivery of chlorhexidine and platelet-derived growth factor-BB for enhanced wound healing and infection control. Acta Biomater. 2013 Feb 1;9(2):4976–84.

238. Checa-Casalengua P, Jiang C, Bravo-Osuna I, Tucker BA, Molina-Martínez IT, Young MJ, et al. Preservation of biological activity of glial cell line-derived neurotrophic factor (GDNF) after microencapsulation and sterilization by gamma irradiation. Int J Pharm. 2012 Oct 15;436(1–2):545–54.

239. Chen XQ, Yang YY, Wang L, Chung TS. Effects of inner water volume on the peculiar surface morphology of microspheres fabricated by double emulsion technique. J Microencapsul. 2001;18(5):637–49.

240. Kersey JP, Broadway DC. Corticosteroid-induced glaucoma: a review of the literature. Eye (Lond). 2006;20(4):407–16.

241. Razali N, Agarwal R, Agarwal P, Kapitonova MY, Kannan Kutty M, Smirnov A, et al. Anterior and posterior segment changes in rat eyes with chronic steroid administration and their responsiveness to antiglaucoma drugs. Eur J Pharmacol. 2015 Feb 15;749:73–80.

242. Sapienza A, Raveu AL, Reboussin E, Roubeix C, Boucher C, Dégardin J, et al. Bilateral neuroinflammatory processes in visual pathways induced by unilateral ocular hypertension in the rat. J Neuroinflammation. 2016;13(1).

243. de Hoz R, Ramírez AI, González-Martín R, Ajoy D, Rojas B, Salobrar-Garcia E, et al. Bilateral early activation of retinal microglial cells in a mouse model of unilateral laser-induced experimental ocular hypertension. Exp Eye Res. 2018 Jun 1;171:12–29.

244. Chen H, Cho KS, Vu THK, Shen CH, Kaur M, Chen G, et al. Commensal microflora-induced T cell responses mediate progressive neurodegeneration in glaucoma. Nature Communications 2018 9:1. 2018 Aug 10;9(1):1–13.

245. Gallego BI, Salazar JJ, de Hoz R, Rojas B, Ramírez AI, Salinas-Navarro M, et al. IOP induces upregulation of GFAP and MHC-II and microglia reactivity in mice retina contralateral to experimental glaucoma. J Neuroinflammation. 2012 May 14;9.

246. Kuehn MH. Immune phenomena in glaucoma and conformational disorders: why is the second eye not involved? J Glaucoma. 2014 Dec 10;23(8 Suppl 1):S59–61.

247. del Amo EM, Rimpelä AK, Heikkinen E, Kari OK, Ramsay E, Lajunen T, et al. Pharmacokinetic aspects of retinal drug delivery. Prog Retin Eye Res. 2017 Mar 1;57:134–85.

248. Weinreb RN, Levin LA. Is neuroprotection a viable therapy for glaucoma? Vol. 117, Archives of Ophthalmology. 1999.

249. Machiele R, Motlagh M, Patel BC. Intraocular Pressure. Drug Discovery and Evaluation: Pharmacological Assay, Fourth Edition. StatPearls Publishing; 2022. 3749–3752 p.

250. Soto I, Howell GR. The complex role of neuroinflammation in glaucoma. Cold Spring Harb Perspect Med. 2014;4(8):14.

251. Li HY, Ruan YW, Ren CR, Cui Q, So KF. Mechanisms of secondary degeneration after partial optic nerve transection. Neural Regen Res. 2014;9(6):565–74.

252. Naik S, Pandey A, Lewis SA, Rao BSS, Mutalik S. Neuroprotection: A versatile approach to combat glaucoma. European Journal of Pharmacology. 2020.

253. Varde NK, Pack DW. Microspheres for controlled release drug delivery. Expert Opin Biol Ther. 2004 Jan;4(1):35–51.

254. Ramazani F, Chen W, Van Nostrum CF, Storm G, Kiessling F, Lammers T, et al. Strategies for encapsulation of small hydrophilic and amphiphilic drugs in PLGA microspheres: State-of-the-art and challenges. Int J Pharm. 2016 Feb 29;499(1–2):358–67.

255. Yeo Y, Park K. Control of encapsulation efficiency and initial burst in polymeric microparticle systems. Vol. 27, Archives of Pharmacal Research. 2004.

256. ICH Q3C (R8) Residual solvents - Scientific guideline . 2022.

257. Rawat A, Burgess DJ. Effect of ethanol as a processing co-solvent on the PLGA microsphere characteristics. Int J Pharm. 2010;394(1–2).

258. Liu G, McEnnis K. Glass Transition Temperature of PLGA Particles and the Influence on Drug Delivery Applications. Polymers (Basel). 2022 Mar 1;14(5).

259. Gallagher KM, Corrigan OI. Mechanistic aspects of the release of levamisole hydrochloride from biodegradable polymers. Journal of Controlled Release. 2000;69(2).

260. Gorrasi G, Attanasio G, Izzo L, Sorrentino A. Controlled release mechanisms of sodium benzoate from a biodegradable polymer and halloysite nanotube composite. Polym Int. 2017;66(5).

261. Yu L, Zhang Z, Ding J. Influence of la and GA sequence in the PLGA block on the properties of thermogelling PLGA-PEG-PLGA block copolymers. Biomacromolecules. 2011;12(4).

262. Wang P, Chu W, Zhuo X, Zhang Y, Gou J, Ren T, et al. Modified PLGA-PEG-PLGA thermosensitive hydrogels with suitable thermosensitivity and properties for use in a drug delivery system. Vol. 5, Journal of Materials Chemistry B. 2017.

263. Liechty WB, Kryscio DR, Slaughter B V., Peppas NA. Polymers for Drug Delivery Systems. https://doi.org/101146/annurev-chembioeng-073009-100847. 2010 Jun 11;1:149–73.

264. Makadia HK, Siegel SJ. Poly Lactic-co-Glycolic Acid (PLGA) as Biodegradable Controlled Drug Delivery Carrier. Polymers (Basel). 2011 Sep 9;3(3):1377.

265. Jonkman JEN, Cathcart JA, Xu F, Bartolini ME, Amon JE, Stevens KM, et al. An introduction to the wound healing assay using live-cell microscopy. http://dx.doi.org/104161/cam36224. 2015 Sep 1;8(5):440–51.

266. Yang X, Yu XW, Zhang DD, Fan ZG. Blood-retinal barrier as a converging pivot in understanding the initiation and development of retinal diseases. Chin Med J (Engl). 2020 Nov 5;133(21):2586–94.

267. Wang P, Zhuo X, Chu W, Tang X. Exenatide-loaded microsphere/thermosensitive hydrogel long-acting delivery system with high drug bioactivity. Int J Pharm [Internet]. 2017 Aug 7 [cited 2023 Feb 16];528(1–2):62–75. Available from: https://pubmed.ncbi.nlm.nih.gov/28579543/

ANEXO I – Patente titulada “A non-human animal mammalian model of chronic glaucoma”

(12) INTERNATIONAL APPLICATION PUBLISHED UNDER THE PATENT COOPERATION TREATY (PCT)

(19) World Intellectual Property Organization
International Bureau

(43) International Publication Date
08 July 2021 (08.07.2021)

WIPO | PCT

(10) International Publication Number
WO 2021/136697 A1

(51) International Patent Classification:
A01K 67/027 (2006.01) *A61K 31/573* (2006.01)
A61K 9/16 (2006.01) *C07K 14/78* (2006.01)

(21) International Application Number:
PCT/EP2020/087153

(22) International Filing Date:
18 December 2020 (18.12.2020)

(25) Filing Language: English

(26) Publication Language: English

(30) Priority Data:
19383213.6 30 December 2019 (30.12.2019) EP

(71) Applicants: **UNIVERSIDAD COMPLUTENSE DE MADRID** [ES/ES]; Rectorado-Avenida de Séneca, 2, 28040 Madrid (ES). **UNIVERSIDAD DE ZARAGOZA** [ES/ES]; Campus Plz. San Francisco (Edif. Interfacultades), c/ Pedro Cerbuna 12, 50009 Zaragoza (ES). **INSTITUTO DE INVESTIGACIÓN SANITARIA ARAGÓN** [ES/ES]; Avda. San Juan Bosco 13, 50009 Zaragoza (ES).

(72) Inventors: **HERRERO VANRELL, María, Rocío**; Universidad Complutense de Madrid, Rectorado-Avenida de Séneca, 2, 28040 Madrid (ES). **GARCÍA MARTÍN, Elena**; Instituto de Investigación Sanitaria, Avda. San Juan Bosco 13, 50009 Zaragoza (ES). **RODRIGO SANJUÁN, Maria, Jesus**; Instituto de Investigación Sanitaria, Avda. San Juan Bosco 13, 50009 Zaragoza (ES). **GARCÍA HERRANZ, David**; Universidad Complutense de Madrid, Rectorado-Avenida de Séneca, 2, 28040 Madrid (ES). **ARAGÓN NAVAS, Alba**; Universidad Complutense de Madrid, Rectorado-Avenida de Séneca, 2, 28040 Madrid (ES). **BRAVO OSUNA, Irene**; Universidad Complutense de Madrid, Rectorado-Avenida de Séneca, 2, 28040 Madrid (ES). **GARCÍA FELJOO, Julian**; Universidad Complutense de Madrid, Rectorado-Avenida de Séneca, 2, 28040 Madrid (ES). **PABLO JÚLVEZ, Luis**; Instituto de Investigación Sanitaria, Avda. San Juan Bosco 13, 50009 Zaragoza (ES).

(74) Agent: **GONZALEZ PECES, Gustavo, Adolfo**; Herrero & Asociados, S.L., Cedaceros, 1, 28014 Madrid (ES).

(81) Designated States *(unless otherwise indicated, for every kind of national protection available)*: AE, AG, AL, AM, AO, AT, AU, AZ, BA, BB, BG, BH, BN, BR, BW, BY, BZ, CA, CH, CL, CN, CO, CR, CU, CZ, DE, DJ, DK, DM, DO, DZ, EC, EE, EG, ES, FI, GB, GD, GE, GH, GM, GT, HN, HR, HU, ID, IL, IN, IR, IS, IT, JO, JP, KE, KG, KH, KN, KP, KR, KW, KZ, LA, LC, LK, LR, LS, LU, LY, MA, MD, ME, MG, MK, MN, MW, MX, MY, MZ, NA, NG, NI, NO, NZ, OM, PA, PE, PG, PH, PL, PT, QA, RO, RS, RU, RW, SA, SC, SD, SE, SG, SK, SL, ST, SV, SY, TH, TJ, TM, TN, TR, TT, TZ, UA, UG, US, UZ, VC, VN, WS, ZA, ZM, ZW.

(84) Designated States *(unless otherwise indicated, for every kind of regional protection available)*: ARIPO (BW, GH, GM, KE, LR, LS, MW, MZ, NA, RW, SD, SL, ST, SZ, TZ, UG, ZM, ZW), Eurasian (AM, AZ, BY, KG, KZ, RU, TJ, TM), European (AL, AT, BE, BG, CH, CY, CZ, DE, DK, EE, ES, FI, FR, GB, GR, HR, HU, IE, IS, IT, LT, LU, LV, MC, MK, MT, NL, NO, PL, PT, RO, RS, SE, SI, SK, SM, TR), OAPI (BF, BJ, CF, CG, CI, CM, GA, GN, GQ, GW, KM, ML, MR, NE, SN, TD, TG).

Declarations under Rule 4.17:
— *as to the applicant's entitlement to claim the priority of the earlier application (Rule 4.17(iii))*

Published:
— *with international search report (Art. 21(3))*

WO 2021/136697 A1

(54) **Title:** A NON-HUMAN ANIMAL MAMMALIAN MODEL OF CHRONIC GLAUCOMA

(57) **Abstract:** The present invention relates to a non-human animal model of chronic glaucoma. In addition, the invention refers to a method for the preparation of said animal model, as well as to the use thereof.

A NON-HUMAN ANIMAL MAMMALIAN MODEL OF CHRONIC GLAUCOMA

FIELD OF THE INVENTION

The present invention belongs to the field of research tools for glaucoma, more specifically it relates to a non-human animal model of chronic glaucoma. In addition, the invention refers to a method for the preparation of said animal model, as well as to the use of thereof.

BACKGROUND OF THE INVENTION

Glaucoma is a degenerative optic neuropathy in which irreversible vision loss is produced by the gradual death of retinal ganglion cells (RGC), although affectation in other retinal layers has also been observed in recent studies (Vidal-Sanz et al., Prog. Brain. Res. 2015; 220:1-35). According to the World Health Organization (WHO), it is the second leading cause of irreversible blindness in the world and the first in developed countries, with over 61 million people affected, although it is estimated that this prevalence is actually 20-25% higher due to frequent undiagnosed cases, as this pathology is asymptomatic until its late stages. It is believed that 7 million glaucoma patients have already lost their vision. Over 2 million cases are registered in the world every year, and the pathology is expected to affect 80 million people (according to "World Glaucoma Association" data). In response to the growing disease burden derived from chronic ocular conditions, the WHO coordinates a worldwide research attempt focused on identifying services and policies to fight neurodegenerative pathologies, being glaucoma among them.

The main modifiable risk factor which is currently known is intraocular pressure (IOP) increase, which hinders blood supply to the retina, compromising it by the pressure excess. This damages neural structures with optic nerve atrophy. Furthermore, it is argued that the pressure increase in the optic nerve connective tissues interrupts the axo-plasmatic flow, blocking the arrival of endogenous neurotrophic factors to the neuronal body from the axons (Pease et al., Invest. Ophtalmol. Vis. Sci., 2000, 41(3):764-774). Although it is considered there is risk of suffering from glaucoma when IOP is high, not every patient with high IOP develops glaucoma, nor a decrease in IOP assures protection against the development of the disease (Ritch et al., Ophtalmol. Clin. North Am., 2005, 18(4):597-609). Therefore, in the last decade other important factors in the genesis and the development of neuronal degeneration in the

retina have been studied, proving that the neurodegeneration process can be described, chronologically, in three steps:

1. Primary axonal damage;
2. Death of damaged neurons;
3. Damage and subsequent death of adjacent neurons, which is known as 'secondary degeneration'. This degeneration occurs in neurons which are not damaged initially, but they end up dying due to exposure to cytotoxic agents released by the death of neurons with primary axonal damage.

There are different types of glaucoma, being primary open-angle glaucoma (OAG) the most frequent as well as one of the most usual causes of blindness in the world. It is characterized by slow and progressive clinical process due to the fact that gradual and chronic IOP increase does not produce pain or discomfort and, at the first stages, loss of visual field is not perceptible by patients, although as it develops it causes malfunctions in the visual field and progressive vision loss. Once these symptoms appear, they are irreversible and might imply the disease is in an advanced stage of its evolution. The main therapy is based on reducing IOP with hypotensive eyedrops, drainage implants or surgery, depending on stage and severity.

In addition, physiopathological studies of OAG showed that once neuronal death starts, even when patients present IOP between limits considered normal, a flood of damaging proinflammatory and proapoptotic substances of RGC is unleashed, which causes the death of the adjacent neurons, known, as mentioned before, as secondary degeneration (Ritch et al., Ophthalmol. Clin. North Am., 2005, 18(4):597-609). Therefore, the use of neuroprotective therapies in the treatment of glaucoma results in an alternative way to therapies based on IOP control, which are sometimes deficient in many glaucomatous pathologies and in patients with normal IOP values.

The main problem to evaluate the efficacy of hypotensive treatments or to develop new therapies resides in the absence of a chronic and slow glaucoma animal model that simulates a human one. Nowadays most animal models in retinal degeneration are acute models, either by genetic failure or induced damage, obtaining abrupt deterioration of the tissue in few weeks. On the one hand, these models do not reproduce the reality of retinal pathologies in human beings, whose nature is chronic and where retinal damage usually takes years to appear (Dey et al Cell Transplant.

2018 Feb;27(2):213-229, Mukai et al PLoS ONE. 2019. 14(1): e02087132019). On the other hand, acute models of degeneration are not useful to assess modified release systems, which present as great potential their capacity to extend the release of active substances in small quantities for months (Nadal-Nicolás et al., Invest. Ophtalmol.Vis. Sci. 2016; 57(3):1183-92). Furthermore, these acute glaucoma animal models do not allow testing the efficacy of new therapies (hypotensive, neuronal protective, etc.) because in few days the optic nerve of the animal is completely and irreversibly atrophied and therefore no treatment has enough time to stop the disease progression.

In order to broaden and improve the knowledge of glaucomatous pathologies, several animal models have been developed in the last decades (Dey et al Cell Transplant. 2018 Feb;27(2):213-229), in which it has been resorted to an increase in IOP secondary to a decrease in the flow of aqueous humor, either through cauterization, ligature and/or sclerosis of episcleral veins, either by mechanical blockage of the trabecular meshwork with non-biodegradable particles injected in the anterior chamber, or through the use of corticoids (which reduce aqueous humor outflow when inhibiting cellular phagocytosis in the trabecular meshwork, thus avoiding the cleaning of the waste channels (Zeng et al. Current Eye Research 2019). The model of episcleral sclerosis using a hypertonic saline solution has proved to increase IOP in a sustained manner with retinotopic death of RGC (Morrison et al., Exp. Eye Res. 1997, 64:84-96; Vecino et al., Glaucoma Basic and Clinical Concepts 2011, First edition, Croatia Intech:319-334; Chen et al., Invest. Ophtalmol.Vis. Sci.2011, 52(1):5-16), albeit acute optic nerve atrophy appears in the animal in merely few weeks.

Further animal models of glaucoma have been reported in the prior art so far (Struebing el al Prog. Mol. Biol. Trans. Sci. 2015; Bouhenni et al. J. Biomed. Biotech., 2012; Agarwal et al Expert Opin Drug Discov. 2017; Biswas and Wan Acta Ophthalmol. 2019) but no research group has achieved the creation of an animal model which mimics OAG and allows assessing new reliable therapies.

The present invention represents a new model of chronic animal glaucoma based on the injection of biodegradable microspheres (Ms) of PLGA, PLA or PGA (poly-lactic-co-glycolic-acid, polylactic acid or polyglycolic acid) in the anterior chamber of the eye in a mammal, preferably a rat, which produces a progressive and chronic increase of IOP and consequently, a chronic neurodegenerative process which simulates the

conditions which appear in chronic glaucoma patients. Until now, biodegradable microparticles had never been used for this purpose. Biodegradable microparticles produce mechanical blockage in the trabecular meshwork which can be accompanied by a pharmacological effect if the particles are loaded with pharmacological agents able to provide damage at this level. All these events cause a slow, persistent and progressive rise of IOP with slow retinal degeneration of the ganglion cell layer and the optic nerve, simulating OAG physiopathology.

This invention allows to use biodegradable microspheres not only as active substance administration systems (Garcia-Caballero et al. Eur J Pharm Sci. 2017a;103:19-26) but also as a useful tool to create ocular hypertensive animal models which are able to reproduce chronic human pathologies.

CLAIMS

1. A non-human animal mammalian model of chronic glaucoma wherein the animal has intraocular PLGA, PLA or PGA microparticles, optionally loaded, in order to induce a increase in intraocular pressure.

2. A non-human animal mammalian model according to claim 1 wherein de microparticles are loaded with dexamethasone or with a combination of dexamethasone and fibronectin.

3. A non-human animal mammalian model according to any of the previous claims wherein the animal is a rodent, preferably a rat, a mouse or a guinea pig.

4. A non-human animal mammalian model according to any of the previous claims wherein chronic glaucoma is open-angle chronic glaucoma.

5. A non-human animal mammalian model according to any of the previous claims wherein the intraocular microparticles optionally loaded have a particle size between 5 µm and 40 µm, preferably between 10 µm and 20 µm.

6. A non-human animal mammalian model according to any of the previous claims wherein the intraocular microparticles optionally loaded are present in the anterior chamber of the eye of the animal.

7. A method for preparing a non-human animal mammalian model of chronic glaucoma according to any of the previous claims comprising the intraocular injection in the animal's eye of a suspension of PLGA, PLA or PGA microparticles optionally loaded.

8. A method according to claim 7 wherein the microparticles are loaded with dexamethasone or with a combination of dexamethasone and fibronectin.

9. A method according to claim 7 or 8 wherein the animal is a rodent, preferably a rat, a mouse or a guinea pig.

10. A method according to claim 7 to 9 wherein the intraocular injection is performed in the anterior chamber of the eye of the animal.

11. A method according to any of previous claims 7 to 10 wherein the aqueous suspension has a concentration of microparticles optionally loaded of 0.005% to 20% by weight of the total suspension.

12. A method according to any of previous claims 7 to 11 wherein 1 to 5 microlitres of the aqueous suspension of microparticles optionally loaded are injected in the animal's eye.

13. A method according to any of previous claims 7 to 12 wherein the microparticles optionally loaded have a particle size between 5 and 40 µm, preferably between 10 µm and 20 µm.

14. Use non-human animal mammalian model according to claim 1 to 7 for the study of physiopathology of glaucoma.

15. Use non-human animal mammalian model according to claim 1 to 7 as a tool for pharmacological, biomaterial and/or surgical studies.